Block and graft copolymers as flocculants for wastewater treatment

by

Udi Narsingh

Dissertation presented for the degree of PhD in Polymer Science

at

Stellenbosch University

Department of Chemistry and Polymer Science

Faculty of Science

Promoter: Prof. Bert Klumperman

March 2018

Declaration

By submitting this dissertation electronically, I declare that the entirety of the work contained therein is my own, original work, that I am the owner of the copyright thereof (unless to the extent explicitly otherwise stated) and that I have not previously in its entirety or in part submitted it for obtaining any qualification.

Date: December 2017

Abstract

Water pollution, due to toxic metals and organic compounds, remains a serious environmental problem. Many of the contaminants found in industrial and municipal wastewaters are known to be toxic or carcinogenic. Heavy metals are not biodegradable and tend to accumulate in living organisms, causing various diseases. The treatment of these wastewaters involves, among other steps, flocculation to remove, not only the suspended, colloidal particles but also heavy metals and other contaminants that get adsorbed on them. In this research, graft and triblock copolymer flocculants were synthesized to flocculate the suspended solids. For graft copolymerized flocculants, acrylamide was grafted onto cellulose. Cellulose is inexpensive and most abundantly available from plant and microbial resources. Polyacrylamide is a synthetic polymer that is polar and widely used for the treatment of wastewaters. Acrylamide was grafted onto cellulose using a conventional chemical free-radical initiation, as well as microwave-assisted and microwave-initiated methods. The synthesis procedure for each of the methods was optimized for percentage grafting using experimental design with response surface methodology. The optimally synthesized graft copolymer, Cell-*g*-PAM, from each of the synthesis methods was compared with highly recommended polyacrylamide based commercial flocculants for the flocculation of a model kaolinite suspension. The flocculant synthesized via the microwave-assisted method outperformed all flocculants tested. For triblock flocculants, two ABA type triblock copolymers were synthesized using single electron transfer living radical polymerization (SET-LRP). For both copolymers, the central block was poly(ethylene glycol) (PEG). PEG is a hydrophobic, pH insensitive polymer that adsorbs strongly onto colloidal particles. The first outer block was poly(*N,N*-dimethylaminoethyl methacrylate) (PDMAEMA). PDMAEMA is temperature and pH responsive and known to interact strongly with anionic colloidal particles and heavy metals. The second outer block was polyacrylamide. Various molecular weight triblock copolymers were synthesized and used for the flocculation of a kaolinite suspension. The mechanism of flocculation changed from patch to bridging as the length of the flocculants increased. The graft copolymer flocculants performed better than the block copolymer flocculants in the flocculation of kaolinite.

Opsomming

Waterbesoedeling, as gevolg van giftige metale en organiese verbindinge bly steeds 'n gevaarlike omgewingsprobleem. Baie van die besoedelingstowwe wat gevind word in industriële en munisipale afvalwater is giftig of kankeropwekkend. Swaarmetale kan nie biochemies afgebreek word nie en versamel in lewende organismes wat verskeie siektes veroorsaak. Die behandeling van hierdie afvalwater behels, benewens ander stappe, flokkulering om nie net die gesuspendeerde kolloïdale partikels te verwyder nie, maar ook ander gifstowwe wat daarop adsorbeer. In hierdie navorsing was ent en trippelblok kogepolimeriseerde flokmiddels gesintetiseer om die opgeskorte vastestowwe te flokkuleer. Vir die ert kopolimeerde flokmiddels, was akrielamied op sellulose ingeënt. Sellulose is goedkoop en geredelik beskikbaar vanaf plant en mikrobiese bronne. Poliakrielamied is 'n sintetiese polimeer en word algemeen gebruik vir die behandeling van afvalwater. Akrielamied is gebind op sellulose deur middel van 'n konvensionele chemiese vryradikaal inisiëring en ook aangehelp deur middel van mikrogolfgeïnisieerde metodes. Vir die sinteseprosesse van elk van die metodes is die optimale kondisies bepaal deur eksperimentele ontwerp deur gekose oppervlakmetodes. Die optimaal gesintetiseerde kopolimeer, Cell-*g*-PAM, vanaf elk van die metodes is vergelyk met die hoogs aangeskrewe poliakrielamied gebaseerde kommersiële flokkulante vir die flokkulering van 'n model kaolinitiese suspensie. Die gesintetiseerde flokkulant wat deur middel van die mikrogolf gebaseerde metodes vervaardig is het alle flokkulante wat ondersoek is oortref. Vir trippelblok flokkulante is twee ABA tipe trippelblok koplimere gesintetiseer deur middel van enkel elektronoordrag lewende radikale polimerisasie (SET-LRP). Die sentrale blok van beide kopolimere was poliëtileenglikool (PEG). PEG is 'n hidrofobiese, pH onsensitiewe polimeer wat sterk aan kolloïdale deeltjies adsorbeer. Die buitenste blok was poli(*N,N*-dimetielamino-etielmetakrilaat) (PDMAEMA). PDMAEMA is temperatuur en pH afhanklik toon sterk interaksie met anioniese kolloïdale partikels en swaarmetale. Die blok aangrensend aan die buitenste blok was poliakrielamied. 'n Aantal trippelblok polimere met verskille molekulêre massas is gesintetiseer en gebruik vir die flokkulering van 'n kaolinietsuspensie. Die meganisme van flokkulasie het van kol na oorbrugging verander namate die lengte van die Flokmiddels verhoog. Die gebinde kopolimeer flokkulante het beter resultate gelewer as die blok kopolimeer flokkulante in die flokkulasie van kaoliniet.

Acknowledgements

I would like to express my sincerest gratitude to my supervisor, Prof Bert Klumperman, for all his patience, support and guidance throughout my studies. Thank you for allowing me to think, and then rethink, many of my ideas about polymers.

To my co-supervisor, Dr Reuben Pfukwa, thank you for our initial discussions and giving me the opportunity to learn the finer aspects of the practical work.

To my fellow students, Anna, Siyasanga, Welmarie, and Nusrat – thank you for "holding" my hand when I was floundering in the deep!

Also, I would like to thank the staff of the Polymer Science department, especially Jim Motshweni and Calvin Maart for always being on hand whenever I required any assistance. For all the input and analyses done by Mohamed Jaffer for TEM, Illana Bergh for TGA, and Elsa Malherbe for NMR analyses.

I would also like to thank Mr Stanley Mbanga (CPUT) and Mr Kelvin Smarts (Scientific Services) for taking in my raw samples and returning with complete NMR and FTIR analyses!

I greatly acknowledge and appreciate the financial support given to me by both my employer institution (Cape Peninsula University of Technology) and the National Research Foundation (NRF).

Lastly to my wife, Natasha, thank you for your constant love, support and encouragement, and holding the fort when things got rough towards the end – you are the best!

To my dearest and most beautiful, Nalini.

Table of Contents

Chapter 4: Synthesis of cellulose-*g*-polyacrylamide through microwave-assisted and microwave-initiated copolymerization and its application as a flocculant

List of Figures

List of Tables

List of Schemes

List of Abbreviations

AA	Acrylic acid
AGU	Anhydroglucose unit
AM	Acrylamide
ANOVA	Analysis of variance
AP	Anionic polymer
APS	Ammonium persulfate
ARGET	Activator regenerated by electron transfer
ATRA	Atom transfer radical addition
ATRP	Atom transfer radical polymerization
BiBB	2-bromoisobutyryl bromide
bPy	2,2'-bipyridine
CAN	Cerium ammonium nitrate
CCD	Central composite design
CMC	Carboxyl methyl cellulose
CP	Cationic polymer
CRP	Controlled/living free radical polymerization
CTA	Chain transfer agent
DADMAC	Diallyldimethyl ammonium chloride
DCC	*N,N'*-dicyclohexylcarbodiimide
DF	Degree of freedom
DMAP	4-dimethylaminopyridine
DMAEMA	*N,N*-dimethylaminoethyl methacrylate
DMF	Dimethylformamide
DMSO	Dimethylsulphoxide
DP	Degree of polymerization
DVLO	Derjaguin, Verwey, Landau and Overbeek
EtOH	Ethanol
F	Faradays constant
FTIR	Fourier transform infrared
I	Ionic strength
ICAR	Initiator for continuous activator regeneration
KOH	Potassium hydroxide
KPS	Potassium persulfate
LMW	Low molecular weight

LRP	Living radical polymerization
Me_6TREN	Tris(2-dimethylaminoethyl)amine
MWP	Microwave power
NMP	Nitroxide mediated polymerization
NMR	Nuclear magnetic resonance
NTU	Nephelometric turbidity unit
OSET	Outer-sphere electron transfer
PAA	Polyacrylic acid
PAM	Polyacrylamide
PDMAEMA	Poly(*N,N*-dimethylaminoethyl methacrylate)
PEG	Polyethylene glycol
PEO	Polyethylene oxide
RAFT	Reversible addition-fragmentation chain transfer
RDRP	Reversible-deactivation radical polymerization
SET-LRP	Single electron transfer-living radical polymerization
TEA	Triethyl amine
TEMPO	2,2,6,6-tetramethylpiperidinyl-1-oxy
TGA	Thermogravimetric analysis
THF	Tetrahydrofuran
UV	Ultraviolet

Chapter 1

Introduction and Objectives

1.1 Introduction

Water is the single most important resource that decides the fate of all living beings. The ever increasing population, coupled with depleting water resources makes a strong case for purifying and recycling both industrial and domestic wastewaters. The treatment of these wastewaters and their reuse are of profound importance, as untreated wastewater not only constitutes a wastage of an important resource, but they also pollute other water bodies whenever they are discharged, thus creating further problems for the already overstressed water resources [1].

Water pollution, as a result of toxic metals and organic compounds, poses a serious environmental problem. Many of the contaminants found in industrial and municipal wastewaters are known to be toxic or carcinogenic [2]. In addition to this, heavy metals found in wastewaters are not biodegradable and accumulate in living organisms causing various diseases and disorders [3]. Most solids in water systems are usually present in the form of suspended particles, colloids, dissolved solids and molecules. These materials need to be removed from potable water supplies because they supply surfaces onto which microbes can adsorb and be protected from disinfection chemicals [4]. Strict legislation on the discharge of these toxic contaminants makes it necessary to develop various technologies for the removal of pollutants from wastewaters. The search, therefore, for cost-effective and economical methods of removing toxic heavy metal ions as well as suspended solids has become the focus of many studies.

Various technologies have been proposed and utilized for the purification of wastewaters. These include: biological treatment [5], membrane processes [6], advanced oxidation processes [7], adsorption processes [8], and coagulation/flocculation [9]. Each of the processes above has certain advantages and disadvantages but coagulation/flocculation remains one of the most popular methods for the primary treatment of wastewater. This is because of its high efficiency, easy handling, and the availability of various kinds of flocculants.

Flocculation is a process of removing organic and inorganic colloidal contaminants from wastewater and involves the aggregation of dispersed particles into larger flocs that can be separated from the water [10]. Flocculation is caused by the addition of minute quantities of chemicals known as flocculants. Both inorganic and organic flocculants are used. Among the

inorganic flocculants, the salts of multivalent metals, such as aluminium and iron, are mostly used. Inorganic flocculants are currently widely used by municipalities for the treatment of domestic wastewaters. These inorganic flocculants have some important disadvantages which include the large amounts required (in parts per thousand range), being pH sensitive, temperature sensitive and producing large amounts of sludge (which will then need to be further treated) [11]. The organic flocculants are essentially polymeric in nature. Polymeric flocculants are preferred because of their low dosage requirements, easy handling, inertness to pH changes, production of large cohesive flocs and versatile tailorability [12].

Organic flocculants may be natural or synthetic. Natural polymers have the advantage of being low cost, non-toxic, and biodegradable. The biodegradability of the natural polymers may however be a drawback in that it reduces the storage-life of the polymer as well as its efficiency due to the lowering of its molecular weight. Synthetic polymers, on the other hand, are highly efficient and can be tailored to the needs of a particular application [13]. Their main drawback, however, is that they are not shear resistant. This is a very important consideration when flocculants are used directly in water pipes or physically mixed with wastewaters and so subjected to shear forces. One could conceivably obtain the best properties of both the natural and synthetic polymers by copolymerizing the synthetic polymer on the natural polymer backbone. This, it is proposed, will yield a polymer that has reduced biodegradability because of the drastic change in the original structure of the natural polymer and reasonably shear stable because of the attachment of the flexible synthetic polymers on the rigid natural polymer backbone. One of the main problems associated with graft copolymers, however, is the lack of commercial methods for their large scale synthesis.

A number of grafting methods have been developed which may be classified into three groups: (i) free radical, (2) ionic, and (3) condensation and ring opening polymerizations. The free radical methods have received the greatest amount of attention due to their practicality [14]. Free radicals are formed on the natural polymer backbone either by chemical means or radiation. With chemical free-radical grafting, free radicals are generated *in situ* by radical/redox initiators. The chemical free-radical grafting of natural polymers has received considerable attention in recent years and has proven to be a useful method for the industrial production of modified polysaccharides.

Other than by the use of chemical free-radical initiators, free radicals are generated through γ-rays [15], UV radiations [16], electron beam [17] and microwave irradiation [18]. Among these methods of synthesis, microwave irradiation exhibits the most potential for synthesizing the grafted polymers, because as the free radicals are generated by means of microwave

photons, the chain opening of polysaccharide backbones does not take place hence rigidity of the backbone is maintained [19]. Further, with this method, the percentage grafting depends on monomer concentration, power and exposure time of the irradiation. These factors can be precisely controlled, leading to high reproducibility of percentage grafting and high batch-to-batch consistency. Another advantage of microwave heating is the almost instantaneous homogeneous heating of material in a selective manner. Microwave based grafting is of two types. The method employs microwave in presence of a free radical initiator (microwave assisted grafting) and use of microwave radiation in absence of any free radical initiator (microwave initiated grafting) [20].

In this research it is proposed to synthesize cellulose-based graft copolymer flocculants for the treatment of wastewater using both microwave-assisted and microwave-initiated polymerization and comparing this method with the conventional free radical technique. Cellulose is inexpensive and abundantly available from plant, forest and microbial resources. Cellulose will be copolymerized with polyacrylamide (PAM) – as extensively used flocculant for wastewater treatment.

In addition to graft copolymers, ABA type triblock copolymer flocculants will be investigated. The triblock copolymers will consist of poly(ethylene glycol) as the central block, and two different outer blocks will be investigated for adhesion to contaminants. The first outer block will be polyacrylamide (PAM). PAM is a pH insensitive, but very polar material that is expected to interact with colloidal particles as well as heavy metal ions. The second outer block will be poly(*N,N*-dimethylaminoethyl methacrylate) (PDMAEMA). PDMAEMA contains a tertiary amine as its active/polar group. It is known to interact strongly with anionic colloidal particles and it also strongly interacts with heavy metals.

1.2 Objectives

The main aim of this study is to synthesize graft and block copolymeric flocculants and compare their flocculating ability with commercially available flocculants. For graft copolymeric flocculants, this research is aimed at developing and applying both a chemical free-radical initiator as well as a microwave technique (both microwave-assisted and microwave-initiated) to synthesize biodegradable polymeric flocculants for the flocculation of a simulated wastewater system. For block copolymeric flocculants, the proposed research is aimed at synthesizing and testing two ABA type triblock polymeric flocculants to flocculate suspended solids in a wastewater system. The central block will be poly(ethylene glycol) and this will be

copolymerized with polyacrylamide (PAM) and poly(N,N-dimethylaminoethyl methacrylate) (PDMAEMA).

In line with the above aim, the objectives are:

1) For synthesis and testing of graft copolymers using chemical free-radical generation method:
   - Carry out graft copolymerization of acrylamide on cellulose and use response surface methodology to optimize the synthesis with percentage grafting as the output variable.
   - Compare the flocculation efficiency of the grafted copolymers with commercially available flocculants.

2) For synthesis and testing of graft copolymers using microwave free-radical generation method:
   - Design and construct a microwave reactor to conduct the polymerization reactions.
   - Carry out graft copolymerization of a functional group (acrylamide) on cellulose backbone using both microwave-assisted and microwave-initiated irradiation technique.
   - Compare the flocculation efficiency of the grafted copolymers with commercially available flocculants.

3) For synthesis and testing of block copolymers:
   - Synthesize ABA type triblock copolymerization with PEG as the central block and PAM as the two outer blocks.
   - Synthesize ABA type triblock copolymerization with PEG as the central block and PPDMAEMA as the two outer blocks.
   - Compare the flocculation efficiency of the grafted block copolymers with commercially available flocculants.

1.3 Layout of the thesis

The thesis can be divided into two parts. The first part entails the synthesis of graft copolymer flocculants using a natural polymer (cellulose) onto which is grafted a synthetic polymer (acrylamide). The second part entails the synthesis and testing of block copolymer flocculants using only synthetic polymers. The thesis is composed of six chapters. Three chapters describe the experimental work done on the grafting of cellulose with polyacrylamide using

the conventional chemical free-radical method, microwave techniques and the synthesis of block copolymers.

Chapter 1: Introduction and objectives

Chapter 2: Theoretical background

Chapter 2 discusses the theory behind flocculation. In this chapter theory common to the various systems (both the graft and block copolymers) are also discussed. In the chapters that follow, dedicated overviews of the relevant literature and theory precede the presentation of research results on the specific topic.

Chapter 3: Grafting of acrylamide onto cellulose using a chemical free-radical technique

This chapter describes the synthesis of the Cell-*g*-PAM graft copolymer using the conventional chemical free-radical method. The synthesized graft copolymer is then tested against commercially available flocculants for the flocculation of a simulated wastewater system. In order to compare the grafting performance of the grafted copolymer flocculant against the commercial flocculants the synthesis of the grafted copolymer is optimized using an experimental design technique (in conjunction with response surface methodology).

Chapter 4: Grafting of acrylamide onto cellulose using microwave techniques

This chapter describes the synthesis of the Cell-*g*-PAM graft copolymer using microwave techniques. The synthesis of the graft copolymer is done using both a microwave-assisted and microwave-initiated technique. The synthesis of the graft copolymers is optimized using response surface methodology with percentage grafting being the output variable. The optimized graft copolymer is then tested against commercially available flocculants for the flocculation of a simulated wastewater system.

Chapter 5: Linear block polymers as flocculants for wastewater treatment

This chapter describes the synthesis and testing of two block copolymers for the flocculation of a synthesized wastewater system. The first block copolymer consists of a poly(ethylene glycol) (PEG) central block with two outer blocks being polyacrylamide (PAM). In the second

copolymer the central block is again PEG but here the outer blocks are changed to poly(2-dimethylaminoethyl methacrylate) (PDMAEMA).

Chapter 6: Conclusions and recommendations for future work.

1.4 References

[1] R. L. Droste, Theory and Practice of Water and Wastewater Treatment, John Wiley & Sons, Inc., New York, 1997.

[2] D. H. Hutson and T. R. Roberts, Environmental Fate of Pesticides, Vol. 7, John Wiley & Sons, New York, 1990.

[3] Bolto, B., Gregory, J., 2007. Water Res. 41, 2301–2324.

[4] Brostow, W., Lobland, H.E.H., Sagar Pal Singh, R.P., J. Mater. Educ., 2009, 31, 157–166.

[5] L. B. Franklin, Wastewater Engineering: Treatment. Disposal and Reuse, McGraw Hill, Inc., New York, 1991.

[6] C. Bellona, J. E. Drewes, P. Xu and G. Amy, Water Res., 2004, 38, 2795–2809.

[7] T. A. Ternes, J. Stüber, N. Herrmann, D. McDowell, A. Ried, M. Kampmann and B. Teiser, Water Res., 2003, 37, 1976–1982.

[8] V. K. Gupta, R. Jain and S. Varshney, J. Hazard. Mater, 2007, 142, 443–448.

[9] Bratby J., Coagulation and Flocculation in Water and wastewater Treatment. IWA Publishing, London, 2006.

[10] N. P. Cheremisinoff, Handbook of Water and Wastewater Treatment Technologies, Butterworth-Heinemann, Boston, 2002.

[11] T. Clark and T. Stephenson, Environ. Technol., 1998, 19, 579–590.

[12] Latifossglu, A. A., Surucu, G and Evirgen, M., Water Pollution, IV: Model. Meas., Predict, 4th Int. Conf., 1997, 733–742.

[13] Dabrowski, A., Hubicki, Z., Podkoscielny, P and E. Robens, Chemosphere, 2004, 56, 91–106.

[14] Singh, R.P., S. Pal, S. Krishnamoorthy, P. Adhikary, S. Ali, Pure Applied Chemistry, 81, 2009, 525–547.

[15] Sen, G., R. Kumar, S. Ghosh, S. Pal, Carbohydrate Polymers, 2009, 77, 822–831.

[16] Bertolini AC, Mestres C, Colonna P, Raffi J. Carbohydrate Polymers, 2001, 44:269–71.

[17] Vahdat A, Bahrami H, Ansari N, Ziaie F. Radiation Physical Chemistry, 2007, 76:787–93.

[18] Sen, G., R. Kumar, S. Ghosh, S. Pal, Carbohydrate Polymers, 2009, 77, 822–831.

[19] Singh, V., A. Tiwari, R. Sanghi, Journal of Applied Polymer Science, 2005, 98, 1652–1662.

[20] Sen, G., S. Pal, Int. J. Biol. Macromol., 2009, 45, 48–55.

Chapter 2: Literature

2.1 Flocculation

2.1.1 Introduction

Water pollution can be attributed to the discharge of untreated domestic waste, dumping of industrial effluent, and run-off from agricultural fields [1]. The impurities found in the water are, in general, colloidal in nature and negatively charged. Various technologies such as ion exchange, membrane filtration, precipitation, flotation, solvent extraction, adsorption, coagulation, flocculation, biological and electrolytic methods have been used to remove the colloidal particles from wastewater [2]. Among these methods, coagulation/flocculation has proven to be one of the most successful and widely used solid–liquid separation processes for the removal of suspended and dissolved solids, colloids and organic matter present in industrial wastewater [3].

Flocculation is a general term for the process of adding a floc-forming chemical reagent (flocculant) to the wastewater and whereby finely divided or dispersed particles (colloids) are aggregated together to form large particles of such a size as to cause their settling or it is the agglomeration of tiny particles to form flocs which settle and cause clarification of the system [3-5]. The term, flocculation, is very often used synonymously with coagulation. There is, however, a subtle difference between the two [6]. Depending on the basis of classification, the two terms may be distinguished as follows. If the type of chemical agents added to induce aggregate formation is the basis of classification, then the process is called coagulation when inorganic materials are used and flocculation in the case when polymeric materials are used. If the mechanism of destabilisation is the basis of classification, then coagulation is electrostatic in nature, brought about by a reduction of the repulsive potential between the colloidal particles. The aggregates formed are compact or dense and there is not much loose space between the constituent particles. Flocculation, on the other hand, primarily involves the adsorption of high molecular weight polymeric molecules simultaneously to the surface of a number of colloidal particles, thus forming large but loose and open agglomerates called flocs.

In the following discussion no such distinction has been made and the two terms, coagulation and flocculation, have been used synonymously.

2.1.2 Impurities and Colloids in Water

Impurities present in water can be in the form of dissolved and colloidal natural organic matter (NOM), as dissolved salts, and as suspended material [7].

The organic material is generally associated with a complex high molecular weight fraction referred to as humic acid and a lower molecular weight less complex fraction, fulvic acid, both of which are products of decaying plant and animal matter [8]. These compounds pose problems of colour, taste, odour, and are a potential health hazard. Humic substances are troublesome materials with respect to flocculation because they have quite variable properties: acidity (pK_a: 3–5), molecular weight (MW) (several hundred to tens of thousands) and molecular structure (mostly phenolic and carboxylic acid functionalities, but also alcohol, quinone, ether, ester, and ketone groups) [9]. They behave as negatively charged colloids or anionic polyelectrolytes at pH levels of 6 to 8.

Most solids in water systems are usually present in the form of suspended particles, colloids, and molecules. These materials needs to be removed from potable water supplies because they supply surfaces onto which microbes can adsorb and be protected from disinfection chemicals [10]. Typical suspended solids levels are 2–200mg/L. These particles range in size from about 0.01 to 100 microns in size (see Figure 2.1).

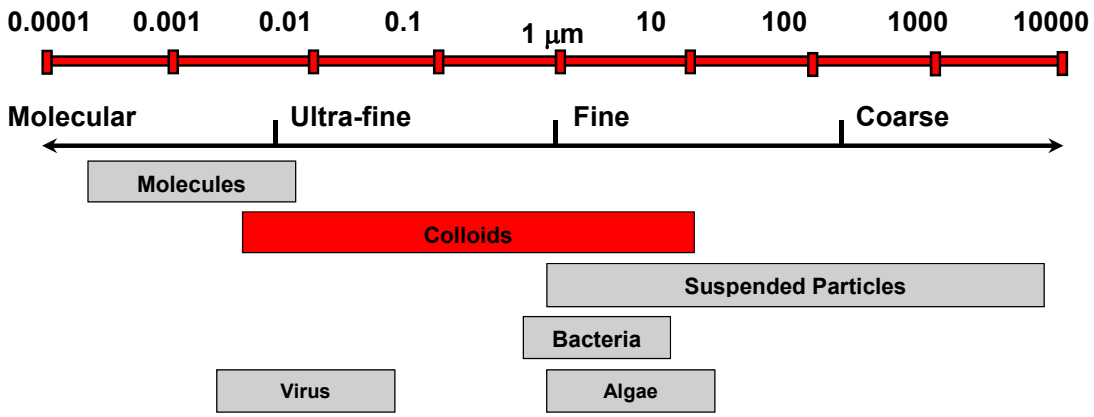

Figure 2.1: Size range of colloidal particles of concern in water treatment

Particles in the coarse to fine range are easily removed by settlement or filtration. Those in the molecular range cannot be removed by these physical processes, unless after precipitation. Colloids, which are very fine particles with diameters between 10 nm and 10 µm, are usually the main focus and the most challenging in water treatment processes [11]. These

particles have very high specific surface area to volume ratio and are therefore more sensitive to surface phenomena than to gravitational forces. Calculations using Stokes Law have shown that some of these particles in the middle of this size range, due to interparticle interactions, can take up to a decade to settle a mere 0.3 m, while the smallest particles will not settle at all due to Brownian motion [12]. The behaviour of colloids in water is strongly influenced by their electrokinetic charge. Each colloidal particle carries a like charge, which in nature is usually negative. These like charges cause adjacent particles to repel each other and prevents effective agglomeration and flocculation. As a result, charged colloids tend to remain discrete, dispersed, and in suspension – the colloid is said to be stable. Colloids can be classified as being either hydrophilic or hydrophobic. Hydrophilic colloids are readily dispersed in water and form colloidal solutions that are not easily destabilized. Their stability depends on their affinity for water molecules rather than the slight charge they possess. Hydrophobic colloids, including clay and non-hydrated metal oxides, have no affinity for water molecules, and owe their stability to the charge they possess [13].

2.1.3 Stability of Colloids

Since the key to effective flocculation is an understanding of how individual colloidal particles interact with each other, it is useful to understand the concept of colloidal stability. The stability and properties of colloidal systems have been studied for decades by a variety of individuals [14].

At the core of colloidal stability are two opposing forces: Van der Waals attractions and electrostatic repulsion [14]. Van der Waals forces arise from atomic and molecular level interactions due to induced and permanent dipoles in the system. They include Keesom interactions (permanent dipole-permanent dipole interactions), Debye interactions (permanent dipole-induced dipole interactions), and London interactions (induced dipole-induced dipole interactions) [15]. These forces are relatively weak and relatively long ranged. The electrostatic repulsive forces are generally Coulombic in origin, relatively strong, and relatively short ranged. In order for a colloidal system to become unstable, the attractive forces between the particles must be greater than the repulsive forces.

The stability of a colloidal particle depends on the surface properties, number, size, and density of solid particles of the dispersed phase and the density of the dispersion medium [16]. The principle mechanism controlling the stability of colloidal particulates is the electrostatic repulsion. The particles of the dispersed phase usually all carry negative electrical charges and hence repel each other. These negative charges are generated on the surface of solid

particles in three ways [17]. First is the differential loss of ions from the crystal lattice. As an example, consider a crystal of silver iodide placed in water. Silver ions dissolve preferentially, leaving a negatively charged surface. Second is from dissociation of inorganic groups (carboxylic or other organic acid groups) located on the particle surface. The magnitude of the surface charge depends on the acidic strengths of the surface groups and on the pH of the solution. The third method is the preferential adsorption of ions or ionisable species from the suspending medium. Besides electrical repulsion, a colloidal suspension may be stable due to the presence of adsorbed water molecules that provide a physical liquid barrier preventing particulates from making collisions and destabilisation.

The aggregation of colloidal particles can be considered to involve two separate and distinct steps [18]. Firstly there is particle transport to effect interparticle contact and this is then followed by particle destabilization to permit attachment when contact occurs. Because of the negative surface charge, ions of opposite charge in the solution will be attracted towards the surface. The counter ions (e.g. Ca^{2+} or Mg^{2+}) are present in surrounding water and accumulate on the surface of the suspended particles.

2.1.4 The Double Layer

The double layer model gives a visualization of the ionic environment in the vicinity of a charged colloidal particle and explains how electrical repulsive forces occur [19] (Figure 2.2). The colloidal particle, being negatively charged, attracts positive ions (counter ions) from the surrounding solution. The total potential at the surface of a primary charged particle is called the Nernst potential [20]. These counter ions form a firmly attached monolayer around the colloidal particle which is called the Stern layer. This monolayer of counter ions is, however, generally slightly less than the amount of counter ions required to achieve complete neutralization of the surface charge of the colloid particle. Additional counter ions are therefore still attracted to the negatively charged colloidal particle but they are now simultaneously repelled by the positive Stern layer. In the solution surrounding the Stern layer, the distribution of counter ions is determined by the movement of counter ions towards the colloid surface to satisfy electroneutrality and this tendency to accumulation is simultaneously opposed by the tendency of the counter ions to diffuse away from the colloidal surface in the direction of decreasing concentration, in accordance with Fick's Law. A dynamic equilibrium results from the two opposite forces, electrostatic attraction and ionic diffusion, and this produces a diffuse cloud of ions surrounding the Stern layer. This diffuse cloud can extend up to about 300 nm into the solution forming the Gouy-Chapman layer. Within the diffuse layer there is a notional boundary (typically another layer of ions) which are not so tightly attached to the colloidal

particle as the Stern layer, but which is nonetheless bound to the particle even as the particle moves [21]. This delimits the shear plane - those ions beyond this boundary stay with the bulk dispersant.

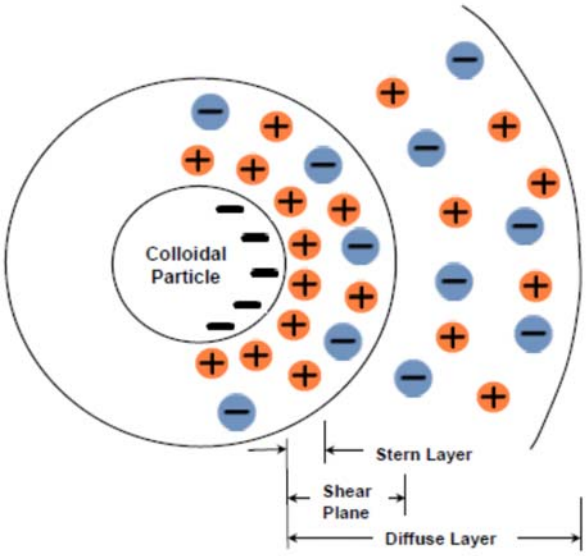

Figure 2.2: A conceptual representation of the electrical double layer [21]

In a similar but opposite fashion, there is a lack of negative ions in the neighbourhood of the colloidal particle, because they are repelled by the negative colloidal surface. These negative ions are called co-ions because they have the same charge as the colloid surface. Their concentration gradually increases with distance from the colloid surface as the repulsive forces of the colloid are screened out by the positive ions, until equilibrium is again reached with the co-ion concentration in solution [22]. This co-existence of original charged surface and the neutralizing excess of counter-ions over co-ions distributed in a diffuse manner in the nearby liquid is known as the electrical double layer [23].

The width of the inner layer, known as Stern Layer is approximately 5 nm deep, corresponding in size to the hydrated cation or nonhydrated anion. The width of the electrical double layer is characterized by the thickness of the diffuse layer or Debye screening thickness which is represented by κ^{-1} (Equation 2.1).

$$\kappa = \left(\frac{2000F^2}{\varepsilon DRT} \right)^{1/2} \sqrt{I} \qquad (2.1)$$

where F (96486.7 C·mol^{-1}) is Faradays constant, T(K) is the temperature, and R(J·mol^{-1}) is the gas constant and I is the ionic strength (M) given by Equation 2.2.

$$I = \frac{1}{2}\sum Z_i^2 C_i^2 \qquad (2.2)$$

where Z_i is the valence of the ion and C_i the concentration.

As shown by Equation 2.1, the double layer thickness is influenced by the valency and concentration of added electrolyte and upon interaction of the ions with the colloid particles. The ionic strength is inversely proportional to κ^{-1}. Therefore, as the ionic strength increases the double layer thickness should decrease, resulting in more agglomeration [23].

The nature of the electrical double layer formed can greatly influence the interaction between charged particles. At low ionic strength, the diffuse layer of counter ions around the colloidal particles extends to a considerable distance. Colloidal particles approaching each other begin to experience repulsion when their diffuse layers overlap and so repulsion can occur at quite large separations. By contrast, at higher electrolyte concentrations, the diffuse layer is less extensive and particles can approach quite closely before repulsion is felt. This has direct implications for the choice and use of coagulants and flocculants, as will be discussed later.

The negatively charged colloidal particle and its positively charged surrounding produce an electrical potential across the diffuse layer. This is highest at the surface and drops off progressively with distance from the surface, approaching zero at the outside of the diffuse layer. The potential curve is useful because it indicates the strength of the repulsive force between colloidal particles and the distance at which these forces come into play.

Figure 2.3 provides a schematic overview of a colloidal particle. The electric potential at the surface of the colloidal particle is called Nernst potential and is denoted by Ψ_o. The electric potential at the Stern plane, located at about a hydrated ion radius from the surface is called the Stern potential, denoted by Ψ_δ. The potential at surface of hydrodynamic shear (shear plane) is the zeta potential, denoted by ζ.

The charge presented to the solution at the Stern layer attracts a diffuse layer of free ions with a net different opposite charge, i.e., the Gouy-Chapman layer [24]. For two colloidal particles to make contact and aggregate, the potential at the Stern layer must be overcome. Unfortunately, this potential, which is of interest in determining particle stability, cannot be measured directly or experimentally. This potential can, however, be closely approximated by the experimentally-accessible Zeta potential. The Zeta potential can be obtained from a number of electrokinetic techniques, in which there is relative motion between particle and solution and a corresponding separation of charge [25]. The most useful technique is

electrophoresis, in which particles migrate under the influence of an applied electrical field. The electrophoretic mobility (velocity/field strength) is measured, from which the zeta potential can be derived.

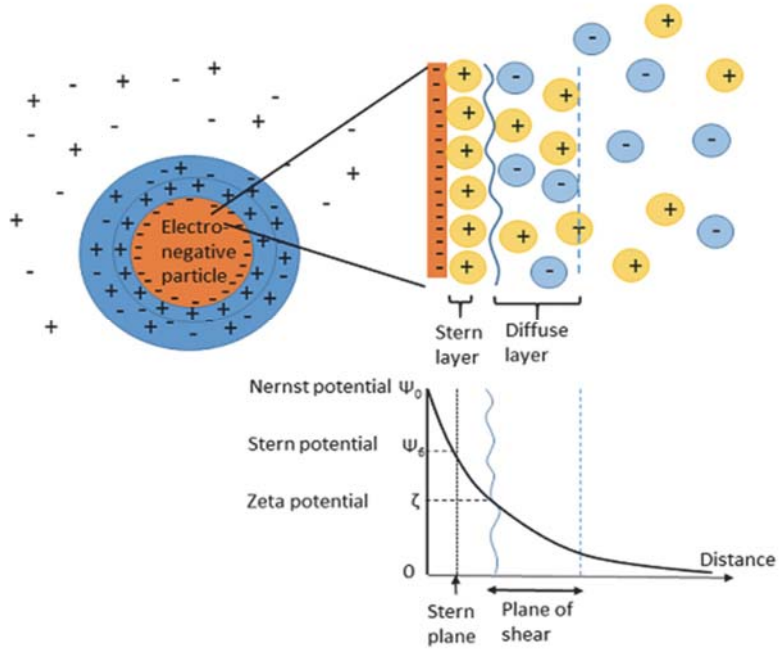

Figure 2.3: Electric double layer potential drop [26]

The magnitude of the zeta potential gives an indication of the potential stability of the colloidal system. If all the particles in suspension have a large negative or positive Zeta potential then they will tend to repel each other and there will be no tendency for the particles to come together. However, if the particles have low Zeta potential values then there will be no force to prevent the particles coming together and flocculating. The general dividing line between stable and unstable suspensions is generally taken at either +30 or -30 mV. Particles with Zeta potentials more positive than +30 mV or more negative than -30 mV will not agglomerate and are considered stable [26].

2.1.5 Colloidal Stability and DVLO Theory

The DVLO theory (named after scientists Derjaguin, Verwey, Landau and Overbeek) gives an explanation of the stability of colloidal systems [27]. This theory suggests that the stability of a colloidal particle in solution is dependent upon its total potential energy, V_T. According to this theory, V_T is the balance of several competing contributions and is given by Equation 2.3.

$$V_T = V_A + V_R + V_S \tag{2.3}$$

V_S is the potential energy due to the solvent and makes only a marginal contribution to the total potential energy over the last few nanometres of separation. Much more important is the balance between V_A and V_R, the attractive and repulsive contributions. Their potentials are much larger and operate over a much larger distance.

V_A is the London-van der Waal's attraction energy between molecules and operates over a very short distance. It is assumed to vary inversely with the sixth power of the inter-molecular distance. In a colloidal system, these forces are approximately additive and the attractive energy between the two particles can be computed by summing the attractions between all pairs of molecules within the particles. For the case of two identical spheres, the London-van der Waal energy of attraction is approximated by Equation 2.4.

$$V_A = -\frac{A\,a}{12\,H} \tag{2.4}$$

where *a* is the radius of spheres (m), H is the shortest distance between spheres (m), and A is the Hamaker constant (J). Van der Waals attractive forces predominate at short particle separations and are weak at large particle separations.

The general expression for the repulsive energy V_R as developed by Verwey and Overbeek is given by Equation 2.5.

$$V_R = 4.62 \times 10^{-6} \left(\frac{a}{\upsilon^2}\right) \gamma \exp(-kH) \tag{2.5}$$

where

a = radius of spheres (m)

υ = valence of counter ions

k T = Boltzmann constant times absolute temperature

$$\gamma = \frac{(\exp(z/2)-1)}{(\exp(z/2)+1)}; \qquad z = \frac{\upsilon \exp\Psi}{k\,T}$$

V_R becomes significant when two colloidal particles approach each other and their double layers begin to overlap and interfere with each other. Energy is required to overcome this repulsion.

An electrostatic repulsion curve is used to indicate the energy that must be overcome if the particles are to be forced together. It has a maximum value when they are almost touching and decreases to zero outside the double layer. The net interaction curve, formed by adding

the attraction curve from the repulsion curve, explains the tendency of colloidal particles to either remain discrete or to flocculate, as shown in Figure 2.4.

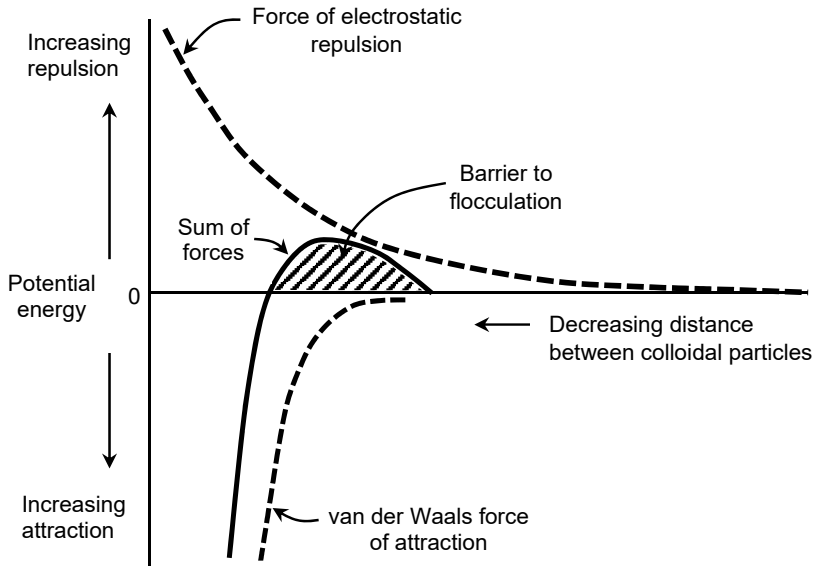

Figure 2.4: Schematic diagram of the variation of potential energy with particle separation according to DVLO theory [27]

The DVLO theory suggests that the stability of a colloidal system is determined by the sum of the van der Waals attractive (V_A) forces and the electrical double layer repulsive (V_R) forces that exist between particles as they approach each other due to the Brownian motion [27]. This theory proposes that an energy barrier resulting from the slightly stronger repulsive forces prevent two colloidal particles from approaching each other and coalescing. However, if the colliding particles have sufficient velocity and the kinetic energy of the approaching particles is large enough to surmount this potential barrier then the particles will come into contact with each other. In that case van der Waals forces of attraction will dominate and the particles will adhere strongly and irreversibly together.

Therefore if the particles have a sufficiently high repulsion, the dispersion will resist flocculation and the colloidal system will be stable. If, however the repulsion mechanism is reduced, then flocculation or coagulation will eventually take place.

2.1.6 Flocculation Mechanism

According to literature, flocculation can occur by a number of mechanisms [28]. These various mechanisms can, however, be grouped into three generally accepted destabilization mechanisms:

- Surface charge neutralisation
- Double layer compression
- Inter-particle bridging

2.1.6.1 Surface Charge Neutralization Mechanism

Charge neutralisation is postulated as the major mechanism for the case where the flocculant and the colloidal particles are oppositely charged [28]. Colloidal particles in wastewater are generally negatively charged and thus cationic poly-electrolytes and inorganic metal salts can be used as flocculating agents. Charge neutralisation involves adsorption of the positively charged coagulant/flocculant on the surface of the colloidal particles. The positively charged flocculant neutralises the negative charge of the colloid and results in a near zero net charge [28]. Flocculation then occurs as a result of the reduced surface charge of the colloidal particles (reduction of zeta potential) and hence a decreased electrical repulsion force between colloidal particles. This allows van der Waals force of attraction to become the dominant force and encourage aggregation of colloidal and fine suspended materials as shown in Figure 2.5.

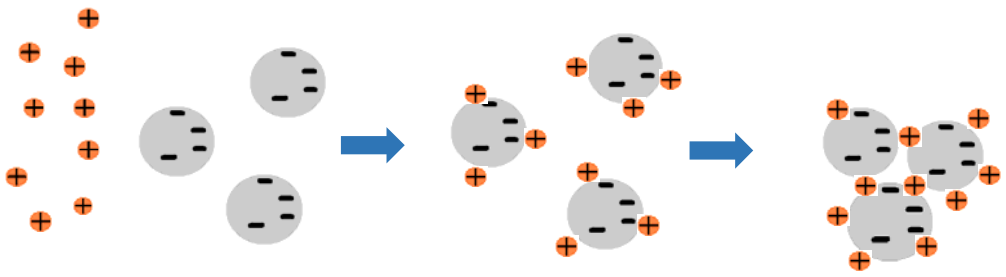

Figure 2.5: Schematic view of a charge neutralisation flocculation mechanism

When using these flocculants, charge neutralization needs to be monitored and controlled using zeta potential because if too much flocculant is used, a charge reversal can occur and the particles will again become dispersed, but with a positive charge rather than with a negative charge [29].

As mentioned above, metal salts can also be used in this mechanism. In this case, when high concentrations of metal salts are introduced into the stabilized colloidal dispersion, the added counter-ions penetrate into the diffuse double layer and compress the double layer. This reduces the long-range repulsion between colloids enabling the aggregation by van der Waals forces. This effect is stronger the higher the charge of the counter-ions in accordance with the Schulze-Hardy rule that indicates the relative effectiveness for coagulation by mono- vs. di- vs. trivalent ions to be in the ratio of 1:100:1000 respectively) [30]. For example, the relative power of Al^{3+}, Mg^{2+}, and Na^{+} for the coagulation of negative colloids is shown to vary in the ratio of 1000:30:1.

2.1.6.2 Bridging Mechanism

Bridging mechanism occurs when long chain flocculant polymers with high molecular weight (up to several million) and low charge density are adsorbed on colloidal particles in such a way that long loops and tails extends some way into the solution far beyond the electrical double layer [31] as shown in Figure 2.6.

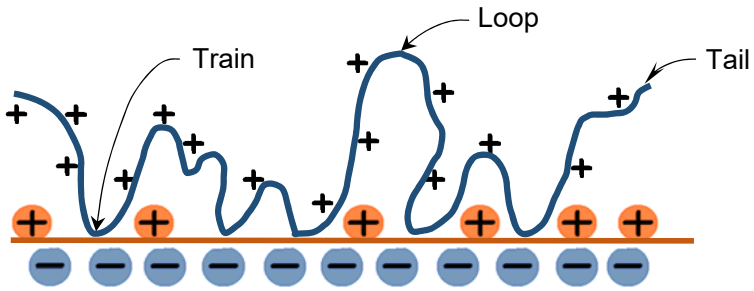

Figure 2.6: Configuration of an adsorbed polymer chain [31]

The extent of the tails and loops depends greatly on the interaction of polymer segments with the solvent (water) and with the particle surface. Generally, if the interactions with the colloidal particle surface are fairly weak, segments of the adsorbed chain extend further into the solution. These dangling loops and tails creates the possibility for interaction and attachment of these polymer segments to other colloidal particles, thus creating ‘bridges’ between particles, as shown in Figure 2.7. The essential requirements for polymer bridging are that there should be sufficient unoccupied particle surface for attachment of polymer segments from chains attached to other particles and that the polymer bridges should be of such an extent that they span beyond the distance over which interparticle repulsion prevails [32]. There should also not be an excessive amount of flocculating polymer (adsorbed amount should not be too high), otherwise the colloidal particle surfaces will be overly coated with the

polymer and no sites would be available to 'bridge' with other particles. Under these conditions the colloidal particles would be stabilised [33], as shown in Figure 2.7.

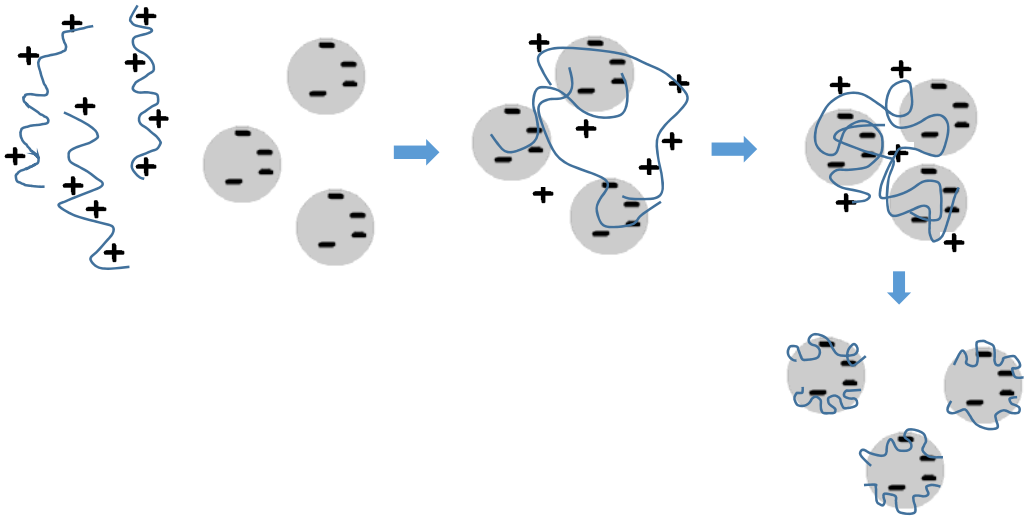

Figure 2.7: Influence of polymer on particle adsorption and interactions leading to flocculation or dispersion [33]

Polymer bridging gives much larger and stronger aggregates (flocs) than those formed from other mechanisms [34]. In addition, bridging contacts are more resistant to breakage at elevated shear levels.

It is generally found that the most effective polymers for bridging are linear chains of high MW (up to several million). Polymers such as polyacrylamide (PAM) and polyethylene oxide (PEO) can adsorb on surfaces with suitable H-bonding sites using the bridging mechanism [35]. Colloidal particles such as silica have surface hydroxyl groups which can form H-bonds with amide groups of PAM or the ether oxygens of PEO.

Cationic, anionic or non-ionic polymeric flocculants can also change the Zeta potential of the colloid surfaces. Although it is expected that the presence of polymeric flocculants (especially non-ionic polymers) will induce no effect on surface charge density and charge distribution in diffuse layer, the opposite is in fact experienced [36]. This can be explained by the displacement of the shear plane which occurs compared to its position in the absence of adsorbed polymer [37], as shown in Figure 2.8.

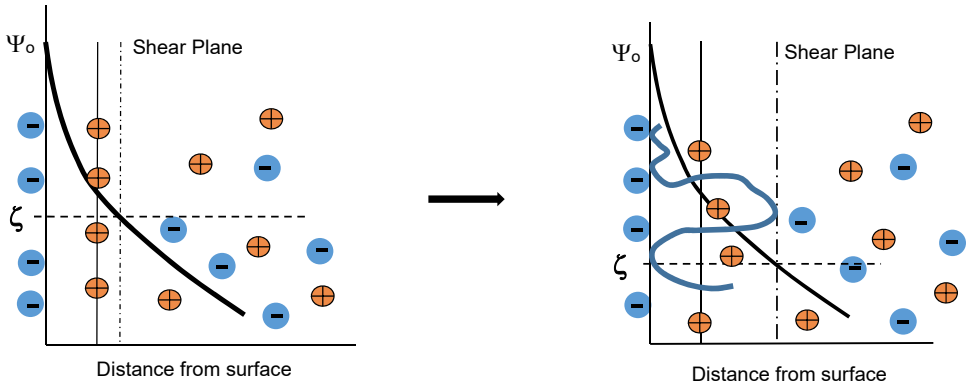

Figure 2.8: Zeta potential change before and after polymer adsorbed on the surface [37]

The displacement of the shear plane depends on the distance of the extension of the loops of the polymers [37]. Due to the inverse relationship between zeta potential and thickness of double layer, the zeta potential value decreases and enables aggregation.

2.1.6.3 Electrostatic patch mechanism

The electrostatic patch mechanism takes place when using flocculant polymers of low molecular weight (LMW = 20 000 to 100 000) and high cationic charge with colloidal particles having fairly low density of charged sites. When these LMW cationic polymers comes into contact with weakly charged anionic colloidal particles, their chains becomes entirely adsorbed onto part of the surface of the colloidal particles thus forming regions of a cationic nature. Under these conditions, the charged polymer is visualized to be much smaller than the surface area of the colloidal particle and forms “islands” or “patches” of cationic charge, surrounded by areas of opposite charge [38]. Also, the high interaction energy favours a flattened adsorbed configuration of the flocculant polymer with significantly reduced loops and trains, and reduced bridging capabilities, as shown in Figure 2.9.

The adsorption of oppositely charged polymer flocculants by the colloidal particle reduces its surface potential and the protection of the particles. Having become true dipoles, these particles are attracted to each other, and collide with each other - there is an electrostatic attraction between positive patches on one colloidal surface and negative areas on other colloidal particles. The van der Waals forces then come into play, binding the two particles and destabilizing the suspension.

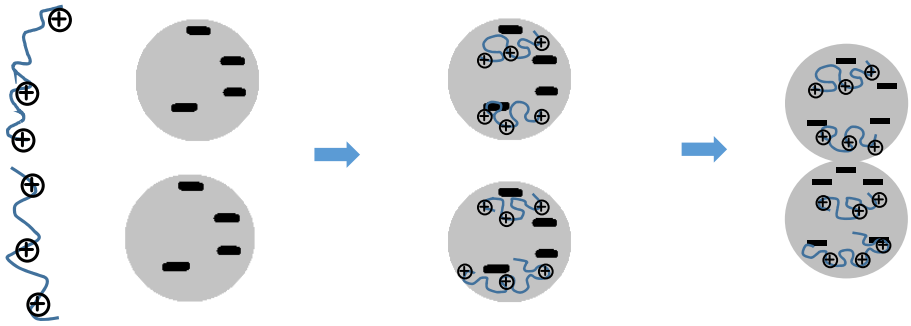

Figure 2.9: Electrostatic patch model for flocculation of negatively charged particles by cationic flocculants [38]

Flocs produced via this mechanism are not as strong as those formed by bridging, but stronger than flocs formed by simple charge neutralisation [39]. Re-flocculation after floc breakage, however, occurs more readily in the case of electrostatic patch than in bridging.

The type of mechanism varies according to the type of flocculants and are summarized in Table 2.1.

Table 2.1: Flocculation mechanisms for different types of flocculants [39]

Category of flocculant	Type of flocculant	Flocculation mechanism
Chemical coagulants	Inorganic metal salts	Charge neutralisation
Chemical flocculants	Polyelectrolytes with low MW and low CD	Charge neutralisation
	Polyelectrolytes with high MW and low CD	Bridging
	Polyelectrolytes with low MW and high CD	Electrostatic patch
	Polyelectrolytes with high MW and high CD	Electrostatic patch + Bridging
Bioflocculants	Cationic (chitosan)	Charge neutralisation + Bridging
	Anionic (cellulose, tannin, sodium alginate)	Bridging
	Anionic/neutral plant based	Bridging
Grafted flocculants	Amphoteric/cationic/anionic graft copolymers	Charge neutralisation + Bridging/ bridging only

2.1.7 Flocculating Materials

The flocculants that are applied in wastewater treatment can generally be divided into three categories: chemical coagulants/flocculants, natural bio-flocculants and grafted flocculants (see Figure 2.10).

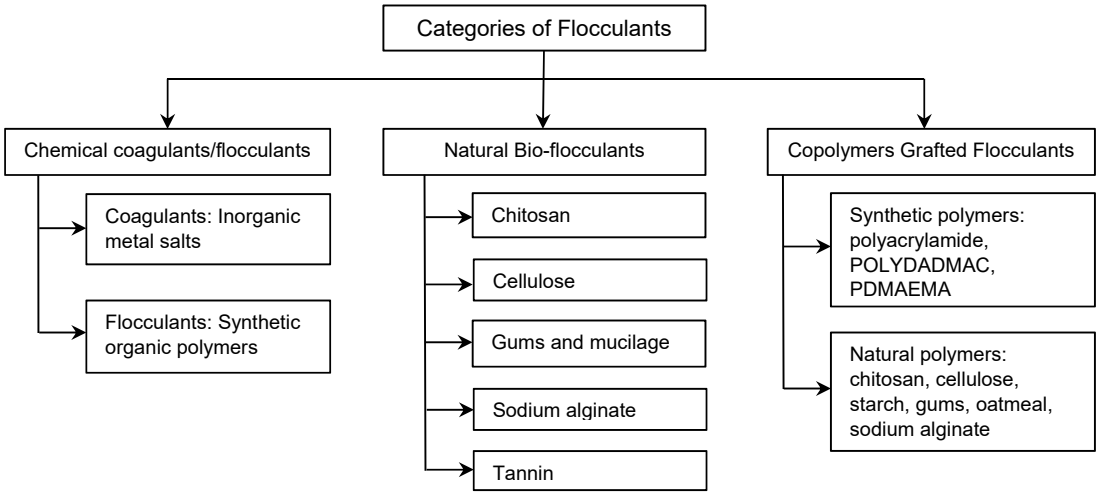

Figure 2.10: Classification of flocculants

2.1.7.1 Chemical coagulants/flocculants

Chemical coagulants/flocculants have been traditionally applied for decades as coagulants and are currently still widely used for industrial and domestic wastewater treatment [40]. They are derived from chemical/petroleum based materials and can be classified into two major groups: inorganic mineral additives/metal salts which are used as coagulants, and organic polymeric materials that are employed as coagulants and flocculants.

With regard to metal salts, the majority of coagulants applied in water treatment are multivalent metals (iron or aluminium) formed by reaction with acids (hydrochloric or sulphuric). These produce compounds such as alum, polyaluminium chloride, ferric chloride, ferrous sulphate, calcium chloride, and magnesium chloride. Metal salts cause sedimentation of impurities from the water using the neutralisation mechanism. Their main advantage is their low cost compared to other types of flocculants [41]. Their use is becoming limited due to several disadvantages. These include the large volumes of sludge produced (which may need further treatment before disposal), large amounts of coagulant required for efficient flocculation, high sensitivity to pH, inefficiency towards very fine particles, inefficiency in cold water (e.g. polyaluminium chloride) and applicability to only a few disperse systems [42].

Synthetic organic flocculants are mostly linear, water soluble polymers which are based on repeating units of various monomers such as acrylamide and acrylic acid. They are derived from oil-based and non-renewable raw materials [43]. These polymers are classified according to the charge, product form and molecular weight. The polymer may carry a negative, a

positive or no charge. They could exist as dry powders, aqueous solutions or as latexes. With respect to molecular weight, synthetic organic polymers can vary from low molecular weight (10^4 - 10^5 g mol^{-1}), to medium (10^5 - 10^6 g mol^{-1}), to high (10^6 - $5x10^6$ g mol^{-1}) and very high (> $5x10^6$ g mol^{-1}) [44]. Although there are over 1500 registered products on the market, they can be grouped into essentially 15 to 20 classes of chemicals. The most commonly used polymers registered for drinking water are shown in Table 2.2 [45].

Table 2.2: Polymers registered for use in drinking water treatment

Common Name	Abbreviation	Chemical Name
Polyacrylamide	PAM	2-Propenamide homopolymer $(C_3H_5NO)_n$
Acrylamide-acrylic acid co-polymer	PAM-PAA	2-Propenoic acid with 2-propenamide copolymer $(C_3H_5NO.C_3H_4O_2)_n$
Diallyldimethyl-ammonium chloride homopolymer	polyDADMAC	N,N-Dimethyl-N-2-propenyl-2-propen-1-aminium chloride homopolymer $(C_8H_{16}N.Cl)_n$
Epichlorhydrin-dimethylamine	EPI-DMA	N-Methyl methanamine with chloromethyl oxirane copolymer $(C_2H_7N.C_3H_5ClO)_n$
Epichlorhydrin-dimethylamine-ethylenediamine	EPI-DMA-EDA	1,2-Ethanediamine with N-methyl methanamine and chloromethyl oxirane copolymer $(C_2H_5N.C_3H_5ClO.C_2H_7N)_n$
Epichlorhydrin-monomethylamine	EPI-MMA	Methanamine with chloromethyl oxirane copolymer $(CH_5N.C_3H_5ClO)_n$
Epichlorhydrin-polyamine	EPI-PA	N,N-Dimethyl-1,3-propanediamine with chloromethyl oxirane copolymer $(C_5H_{14}N_2.C_3H_5ClO)_n$
Polyethyleneimine	PEI	Ethanimine homopolymer $(C_2H_5N)_n$
Polyethylene polyamine	PEPA	1,2-Dicloroethane with ammonia $(C_2H_4Cl_2.H_3N)_n$ or 1,2-Ethanediamine with 1,2-dichloroethane $(C_2H_8N_2.C_2H_4Cl)_n$
Melamine formaldehyde		1,3,5-Triazine-2,4,6-triamino polymer with formaldehyde $(C_3H_6N_6.CH_2O)_n$
Mannich reaction modified polyacrylamide	AMPAM	N,N-[Dimethyl(amino)methyl]-2-propenamide homopolymer $(C_6H_{12}N_2O)_n$
Dimethylaminoethyl methacrylate	Poly(DMAEMA)	N,N-Dimethylaminoethyl-2-methyl-2-propenoic acid homopolymer $(C_8H_{15}NO_2)_n$

Some of the advantages flowing from the use of polymers in water treatment are that they are convenient to use, immediately soluble in aqueous systems, and do not affect the pH of the medium. The synthetic polymers can be tailor-made by controlling the molecular weight, molecular weight distribution, chemical structure of polymers, nature and ratio of functional

groups on polymeric backbone to suit to a particular application [46]. They are also highly efficient with small doses (1–5 ppm) producing smaller volumes of sludge that are strong, dense, of regular shape, and which have good settling characteristics [47]. The use of these flocculants result in substantial cost savings of between 25–30%.

There are, however, a few disadvantages associated with the use of synthetic polymers. These include their market cost which is at least ten times higher compared to chemical coagulants, a greater sensitivity to incorrect dosage with turbidity and natural organics removal, health hazards and environmental consequences. Residual, unreacted monomers (such as acrylamide, ethyleneimine) and unreacted chemicals used to produce the monomer units (such as epichlorohydrin, formaldehyde and dimethylamine) are toxic to aquatic organisms and may have neurotoxic effects on humans [48].

2.1.7.2 Natural Bio-flocculants

Bio-flocculants are sourced from natural materials and have been extensively researched over the past few years. In recent years polysaccharides such as guar gum [49], starch [50], chitosan [51], cellulose [52] and their derivatives such as dextran [53] and pullulan [54] have attracted particularly attention as flocculation and adsorption aids.

Bio-flocculants destabilise the colloidal particles by increasing the ionic strength, giving some reduction in the zeta potential and thus a decreased thickness of the diffuse part of the electrical double layer. Alternatively, they could specifically adsorb counter-ions to neutralise the colloidal particle charge because they have particular macromolecular structures with a variety of functional groups (e.g. carboxyl and hydroxyl groups) which can interact with contaminants [55].

Natural organic flocculants which are based on polysaccharides or natural polymers are safe and biodegradable, fairly shear stable, easily available from reproducible agricultural resources and produce no secondary pollution [56]. In addition, as biopolymers are biodegradable, the sludge can be efficiently degraded by microorganisms [57]. Thus, they have high potential to be applied in water and wastewater treatment.

One of the biggest advantages of natural polymers is their biodegradability. This very advantage, however, becomes a drawback in reducing its storage life and reducing their efficiency as a result of molecular breakdown. Their efficiency is also low, and therefore requires high dosages that varies with the origin of natural polymers.

2.1.7.3 Grafted Flocculants

The continuous increase of market needs for efficient and effective flocculants in wastewater treatment has induced the development of improved flocculants. As a result of this, hybrid materials such as graft- and block-copolymer flocculants have emerged as new materials with tremendous potential in treating wastewater. These materials have unique properties and superior performance compared to original conventional polymeric flocculants [58].

Graft copolymers consists of polymeric backbones with covalently linked polymeric side chains. In principle, both backbone and side chains could be homopolymers or copolymers. Grafting can be carried out in such a way that the properties of the side chains can be added to those of the substrate polymer. The modification of natural bio-flocculants has been carried out with the aim of combining their best attributes with those of synthetic polymers and enhancing the aggregating power of the copolymer flocculants [59].

Graft copolymerization can be carried out one of the following three methods: (1) free radical polymerization, (2) ionic and ring-opening polymerization (ROP), and (3) controlled/living radical polymerization (CRP) [60].

There are many synthetic polymers that can be used to modify the properties of the backbone substrate. Only those polymers that are pertinent to the current research will be discussed in more detail.

2.1.7.3.1 Polyacrylamide (PAM)

There are hundreds of specific PAM formulations that vary in polymer chain length and number and kinds of functional group substitutions [61]. The molecular weights of PAM can vary and in extreme cases, the molecular weight of polyacrylamides can be up to 30 million. PAMs can be polymerized as either linear or cross-linked forms. However, in the field of water treatment linear PAMs are mainly used. Due to their characteristics of high solubility, viscosity and molecular weight, PAMs have been used as inter-particle bridging flocculants to agglomerate non-settleable colloidal particles [62]. Based on the functional groups along backbone chains, PAM derivatives can be classified into three types, non-ionic, anionic, and cationic PAM derivatives.

Non-ionic Polyacrylamides:

Polyacrylamide is a polymer ($–CH_2CHCONH_2–$) formed from acrylamide (Scheme 2.1)

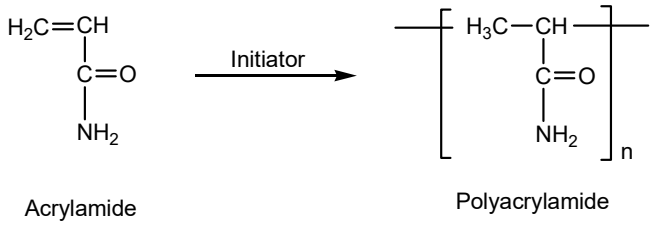

Scheme 2.1: Schematic representation of the synthesis of polyacrylamide

Polyacrylamide can be synthesised by free radical polymerisation from the acrylamide monomer using initiators such as azo compounds, redox catalysts, light and radiation. Polyacrylamides can also be prepared via solution inverse emulsion, inverse micro-emulsion or precipitation techniques [63].

Flocculation by non-ionic polyacrylamide is brought about by hydrogen bonding, as shown in Figure 2.11.

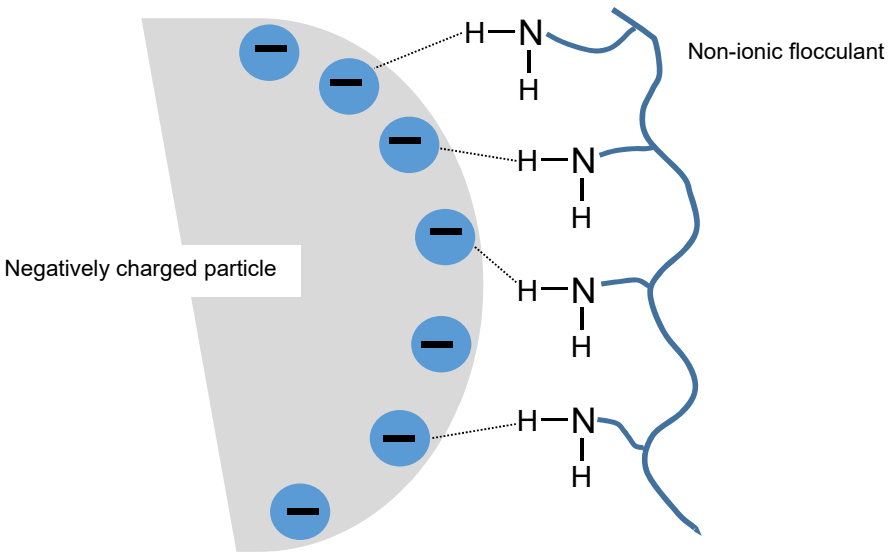

Figure 2.11: Diagrammatic representation of adsorption by hydrogen bonding

Polyacrylamides are not sensitive to pH and remain unchanged over a wide range of pH values. The polyacrylamides attach themselves on colloidal particle surfaces by forming

hydrogen bonds between the amide groups and the active sites of the particle surface. Whilst the individual hydrogen bond may be weak the overall adsorption is strong due to the relatively large numbers of bonds that can be formed. For hydrophilic colloidal particles, polyacrylamide also attaches to the surrounding water molecules by weak hydrogen bonding [64].

Anionic polyacrylamide derivatives

Anionic flocculants are obtained either by hydrolysis of the amide groups on a polyacrylamide chain or by copolymerization of the acrylamide with a suitable carboxylic or sulphonic acid salt. The most commonly used method is by use of acrylic acid [65], as shown in Scheme 2.2.

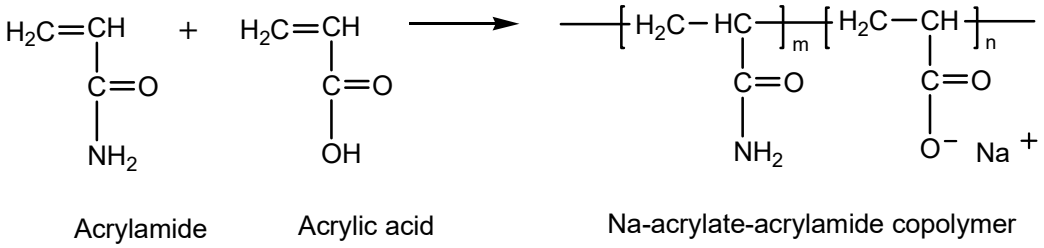

Scheme 2.2: Schematic representation of synthesis of anionic polyacrylamide derivative

The number of anionic groups along the copolymer chain, also called the charge density or frequency, is controlled by controlling the ratio of acrylamide and acrylic acid present during polymerization - the fraction of (acrylic) acid in these copolymers can vary between 0% and 100%. The properties of the anionic acrylamide-based copolymer is entirely different, chemically and biologically, compared to the acrylamide monomer. Whereas acrylamide is a reactive species due mainly to the double bond, polymerization eliminates the double bond and renders polyacrylamide relatively chemically inert [66]. The effects of this is that while the acrylamide monomer has neurotoxic, carcinogenic, and genotoxic effects on humans, the high molecular weight non-ionic polyacrylamide reduces its ability to be absorbed and, therefore, its toxicity to humans and animals. Anionic acrylamide-based copolymer flocculants can therefore be safely used as flocculants for the production of potable water.

The way in which the anionic acrylamide-based copolymer adsorbs onto the colloidal particle is key to its effectiveness as a flocculant. Anionic acrylamide-based copolymers, being negatively charged like the colloidal particle surface, would be expected to experience repulsion from the colloidal particle [67]. Adsorption and flocculation, however, occurs because of hydrogen bonding and van der Waals attractions on the particle surfaces which

are able to overcome any initial electrostatic repulsion [68]. Anionic acrylamide-based copolymers can also bind onto the negative sites of the colloidal particles through a process called cation bridging [68]. Divalent ions such as Ca^{2+} and Mg^{2+} are able to bridge two negatively charged particles together. Each positive charge of the divalent cation binds to one of the negative sites, one on the colloidal particle surface and the other on the anionic acrylamide-based copolymer, as shown in Figure 2.12. Hence the presence of divalent cations in the solution is essential for the use of anionic acrylamide-based copolymers [69].

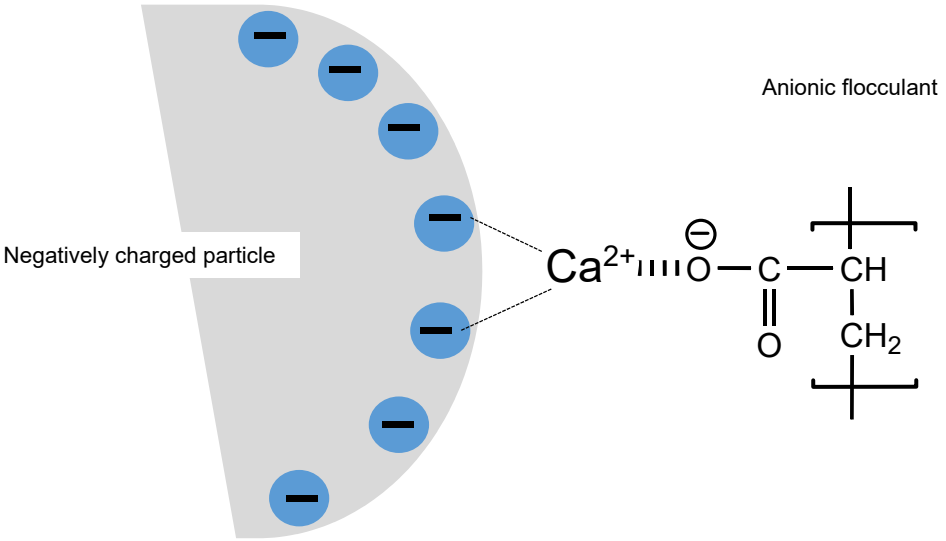

Figure 2.12: Diagrammatic representation of adsorption by salt linkage

Divalent cations present in the solution can increase the adsorption rate of colloidal particles by anionic flocculants by up to 30 times when compared to monovalent cations [69].

Cationic polyacrylamide derivatives

Cationic acrylamide-based copolymers usually contain quaternized amine functional groups, as shown in Figure 2.13.

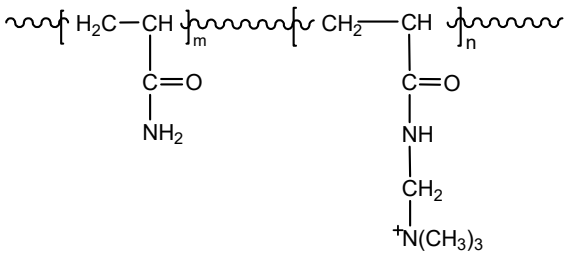

Figure 2.13: Schematic representation of a cationic acrylamide-based copolymer

Cationic acrylamide-based copolymers are produced by either copolymerization of polyacrylamide with another vinyl-type monomer containing a quaternized amine functional group or by direct modification of polyacrylamide to introduce quaternized amine functional groups [70]. Both the Hoffmann degradation reaction followed by methylation or the Mannich reaction followed by methylation have been used to introduce quaternized amine functional groups into polyacrylamide [71].

Since the particles of most colloidal suspensions are negatively charged, cationic acrylamide-based copolymers have found commercial application mainly as flocculants. Yu *et al*. [72] discovered that for a low molecular weight cationic polyacrylamide-based flocculant, charge neutralisation was the main flocculation mechanism, whilst for high molecular weight cationic acrylamide-based copolymers, bridging flocculation was predominant. McCarron *et al.* [73] found that flocculation of kaolin dispersions with high molecular weight cationic acrylamide-based copolymers at low concentrations had bridging flocculation as the predominant mechanism, but that at higher concentrations, charge neutralisation was predominant. Petzold *et al*. [74] determined that dual flocculation by the addition of a cationic acrylamide-based copolymer followed by an anionic polyacrylamide was most successful in terms of both settling rate and consolidation. A combination of charge patch and bridging flocculation was believed to be the mechanism of flocculation.

Cationic acrylamide-based copolymers are very sensitive to pH of environment whereas anionic and non-ionic acrylamide-based flocculants are less sensitive to pH (especially non-ionic flocculants which work successfully even at high pH values).

2.1.7.3.2 Polyethylene oxide (PEO)

Polyethylene oxide (PEO) is a water soluble, non-ionic, linear polymer with the following generalized formula:

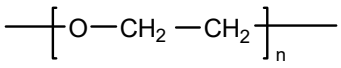

PEO polymers are commercially made by catalytic polymerization of ethylene oxide in the presence of one of several catalyst systems. They are available in a wide range of molecular weights from as low as 200 up to 5 x 10^6 g mol^{-1}. The polymers with molecular weights below about 100 000 g mol^{-1} are viscous liquids or waxy solids and are commonly referred to as polyethylene glycols (PEG). Those with molecular weights in the range from about 1 x 10^5 to

5×10^6 g mol^{-1} are called polyethylene oxides (PEO). They are dry, free flowing, white powders completely soluble in water and certain organic solvents.

The non-ionic character of PEO makes the polymer insensitive to anionic species in suspensions. Mpofu *et al*. [75] also found the polymer to be durable against mechanical mixing – this allows the production of strong and dense flocs under moderate to high shear rates. Adsorption behaviour of PEO on oxides was studied by several authors [76]. Polyethylene oxide has been successfully used as flocculant for clays and ultra-fine silica particles since 1980s [77]. These previous studies found the main mechanisms of PEO adsorption on mineral surfaces to be hydrogen bonding, electrostatic interaction, and cation bridge formation. It has been proposed that hydrogen bonding (or covalent bonding) takes place in the case of strong floc formation and electrostatic attraction (through cation bridge mechanism) in the case of weak floc formation [78].

With respect to hydrogen bonding, Rubio and Kitchener [79], concluded that isolated silanol groups on colloidal surfaces acted as the main adsorption sites for PEO. The interaction between PEO flocculant and the colloidal particle was believed to be through strong hydrogen bonding mechanism that included the ether oxygen of the PEO and surface hydroxyls of colloidal surfaces - ether oxygen of PEO which with two lone pair of electrons could be considered to be an electron donor, Lewis base.

PEOs are subjected to unavoidable hydrolysis during the production cycle and this results in the slightly anionic character. These slightly charged anionic flocculants can be attracted to the negatively charged colloidal surfaces through electrostatic interactions and result in a weak floc structure being formed. This mechanism depends only on the ineffectual electrostatic attractive force and hence is considered to be weaker than the hydrogen bonding mechanism.

Polyvalent cations such as Al^{3+}, Ca^{2+}, Fe^{3+}, Cd^{2+}, Cu^{+2}, *etc*. can also attach themselves on negatively charged colloidal surfaces. PEO can then be adsorbed on to this anchor points on the colloid particle surfaces [80].

2.1.7.3.3 Poly(2-(dimethylamino)ethyl methacrylate) (PDMAEMA)

PDMAEMA can be synthesised from the monomer 2-(*N,N*-dimethylamino)ethyl methacrylate, DMAEMA, a methacrylic ester.

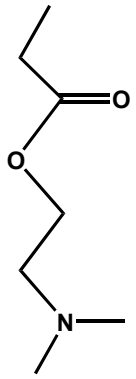

DMAEMA is a readily polymerizable monomer and provides a means of incorporating amino groups into the polymer system. The amine group imparts cationic properties to the polymer and this provides binding abilities to a variety of colloidal materials. Polymerization occurs through anionic polymerization, group transfer polymerization or radical polymerization. Due to their robustness, controlled radical polymerizations (ATRP, RAFT and NMP) are usually the first choice for the preparation of advanced PDMAEMA-related architectures [81].

The properties of PDMAEMA include hydrophilicity, pH and temperature sensitivity, ease of quaternization, and availability of the functional amine/ammonium moiety for complexation with acidic/anionic substances. These properties make PDMAEMA attractive for a wide range of applications, including as flocculation agents, as biocides, and in gene delivery [82]. PDMAEMA belongs to the class of weak cationic polyelectrolytes (pKa ~ 6). It can react to external stimuli with respect to both pH and temperature, i.e., it is both pH- and thermo-responsive. When subjected to changes in pH and/or temperature it can switch from a hydrophilic to a hydrophobic character [83].

PDMAEMA can also be easily modified by quaternization, with for example methyl iodide (MeI), leading to strong polyelectrolytes [84]. Decreasing the pH results in a weak polyelectrolyte, as shown in Figure 2.13.

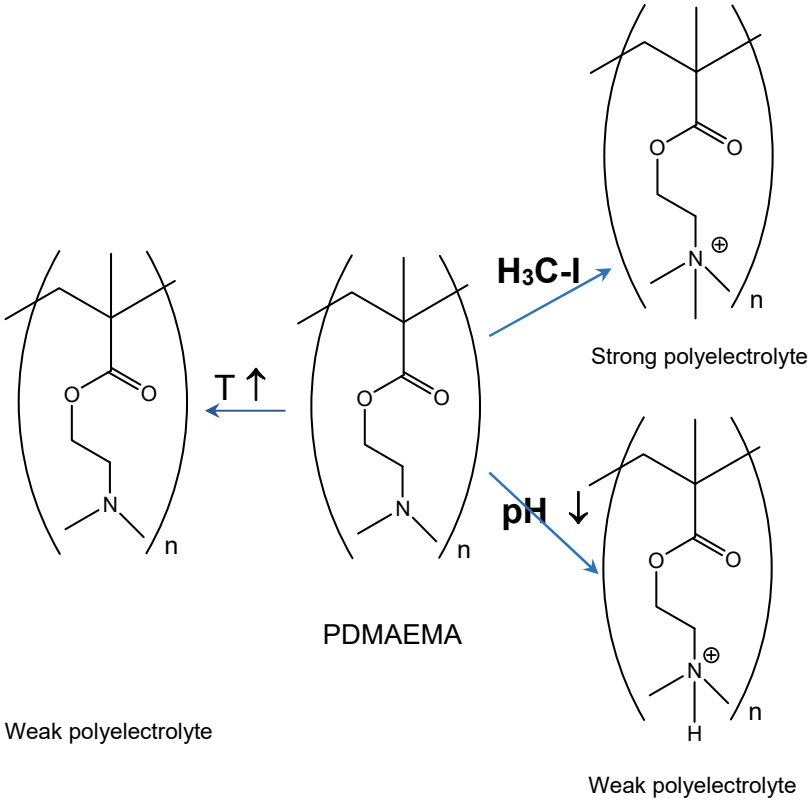

Figure 2.13: Modification of PDMAEMA for use as flocculants

The molecular weight of the polymer plays an important role in its stimuli-responsiveness [85]. Higher molecular weight PDMAEMA result in more effective flocculation and sediment compaction - with larger molecular weight there are enough segments on the polymer chains for bridging flocculation. PDMAEMA can also be copolymerized with other monomers such as vinyl monomers and its conformation in the copolymer adjusted by both pH and temperature. Jian Guou [86] synthesised poly(DMAEMA-co-AM-co-AA) copolymer to improve the flocculation abilities of a polyacrylamide flocculant. The copolymer flocculant was added to the wastewater at low pH. There was a high degree of protonation and an extension of the polymer coil, caused by electrostatic repulsion. At this pH, the long-chain polymer was soluble in the water phase and able to bridge between colloidal particles causing flocculation of the fines. On increasing the pH, the rate of settling of the flocs increased due dense flocs being formed when the coils collapsed. This also led to the release of trapped water from the sediment and increased the strength of the compacted sediment, as shown in Figure 2.14.

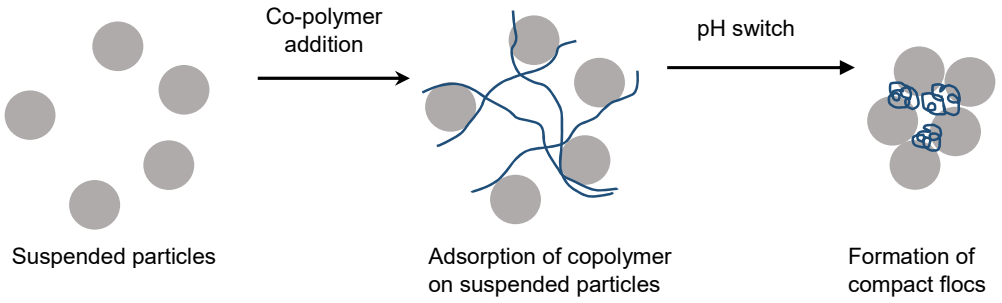

Figure 2.14: Scheme of enhancing consolidation of flocs by switching polymer such PEO-*b*-PDMAEMA [86]

The range of potential applications of PDMAEMA can be further increased by incorporating it into block copolymers with either hydrophilic or hydrophobic polymers [87]. Block copolymerisation with hydrophobic polymers leads to amphiphilic block copolymer systems that are characterized by unique self–assembling properties that can be controlled by external stimuli like temperature, solvent variation and pH. Thus, PDMAEMA diblock copolymers with, various other polymethacrylates [88] poly(caprolactone) [89] poly(ethylene oxide) or poly(ethylene oxide)–poly(propylene oxide) [90] polystyrene [91] poly(2–vinyl pyridine) [92] and poly(ethylene–co–butylene) [93] have been studied.

2.2 Cellulose Chemistry

2.2.1 Introduction

Cellulose is the most abundant, naturally occurring polymer available in the world. It is estimated that between 10^{11} – 10^{12} tons/y of cellulose are synthesised by photosynthesis alone [95]. Cellulose has many attractive physical and chemical properties, which include biocompatibility, hydrophilicity, stereoregularity, reactive hydroxyl groups and the ability to form suprastructures. Cellulosic materials are also relatively cheap, reasonably strong, safe to living organisms, reproducible, recyclable, and biodegradable. However, only about 0.2% of the cellulose produced annually has been effectively used, and this mainly in the paper and textile industries [96]. Despite all its attractive and interesting properties, cellulose lacks some of the versatile properties of synthetic polymers. This explains the continued research into the nature of cellulose and its derivatives.

Since its first discovery and isolation by Anselme Payen in 1838 many technologies have been applied to produce modified cellulosic materials for our daily and industrial needs [97].

2.2.2 Sources of Cellulose

Cellulose is produced in plants, certain bacteria, and certain living higher organisms such as the sea animal tunicates [98].

The primary source of cellulose is the lignocellulosic material found in plants. The cellulose content of plants vary significantly. Young leaves contain about 10% cellulose while older leaves tend to contain about 20% cellulose [99]. The woody tissues of trees and shrubs contain about 60% cellulose. The highest cellulose content (more than 90%) of any naturally occurring substance is found in the seed hair of the cotton plant [100].

In addition to plants, cellulose is also produced by a large variety of other living organisms. Cellulose can be found in bacteria and prokaryotes such as acetobacter, rhizobium, and agrobacterium. It is also found in some fungi, amoeba, green algae and slime molds. *Valonia ventricosa* and *Chaetamorpha melagonicum*, found in green algae, contains about 20-30% cellulose. There are several celluloses of animal origin - some simple marine animals such as tunicates deposit cellulose in their cell walls.

2.2.3 Cellulose Structure and Polymorphy

An understanding of the structure of cellulose is a pre-requisite to controlling its modification as the chemical structure and composition of cellulose determines its chemical and physical properties. Cellulose is the trivial name for (1 → 4)-β-D-glucopyranan. Payen determined, by elemental analysis, the molecular formula for cellulose to be $C_6H_{10}O_5$. In the cellulose chain, these glucose units occur as 6-membered rings, called pyranoses. Two unlinked molecules of β-D-glucose are depicted in Figure 2.15.

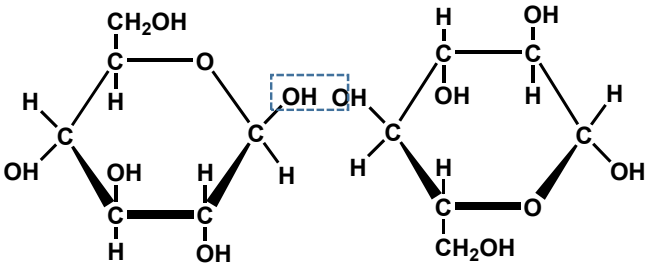

Figure 2.15: Removal of water molecule to form cellobiose unit

The glucose units are linked when water is eliminated by combining the H and –OH group of adjacent anhydroglucopyranose units. They are then joined by single oxygen atoms (acetal

linkages) between the C-1 of one pyranose ring and the C-4 of the next ring. Linking two of these sugars produces a disaccharide called cellobiose which is considered to be the basic repeat unit of the natural polymer. Since a molecule of water is lost, the glucose units in the cellulose polymer are referred to as anhydroglucose units (AGU). Linking additional sugars in exactly the same way produces cellulose (Figure 2.16):

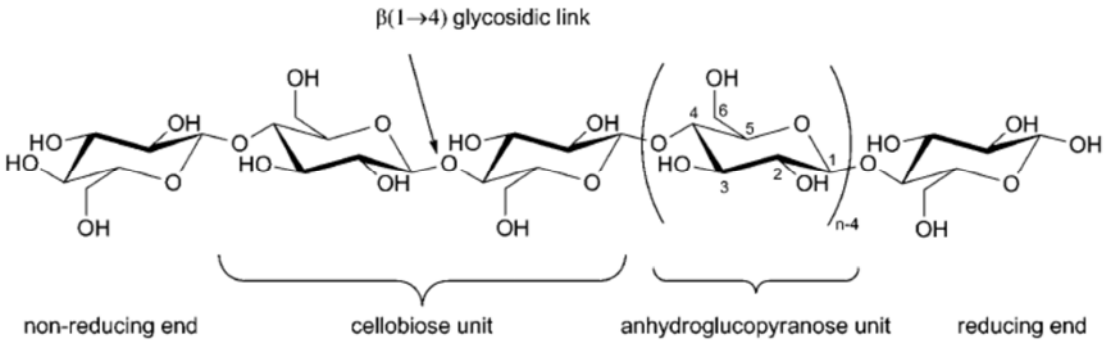

Figure 2.16: Molecular Structure of Cellulose

The basis of the cellulose structure is thus the chair-conformed AGU whose number determines the degree of polymerization. The length of the chain varies greatly, from a few hundred AGUs in wood pulp to over 6000 for cotton [101].

Every two AGU unit in cellulose are rotated by 180° in the plane about their axial chain as compared to the neighbouring two units. Because of the orientation of the glycosidic bonds linking the glucose monomers, the rings of glucose are arranged in a flip-flop manner. The β-(1-4) glycosidic linkage gives cellulose the linearity that results in a rigid rod-like molecule. The cellulose molecule contains three different kinds of AGUs: the reducing end with a free hemiacetal (or aldehyde) group at C-1, the nonreducing end with a free hydroxyl at C-4 and the internal rings joined at C-1 and C-4. Because of large chain length, the chemistry of the alcohol groups of the internal units predominates.

The hydroxyl groups of the cellulose chain are placed at positions C2 and C3 (secondary) as well as C6 (primary). The pyranose rings are in the $^4C_1$ conformation, which means that the $–CH_2OH$ and –OH groups as well as glycosidic bonds are all equatorial with respect to the mean planes of the rings [102]. The CH_2OH side group is arranged in a trans-gauche (*tg*) position relative to the O5–C5 and C4–C5 bonds [102]. When the cellulose molecule is fully extended it takes the form of a flat ribbon with hydroxyl groups protruding laterally. These structural arrangements of the molecule enable it to form both inter- and intra-molecular hydrogen bonds. With respect to intramolecular bonding, the OH groups on the carbon atoms

(C3) on one AGU are involved in intramolecular hydrogen bonds with the oxygen atom (O5') of a neighbouring AGU in the same molecular chain. A possible second intramolecular hydrogen bonding exists between the OH groups on the carbon atoms C6 of one AGU and C2' of neighbouring AGU [103], as shown in Figure 2.17.

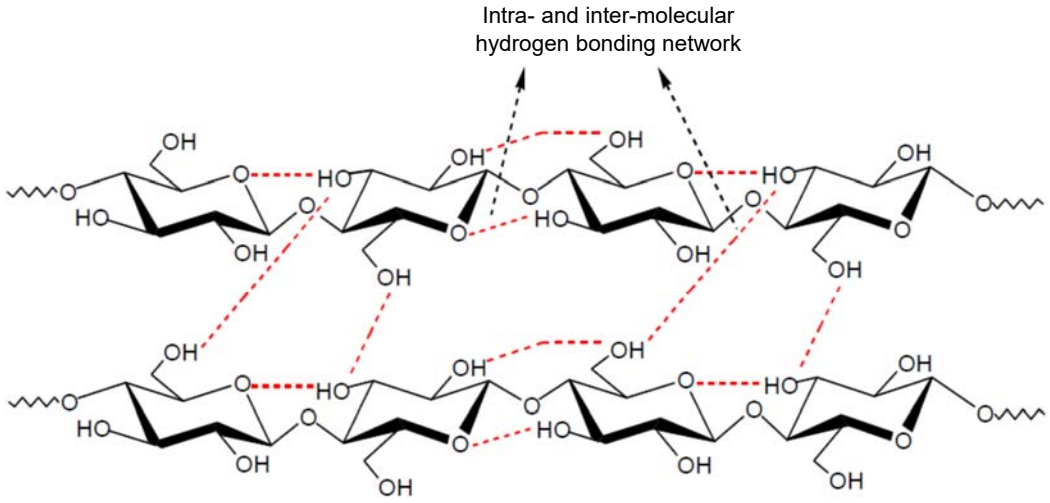

Figure 2.17: Representation of the extensive intra- and inter-molecular hydrogen bonding network [103]

Intermolecular hydrogen bonding exists between the OH groups on the carbon atoms C6 and C3'' of cellulose molecules that are adjacently located on the same plane. The intramolecular hydrogen bonding between adjacent AGUs, strengthens the linear nature of the polymer chain and affects the reactivity of the hydroxyl groups. Further, although it contains two types of hydroxyl groups, a primary hydroxyl in methylol group ($–CH_2OH$) at C-6 and two secondary hydroxyl groups (–OH) at C-3 and C-4, both of which are hydrophilic, it does not dissolve in water and in common solvents due to the strong hydrogen bonds between the cellulose chains.

The hydrogen bonds between the cellulose chains and van der Waals forces between the glucose units also cause the chains to group together in highly ordered, crystal-like structure [104]. As a result of the supramolecular structure of cellulose, the solid state is represented by both high order (crystalline) areas as well as low order (amorphous) areas (Figure 2.18).

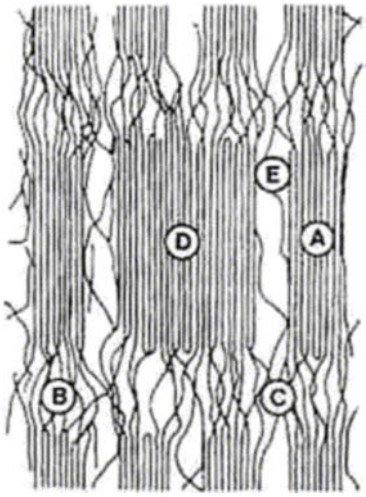

Figure 2.18: Fine structure of cellulose fibre [104]

The crystallites (A) in Figure 2.18 are characterized by their well-ordered size and their orientation. Less-ordered amorphous regions (B) connect successive crystallites length-wise. Lateral tie molecular region (C) connects adjacent amorphous regions. The cluster formations (D) are regions where crystallites are fused to large aggregates and region (E) represents the voids.

In the less ordered regions, the chains are further apart and more available for hydrogen bonding to other molecules, such as water [105], as shown in Figure 2.19.

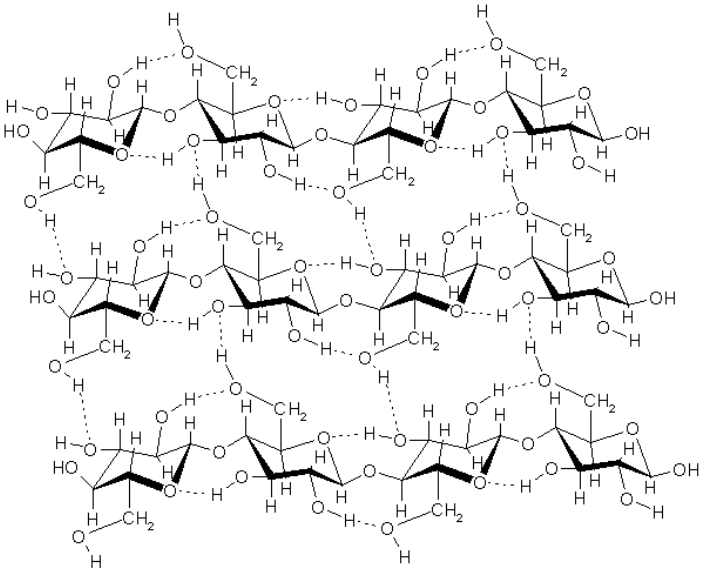

Figure 2.19: Structure of cellulose microfibril, showing hydrogen bonding with water [105]

Cellulose can exist in four different allomorphic forms (Cellulose I (α and β), II, III, and IV), as shown in Figure 2.20, depending on its origin and treatment. Cellulose I (α and β) is produced by plants and is referred to as native cellulose. The two allomorphs exists in different ratios depending on the origin of the cellulose. Cellulose II occurs naturally in marine algae but can be formed when cellulose I is treated with aqueous sodium hydroxide.

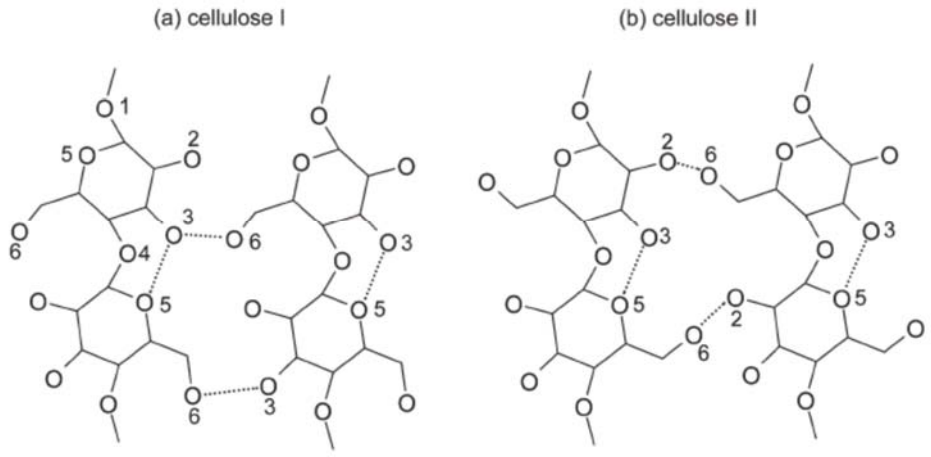

Figure 2.20: (a) Cellulose I and (b) Cellulose II [106]

The distinction between cellulose I and cellulose II is shown in Figure 2.20. Intramolecular hydrogen bonds (O3-H---O5) exist in both of the polymorphs. The difference occurs in the intermolecular hydrogen bonding. The dominant hydrogen bond for cellulose I is the O6-H---O3 whereas cellulose II has it at O6-H---O2 [106]. Furthermore, cellulose II has chains that are in an anti-parallel arrangement where reducing and non-reducing end groups alternate in a microfibril. Among the four different crystalline polymorphs cellulose I, II, III, and IV, cellulose I is thermodynamically less stable while cellulose II is the most stable structure.

The morphology of cellulose has a profound effect on its reactivity. Each AGU of cellulose contains three hydroxyl groups. These hydroxyl groups presents opportunities to modify the cellulose into products with desirable properties for specific applications in industry, pharmaceutics and domestic use. One needs to bear in mind, however, that although the hydroxyl groups that are located in the amorphous regions are highly accessible and react readily, those in crystalline regions with close packing and strong intermolecular hydrogen bonding can be completely inaccessible [107].

2.2.4 Graft Polymerisation of Cellulose

2.2.4.1 Introduction

A polymer is a homopolymer if it consists of only one unique repeat unit, and a copolymer if two different monomers are the repeat units. Graft copolymers involve a preformed polymeric back-bone (substrate) to which polymeric chains of a different chemical nature are attached at several points. Stannett [108] defined graft copolymers as: “Graft copolymers consist of a polymer back-bone with lateral covalently linked side chains.” Both the substrate and the side chain polymers could be homopolymers or copolymers. Graft copolymerization permits one to combine the best properties of two or more polymers in one physical unit.

Graft copolymerization to the cellulose substrate offers an attractive and versatile means of imparting a variety of functional groups to the substrate in order to meet required and specialized applications. Tailor-made graft copolymers can be synthesised using specific polymerisation methods to meet desired end use. With respect to cellulose, this is achieved by modifying the cellulose substrate through the creation of grafts of synthetic polymers that impart specific properties onto the cellulose substrate, without destroying its intrinsic properties. Graft copolymerization of cellulose has been widely studied to give new materials for drug delivery, sorption agents, flocculation, coatings, and membranes [109]. Various techniques (Figure 2.21) for graft copolymerization of various monomers on the cellulose backbone have been developed [110]. These techniques include free radical polymerization (initiated by chemical or radiation methods), ring-opening polymerization, nitroxide-mediated polymerization (NMP), reversible addition–fragmentation chain transfer (RAFT) polymerization and atom transfer radical polymerization (ATRP).

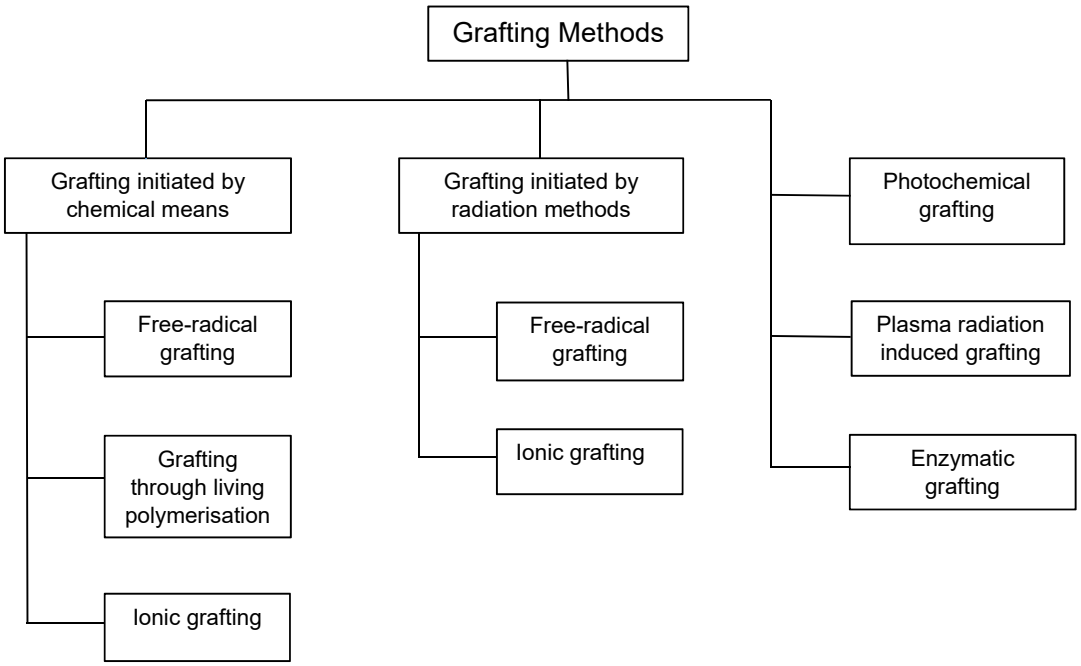

Figure 2.21: Various techniques for graft copolymerisation onto cellulose

2.2.4.2 Approaches to Grafting

There are three approaches to prepare cellulose based graft copolymers, the “grafting-to”, the “grafting-from”, and the “grafting-through” approach.

2.2.4.2.1 Grafting-to Approach

In the “grafting-to” approach, a pre-prepared or pre-formed polymer with desired functionality is covalently attached to the cellulose backbone via a chemical reaction.

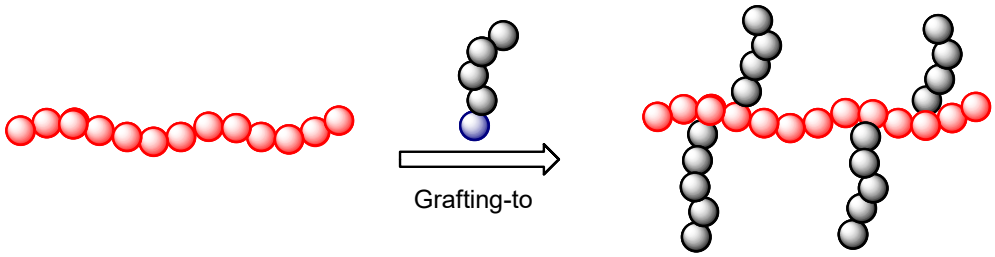

.

Figure 2.22: Modification of cellulose substrate with a polymer via the “grafting-to” approach

This approach therefore allows accurate synthesis of the graft polymer as well as full characterisation of both the grafts and the cellulose backbone prior to the coupling reaction

[111]. An important disadvantage of this approach is that, depending on the molecular weight of the grafting polymer, it may be difficult to obtain a high grafting density – high molecular weight grafting polymers cause steric hindrance and this may cause low mobility of polymer chains across a concentration barrier of already grafted polymers. Common reaction mechanisms used to synthesize these copolymers include free-radical polymerization, anionic polymerization, atom-transfer radical-polymerization, and living polymerization techniques.

2.2.4.2.2 Grafting-from Approach

In this approach, the cellulose backbone is first chemically modified in order to introduce active sites capable of initiating a polymerization reaction. Copolymer chains are then built up through successive monomer unit additions from these initiating site, as shown in Figure 2.23.

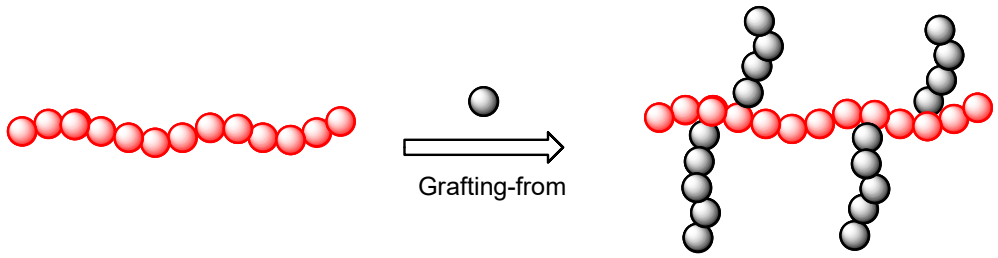

Figure 2.23: Modification of cellulose substrate with a polymer via the "grafting-from" approach

An advantage of this approach is that a high graft density can be achieved due to the easy access of the reactive groups to the chain ends of the growing polymers – there is less steric hindrance and a higher mobility of low molecular weight monomers and catalyst compared to the grafting-to approach. Even though the number of grafted chains can be controlled, there may be a difference in the lengths of each grafted chain due to kinetic and steric hindrance effects [112]. This can, however, be overcome if the copolymerization reaction is carried out using a living/controlled polymerisation method that allows the grafts to grow simultaneously and result in a well-defined polymer structure [112]. Different techniques such as anionic grafting, cationic grafting, atom-transfer radical-polymerization, and free radical polymerization have been used in the synthesis of grafting from-copolymers.

2.2.4.2.3 Grafting-through Approach

In the ''grafting-through'' approach, a macromonomer, usually a vinyl macromonomer of cellulose, is copolymerised with a low molecular weight co-monomer.

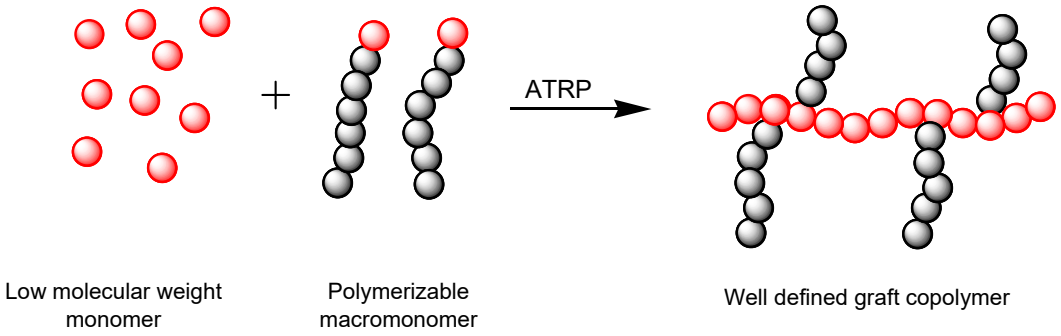

Figure 2.24: Modification of cellulose substrate with a polymer via the "grafting-through" approach

This method allows incorporation of the cellulose-derived macromonomers onto a backbone prepared by a controlled radical polymerisation method [113]. The ratio of monomer to macromonomer molar concentrations determines the number of chains that are grafted. As the reaction proceeds, the concentrations of monomer to macromonomer change causing random placement of branches and formation of graft copolymers with different number of branches.

2.3 References

[1] Faust, S. D. & Aly, O. M. 1998. Chemistry of Water Treatment, Second Edition, Ann Arbor Press.

[2] HDR Engineering Inc. 2001. Handbook of Public Water Systems, Second Edition, John Wiley & Sons, New York.

[3] Montogomery, J. M. 1985. Water Treatment Plant Design, Wiley-Interscience Publication.

[4] Nozaic, D. J., Freese, S.D., & Thompson, P. Water Science and Technology: Water Supply, 2001, 1, 43-50.

[5] Singh R.P., Nayak B.R., Biswal D.R., Tripathy T., Banik K., Materials Research Innovations, 2003, 7, 331-340.

[6] Metcalf and Eddy, I., 1993. Wastewater Engineering, 3rd Edition, McGraw-Hill, New York.

[7] Lin, W. W., Sung, S. S., Chung, H. Y., Chen, L. C., Wang, C.C, Wu, R.M., Lee, D.J., Huang, Chihpin, Journal of Environmental Engineering, 2004, 130,12, 1481-1487.

[8] Snoeyink, V.L., & Jenkins, D. Water Chemistry. John Wiley & Sons, New York, 2000.

[9] Crittenden, J. C., Trussell, R. R., Hand D.W., Howe K.J., G. Tchobanoglous. 2005. Water Treatment: Principles and Design, 2nd edition, John Wiley & Sons, New York.

[10] Bayramoglu, G., Bektas, S., Arica, M.Y., Journal of Hazardous Materials, 2003,101, 3, 285–300.

[11] Sojka, R. E., Lentz, R. D., Westermann, D. T. Soil Science Society of America Journal, 1998, 62, 1672-1680.

[12] Kawamura, S., Journal-American Water Works Association, 1976, 68, 6, 328-336.

[13] Atesok, G., Somasundaran, P., and Morgan, L.J., Powder Technology, 1988, 54, 77-83.

[14] Bohuslav, D. 2005. Coagulation and Flocculation, 2nd ed. CRC Press, Taylor & Francis Group, United States of America.

[15] Bratby, J. 2006. Coagulation and Flocculation in Water and Wastewater Treatment, 2nd ed. IWA Publishing, London.

[16] Hiemenz, P. C. and Rajagopalan, S. 1997. Principles of Colloid and Surface Chemistry. Marcel Dekker Inc., New York.

[17] Hogg, R., Flocculation and Dewatering, International Journal of Mineral, 2000, 58, 4, 223-236.

[18] Hunter, R. J. 1981. Zeta Potential in Colloid Science: Principles and Applications. Academic Press, London.

[19] Israelachavili, J., 2006. Intermolecular and Surface Forces. Academic Press, London and New York.

[20] Jones, F., J. B. Farrow and van Bronswijk, W. Colloids and Surfaces A: Physicochemical and Engineering Aspects, 1998, 142, 1, 65-73.

[21] Missana, T. and A. Adell. J. Colloid and Interface Science, 2000, 230, 1, 150-156.

[22] Nabzar, L., A. Carroy and E. Pefferkorn. J. Colloid Interface Science, 1986, 14,113-1, 19.

[23] Connelly, L. J., Owen D. O., and P. F. Richardson. Light Metals, 1986, 247-261.

[24] Csempesz, F. Journal of Colloid Interface Science, 2000, 80, 43-49.

[25] Dustan, A. C., B. Cohen and J. G. Petrie. Advances in Colloid and Interface Science, 2005, 113: 85-97.

[26] Fleer, G.J. and Scheutjens, J.M.H.M. 1993. Coagulation and Flocculation, Theory and Applications, Marcel Dekker, New York.

[27] Verwey, E.J.W., Journal of Physical and Colloid Chemistry, 1947. 51, 3, 631-636.

[28] Zbik, M. and R.G. Horn. Colloids Surfaces, 2003. 222(1-3): 323-328.

[29] Scales, P.J., S.B. Johnson, and P.C. Kapur, Mineral Processing and Extractive Metallurgy Review: An International Journal, 1999. 20(1): 27 - 40.

[30] Addai-Mensah, J. and J. Ralston. Powder Technology, 2005, 160(1): 35-39.

[31] James, R.O., G.R. Wiese, and T.W. Healy, Journal of Colloid and Interface Science, 1977, 59(2): 379-385.

[32] Mabire F, Audebert R, Quivoron C, J Colloid Interface Science. 1984, 97(1):120.

[33] Zhang CK, Yang ZYM, Qu X., Huaxua Shijie, Chem. Abstr., 1994, 317-238, 122.

[34] Sharma, B.R., Kumar, V, Soni, P.L., Trends Carbohydr Chem. 1999, 5, 75.

[35] Farinato, R.S., Huang, S., and Hawkins, P. 1999. Polyelectrolyte-assisted dewatering, fourth edition. John Wiley & Sons, USA.

[36] Gill, R.I.S. and Herrington, T.M. Colloids and Surfaces, 1987, 28, 41-52.

[37] Hiemenz, P.C. and Rajagopalan, R. 1997. Principles of colloid and surface chemistry, third edition. Marcel Dekker, New York.

[38] Gregory, J., Colloids and Surfaces, 1988, 31, 231-253.

[39] Krishnamoorthy, S., D. Mal, R. P. Singh. Carbohydr. Polym. 2007, 69, 371.

[40] Ungeheur, S., H. W. Bewersdorff, R. P. Singh. J. Appl. Polym. Sci. 1989, 37, 2933.

[41] Nystrom, R., K. Backfolk, J. B. Rosenholm, K. Nurmi. Colloids Surfaces, 2003, 219, 55.

[42] Morgen, S. E., McCormic, C. L., Prog. Polym. Sci. 1990, 15, 103.

[44] H. Barkert, J. Hartmann. Encyclopedia of Industrial Chemistry, 1988. 5th ed., Vol. 11, VCH, Weinheim.

[46] Singh, R. P., T. Tripathy, G. P. Karmakar, S. K. Rath, N. C. Karmakar, S. R. Pandey, K. Kannan, S. K. Jain, N. T. Lan. Curr. Sci. 2000, 78, 798.

[47] Grano, H., J. Y. Kauhaluoma, T. Suortti, J. Kaki, K. Nurmi. Carbohydr. Polym. 2000, 41, 277.

[48] Brostow, W., M. Drewniak, N. N. Medvedev. Macromol. Rapid Commun. 1995, 4, 745.

[49] Pal, S., D. Mal, R. P. Singh. J. Appl. Polym. Sci. 2007,105, 3240.

[50] Nayak, B. R., R. P. Singh. J. Appl. Polym. Sci. 2001, 81, 1776.

[51] Adhikary, P., K. N. Tiwari, R. P. Singh. J. Appl. Polym. Sci. 2007,103, 773.

[52] Adhikary, P., K. N. Tiwari, R. P. Singh. J. Appl. Polym. Sci. 2007,103, 773.

[53] Deshmukh, S. R., R. P. Singh. J. Appl. Polym. Sci. 1991, 43, 1091.

[54] Nayak, B. R., R. P. Singh. J. Appl. Polym. Sci. 2001, 81, 1776.

[55] Kan C., Huang C., Ruhsing, P.J. Colloids and Surfaces, A: Physicochemical and Engineering Aspects, 2001, 203, 1-9.

[56] Napper, D.H. Polymeric Stabilization of Colloidal Dispersions. 1983. Academic Press: London, U.K.

[57] Koskinen, W. C.; Clay, S. A. Soils. Rev. Environ. Contam. Toxicol. 1997, 151, 117-165.

[58] Singh, V., Tiwari, A., Pandey, S., & Singh, S. K., Express Polymer Letters, 2007, 1, 51–58.

[59] Varma, R. S. Green Chemistry, 1999, 1, 43–55.

[60] Pradip, R.A. Kulkarni, S. Gundiah. B.M. Moudgil, Int. J. Mineral Processing, 1991, 32, 259.

[61] Hogg, R. International Journal of Mineral, 2000, 58(1-4), 223-236.

[62] Hiemenz, P.C. Principles of Colloid and Surface Chemistry. 1986. 2nd edition. Marcel Dekker, New York.

[63] James, R.O. and Healy, T.W., J. Colloid Interface Science. 1972, 40, 53-64.

[64] Jenkins, P. and Ralston, J. Colloids and surfaces A: Physicochemical and Engineering Aspects. 1998, 139, 27-40.

[65] Cheng, W.P., Chemosphere. 2002, 47 (9) 963–969.

[66] Bell-Ajy, K., M. Abbaszadegan, E. Ibrahim, D. Verges, M. Le Chevallier l, J. Am. Water Works Assoc. 2000, 92 (10) 44–58.

[67] Bache, D.H., E. Rasool, D. Moffatt, F.J. McGilligan, Water Sci. Technol. 1999, 40, 9, 81–88.

[68] Bolto, B., G. Abbt-Braun, D. Dixon, R. Eldridge, F. Frimmel, S. Hesse, S. King, M. Toifl. Water Sci. Technol. 1999, 40 (9), 71–79.

[69] Besra, L., Min. Proc. Extract. Metall. Rev., 1998, 18, 67–103.

[70] Kalia, S., A. Dufresne, B.M. Cherian, B.S. Kaith, L. Avérous, J. Njuguna, International Journal of Polymer Science. 2011 (2011) 1–35.

[71] Ross, S. and Morrison, I.D. 1988. Colloidal Systems and Interfaces, Wiley, New York.

[72] XiangYu, P.Somasundaran Colloids and Surfaces A: Physicochemical and Engineering Aspects. 1993, 81, 17-23.

[73] McCarron, A. M., Crispo, S. and Smith-Palmer, T., J. Appl. Polym. Sci. 2002, 83: 2382–2389.

[74] Petzold, G., M. Mende, K.Lunkwitz, S.Schwarz, H.M. Buchhammer, Colloids and Surfaces A: Physicochemical and Engineering Aspects, 2003, 47-57.

[75] Mpofu, P., J. Addai-Mensah and J. Ralston. Journal of Colloid and Interface Science. 2003, 261(2): 349-359.

[76] Nishimura, S., M. Kodama, K. Yao, Y. Imai and H. Tateyama, Langmuir. 2002, 18, 468, 1-4688.

[77] Parks, G. A. Chemical Reviews. 1965, 65, 177-198.

[78] Pefferkorn, E. Journal of Colloid and Interface Science. 1999, 216, 2, 197-220.

[79] Rubio, J. Journal of Colloid and Interface Science. 1981, 2, 1, 79-95.

[80] Sastry, N. V., P. N. Dave, M. K. Valand, European Polymer Journal. 1999, 35, 3, 517-525.

[81] Virtanen J., Arotcarena M., Heise B., Ishaya S., Laschewsky A. Langmuir, 2002, 18, 5360.

[82] Chen M., BriscoeW. H., Armes S. P., Klein J. Science. 2009, 323, 1698.

[83] Georgiou T. K., Vamvakaki M., Phylactou L. A., Patrickios C. S.: Biomacromolecules, 2005, 6, 2990.

[84] Li J., Guo Z., Xin J., Zhao G., Xiao H., Carbohydr. Polym. 2010, 79, 277.

[85] Plamper F. A., Gelissen A. P., Timper J., Wolf A., Zezin A. B., Macromol. Rapid Commun. 2013, 34, 855−860.

[86] Jian Guo, K.M. Cooklock, Drug Dev. Ind. Pharm. 1995, 21, 2013-2019.

[87] Chen W.X., Fan X.-D., Huang Y., Liu Y., Sun L. React. Funct. Polym. 2009, 69, 97.

[88] Savoji M. T., Strandman S., Zhu J. X. X., Langmuir. 2013, 29, 6823.

[89] Crystal R. G.: Science. 1995, 270, 404.

[90] Wong S. Y., Pelet J. M., Putnam D. Prog. Polym. Sci. 2007, 32, 799.

[91] Cherng J.Y., van de Wetering P., Talsma H., Crommelin D. A., Hennink W., Pharm. Res. 1996, 13, 1038.

[92] van de Wetering P., Cherng J.Y., Talsma H., Hennink W. E. J. Controlled Release 1997, 49, 59.

[93] Yang C., Li H., Goh S. H., Li J.: Biomaterials. 2007, 28, 3245.

[94] Schallon A., Jérôme V.,Walther A., Synatschke C. V., Müller A. H. E. React. Funct. Polym. 2010, 70, 1.

[95] Bikales NM, Segal L. 1971. Cellulose and cellulose derivatives. Wiley Interscience, New York, NY.

[96] Bianchi E, Bonazza A, Marsano E, Russo S., Carbohydr Polym., 2000, 41, 47–53.

[97] El Seoud OA, Fidale LC, Ruiz N, D'Almeida MLO, Frollini E., Cellulose. 2008, 15, 371–392.

[98] Bhattacharya A, Misra BN., Prog Polym Sci., 2004, 29,767–814.

[99] Roy D, Semsarilar M, Guthrie JT, Perrier S., Chem Soc Rev., 2009, 38, 2046–2064.

[100] Bicak N, Sherrington DC, Senkal BF., React Funct Polym.,1999, 41,69–76.

[101] Hebeish A, Guthrie JT. 1981. The Chemistry and Technology of Cellulosic Copolymers. Springer, New York, NY.

[102] Misra M, Mohanty AK, Singh BC., J Appl Polym Sci., 1987, 33, 2809–2819.

[103] Ifuku S, Kadla J., Biomacromolecules. 2008, 9, 3308–3313.

[104] McDowall DJ, Gupta BS, Stannett VT., Prog Polym Sci. 1984, 10,1–50.

[105] Tsubokawa N, Iida T, Takayama T., J Appl Polym Sci. 2000, 75, 515–522.

[106] Gurdag G, Yasar M, Gurkaynak MA., J Appl Polym Sci. 1997, 66, 929–934.

[107] Yang F, Li G, He YG, Ren FX, Wang J. X., Carbohydr Polym. 2009, 78, 95–99.

[108] El-Hady BA, Ibrahim M. M., J Appl Polym Sci. 2004, 93, 271–278.

[109] Zhu J, Dong XT, Wang XL, Wang Y. Z., Carbohydr Polym. 2010, 80, 350–359.

[110] Zhou Q, Greffe L, Baumann MJ, Malmstrom E, Teeri TT, Brumer H., Macromolecules. 2005, 38, 3547–3549.

[111] Perrier S, Takolpuckdee P, Westwood J, Lewis D. M., Macromolecules. 2004, 37, 2709–2717.

[112] Takolpuckdee P., Aust J Chem. 2005, 58, 66–66.

[113] Fernandez MJ, Casinos I, Guzman GM., Makromol Chem. 1990, 191, 1287–1299.

Chapter 3

Synthesis of cellulose-*g*-polyacrylamide copolymer through chemical free-radical technique and its application as a flocculant

3.1) Introduction

Grafting is an effective technique for modifying the physical and chemical properties of cellulose and combining the advantages of natural cellulose and synthetic polymers. Grafting can be achieved through free-radical, ionic, or condensation and ring opening polymerization techniques. The free radical methods have received the greatest attention due to their practicality. In the grafting of vinyl monomers onto cellulose by free radical polymerisation, the initiation can be performed by chemical initiators or by (ir)radiation.

Among the chemical initiated methods, redox-initiated grafting is advantageous because, in the presence of redox systems, grafting can be carried out under milder conditions with minimum side reactions [1]. Free radical sites may be generated on the cellulose backbone by certain transition metal ions such as Ce^{4+}, Cr^{6+}, V^{5+}, and Co^{3+}. The redox potential of the metal ion is an important parameter in controlling the grafting efficiency - metal ions with low oxidation potential are preferred for better grafting efficiency. Various redox initiators such as ceric (IV) ion (ceric ammonium nitrate: $(NH_4)_2Ce(NO_3)_6$) (CAN)-HNO_3 or cerium (IV) sulphate-nitric acid [2], ceric ammonium sulphate (CAS)-HNO_3 [3, 4], iron(II)–hydrogen peroxide (Fe^{2+}–H_2O_2: Fenton reagent), cobalt (III) acetylacetonate complex salts [5], Co(II)–potassium monopersulphate [6], and sodium sulphite–ammonium persulphate [7], and free radical generators such as azobisisobutyronitrile ($C_8H_{12}N_4$: AIBN) [8], potassium persulfate ($K_2S_2O_8$: KPS) [9, 10, 11, 12, 13, 14], ammonium persulphate ($(NH_4)_2S_2O_8$: APS) [15, 16, 17], and benzoyl peroxide ($C_{14}H_{10}O_4$: BPO) [18, 19] have been used. Of the methods mentioned above, the formation of free radicals on cellulose molecules by direct oxidation with Ce^{4+} ions has gained considerable importance, due to its ease of application and its high grafting efficiency compared with the other redox systems [20]. Cerium possesses two oxidation states, Ce^{3+} and Ce^{4+}. The stability of Ce^{4+} is attributed to the empty 4f shell in its electron configuration. In acidic medium, it is known to be an oxidant and a strong electron acceptor. The use of Ce^{4+} ion in free radical initiator has also shown a substantial decrease in ungrafted polymers due to the participation of a single-electron process in the formation of active sites on cellulose [21]. As the Ce^{4+} ions produce free radicals almost exclusively on the cellulose backbone, in principle, no (ungrafted) homopolymer should be formed. Small amounts of homopolymer are,

however, always observed as a result of the direct reactions between Ce^{4+} ions and the monomers or due to chain transfer [22].

The use of ceric ions to initiate graft polymerization was first used by Mino and Kaizerman in 1958 [23]. Schwab and coworkers [24] were among the first to extend this method to the grafting of cellulose. Following their work, numerous papers have appeared in the literature on the grafting of various monomers onto cellulose by this technique. Temperature-responsive cellulose was obtained by Gupta and Khandekar [25] by graft polymerization of *N*-isopropyl acrylamide (NIPAM) using CAN-HNO_3 as initiator in acidic media. Hebeish *et al*. [26] reported the graft copolymerization of vinyl monomers onto modified cotton using ceric ion-nitric acid as the initiator. Hamma *et al.* [27] grafted acrylamide monomer (AM) onto Bombax Costatum Calyx (BCC) using ceric ammonium nitrate as initiator in aqueous medium to form grafted copolymer (BCC-*g*- PAM). Khullar *et al*. [28] optimized the reaction conditions for grafting of acrylonitrile onto cellulosic material obtained from bamboo using a two-phase system by varying the reaction parameters such as the duration of soaking cellulosic material in CAN, concentration of CAN, polymerization time, temperature and concentration of acrylonitrile and studying their effects on %G and %GE. Wassila *et al*. [29] grafted acrylic acid (AA) and acrylonitrile (AN) onto cellulose fluff pulp using CAN-HNO_3 as initiator. In this system the resulting copolymers were saponified with dilute sodium hydroxide. Okieimen [30] synthesised copolymers of acrylamide on cellulose obtained from *Terminalia superba* wood and its carboxymethylated derivative using a CAN-HNO_3 initiator in both batch polymerization and modified batch polymerization processes. The grafting efficiency, molecular weight of grafted polymer chains, and frequency of grafting as a function of the polymerization medium, and initiator and monomer concentrations were measured. Singha and Rana [31] studied the functionalization of cannabis indica fibre with acrylic acid (AAc) using a CAN-HNO_3 redox initiator in an aqueous medium. Different reaction parameters such as reaction time, pH, reaction temperature, concentrations of initiator, monomer and nitric acid were optimized to achieve the maximum percentage of grafting.

Even though many investigations have reported on conditions for optimising the grafting of vinyl monomers onto cellulose, there is as yet not a comprehensive understanding of optimised conditions. Investigations, to date, have used the one-variable-at-a-time technique in order to try and optimize the copolymerization of monomers onto cellulose. In this approach, investigators have kept all parameters constant except the factor to be investigated. The major disadvantage of this technique is that it does not take into account the many possible interactive effects among the variables and, thus, does not depict the complete effects of the

parameters on the process. Further, the investigators have given no justification for the values at which they have kept the factors constant whilst investigating the effect of the chosen factor. Using the one-factor-at-a-time approach in order to obtain a complete study of all the parameters and their interactions would, however, have increased the number of experimental runs beyond practical limitations. The factorial design or design of experiment (DOE) method provides for a way out of this dilemma. By applying this method in the investigation, most of the possible variations of the reaction conditions and their interactions could be included in a limited number of experiments. Factorial design also allows effects of a factor to be estimated at several levels of the other factors, yielding conclusions that are valid over a range of experimental conditions.

3.2) Mechanism

The precise mechanism and kinetics governing the grafting of vinyl monomers onto cellulose are difficult to determine since the reaction is heterogeneous [32]. Extensive research has, however, been performed on alcohols and other model compounds and the results gleaned from these experiments used to infer the mechanism and kinetics of cellulose copolymerisation.

It has been proposed that when Ce^{4+}-HNO_3 is used as initiator in the grafting of vinyl monomers onto cellulose, the first step is the oxidation of cellulose to form an intermediate, reversible complex (which may be a chelated species) between the Ce^{4+} ion and the cellulose. This is followed by the disproportionation of the complex to form Ce^{3+} ion and in the process, creating a cellulose radical by hydrogen abstraction [33, 34]. Thus, the initiation sites for grafting are created on the cellulose backbone. There are, however, several possible sites on the cellulose molecule at which the radicals can be produced for grafting to occur: the hydroxyl at the C6 position, the glycol group at the C2-C3 position and the hydroxyl at the end of the cellulose chain [35, 36].

According to Mino and Kaizerman [23], the radical formation on the cellulose backbone may occur on the carbon (C6) or on the oxygen atom of methylol ($–CH_2OH$) group, as shown in Scheme 3.1.

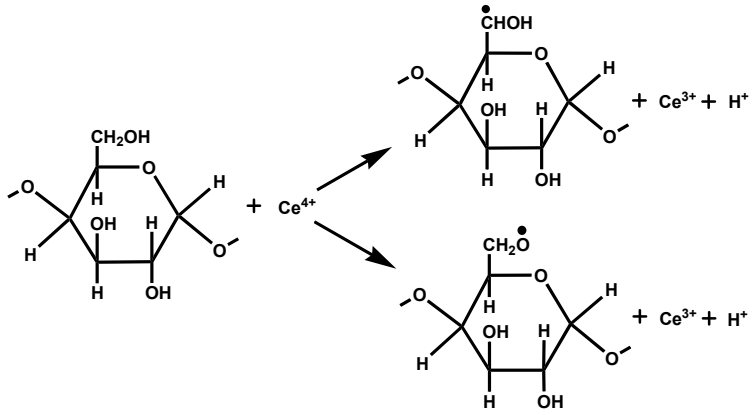

Scheme 3.1: Radical formation on cellulose backbone according to Mino and Kaizerman [23]

Iwakura, *et al*. [37] showed that, in ceric ion-ethanol initiated styrene polymerization, the resulting polystyrene contains hydroxyl groups. The presence of the hydroxyl groups confirms the existence of the carbon radical, R*OH, rather than the alkoxy radical, RO*, as the initiating species. This was further confirmed by Bergam *et al.* [38] who found evidence of oxidation at the C6 position. When they treated paper with NO_2 no grafting was observed – NO_2 preferentially attacks the C6 carbon.

To further examine the most likely site for grafting, Imai *et al*. [39] grafted several polymers containing glucose with methyl methacrylate. Reduced reaction rates were noticed only for the polymers in which the site of glucose attachment to the polymer chain was the C_1 position. On the basis of these results they proposed that the oxidation of cellulose by ceric ions occurred primarily at the hemiacetal unit (Scheme 3.2).

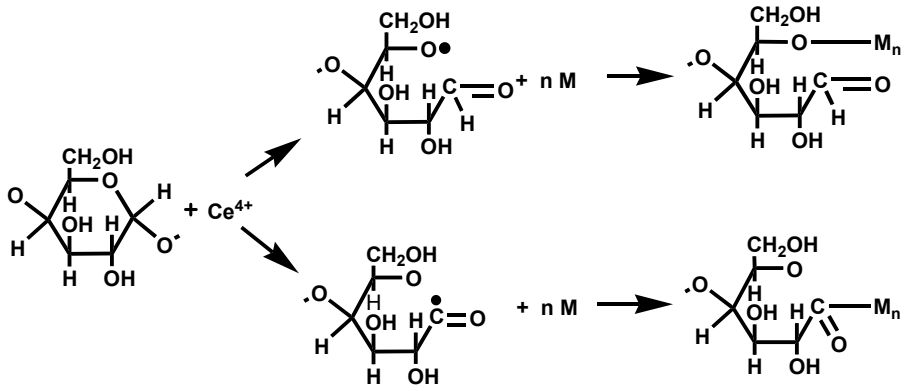

Scheme 3.2: Radical formation on cellulose backbone according to Imai *et al.* [39]

Terasaki and Matsuki [40] attributed the initial fast rate of ceric ion consumption, which was observed during grafting, to the presence of the hemiacetal units in the cellulose chains.

Arthur *et al.* [41] obtained evidence from electron spin resonance (ESR) spectra to support their proposal that cleavage of the C2-C3 glycol group of the anhydroglucose unit occurs when ceric ion is used to generate the free radicals. The importance of the glycol groups along the cellulose chain was also demonstrated by Hebeish, *et al.* [42] who found that partial blocking of these groups decreased the rate of grafting. The complex formed between Ce^{4+} ion and the 1,2-glycol may be either a chelated or an acyclic species. Work done by Hinz and Johnson [43] showed that in the oxidation of monohydric alcohols (which cannot form chelate intermediates) and 1,2-glycols by Ce^{4+}, the equilibrium constant for complex formation was significantly larger for the 1,2-glycols [44]. This increase was attributed to chelate stabilization of the Ce(IV)-1,2-glycol complex. This not only indicated the complex formed to be a chelated one, but also minimized the possibility of involvement of the hydroxyl group at 6-position in complex formation.

On the basis of the available evidence, the following mechanism has been proposed for the graft copolymerization of acrylamide on the anhydroglucose units by Ce^{4+} ion (Scheme 3.3).

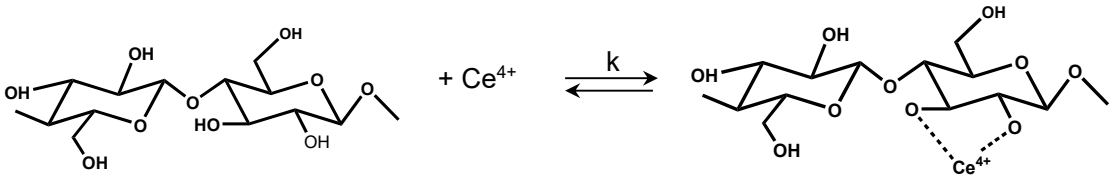

Cellulose

Cellulose – Ce^{4+} Complex

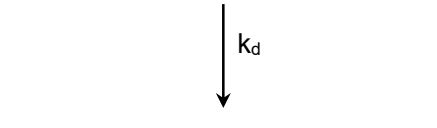

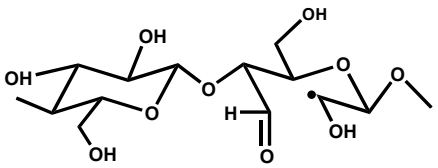

Cellulose free radical

Chain Initiation

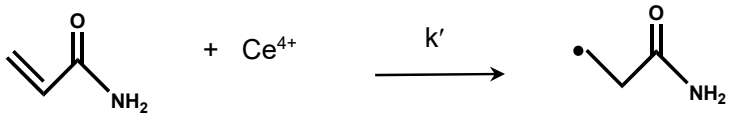

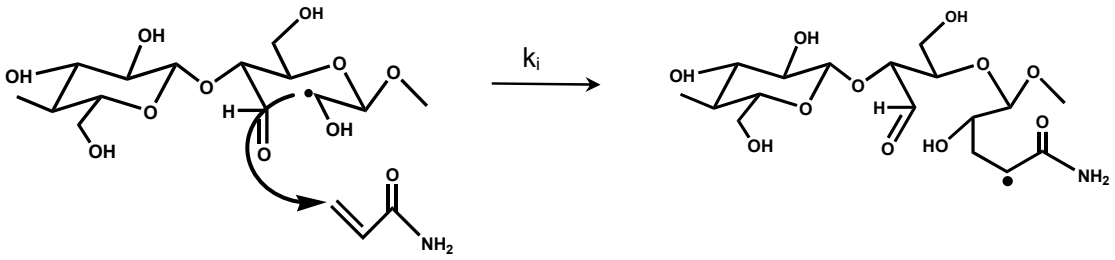

Chain Propagation:

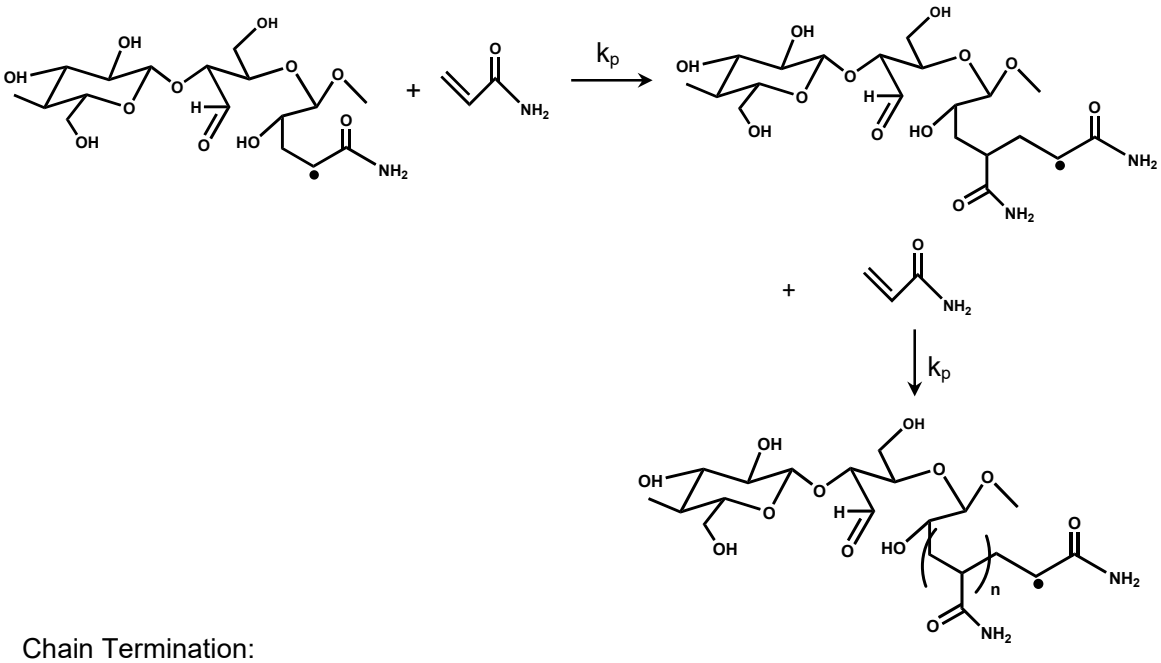

Chain Termination:

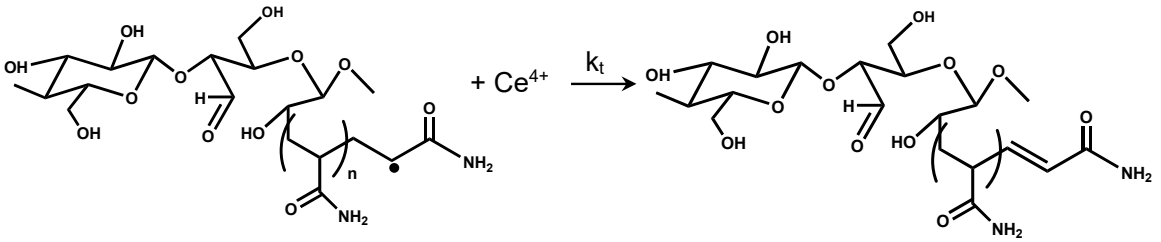

Cell-*g*-PAM free radical

Cell-*g*-PAM

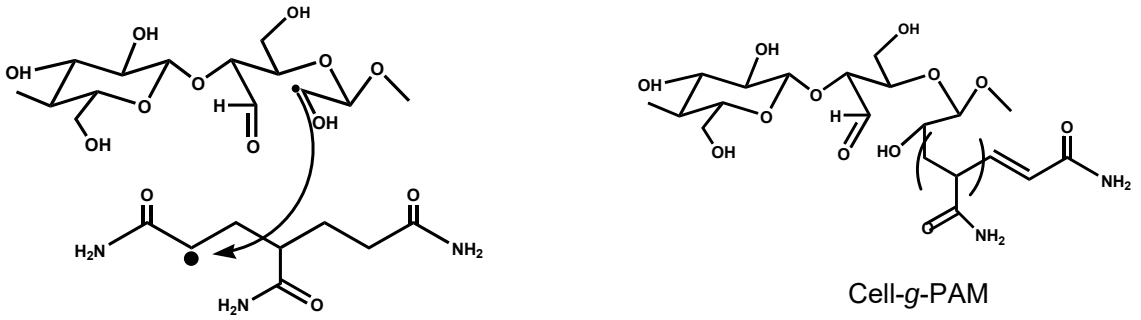

Cell-*g*-PAM

Scheme 3.3: Possible mechanism for graft copolymerization of acrylamide onto cellulose

3.3) Kinetics

Ogiwara *et al*. [45], using the results of free radical copolymerization of vinyl monomers onto alcohols initiated by Ce^{4+} ions, proposed the reaction scheme for cellulose shown in Scheme 3.4.

Initiation:

$$Ce^{4+} + Cell\text{-}OH \overset{K}{\rightleftharpoons} Complex \xrightarrow{k_d} Cell\text{-}O^{*} + Ce^{3+} + H^{+} \quad (3.1)$$

$$Cell\text{-}O^{*} + M \xrightarrow{k_i} Cell\text{-}O\text{-}M^{*} \quad (3.2)$$

$$Ce^{4+} + M \xrightarrow{k_i'} M^{*} + Ce^{3+} + H^{+} \quad (3.3)$$

Propagation:

$$Cell - O - M^{*} + M \xrightarrow{k_p} Cell - O - M^{*}_{n+1} \quad (3.4)$$

$$M^{*}_{m} + M \xrightarrow{k_p''} M^{*}_{m+1} \quad (3.5)$$

Termination:

$$Cell - O - M^{*}_{n} + Ce^{4+} \xrightarrow{k_t} Cell\text{-}O\text{-}M_{n} + Ce^{3+} + H^{+} \quad (3.6)$$

$$M^{*}_{m} + Ce^{4+} \xrightarrow{k_t'} M_{m} + Ce^{3+} + H^{+} \quad (3.7)$$

$$Cell - O - M^{*}_{n} + Cell\text{-}O^{*} \xrightarrow{k_t''} Stabilisation \quad (3.8)$$

$$Cell\text{-}O^{*} + Ce^{4+} \xrightarrow{k_o} Oxidation\ products + Ce^{3+} + H^{+} \quad (3.9)$$

Scheme 3.4: Reaction scheme for cellulose as proposed Ogiwara *et al.* [45]

Using the above reaction scheme, Ogiwara *et al*., derived the following expression for the rate of polymerisation:

$$R_p = \frac{k_p}{k_t}[M]^2 \left\{ k_i' + \frac{k_i k_d K[Cell - OH]}{k_o[Ce^{4+}]} \right\} \quad (3.10)$$

As seen in equation (3.10), the rate of polymerization, Rp, is inversely proportional to the concentration of Ce^{4+}. This implies that the rate of polymerization may be greater at lower Ce^{4+} ion concentrations. In their experimental work, however, the grafting yields were found to firstly increase and then decrease with increasing concentration of Ce^{4+}. Varma and Narasimhan [46] proposed that the initiation reactions (3.1, 3.2, and 3.3) should be reversible reactions since according to their results, increases in the proton concentration suppressed grafting. Accordingly, they obtained the following expression for the rate of polymerization:

$$R_p = \frac{k_p k_i [M]^2}{(k_{-i}) + k_t [Ce^{4+}]} \left\{ \frac{k_1 [Ce^{4+}][CeII - OH]}{(k_{-1})[Ce^{3+}][H^+] + k_i [M] + k_o [Ce^{4+}]} \right\} \quad (3.11)$$

where k_1 is the rate of complex formation, k_i the rate of initiation and k_{-1} and k_{-i} the rates of the reverse reactions. At low ceric ion concentrations, Equation (3.11) becomes:

$$R_p = \frac{k_p k_i [M]^2}{(k_{-i}) + k_t [Ce^{4+}]} \left\{ \frac{k_1 [Ce^{4+}][CeII - OH]}{(k_{-1})[Ce^{3+}][H^+] + k_i [M]} \right\} \quad (3.12)$$

which predicts that the rate of polymerization will increase with Ce^{4+} concentration. At higher ceric ion concentrations, $k_{-i} < k_t [Ce^{4+}]$ and Equation (3.11) becomes:

$$R_p = \frac{k_p k_i [M]^2}{k_t} \left\{ \frac{k_1 [CeII - OH]}{(k_{-1})[Ce^{3+}][H^+] + k_i [M] + k_o [Ce^{4+}]} \right\} \quad (3.13)$$

This indicates a decrease in the rate of polymerization as ceric ion concentration increases.

3.4) Design of Experiment (DOE) and Response Surface Methodology (RSM)

3.4.1) Introduction

In order to compare the flocculating ability of the synthesised bioflocculant against currently available commercial flocculants, it was necessary to produce an optimally synthesised bioflocculant, *i.e.* one with the highest percentage grafting. Design of Experiments and Response Surface methodology were used to optimise the synthesis of the bioflocculant.

Response Surface Methodology (RSM) is a collection of mathematical and statistical techniques used for the analysis and modelling problems in which one or more responses of interest is/are influenced by several input (independent) variables and in which the objective is to optimize this response [47]. RSM defines the effect of the independent variables on the output response when the independent variables are acting either alone or in combination

(interacting) with each other. Interaction occurs when the effect of one factor is dependent on the level of another factor. This is an important feature of factorial design that is not catered for in the one-factor-at-a-time approach. A factor with a small individual effect can contribute greatly to the response by interacting with another [48]. In addition to analyzing the effects of the input variables, RSM also generates a mathematical model which can be graphically depicted – hence the term Response Surface Methodology.

The relationship between the response and the input, independent variables is given by Equation 3.14.

$$y = f(x_1, x_2, ..., x_n) + \varepsilon \tag{3.14}$$

where y is the response or desired outcome, f is the response function, $x_1, x_2, \ldots, x_n$ the independent/natural/input variables, n is the number of independent variables and ε is the error term that represents other sources of variability not accounted for by f. The input variables are also termed natural variables as they are given in their respective units. It is generally assumed that ε has a normal distribution with mean of zero and variance σ^2.

3.4.2) Steps in Response Surface Methodology

The application of RSM as an optimisation technique is done sequentially and details of each of the steps are discussed below.

3.4.2.1) Screening of Variables

Numerous variables may affect the response of the system being studied, and it is not always practical nor possible to identify and control the effects of all input variables, especially those that make minor contributions. To develop a useable and practical model, it is necessary to select those variables that have major effects. Screening experiments are therefore carried out to identify which of the numerous input variables and their interactions present more significant effects. Full or fractional two-level factorial designs are used to achieve this.

3.4.2.2) Selection of the experimental design

The simplest model that can be used in RSM is based on a linear function and is represented by the Equation 3.15 – a first-order equation.

$$y = \beta_o \sum_{i=1}^{k} \beta_i x_i + \varepsilon \tag{3.15}$$

where k is the number of variables

β_o is the constant term

β_i represents the coefficients of the linear parameters

x_i represents the variables

ε is the residual or error associated with the experiments

The above model assumes no curvature in the response. First-order factorial designs are important in RSM because they can be used in screening experiments to help identify the important variables in an experiment and helps the researcher in deciding which input variables to eliminate. They also function as building blocks for other response surface designs, including the central composite designs, which will be discussed in the next section. The 2^k full factorial designs have only 2 levels for each of the k factors and these are coded as -1 for the low level and +1 for the high level.

Codifying the levels of the independent variable consists of transforming each real value of each natural variable into coordinates inside a scale with dimensionless values, and these dimensionless values must be proportional to the location of the real values in the experimental space [49]. Codifying the values of the independent variables is important because this transformation normalizes the variables before regression analysis and eliminates the effect of different units and ranges in the experimental domain and allows parameters of different magnitude to be investigated more evenly in a range between -1 and +1, *i.e.* it prevents variables with higher ranges having a greater influence on the regression analysis than variables with smaller ranges. The formula used for coding is given by Equation 3.16.

$$X = \frac{x - (x_{max} + x_{min})/2}{(x_{max} + x_{min})/2} \tag{3.16}$$

where X is the coded variable, x is the natural variable value, and x_{max} and x_{min} are the maximum and minimum values of the natural variable.

As the number of input variables (k) increase in an experiment, the number of experimental runs required to perform the full factorial design become unrealistically large. For these situations, 2^{k-s} fractional factorial design is used. The 2^{-s} corresponds to the fraction part of the design.

If the response is non-linear, then the curvature is evaluated using a second-order model represented by Equation 3.17.

$$y = \beta_o + \sum_{i=1}^{k} \beta_i x_i + \sum_{i=1}^{k} \beta_{ii} x_i^2 + \sum_{1 \le i \le j}^{k} \beta_{ij} x_i x_j + \varepsilon \qquad (3.17)$$

where β_o, β_i, β_{ii}, and β_{ij} are regression coefficients for intercept, linear, quadratic and interaction coefficients respectively and x_i and x_j are coded independent variables. To estimate the parameters in the above equation, an experimental design has to be chosen that will provide sufficient data to estimate the β's. Among the more well-known second-order response surface designs, the central composite design (CCD) introduced by Box and Wilson [50] in 1951 is one of the most popular designs.

CCD is composed of three components: a factorial (cubic) design, a set of central points, and axial (star) points equidistant from the center point:

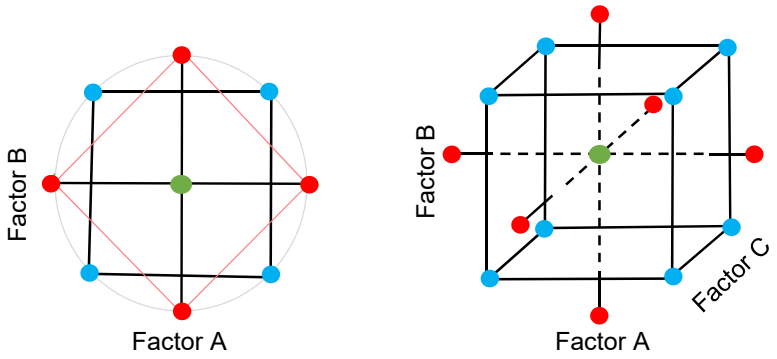

Figure 3.1: Central Composite Design for k = 2 and k=3

In the above diagram, the points in blue are a 2k factorial design, and the points in red are a star design.

The factorial (cubic) points of the CCD are the same as those of the full factorial (2^k) or fractional factorial (2^{k-s}) designs of the first-order system. Each of the variables is taken at two levels, meaning that each variable has a low and high numeric value. A coded numerical value of -1 and +1 is assigned to represent the variable's low and high values. These points are used primarily for the estimation of the linear terms, and the 2-way interactions. The geometric

representation of a factorial is a cube in which each corner represents an interaction of the factors. Thus for 3 independent variables, there will be 8 interactions [50].

The central point component in the CCD is the average of the high and low values determined in the factorial design. The center point contains information about the curvature of the surface and helps in the estimation of the quadratic terms. The center point runs are repeated 3 – 6 times and provide a good estimate of the experimental or pure error. If the center point runs indicate that curvature is significant then the researcher completes the design with the axial points.

The axial component of the CCD (also called the star points) refers to the points that are at an equidistance of α from the center of the cube formed for the factorial design. For a 3-factor design, they are located at (0, 0, ±α), (0, ±α, 0) and (±α, 0, 0). α-values depend on the number of variables and can be calculated by $\alpha = 2^{(k-p)/4}$. The axial points completes the estimation of the quadratic terms.

Using the CCD, second-order model, evaluated at 5 levels, the response surface, for 2 factors at a time, can represent maximum, minimum, ridge or saddle point, as shown in Figure 3.2.

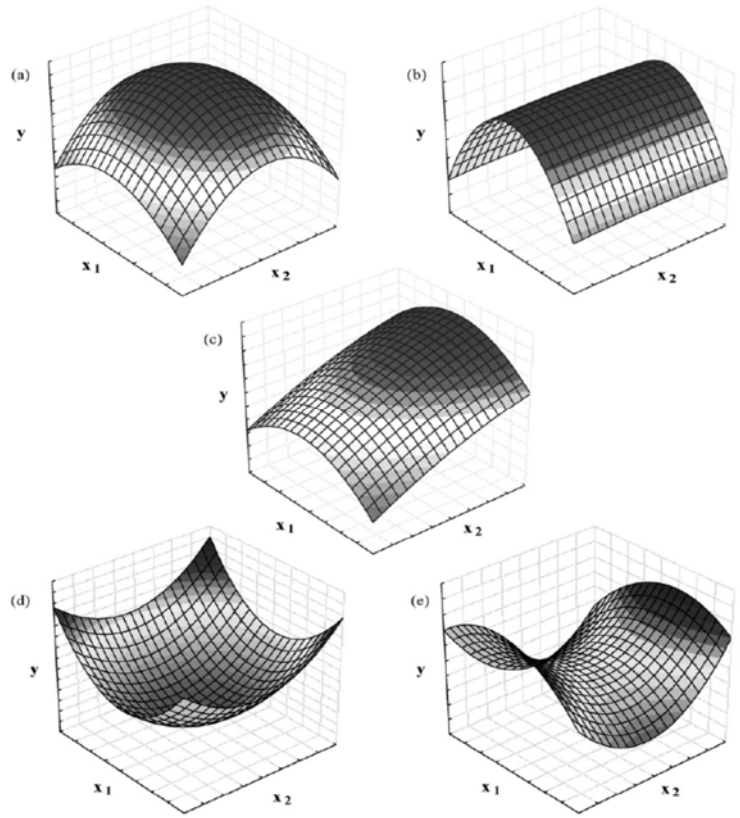

Figure 3.2: Outputs from Response Surface Methodology

The above graphs are helpful tools in understanding the surface of a response or the effects of single input variables on the response. However, when more than two independent variables are considered simultaneously (as in the actual situation), graphs are difficult or almost impossible to use to illustrate the response surface, since it is beyond 3-dimension. For this reason, response surface models are essential for analysing the unknown function f.

3.4.2.3) Prediction and Evaluation of Model Equation

After acquiring the necessary data, as per the selected design, it is necessary to fit a mathematical equation to describe the behavior of the response according to the levels of values studied. In other words, it is necessary to estimate values for the β parameters. The matrix notation of the second-order model equation is given by Equation 3.18.

$$\begin{bmatrix} y_1 \\ y_2 \\ . \\ . \\ . \\ y_n \end{bmatrix} = \begin{bmatrix} 1 & x_{11} & x_{12} & . & . & x_{1k} \\ 1 & x_{21} & x_{22} & . & . & x_{2k} \\ . & . & . & . & . & . \\ . & . & . & . & . & . \\ . & . & . & . & . & . \\ 1 & x_{n1} & x_{n2} & . & . & x_{nk} \end{bmatrix} \begin{bmatrix} \beta_o \\ \beta_1 \\ . \\ . \\ . \\ \beta_k \end{bmatrix} + \begin{bmatrix} \varepsilon_1 \\ \varepsilon_2 \\ . \\ . \\ . \\ \varepsilon_n \end{bmatrix} \tag{3.18}$$

The above system of equations can be solved using the method of least squares (MLS). MLS is a multiple regression technique used to fit a mathematical model to a set of experimental data whilst generating the lowest possible error or residual. In MLS, it is assumed that random errors are identically distributed with a zero mean and a common unknown variance and they are independent of each other. The difference between the observed response (y) and the fitted value ($\hat{y}$) for the i th observation is called the error or residual.

The mathematical model determined by solving the above equations does not always adequately represent the true system and an objective way of evaluating the quality of the fitted model is by the application of analysis of variance (ANOVA). By applying the analysis of variance, the contribution of each term in the regression and the statistical significance of the fitted model can be obtained. This is done by analyzing the magnitude of the sum of square (SS), mean square (MS), the Fischer test (F-test) and the lack-of-fit test (LOF). The ANOVA for model validation is given in Table3.1.

Table 3.1: ANOVA Table for fitted mathematical model to an experimental data set using multiple regression

Source of variation	Sum of squares	Deg. of freedom	Mean square
Regression	$SS_{reg} = \sum_{i}^{m}\sum_{j}^{n_i}(\hat{y}_i - \bar{y})^2$	p -1	$MS_{reg} = \frac{SS_{reg}}{p-1}$
Residual	$SS_{res} = \sum_{i}^{m}\sum_{j}^{n_i}(y_{ij} - \hat{y}_i)^2$	n - p	$MS_{res} = \frac{SS_{res}}{n-p}$
Lack of fit	$SS_{lof} = \sum_{i}^{m}\sum_{j}^{n_i}(\hat{y}_i - \bar{y}_i)^2$	m - p	$MS_{lof} = \frac{SS_{lof}}{m-p}$
Pure error	$SS_{pe} = \sum_{i}^{m}\sum_{j}^{n_i}(y_{ij} - \bar{y}_i)^2$	n - m	$MS_{pe} = \frac{SS_{pe}}{n-m}$
Total	$SS_{tot} = \sum_{i}^{m}\sum_{j}^{n_i}(y_{ij} - \bar{y})^2$	n - 1	

where n_i is the number of total observations;

m is the total number of levels in the design;

p is the number of parameters or coefficients of the mathematical model;

$\hat{y}_i$ is the estimated value by the model for the level i;

$\bar{y}$ is the overall mean;

y_{ij} are the replicates performed in each individual levels;

$\bar{y}_i$ are the means of replicates performed in the same set of experimental conditions.

SS_{reg} represents the sum of the squares of differences between values predicted by the regression and the grand average of all the response values. SS_{res} represents the sum of the squares of differences or residuals between all the experimental values and the predicted values from the model. Large SS_{reg} and small SS_{res} values describe models that accurately represent the experimental data [51]. The significance of regression can be evaluated by performing an F-test by comparing the ratio between the mean square of regression (MS_{reg}) and the mean square of residuals (MS_{res}) with tabled F value for p-1 and n-p degrees of freedom at the desired confidence, usually 95%.

$$\frac{MS_{reg}}{MS_{res}} \approx F_{p-1,n-p} \tag{3.19}$$

Thus, a statistically significant value for this ratio must be higher than the tabulated value for *F*. This is an indication that the mathematical model is well fitted to the experimental data.

The overall predictive capability of the model is commonly explained by the coefficient of determination (R^2), where $R^2 = SS_{reg}/SS_{tot}$. The value of R^2 lies between 0 and 1 and a value close to 1 indicates that most of the variability in y is explained by regression model. It should be noted that it is always possible to increase the value of R^2 by considering more regression variables, regardless of whether the additional variable is statistically significant or not. Therefore, an adjusted R^2 value is calculated using Equation 3.20.

$$R^2_{adj} = 1 - \frac{n-1}{n-p}\left(1 - R^2\right) \tag{3.20}$$

For a good model, values of R^2 and adjusted R^2 should be close to each other and they should also be close to 1 [52].

Another way to evaluate the model is the lack of fit test. SS_{pe} represents the sum of the squares of differences between all the individual experimental values and the average of the experimental values at the same level. SS_{lof} represents the sum of the squares of differences between the values predicted at each level and the average experimental value at that level. Regression lack of fit is determined performing an F-test by comparing the SS_{lof}/SS_{pe} ratio with the tabled F value for m−p and n−m degrees of freedom at the desired confidence level, usually 95%. If the calculated quotient is greater than the tabled value then it can be concluded that there is evidence of lack of fit and the model must be discarded. If not, the model can be accepted at this confidence level as providing an adequate representation of the data.

3.5) Performance of Flocculant

3.5.1) Introduction

Once a flocculant has been synthesised, it is necessary to test its efficacy in removing suspended solids from wastewaters. The main purpose of conducting flocculation tests in the laboratory is to determine the optimal conditions for the removal of these suspended colloids via floc formation and settling. The nature of these tests are determined by the end use of the results obtained. If the aim of flocculation process is to remove suspended solids from turbid water, then the optimum conditions might be judged in terms of minimum supernatant turbidity after sedimentation of flocs [53]. If, however, solids recovery is the main purpose, then settling rate could be the chosen parameter.

Ideally, a flocculation test procedure should simulate the operation of a full-scale industrial unit and be capable of predicting plant performance on the basis of laboratory trials [54]. In the

actual plant, the removal of suspended solids using polymer flocculants occurs through several stages. These steps are the addition of the polymer flocculant to the suspension, mixing, adsorption of the polymer to the suspended solids, rearrangement of adsorbed chains on the solids, and finally flocculation (Figure 3.3).

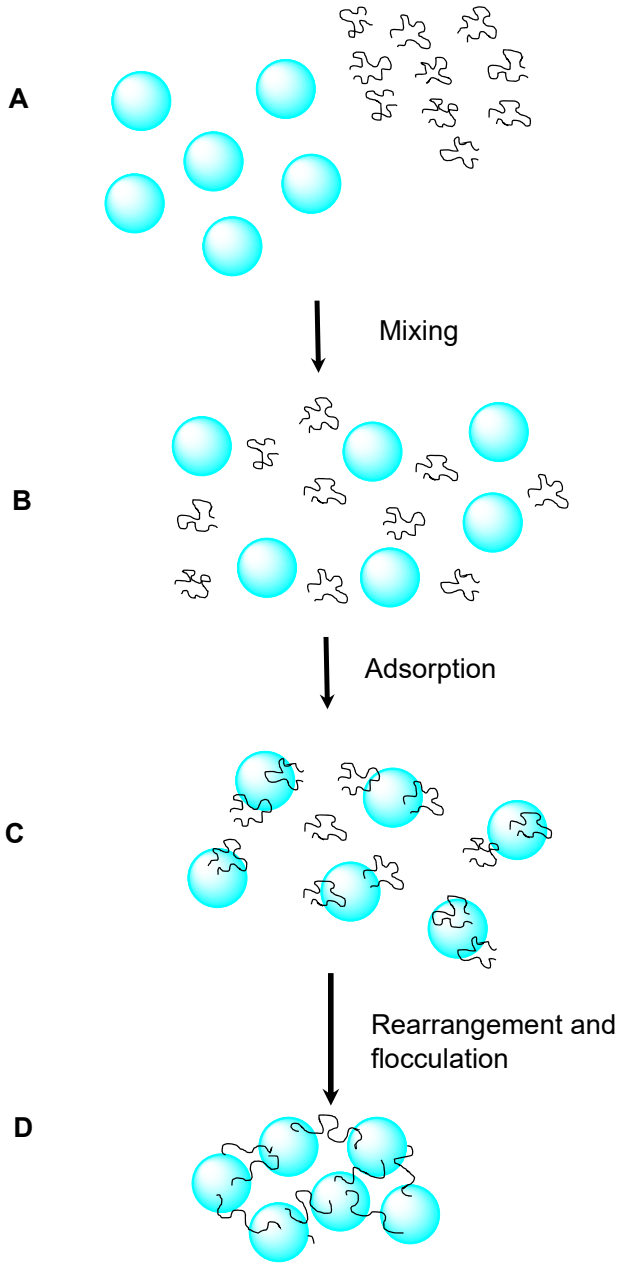

Figure 3.3: Steps in flocculation of suspended solids

Polymer flocculants are added to the suspension directly as powders or as concentrated solutions. These powders and viscous solutions do not readily disperse without mixing. During mixing the polymers begin to adsorb onto the surface of the suspended solids. Adsorption of

the polymer to the solids is a second-order reaction, the rate being proportional to the concentrations of the solids in solution and the polymer [55].

3.5.2) Equipment used to test flocculant

To test the performance of a flocculant, a laboratory jar test is normally carried out. The laboratory jar test is a simple and effective method that simulates the coagulation/flocculation process in an industrial treatment plant and is widely used for obtaining operating parameters and design conditions for water treatment plants. The laboratory apparatus that is generally used for assessing flocculation performance is the jar test apparatus (Figure 3.4).

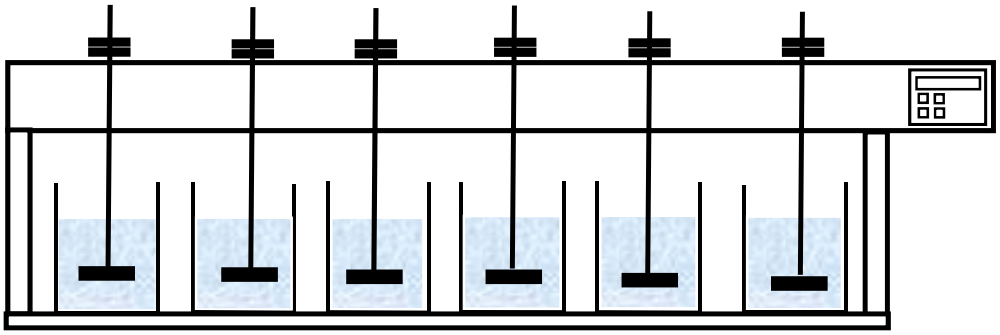

Figure 3.4: Laboratory jar test apparatus

The bench scale jar test apparatus consists of a series of standard 1000 -1500 mL beakers/jars and multiple stirrers with paddles all connected to a single variable speed motor to drive those stirrers. An equal volume of effluent wastewater is fed to each of the beakers/jars in which the jar test is to be performed. The stirrers are then lowered so that they are immersed in the wastewater. The operation of the jar test apparatus has to simulate what happens in the industrial treatment plant - the jar test apparatus puts the solution in the jars through a stirring program intended to mimic the flash mixing, flocculation, and settling unit operations of an actual treatment plant. In this regard, the mixing paddles are first run at high speed (75, 150, 225, or 300 rpm) to cause intimate mixing between suspended particles and flocculant for a specified duration, then at a slow-mix speed (10, 20, 30, or 40 rpm) for a specified duration to allow adsorption of flocculants onto suspended particles. After this time period, the paddles are withdrawn and the floc allowed to settle for a specified time period (0, 5, 10, 15, 20, 30, or 45 minutes).

A sample of the supernatant is then withdrawn and tested for clarity. Measurement of the supernatant turbidity is interpreted as an indicator of flocculant performance. Turbidity is the cloudy or opaque appearance of water caused by suspended solid particles. It is often used

as a general water quality indicator, particularly for clean water such as potable water. Ideally, a well-flocculated suspension should settle, leaving no suspended solids in the supernatant liquid and hence a very low turbidity. The apparatus used to measure the turbidity of the supernatant is the turbidity meter and turbidity values are expressed in terms of the nephelometric turbidity units (NTU). The principle of operation of this instrument is based on the well-known Tyndall effect. A beam of light passing through a turbid liquid being tested, scatters the light, which in turn, is collected at right angles by a photocell and is indicated on a digital display (Figure 3.5). The amount of scattered light is proportional to the turbidity of the solution under test.

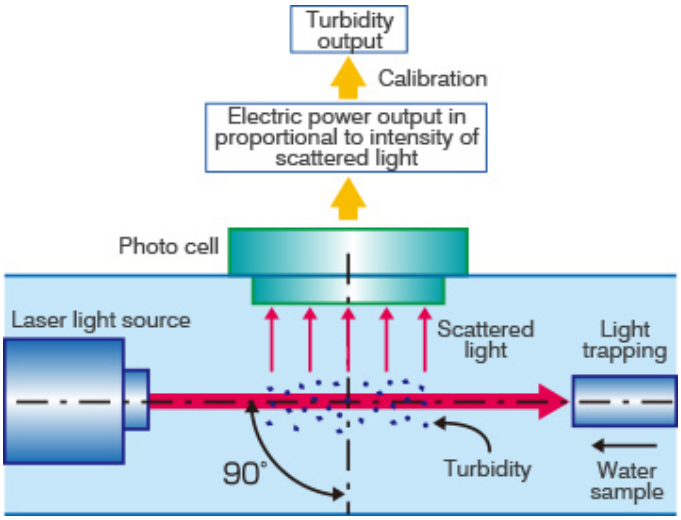

Figure 3.5: Operating principle of a turbidity meter

Another simple test which can be performed to determine the efficiency of a flocculant is the settling test [56]. It involves pouring the suspension, together with the flocculant, into a vertical cylinder and observing the rate at which the suspension settles under the influence of the flocculant. When a flocculant is introduced into the colloidal suspension, an interface or “mud line” begins to form. Above the interface is the clear supernatant liquid while below the interface is the suspension containing the contaminants. Under the action of the flocculating agent, i.e. along with the progress of the flocculation process, that interface descends with the colloidal particles until all contaminants are settled at the bottom of the cylinder. In this experiment the settling times are plotted as a function of the height of the interface. Curves of the interface height as a function of time are linear, except at the last stages of settling where the curves are concave. The linear parts of such diagrams provide information regarding the settling velocities which are used as a measure of the flocculant efficacy of a flocculant in a given suspension medium [56].

3.5.3) Wastewater

According to Rafael *et al*. [57]: “For an assay in which the performance of the flocculant is the object of study, rather than the “wastewater”, it is advantageous to use a wastewater that is very stable, so that changes that are observed (when adding the flocculant) are all attributable to the action of the flocculant and not confounded with changes that the wastewater would experience in the absence of the flocculant.” In line with this, researchers normally use simulated wastewater that is made by dissolving either kaolinite, bentonite, or iron ore in water to test the efficiency of a flocculant. Of these, kaolinite is the most widely used clay in the flocculation research area [58]. This is because the surface characteristics of kaolinite are sufficiently well understood to allow analysis and interpretation of sedimentation data in terms of particle–particle interactions. Also the turbidity of an unagitated suspension of kaolinite remains usable and essentially constant for extended periods of time and stock suspensions can be resuspended to the initial turbidity for at least 6 weeks after preparation. This is important because one can mix a large quantity of a single stock suspension and use it over many days, as opposed to making smaller quantities of fresh suspensions each day where small variations in concentration are bound to occur.

Kaolinite has the general formula $Al_2O_3 \cdot 2SiO_2 \cdot 2H_2O$ and is a two-layer mineral having two different basal faces. One layer is composed of a tetrahedral siloxane (silica) sheet of SiO_4 and the other an octahedral (gibbsite) sheet of $Al(OH)_6$. (Figure 3.6).

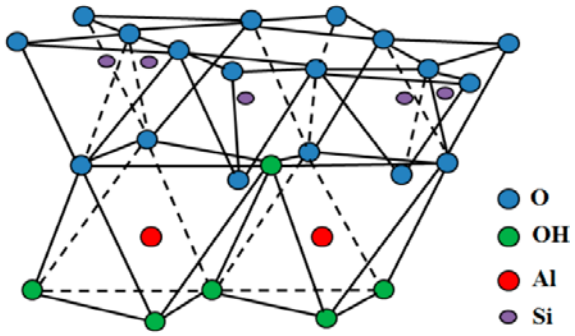

Figure 3.6: Molecular structure of kaolinite

Both the silica and gibbsite sheets combine to form a common layer such that the tips of the silica tetrahedral structure point towards the octahedral layer. The tetrahedral layer is inverted over the octahedral layer and both layers are held strongly together by shared oxygen atoms. Strong hydrogen bonds hold the layers together so that very little swelling occurs.

Kaolinite has a platelet structure with two different surfaces: two basal faces and an edge face. One basal face is made up of tetrahedral siloxane (–Si–O–Si–) species while the other consists of an octahedral, alumina (Al_2O_3) sheet. The basal face, while consisting of inert siloxane groups, carries a permanent negative charge as a result of isomorphous substitution of Si^{4+} by Al^{3+} groups [59]. This negative charge, although small, is responsible for the surface not being completely inert. At the edges of the kaolinite crystal, the octahedral alumina and tetrahedral silica sheets are disrupted/broken and exposes aluminol (Al–OH) and silanol (Si–OH) groups. The edge face may be charged as a result of protonation and deprotonation of the surface hydroxyl groups, depending upon slurry pH:

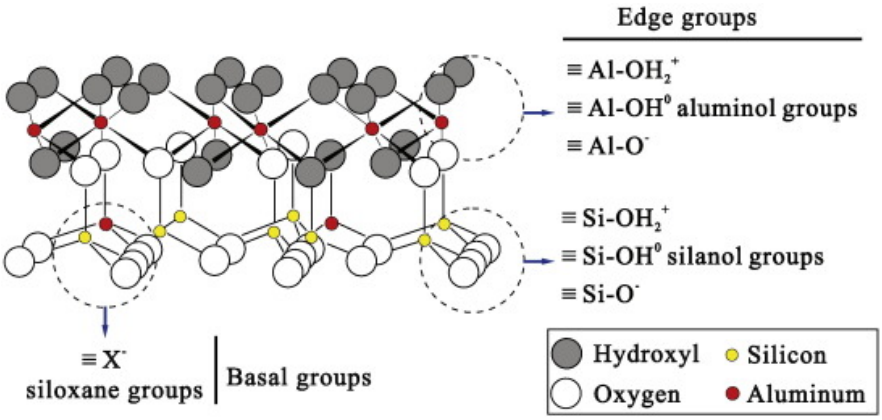

Figure: 3.7 Charge associate with kaolinite particle [59]

Due to its colloidal size, shape and permanently negatively charged basal faces, kaolinite tends to form a turbid and stable dispersion when it is dispersed in an aqueous medium. Thus the addition of a flocculant is required to induce settling of particles.

3.6) Experimental

3.6.1) Reagents and Glassware

The following chemicals were required for the synthesis of cellulose-*g*-polyacrylamide (Cell-*g*-PAM). The natural polymer, α-cellulose, was purchased from Sigma Aldrich (Germany) and was washed with water and then ethanol and vacuum dried at 60 °C to a constant weight before use. The monomer acrylamide, also from Sigma Aldrich, was recrystallized from acetone before use. Ceric ammonium nitrate (CAN) and hydroquinone were obtained from E. Merck, Germany and used as received. *N,N*-Dimethylformamide, acetone, and acetic acid, purchased from KIMIX (SA), used for extraction were reagent grade and used as received. Oxygen free nitrogen (Afrox, SA) was used for purging the polymerization solution. All solutions were prepared by deionized water from a Millipore Direct-Q 5 ultrapure water system.

The following chemicals were purchased for the flocculation tests. Kaolinite power, having a particle size range of 0.1 – 4 μm, was purchased from Sigma Chemicals and was used as received. Industrial flocculants: Magnafloc 351, Magnafloc 10, Magnafloc 380, and Magnafloc 4240 were purchased from BASF (SA). Hydrazine sulphate and hexamethylene tetramine, required to calibrate the turbidity meter were purchased from Sigma Aldrich (Germany).

All glassware were cleaned thoroughly before use. The vessels were first soaked in an alkali wash, rinsed with deionized water and left to stand in a dust-free cabinet. They were then dried in an oven prior to use.

3.6.2) Synthesis of graft polymer (Cell-*g*-PAM)

Grafting of acrylamide onto cellulose was performed by using CAN-HNO_3 as the initiator and was based on the method described by Lepoutre and Hui [60]. The synthesis procedure is shown in Figure 3.8.

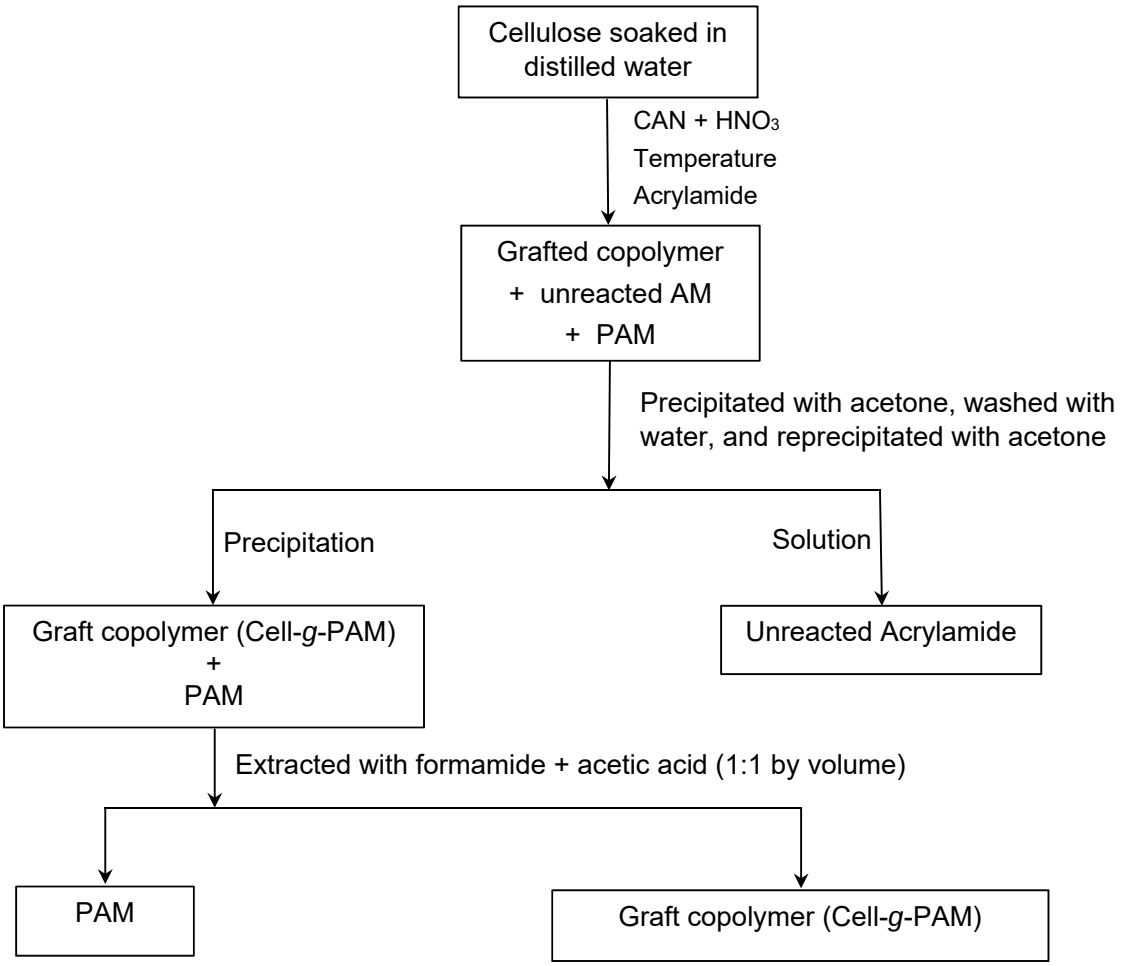

Figure 3.8: Procedure to synthesize and purify Cell-*g*-PAM

The various factors that affect the percentage grafting were identified and varied simultaneously using a factorial design template. The values of the various parameters are given Table 3.2. In all experimental runs, the mass of cellulose was held constant at 4 g (0.025 mol).

Table 3.2: Range of factors affecting graft polymerization of acrylamide onto cellulose

Independent variables	Units	Variable values				
Time	Hours	1	2	3	4	5
Temperature	°C	30	40	50	60	70
[AM] : [cellulose]	-	2	4	6	8	10
[CAN] : [cellulose]	-	0.02	0.065	0.11	0.16	0.2
[HNO_3] : [cellulose]	-	3	4.5	6	7.5	9

The graft copolymerization procedure was started by soaking 4 g (0.0246 mol) of cellulose in 70 mL of distilled water overnight in a 250 mL, three necked, round bottomed flask. The flask was then fitted with a reflux condenser, an oxygen-free nitrogen inlet line and an overhead stirrer and immersed in a constant temperature water bath. The reactor vessel was continuously purged with the supply of nitrogen throughout the reaction period. The water bath was set to the desired temperature (30 – 70 °C) and the contents of the reactor allowed to equilibrate to the desired temperature. After 30 minutes, a freshly prepared, 10 mL solution of CAN (4.9×10^{-4} – 4.9×10^{-3} mol) in nitric acid (0.07 – 0.22 mol) was added and stirred for a further 30 minutes. The required amount of acrylamide monomer (0.05 – 0.246 mol) was then dissolved in 20 mL distilled water and added to the reaction mixture. The grafting reaction was allowed to proceed for the desired time period (1 – 5 hours) with the zero time of the reaction being considered as the time of monomer addition. In all the reactions, total volume of the reaction was kept constant (100 mL). After the desired time period, the reaction was stopped by the addition of 1 mL of 2% hydroquinone solution to the reaction mixture.

At the end of the reaction, the reaction mixture may contain a small amount of unreacted acrylamide monomer. The reaction mixture was therefore poured into a 1L beaker, in which it was made into a homogeneous slurry with the addition of distilled water. The viscous slurry was then precipitated by the addition of an excess quantity of acetone. The precipitated product was filtered and dried overnight in a vacuum oven at 40 °C. The dried product from the above step was then extracted with a DMF : acetic acid mixture (1:1) for 24 h and washed with methanol to remove the homopolymer (polyacrylamide). The grafted cellulose (cell-*g*-AM) was finally dried to a constant weight under vacuum for 24 h at 40 °C.

The percentage grafting (%G) were determined from the increase in the weight of cellulose after grafting and is given by Equation 3.21.

$$\%G = \frac{\text{final cellulose weight - initial cellulose weight}}{\text{initial cellulose weight}} \times 100 \qquad (3.21)$$

3.6.3) Experimental Design and Statistical Analysis

The graft polymerization of acrylamide onto cellulose is affected by many variables as identified above. To determine the effect of each of these variables for all combinations of the other variables using the classical approach of changing one variable at a time will not only be time consuming, but will also ignore any possible interactions between the various variables. Hence, in this study, an alternate strategy of Response Surface Methodology (RSM)

was applied. The procedure involves carrying out the statistically designed experiments, evaluating the coefficients in a mathematical model, examining the adequacy of the model, and then describing the effects of the various parameters on the percentage grafting [61].

In this study, the effect of five variables: monomer to cellulose ratio, initiator to cellulose ratio, nitric acid to cellulose ratio, duration of reaction, and temperature of reaction, on the percentage grafting were investigated. Previous researchers [62, 63, 64] have reported on the effect of the absolute concentration of the various variables (substrate, monomer, and initiator system) on the graft copolymerization reaction. In the current research, however, the molar ratio of the above variables to cellulose was considered more appropriate than the absolute concentrations.

A Central Composite Design (CCD) was used to study the effects of the variables on the percentage grafting. This method is designed for fitting a quadratic surface and is used to optimize the effective parameters with a minimum number of experiments, as well as to analyze the interaction between the parameters. The central composite design, used throughout this study, pertains to the estimation of response surface following the general model equation (Equation 3.22).

$$y = \beta_o + \sum_{i=1}^{5} \beta_i x_i + \sum_{i=1}^{5} \beta_{ii} x_i^2 + \sum_{1 \le i \le j}^{5} \beta_{ij} x_i x_j + \varepsilon \qquad (3.22)$$

where y is the response (percentage grafting), β_o the value of the fitted response at the center point, and β_i, β_{ii}, and β_{ij} are the linear, quadratic, and cross-product (interaction) regression terms, respectively.

In this study a five-level-five-factor CCD was employed. The number of experimental runs was determined by Equation 3.23.

$$N = 2^{(k-s)} + 2k + n_c = 32 \qquad (3.23)$$

where k is the number of factors (5), s = 1 (corresponding to half factorial), and n_c, the number of center point replicates. In this experiment the fractional factorial design consisted of 16 factorial points, 10 axial points (two axial points on the axis of each design variable at a distance of 2 from the design center), and 6 center points. After doing preliminary experiments to determine the range of the various variables, the variables and their levels selected were: reaction time (2 – 6 h); synthesis temperature (30 – 70 °C); monomer amount (in mol) to cellulose ratio (2:1 – 10:1); ceric ammonium nitrate initiator (in mol) to cellulose ratio (0.02:1 – 0.2:1); and nitric acid (in mol) to cellulose ratio (3:1 – 9:1).

In line with factorial design, the variables were coded according to Equation 3.24.

$$X_i = \frac{x_i - x_{io}}{\Delta x_i} \tag{3.24}$$

where X_i is the independent variable coded value, x_i the corresponding independent variable actual value, x_{io} the independent variable actual vale on the center point and Δx_i is the step change value. The independent variables were coded using the above equation because their units differed from one another and although some of the parameters had the same units they were not in the same range. Since the parameters have different units and/or ranges in the experimental domain, the regression analysis could not be performed without first normalizing the parameters. Each of the coded variables is forced to range from -2 to 2, so that they all affect the response more evenly, and so the units of the parameters are irrelevant. The range of the independent variables and their levels are shown in Table 3.3.

Table 3.3: Experimental range and levels of the independent variables

Independent variables	Code	Units	Factor level				
			-2	-1	0	1	2
Time	X_1	Hours	1	2	3	4	5
Temperature	X_2	°C	30	40	50	60	70
[AM] : [cellulose]	X_3	-	2	4	6	8	10
[CAN] : [cellulose]	X_4	-	0.02	0.065	0.11	0.16	0.2
[HNO_3] : [cellulose]	X_5	-	3	4.5	6	7.5	9

A sequence of experiments for the CCD was generated by Design Expert Software (Stat-Ease Inc., Statistic made easy, Minneapolis, MN, USA, version 7.0.0) – see Table 3.4. The experiments were performed in random order to avoid systematic error. Each experiment involved a different combination of experimental data points for the five variables. Replications of factor combinations were necessary to estimate the experimental error, thus, the center point was run six times.

Table 3.4: Experimental design matrix for the synthesis of Cell-*g*-PAM

Standard Order	Run Order	Time	Temp	[AM]/[Cell]	[CAN]/[Cell]	[HNO_3]/[Cell]	%G
1	17	-1	-1	-1	-1	1	
2	9	1	-1	-1	-1	-1	
3	15	-1	1	-1	-1	-1	
4	20	1	1	-1	-1	1	
5	3	-1	-1	1	-1	-1	
6	18	1	-1	1	-1	1	
7	4	-1	1	1	-1	1	
8	22	1	1	1	-1	-1	
9	5	-1	-1	-1	1	-1	
10	31	1	-1	-1	1	1	
11	8	-1	1	-1	1	1	
12	1	1	1	-1	1	-1	
13	10	-1	-1	1	1	1	
14	28	1	-1	1	1	-1	
15	24	-1	1	1	1	-1	
16	25	1	1	1	1	1	
17	14	-2	0	0	0	0	
18	27	2	0	0	0	0	
19	12	0	-2	0	0	0	
20	26	0	2	0	0	0	
21	23	0	0	-2	0	0	
22	11	0	0	2	0	0	
23	16	0	0	0	-2	0	
24	7	0	0	0	2	0	
25	13	0	0	0	0	-2	
26	30	0	0	0	0	2	
27	21	0	0	0	0	0	
28	29	0	0	0	0	0	
29	2	0	0	0	0	0	
30	32	0	0	0	0	0	
31	19	0	0	0	0	0	
32	6	0	0	0	0	0	

Design Expert Software (Stat-Ease Inc., Statistic made easy, Minneapolis, MN, USA, version 7.0.0) will also be used to conduct regression and the analysis of variance (ANOVA) of the model equation. Analysis of variance will also be used to check the significance of each input variable for the response in the experiment. ANOVA calculates the Fishers F-ratio, which is the ratio between the regression mean square and the mean square error. If the calculated value of F turns out to be higher than the tabulated F-value, then the model will be concluded to be adequate at desired significance level α. In the current work the α-level is set at 0.05,

i.e. the confidence level is set at 95%. The ANOVA will also be performed to test the effect of linear, quadratic and interaction terms on the predicted responses.

Additional checks will also be done to determine the goodness of fit of the mathematical models by determining the coefficient of determination (R^2) and adjusted coefficient of determination (R^2_{adj}). The R^2 is the proportion of the variation in the dependent variable explained by the regression model. On the other hand, R^2_{adj} is the coefficient of determination adjusted for the number of independent variables in the regression model. For a good model, values of R^2 and R^2_{adj} should be close to each other and also they should be close to 1.

3.6.4) Flocculation Studies

3.6.4.1) Introduction

Flocculation studies of the optimally synthesized copolymer, Cell-*g*-PAM, as well as those of the commercially available flocculants were conducted with kaolinite suspension simulating the industrial effluent. The flocculant performance was determined using both the Jar Test as well as the Settling Test.

3.6.4.2) Turbidity Measurement

Before measuring the turbidity of test suspensions, the turbidity meter was calibrated with a standard formazin suspension. Formazin polymer is used as the reference turbidity standard suspension, because it is easy to prepare and is more reproducible in its light scattering properties than clay or turbid natural water.

The first step in the calibration procedure involved preparation of standard turbidity suspensions. For this, hydrazine sulphate [$(NH_2)_2 \cdot H_2SO_4$] (1 g) was dissolved in freshly prepared distilled water (100 mL). Hexamethylene tetramine, $(CH_2)_6N_4$ (10 g), was then dissolved in 100 ml of distilled water. 5 mL each of the above solutions was poured into a 100 mL volumetric flask and allowed to stand for 24 hours. The volume was then made up to 100 mL. This was a stock solution of 400 Nephelometric Turbidity Units (NTU). 10 mL of this stock turbidity suspension was diluted to 100 mL with distilled water and the turbidity of this suspension was defined as 40 NTU.

The following procedure was then used to calibrate the Turbidity Meter: (i) The calibration control was set to maximum. (ii) The measuring cell with distilled water was introduced into

the cell holder and was covered with the light shield. (iii) The set zero controls (both coarse and fine) were adjusted till the meter indicated zero reading. (iv) The cell was removed and the distilled water replaced with the standard solution of 40 NTU. Care was taken to align the cell properly with the marking on the cell holder. (v) The calibration control was now adjusted such that the turbidity of the standard solution (40 NTU) was shown on the digital panel meter. This position of calibration control was kept fixed for this range (0-40 NTU), unless a separate calibration was necessary for a different range (say 0-100 NTU).

3.6.4.3) Synthetic Wastewater Preparation

For all flocculation experiments, kaolinite power purchased from Sigma Chemicals and having a particle size range of 0.1 – 4 μm was used. The turbid water was prepared by mixing the kaolinite powder with tap water. The tap water had a Ca^{2+} and Mg^{2+} ion concentration of 11.8 mg/L and 1.32 mg/L respectively. A mass of 125 g of kaolinite powder was added to 50 L water, making up a 0.25% (w/v) suspension. The kaolinite suspension solution was then placed under slow stirring (20 rpm) for 1 hour, using an overhead stirrer, to ensure the uniform dispersion of the kaolinite particles. This suspension was then allowed to stand for 24 hours to complete the hydration of the kaolinite particles. Immediately prior to the Jar Test experiment, the suspension was again stirred at 50 rpm for 10 minutes to ensure uniformity.

From literature it is known that polyacrylamide based flocculants are sensitive to changes in pH [65]. At low pH values, the macromolecules coil up and they do not adsorb effectively on the kaolinite colloidal particles. Increasing pH to around 9 causes the macromolecules to uncoil and have a stretched conformation. This stretched conformation enables the bridging mechanism of flocculation and increases the flocculant performance. There is, however, another aspect of flocculation that comes into play on increasing the pH - the surface charge of the kaolinite particles become more negative whilst at the same time the anionic charge density of the flocculant also increases. There is thus a repulsion between the flocculant and the kaolinite particles, decreasing the flocculant efficiency. As a result, the optimum flocculation pH was defined by many authors as being around a neutral pH of 7. Therefore in the current research, the pH of the simulated wastewater was adjusted to a pH of 7 before testing of the flocculants.

3.6.4.4) Flocculants

The commercially available flocculants used in the experiments and their properties are shown in Table 3.5. The flocculants were supplied by BASF (South Africa) and were chosen based on their varying charge and molecular weights. The actual molecular weights, structures and compositions of the flocculants were considered proprietary information and not revealed by the manufacturer. Since they are also polyacrylamide based, they are taken for comparison purposes.

Table 3.5: Properties of commercial flocculants

Flocculant Name	Flocculant Type	Molecular Weight	Physical Form	Particle Size
Magnafloc 351 (Polyacrylamide)	Nonionic (linear polymer)	High molecular weight	Powder	98% < 1000 μm
Magnafloc 10 (Polyacrylamide)	Anionic (linear polymer)	Very high molecular weight	Powder	98% < 1000 μm
Magnafloc 380 (Polyacrylamide)	Cationic (linear polymer)	High molecular weight	Powder	98% < 1750 μm
Magnafloc 4240 (polyacrylamide)	Anionic (branched polymer) with UMA technology	High molecular weight	Powder	98% < 1000 μm

3.6.4.5) Jar Tests

All flocculation tests were carried out using a Phipps and Bird Six-Paddle Stirrer with illuminated base, model PB-7790910 jar test apparatus, Figure 3.9.

The Phipps and Bird Six-Paddle Stirrer has six 1.5 L square jars, called Gator Jars. Each Gator Jar is provided with a sampling port, located 5 cm above the base of the jar, which allows for repetitive sampling of the supernatant with minimal disturbance to the supernatant. The experiments were started off by adding 1000 mL of the prepared kaolinite suspension to each of the jars. The stirrers were lowered into the suspensions and the suspensions gently stirred at 5 rpm. In the first set of runs the performance of the synthesized copolymer (Cell-g-PAM) was tested. For this, six different masses (dosages ranging from 0.05 to 2.0 ppm) of the copolymer were added to the six different jars respectively. Immediately after the addition of the flocculant to the suspension solution, the solution needed to be thoroughly and vigorously

mixed so that the flocculant became fully dispersed in the entire suspension solution. The suspensions were therefore rapidly stirred at 125 rpm for 2 min to ensure that flash mixing occurred. At the end of this stage the slow mixing stage was initiated with the stirring paddles operating at 20 rpm for 15 minutes to allow complete agglomeration to take place. After the slow mixing period, the paddles were gently withdrawn from each of the jars and a 30 minute settling time was allowed for sedimentation to occur. This procedure was then uniformly applied to each of the other flocculants.

Figure 3.9: Phipps and Bird Six-Paddle Stirrer used for flocculation jar tests

Turbidity samples were obtained from the supernatant immediately following the settling stage. The turbidity measurements were done using the nephelometric method in accordance with Standard Methods No. 2130 (Standard Methods, 2005). A HANNA model HI88703 turbidimeter was used throughout the experiments. The procedure involved slowly drawing 10 mL of the supernatant into a glass cuvette for analysis. The cuvette was wiped clean with a disposable lens cloth and then gently inverted three times just before analysis in order to resuspend any particles that may have settled in the cuvette. The cuvette was then inserted into the turbidity meter and the turbidity determined and expressed in terms of nephelometric turbidity unis (NTU). Turbidity removal (%) was then calculated according to Equation 3.25.

$$\text{Percentage turbidity removal} = \frac{T_o - T_t}{T_o} \qquad (3.25)$$

where T_o is the turbidity of the suspension just before flocculant addition and T_t is the turbidity of the suspension at the end of the predetermined settling time (t) after the flocculant addition.

The jar test experiments were done in triplicate and the average of the obtained turbidities recorded.

3.6.4.6) Settling Test

After the jar tests, sedimentation tests were performed in order to determine the settling rate. The settling tests were performed by using a 1000 mL stoppered graduated cylinder having a height of 400 mm and an inner diameter of 50 mm – these dimensions were sufficient to avoid wall effects and to allow flocs to reach terminal velocity. Each sedimentation test began by adding 1000 mL of the prepared kaolinite suspension to a Gator Jar of the jar test apparatus. The stirrer was then lowered into the suspension and the suspension gently stirred at 5 rpm. The optimally determined dosage of the graft copolymer flocculant (Cell-g-PAM) from the previous jar test experiment was then added to the Gator Jar. Immediately after the addition of the flocculant to the suspension solution, the suspension was rapidly stirred at 125 rpm for 2 minutes to ensure that flash mixing occurred. The contents of the jar were then immediately transferred to the graduated cylinder up to a height of 400 mm. The suspension was further mixed by inverting the cylinder end-over-end 10 times and then placed upright in front of a diffuse light source. The descent of the solids/liquid interface (mud line) was carefully observed and recorded as a function of settling time. This procedure was then repeated for the other flocculants.

3.7) Results and Discussion

3.7.1) Percentage grafting of Cell-g-PAM

The actual values of the five variables, as well as composites of their combination sets are presented in Table 3.6. Also presented in Table 3.6 are the experimental values of the percentage grafting and the corresponding values predicted from the model.

Table 3.6: Experimental design matrix for the synthesis of Cell-*g*-PAM with results

Std Order	Run Order	Time	Temp	[AM] / [Cell]	[CAN] / [Cell]	[HNO_3] / [Cell]	%G (Actual)	%G (Predicted)
1	10	2	40	4	4.5	0.16	70.86	71.00
2	3	4	40	4	4.5	0.07	105.5	104.37
3	11	2	60	4	4.5	0.07	94.89	92.15
4	15	4	60	4	4.5	0.16	104.52	105.83
5	19	2	40	6	4.5	0.07	87.1	81.97
6	7	4	40	6	4.5	0.16	117.13	116.05
7	18	2	60	6	4.5	0.16	101.79	99.10
8	6	4	60	6	4.5	0.07	118.53	114.57
9	14	2	40	4	7.5	0.07	78.08	76.65
10	1	4	40	4	7.5	0.16	65.2	67.81
11	21	2	60	4	7.5	0.16	58.99	59.99
12	2	4	60	4	7.5	0.07	110.4	110.14
13	16	2	40	6	7.5	0.16	78.5	77.11
14	32	4	40	6	7.5	0.07	120.89	118.24
15	13	2	60	6	7.5	0.07	111.99	107.73
16	25	4	60	6	7.5	0.16	119.51	119.29
17	22	1	50	5	6	0.11	66.59	72.11
18	24	5	50	5	6	0.11	119.81	119.76
19	31	3	30	5	6	0.11	76.2	78.49
20	20	3	70	5	6	0.11	99.22	102.39
21	9	3	50	3	6	0.11	85.95	83.46
22	27	3	50	7	6	0.11	112.04	119.99
23	30	3	50	5	3	0.11	102.95	107.86
24	4	3	50	5	9	0.11	95.28	95.84
25	5	3	50	5	6	0.02	107.1	115.14
26	29	3	50	5	6	0.21	95.3	92.73
27	26	3	50	5	6	0.11	112.89	113.38
28	23	3	50	5	6	0.11	113.3	113.38
29	17	3	50	5	6	0.11	113.24	113.38
30	28	3	50	5	6	0.11	114.62	113.38
31	8	3	50	5	6	0.11	116.6	113.38
32	12	3	50	5	6	0.11	115.11	113.38

3.7.2) ANOVA analysis and fitting of quadratic model

It was previously stated that test for significance of the regression model, test for significance on individual model coefficients and test for lack-of-fit need to be performed. The analysis of variance (ANOVA) table is used to summarize the tests performed.

Table 3.5 gives a summary of relevant statistics for the model from Fit Summary of Design Expert.

Table 3.7: Model Summary Statistics

Source	Standard Deviation	R^2	Adjusted R^2	Predicted R^2	PRESS
Linear	11.0183	0.6962	0.6378	0.5657	4512.7384
2FI	11.2777	0.8042	0.6206	-0.4248	14805.4649
Quadratic	5.4267	0.9688	0.9121	0.8305	7996.2947
Cubic	4.4670	0.9885	0.9405	-10.4456	118935.0332

The predicted R^2 and adjusted R^2 values are important parameters to consider in determining how well the model can predict the %G responses. The predicted R^2 value predicts how well the model can predict the response while the adjusted R^2 value gives a measure of the amount of variation around the mean explained by the model. For the model to be statistically significant, the adjusted R^2 value and predicted R^2 value should be as high as possible and within approximately 0.20 of each other. As shown in Table 3.7, the quadratic model has higher R^2, adjusted R^2 value and predicted R^2 values than the other models. Further, in the quadratic model, the difference between the adjusted R^2 and predicted R^2 is 0.0816 – well lower than the 0.2 limit. The quadratic model was therefore chosen as the predictive model.

Table 3.8 below shows the ANOVA results of the quadratic model for percentage grafting of acrylamide onto cellulose.

Table 3.8: ANOVA of Response Surface Quadratic Model for Percentage Grafting

Source	Coeff	Sum of Squares	DF	Mean Square	F Value	Prob > F
Model		10067.39	20	503.37	17.0927	< 0.0001
A	12.01	3406.26	1	3406.26	115.6649	< 0.0001
B	5.98	856.82	1	856.82	29.0945	0.0002
C	9.13	2001.66	1	2001.66	67.9696	< 0.0001
D	-3.00	216.60	1	216.60	7.3550	0.0202
E	-5.60	753.54	1	753.54	25.5875	0.0004
A^2	-4.24	558.20	1	558.20	18.9544	0.0011
B^2	-5.76	964.70	1	964.70	32.7580	0.0001
C^2	-2.94	249.00	1	249.00	8.4552	0.0142
D^2	-2.91	243.90	1	243.90	8.2819	0.0150
E^2	-2.39	163.69	1	163.69	5.5583	0.0380
AB	-0.56	4.93	1	4.93	0.1674	0.6903
AC	0.87	12.04	1	12.04	0.4089	0.5356
AD	-0.16	0.42	1	0.42	0.0143	0.9068
AE	0.81	10.50	1	10.50	0.3565	0.5626
BC	-0.06	0.06	1	0.06	0.0020	0.9655
BD	1.19	22.75	1	22.75	0.7726	0.3982
BE	0.55	4.93	1	4.93	0.1674	0.6903
CD	4.34	301.37	1	301.37	10.2335	0.0085
CE	4.23	286.62	1	286.62	9.7328	0.0098
DE	-5.47	477.86	1	477.86	16.2265	0.0020
Residual		323.94	11	29.45		
Lack of Fit		313.78	6	52.30	25.7370	0.0013
Pure Error		10.16	5	2.03		
Cor Total		10391.33	31			

Std. Dev.	5.43	R-Squared	0.9688
Mean	99.69	Adj R-Squared	0.9121

The significant factors can be determined by considering the F-value or P-value (also named "Prob. > F" value). The larger the magnitude of F-value and correspondingly the smaller the P-value, the more significant is the corresponding coefficient [66]. Values of P less than 0.05 indicate that the model term is significant [67]. The ANOVA results indicate a Fisher's F-Test (F_{model} = 17.0927) with a very low probability value (P_{model} = 0.0001). This calculated F-value of 17.0927 needs to be compared with the critical F-value ($F_{0.05,\ df,\ (n\text{-}df\text{-}1)}$) for the considered probability (p = 0.05) and degrees of freedom. Since, the df for model is 20 and n = 32, it gives (n-df-1) = 11. Hence, the critical F-value ($F_{0.05,\ 20,\ 11}$ = 2.65) is less than the calculated F-value of 17.0927. This suggests that the computed Fisher's variance ratio at this level was large enough to justify a very high degree of adequacy of the quadratic model, implying that the model is significant [68].

The P-values are also used to determine the significance of each of the coefficients of the quadratic model - values of P less than 0.05 indicate significant terms [69]. In this work, the main effects of reaction time (A), reaction temperature (B), molar ratio of acrylamide to cellulose (C), molar ratio of nitric acid to cellulose (D), and molar ratio of ceric ammonium nitrate to cellulose (E) are all significant terms. The P-values of all quadratic effects (A^2, B^2, C^2, D^2, and E^2) are less than 0.05 and therefore also significant. With respect to the inter-effect terms, the inter-effect of acrylamide concentration and nitric acid concentration (CD), acrylamide concentration and CAN concentration (CE), and nitric acid concentration and CAN concentration (DE) are significant.

The mean square value of lack of fit for the model is 0.0013. This implies the lack of fit is not significant relative to the pure error, and hence the model is accepted [70].

The Post-ANOVA statistics given at the bottom of Table 3.8 shows that the R^2 value for the percentage grafting of acrylamide on cellulose is calculated as 0.9688. This value is close to 1 and implies that the sample variation of 96.88% for the %G is attributed to the independent variables, and only about 3.12 % of the total variation cannot be explained by the model. The high R^2 value also indicates that the accuracy of the modified quadratic model is good. The adjusted R^2 value for the modified model is 0.9121 is also high and close to the R^2 value. This means that the regression model provides an excellent explanation of the relationship between the independent variables and the response (%G).

After dropping the insignificant coefficients from the regression equation the final mathematical model was developed, which further added to the simplicity of use of the model. Based on the

above discussion, the quadratic regression model for the grafting percentage of acrylamide on cellulose is given by equation 3.26.

$$\begin{aligned} \%G = {} & +113.41 + 12.01\,A + 5.98\,B + 9.13\,C - 3.00\,D - 5.60\,E \\ & - 4.24\,A^2 - 5.76\,B^2 - 2.94\,C^2 - 2.91\,D^2 - 2.39\,E^2 \\ & + 4.34\,CD + 4.23\,CE - 5.46\,DE \end{aligned} \qquad (3.26)$$

As the accuracy and adequacy of the above model equation is vitally important in determining the main effects of the independent variables and the interactions between them, the adequacy of quadratic model was further checked. The diagnostic plots are shown in Figures 3.10 – 3.12.

Figure 3.10 compares experimental %G to the predicted values obtained from the model, Equation 3.26. A check on the plot reveals that the residuals generally fall on a straight line, implying that the errors are distributed normally. The agreement between the predicted and experimental values implies good accuracy of the model. Therefore, this model could be used to predict the percentage grafting of acrylamide on cellulose.

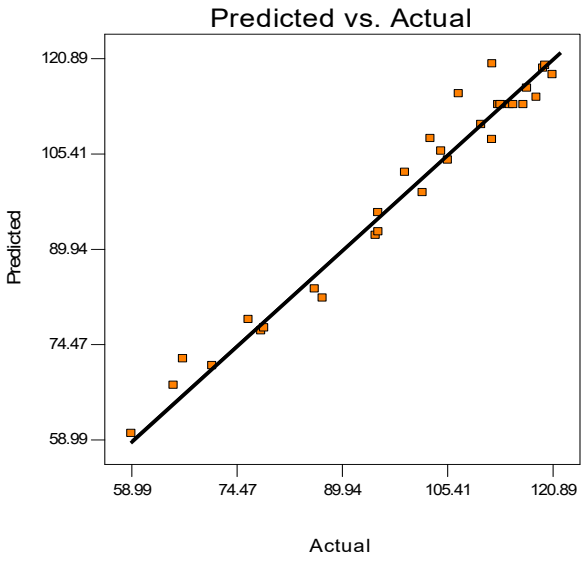

Figure 3.10: Plot of predicted vs. actual Percentage Grafting

In Figure 3.11, the normal % probability is plotted against internally studentized residuals. All points lie close to the straight line. This indicates that there are no serious violations in the quadratic assumptions that: (i) the errors are normally distributed and are independent of each other; (ii) the error variances are homogeneous and (iii) the residuals are independent.

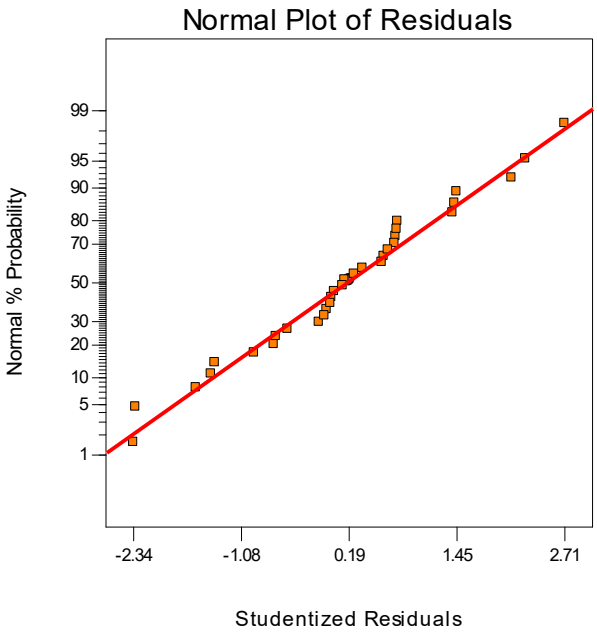

Figure 3.11: Normal plot of residuals for Percentage Grafting

Figure 3.12 reveals that the points are randomly scattered with no obvious pattern and unusual structure. This implies that the models proposed are adequate and there is no reason to suspect any violation of the independence or constant variance assumption. It can also be seen that all values lie within the range of −2.338 and 2.714 (values between −3 and +3 are considered as the top and bottom outlier detection limits).

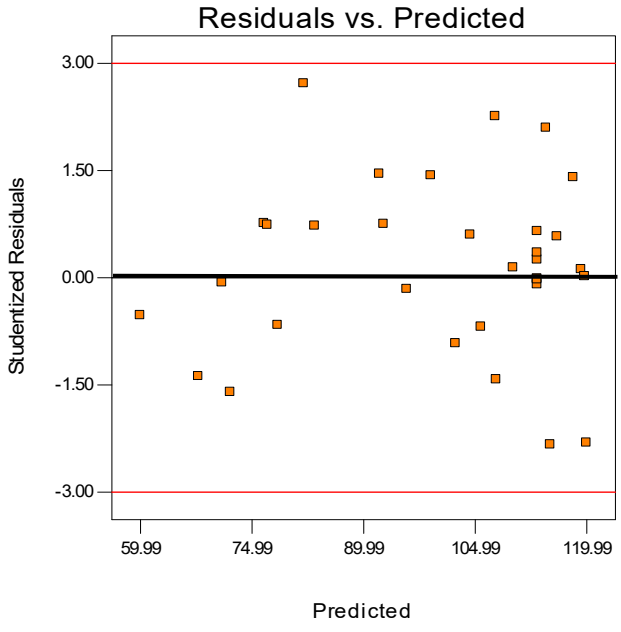

Figure 3.12: Plot of residual vs predicted response for percentage grafting

3.7.3) Effects of Process Variables on the Percentage Grafting

3.7.3.1) Introduction

To optimize the conditions for the grafting of acrylamide onto cellulose, the concentration of CAN, nitric acid, monomer, time and temperature were varied simultaneously. Since each of these polymerization variables influence the percentage grafting, it is important to determine the effect of each of these parameters individually (main effects) as well as their effects in combination with each other. The following sections discuss the effects of the various reaction conditions on the percentage grafting.

3.7.3.2) Main Effects

3.7.3.2.1) Effect of Time

With respect to the grafting of vinyl monomers onto cellulose derivatives, many researchers have shown that the grafting percentage increases with time and generally follow one of three curves as shown in Figure 3.13.

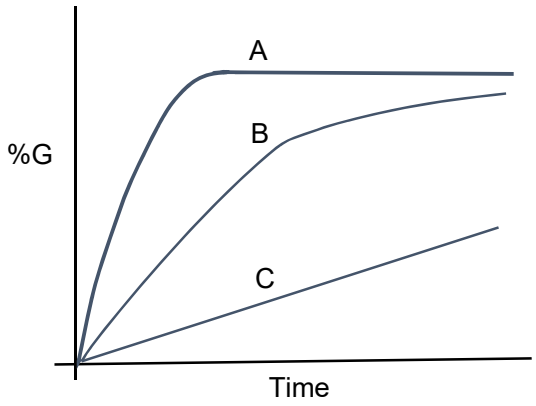

Figure 3.13: Typical curves of percentage grafting as a function of reaction time

The behaviour most often observed is curve A, where the percentage grafting eventually levels off with time. In curve B, although the percentage grafting continues to increase with time, the rate of grafting gradually decreases and an eventual levelling off can be predicted.

In the current research, the effect of time on the percentage grafting is shown in Figure 3.14.

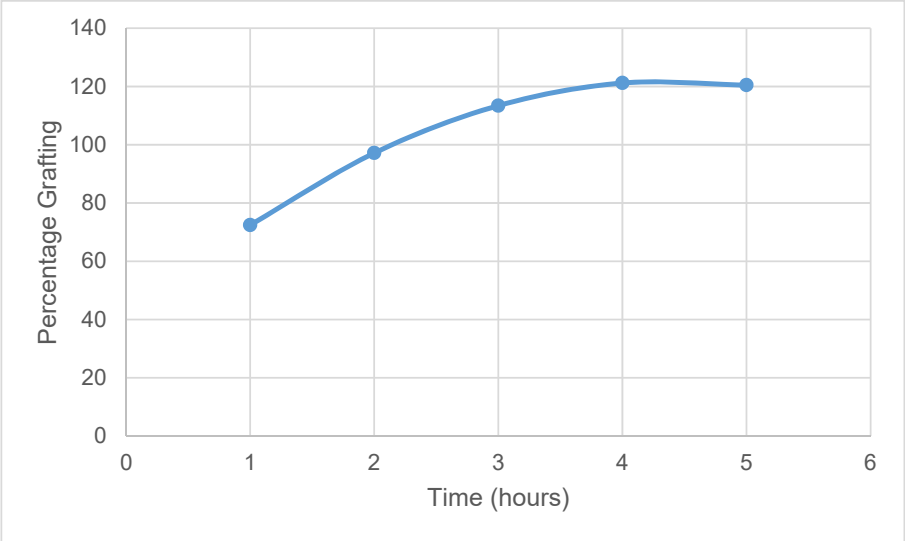

Figure 3.14: Effect of time on percentage grafting of acrylamide on cellulose

Preliminary experiments indicated that the reaction hardly begins in the first 30 minutes. Hence it can be said that, some induction period is involved in the grafting of acrylamide on cellulose during which grafting reaction does not take place. It can be seen from Figure 3.14 that the %G increases with increase in time up to 4 hours, reaching a value of 120%, after which it levels off.

Reaction time allows ceric solution to diffuse into the cellulose backbone prior to grafting reaction thereby allowing initiation of free radicals on cellulose sample by oxidation with Ce^{4+} ions. The increase in %G up to 4 hours may be accounted for by the increase in number of grafting sites on the cellulose backbone in the initial stages of reaction due to high rate of ceric ion participation in the formation of reactive sites.

The levelling off of the %G after 4 hours could be due to several factors acting simultaneously on the system. After 4 hours there is an overall decrease in concentration of the acrylamide monomers in the reaction mixture resulting in a decrease in the rate of reaction. After the optimum time there is a decay in the free radical activity of Ce^{4+} oxidized cellulose resulting from the free radical termination by charge transfer. Beyond the optimum time, most of the active sites on the cellulose backbone are been used and the formation of the homopolymer begin to dominate over graft copolymerization. In addition to this, as the reaction time gets longer, the reaction medium becomes more viscous and forms a gel-like latex, reducing the rate of diffusion of the monomer to the reactive sites. The steric hindrance offered to diffusing monomers by the already grafted chains also contribute in retarding the extent of grafting after 4 h of graft copolymerization.

3.7.3.2.2) Effect of Temperature

Temperature is one of the important reaction parameters that controls the extent of grafting. According to literature, various grafting behaviours were observed with increasing temperature. It was observed that the grafting percentage increased with increasing temperature [76, 77, 78, 79, 80, 81], decreased with increasing temperature [82, 83], and no change in grafting percentage with increasing temperature [84, 85, 86]. It was also widely observed that grafting percentage initially increased up to an optimum value and then decreased with further increase in temperature [87, 88, 89, 90, 91].

In the current research, preliminary experiments were conducted to determine the experimental range of the temperature parameter. It was found that below 20 °C practically no reaction took place while at 80 °C it was observed that some evaporation of the solution occurred. It was therefore decided to conduct the experiments in the 30 – 70 °C range while simultaneously varying the other parameters. The main effect of temperature on percentage grafting is shown in Figure 3.15. As shown in the figure, the %G increases with the rise in temperature from 30 to 55 ◦C, but decreases with further increase in temperature. The maximum %G of 115 was obtained at 55 ◦C. The changes in %G with temperature can be related to a variety of temperature dependent factors such as diffusion, adsorption of monomer onto the substrate, and changes in the rate constants of initiation, propagation, and (to a lesser extent) termination.

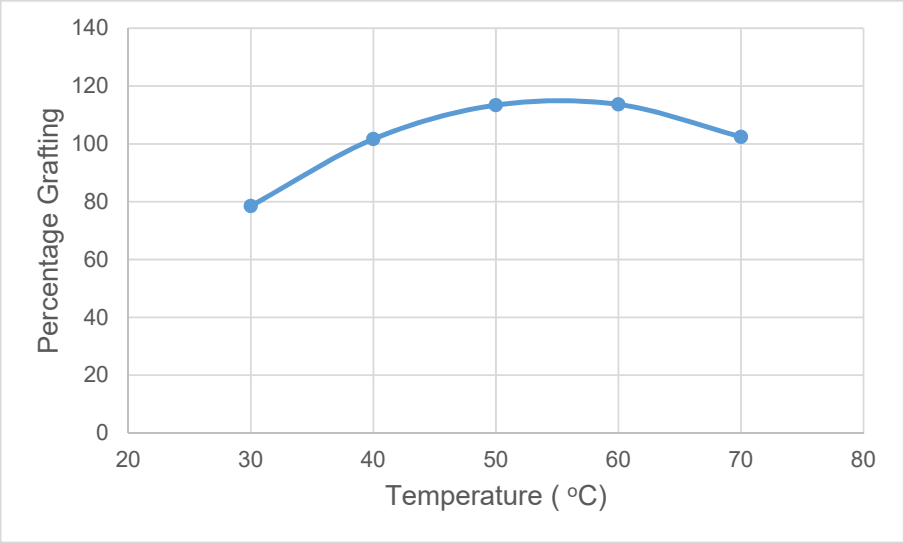

Figure 3.15: Effect of temperature on percentage grafting of acrylamide on cellulose

The initial increase in %G with increasing temperature can be ascribed to several factors acting simultaneously on the system. An optimum temperature is required for the

decomposition of the redox system. With increasing temperature there is an increase in the rate of thermal decomposition of the CAN redox system and consequently an increase in the generation of free radicals on the cellulose substrate. Increasing temperature imparts energy to the reaction system, enhancing the diffusion rate and consequently the mobility of both the initiator and acrylamide monomer to the active sites on the cellulose substrate. Enhanced energy also increases the collision rate of the initiator and acrylamide molecules with active sites on the growing copolymer chain, increasing the chances of a favourable reaction. The initial increase in %G may also be due to swelling of the cellulose substrate with increasing temperature and this helps in exposing the active sites on the substrate. The maximum graft yield occurs at 55 ^{o}C.

With further increase in temperature beyond the optimal value, the decrease in %G is most likely due to an increased probability of chain transfer, resulting in an increase in the amount of homopolymer being formed. Kulkarni and Mehta [92] proposed that at elevated temperatures, there is a rapid increase in the decay of free radical activity with increasing temperature.

3.7.3.2.3) Effect of Monomer Concentration

When determining the effect of monomer concentration on %G, most of the researchers used the absolute concentration of monomer as a variable in the graft copolymerization reaction. In the current research, however, the ratio of the moles of monomer (acrylamide) to substrate (cellulose) was chosen as the variable and varied between 2 and 10. This was done to enable scale-up of the optimized process.

Many researchers [93, 94, 95, 96] observed an increase in %G with increasing concentration of monomer and explained this behaviour to be in line with the kinetic equation (3.10). Their results showed the %G to be proportional to the square of the monomer concentration. Many other researchers [97, 98, 98] also observed an initial increase in %G with monomer concentration up to a certain value, beyond which there was a downward trend in %G.

In the current research the effect of monomer concentration on %G can be seen in Figure 3.16. It can be seen from the results of Figure 3.16 that as the acrylamide concentration increased, the %G increased in the initial stages up to 120%. With further increase in the acrylamide concentration the %G decreased. These observations are in line with many results cited in literature.

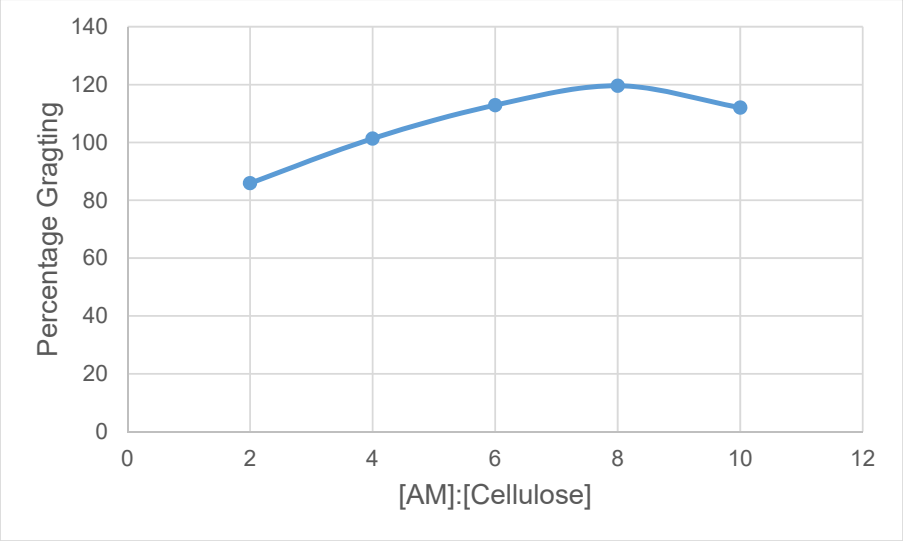

Figure 3.16: Effect of acrylamide to cellulose molar ratio on percentage grafting of acrylamide on cellulose

The initial increase in %G may be due to the higher availability of acrylamide monomer molecules in the vicinity of the active sites on the cellulose macromolecule with increasing concentration of the monomer. The subsequent decrease in %G on further increasing the monomer concentration is due mainly to an increase in chain transfer. Thus, more of the acrylamide monomer is preferentially used up in the formation of homopolymers than on copolymerization, on increasing the monomer concentration. The polyacrylamide homopolymers has the added effect of increasing the viscosity of the solution and hence reducing the diffusion of the monomers to the active sites on the cellulose macroradical and resulting in a lower percentage of grafting. The already growing acrylamide copolymer chains on the cellulose substrate cause steric hindrance which results in a retardation in the rate of graft copolymerization.

3.7.3.2.4) Effect of Initiator Concentration

The effect of initiator concentration on percentage grafting was examined by a number of researchers, with the most prevalent trend shown in Figure 3.17.

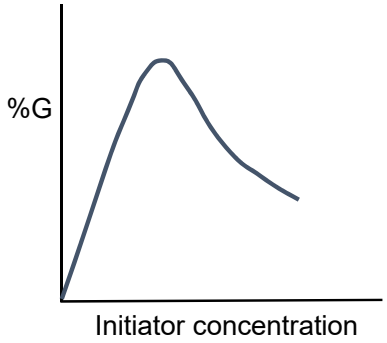

Figure 3.17: Typical curves of percentage graft as a function of initiator concentration [101]

The percent grafting was found to increase with the initiator concentration up to a maximum value after which there was a decrease in percent grafting [99, 100]. Other trends, such as: decreasing %G [101]; increasing %G [102]; increasing grafting with a levelling off [103]; and little change in grafting values [104] have also been observed.

In the current research, ceric ammonium nitrate was used as the initiator. The ceric ion- HNO_3 induced redox initiation system has been preferred for grafting acrylamide onto cellulose because the redox process initiates free radical sites mainly on the cellulose backbone, and this reduces the homopolymerization of acrylamide [105]. The [CAN]/[Cell] ratio was increased from 0.02 to 0.2 and the effect of increasing this ratio on percentage grafting is shown in Figure 3.18.

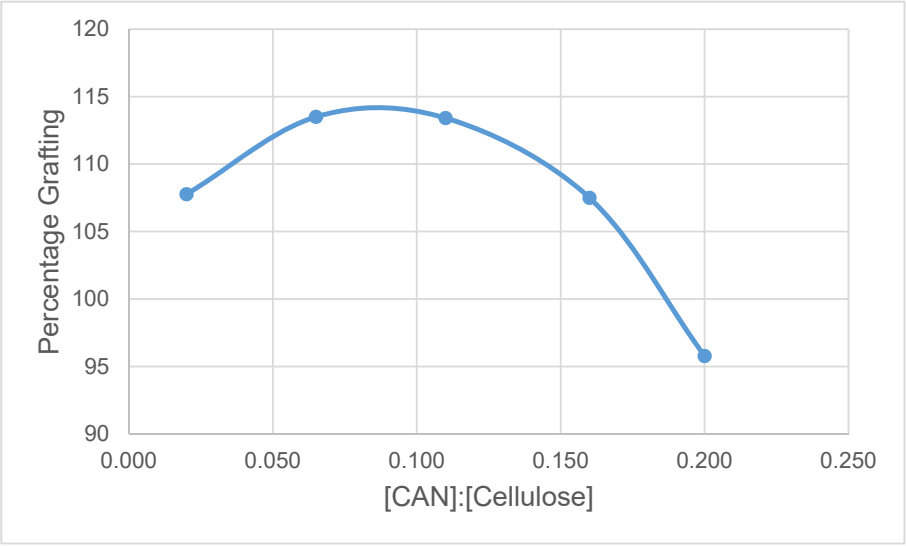

Figure 3.18: Effect of CAN to cellulose molar ratio on percentage grafting of acrylamide on cellulose

It can be seen from Figure 3.18 that the %G increases with an incease in initiator concentration and reaches a maximum value of 114% at a molar ratio of 0.08. Further increases in the initiator concentration is accompanied by a decrease in percentage grafting.

The initial increase in %G may be explained in terms of the mechanism of Ce^{4+} initiation which involves the formation of a chelate complex with cellulose that decomposes to generate free radical site on the cellulose backbone [106]. As the Ce^{4+} concentration increases, the number of active free radical sites on the cellulose backbone at which the acrylamide can be grafted also increases and these active free radical sites, in the presence of the acrylamide monomer, generate more graft copolymers [107].

When the initiator concentration is increased beyond what is required for maximum percentage grafting there is a decrease in the percentage grafting due to several reasons: (1) with higher concentrations of the initiator more and more polyacrylamide homopolymers are formed at the expense of the copolymers. This occurs since ceric ion is a very good oxidizing agent with high oxidation potential and it interacts with acrylamide, forming polyacrylamide rather than the graft copolymer at high concentrations [108]. (2) at higher concentrations of the initiator the ratio of nitric acid to CAN decreases and this results in a hydrated form of Ce^{4+} ions, $[Ce\text{-}O\text{-}Ce]^{6+}$, being produced. This hydrated form is not able to produce active sites onto the cellulose backbone thus reducing the generation of copolymers – this will be discussed in more detail when discussing the effect of nitric acid on percentage grafting. (3) the Ce^{4+} ions start participating in oxidative termination of the growing chains of the copolymer, and this could result in chain transfer reactions.

3.7.3.2.5) Effect of Nitric Acid Concentration

Previous research [109] on the effect of acid concentration on the percentage showed the general trend indicated in Figure 3.19.

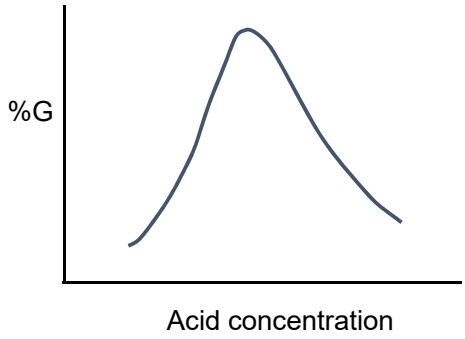

Figure 3.19: Typical curves of percentage graft as a function of acid concentration [109]

Other trends with increasing acid concentration reported also include: (1) decreasing percentage grafting [110]; (2) increasing grafting [111]; and no influence [112].

In the current research the effect of [HNO_3]/[Cell] ratio on the percentage grafting is shown in Figure 3.20.

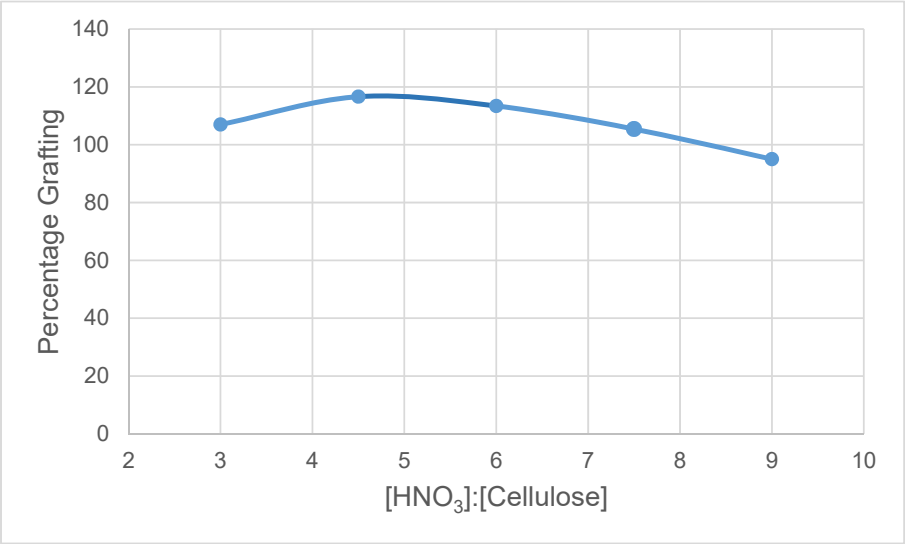

Figure 3.20: Effect of HNO_3 to cellulose molar ratio on percentage grafting of acrylamide on cellulose

The ratio of [HNO_3]/[Cell] was varied between 3 and 9. It is observed that, initially, increases in nitric acid concentration in the reaction mixture led to enhanced percentage grafting. A critical concentration of nitric acid to cellulose concentration of 4.3, which permits the maximum percent grafting of 118%, may be also observed. Further increases in the acid concentration results in a decrease in the percentage grafting.

The observed initial increase in percentage grafting with increasing HNO_3 concentration may be explained as follows: In an aqueous medium, Ce^{4+} is believed to combine with water in the following manner [113]:

$$Ce^{4+} + H_2O \rightleftharpoons [Ce(OH)_3]^{3+} + H_2^+ \quad (3.27)$$

$$2\,[Ce(OH)_3]^{3+} \rightleftharpoons [Ce-O-Ce]^{6+} + H_2O \quad (3.28)$$

Thus in aqueous medium, CAN exists as Ce^{4+}, $[Ce(OH)]^{3+}$ and $[Ce–O–Ce]^{6+}$ ions. Due to their large size, $[Ce(OH)]^{3+}$ and $[Ce–O–Ce]^{6+}$ ions are not able to form complexes with the cellulose substrate. With increasing HNO_3 acid concentration, however, equilibria (3.27) and (3.28) shifts towards the formation of more Ce^{4+} at the expense of $[Ce\text{-}O\text{-}Ce]^{6+}$ and $[Ce(OH)]^{3+}$. Ce^{4+}

ions, being smaller in size, are more effective in forming complexes with the cellulose substrate molecules and thus results in a higher percentage of grafting.

A decrease in the grafting percentage beyond the optimum could be attributed to the generation of higher concentrations of $Ce^{4+}$and $[Ce(OH)]^{3+}$ with increasing concentrations of HNO_3. These species, at higher concentrations of HNO_3, affect the copolymerization negatively – instead of propagating the polymeric chain, these species affect the termination steps and thus reduce the percentage grafting. In addition to this, the increased concentration of nitric acid may result in hydrolysis of the cellulose substrate [114]:

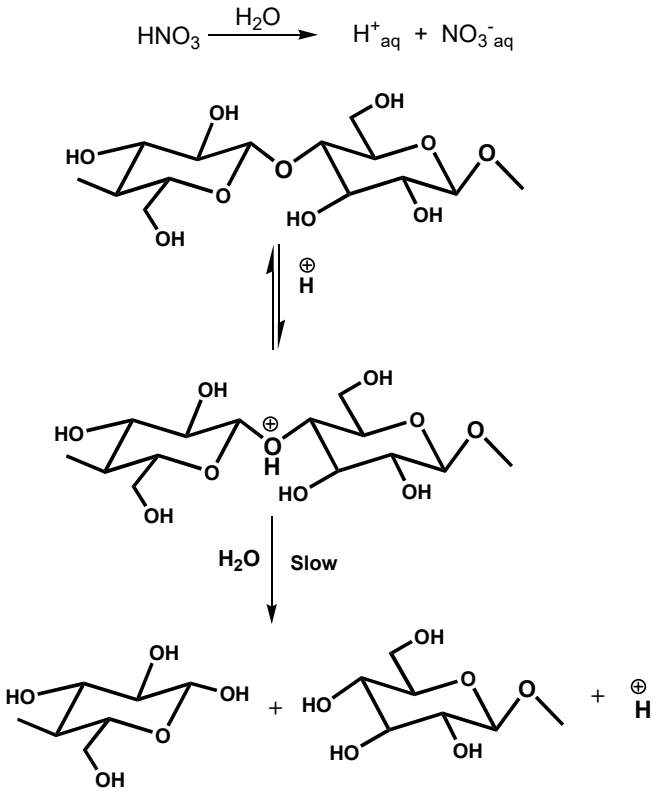

Scheme 3.4: Hydrolysis of cellulose due to increased HNO_3 concentration [114]

3.7.3.3) Interactive Effects

In addition to the main effects, the percentage grafting (%G) is also influenced by the interaction effects between the various input variables. Interaction effects mean that certain combinations of input factors significantly influence the response, and there is a difference in the effect of one factor when a second factor is changed from one level to another. Statistical analysis of the results (Table 3.8) shows the existence of significant interaction effects

between some of the input parameters. The study of these interaction effects helps in gaining more understanding about the behaviour of the copolymerization process. As the interaction of several variables simultaneously becomes extremely complicated to analyze, it was decided to include only two way interactive effects for the present study. Three-dimensional response surfaces were plotted to investigate the interaction among the input variables. To prepare these surfaces, only interaction terms found to be significant at $P \leq 0.05$, were considered. The interaction effect between acrylamide concentration and initiator concentration (C-D), acrylamide concentration and nitric acid concentration (C-E), and initiator concentration and nitric acid concentration (D-E) are significant in the copolymerization process and are discussed in the following sections. When analyzing the interactive effects of two factors on the response, the other factors were maintained at their central (0) levels.

The combined effect of acrylamide to cellulose ratio (C) and CAN to cellulose ratio (D) on the percentage grafting at a constant reaction time of 3 hours, constant temperature of 50 °C, and constant nitric acid to cellulose ratio of 6 is presented in Figure 3.21.

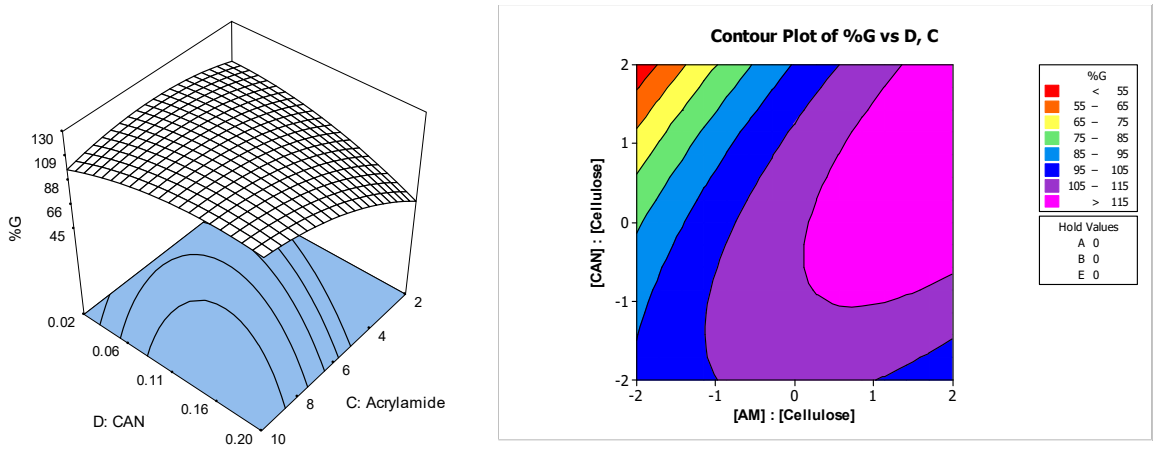

Figure 3.21: Response surface plot and contour plot showing the effect of acrylamide and initiator concentration on percentage grafting

As shown in Table 3.8, the effect of the interactions between acrylamide to cellulose ratio (C) and CAN to cellulose ratio (D) on the percentage grafting (%G) are positive effects. A synergetic effect of these process variables are observed in Figure 3.21. A high percentage grafting (greater than 120%) is obtained at higher acrylamide concentrations and higher initiator concentrations while low percentage grafting occurs at reversed operating conditions. As shown in Figure 3.21, at the lower acrylamide to cellulose molar ratio (C) of 2 the percentage grafting was influenced by change in the levels of molar ratio of CAN to cellulose (D) and as factor C was increased to a higher level of 10, the percentage grafting attained a

maximum value of 123%. As the ratio of acrylamide to cellulose was always in excess of that required stoichiometrically, the lower percentage grafting at the lower levels of both factors C and D can be attributed to fewer active sites being generated on the cellulose backbone by the CAN initiator. At the higher levels of both factors C and D, the higher percentage grafting is due to higher availability of the acrylamide monomers as well as more active sites being generated on the cellulose backbone by the higher concentration of CAN. Also significant is that the effects of steric hindrance and homopolymer formation is reduced at the higher levels by the combined effect of factors C and D acting together when compared to their individual (main) effects.

Figure 3.22 shows the 3-D plot of the interaction between acrylamide to cellulose molar ratio (C) and nitric acid to cellulose molar ratio (E) and their combined effect on the percentage grafting. The reaction time, temperature, and CAN to cellulose molar ratio was fixed at 3 hours, 50 °C, and 0.11 respectively.

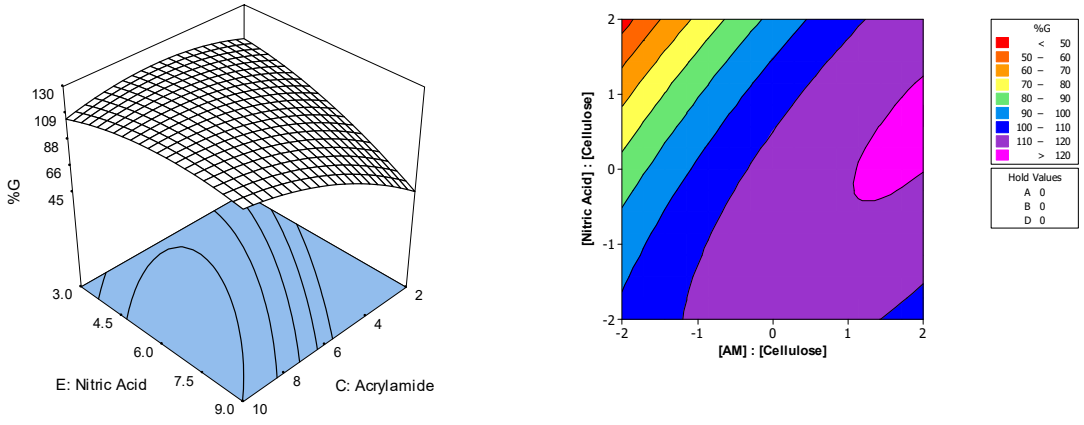

Figure 3.22: Response surface plot and contour plot showing the effect of acrylamide and nitric acid concentration on percentage grafting

A quadratic effect of both variables is observed, but acrylamide to cellulose molar ratio has a greater influence on the percentage grafting than the nitric acid to cellulose molar ratio. The effect of nitric acid to cellulose ratio on the percentage grafting was influenced by the level of acrylamide to cellulose molar ratio. At the lower level of acrylamide to cellulose molar ratio (2) there was a monotonic increase in grafting percentage with increase in nitric acid to cellulose molar ratio. The maximum grafting percentage obtained was 121% and this was achieved at an acrylamide to cellulose molar ratio of 10 and a nitric acid to cellulose molar ratio of 7. When factor C was maintained at its high value of 10, the percentage grafting firstly increased from 105.8 % to the maximum value of 121% and then decreased to 116.9% with increase in nitric acid to cellulose molar ratio.

The combined effect of CAN to cellulose molar ratio (D) and nitric acid to cellulose molar ratio (E) on the percentage grafting at a constant reaction time of 3 hours, constant temperature of 50 °C, and constant acrylamide to cellulose ratio of 6 is presented in Figure 3.23.

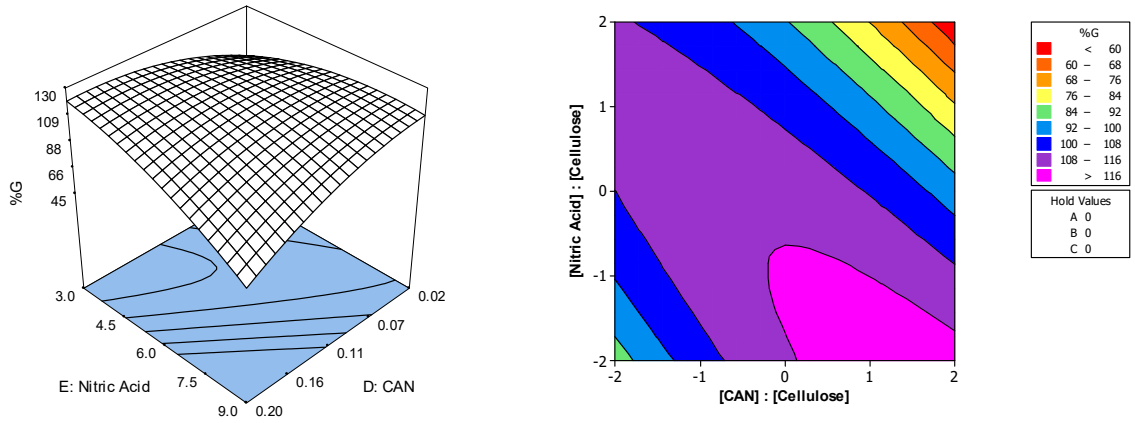

Figure 3.23: Response surface plot and contour plot showing the effect of CAN and nitric acid concentration on percentage grafting

As shown in Table 3.8, the effect of the interactions between CAN to cellulose ratio (D) and nitric acid to cellulose ratio (E) on the percentage grafting (%G) are negative effects. A suppressive effect or interplay of these process variables are also observed in Figure 3.23. At a low value of factor D (0.02), increasing the molar ratio of nitric acid to cellulose increases the percentage grafting but a high value of factor D (0.2), increasing the molar ratio of nitric acid to cellulose causes a steady decrease in the percentage grafting. The highest percentage grafting of 119.8% was obtained at the lowest level of nitric acid to cellulose ratio of 3 and a high CAN to cellulose molar ratio of 0.17. The interaction between the nitric acid concentration and the initiator concentration and their effects on the percentage grafting was explained in detail when discussing their partial effects.

3.8) Results of Flocculation Tests

The performance of the newly prepared Cell-*g*-PAM graft copolymer flocculant along with four commercially available flocculants are presented in Figure 3.24.

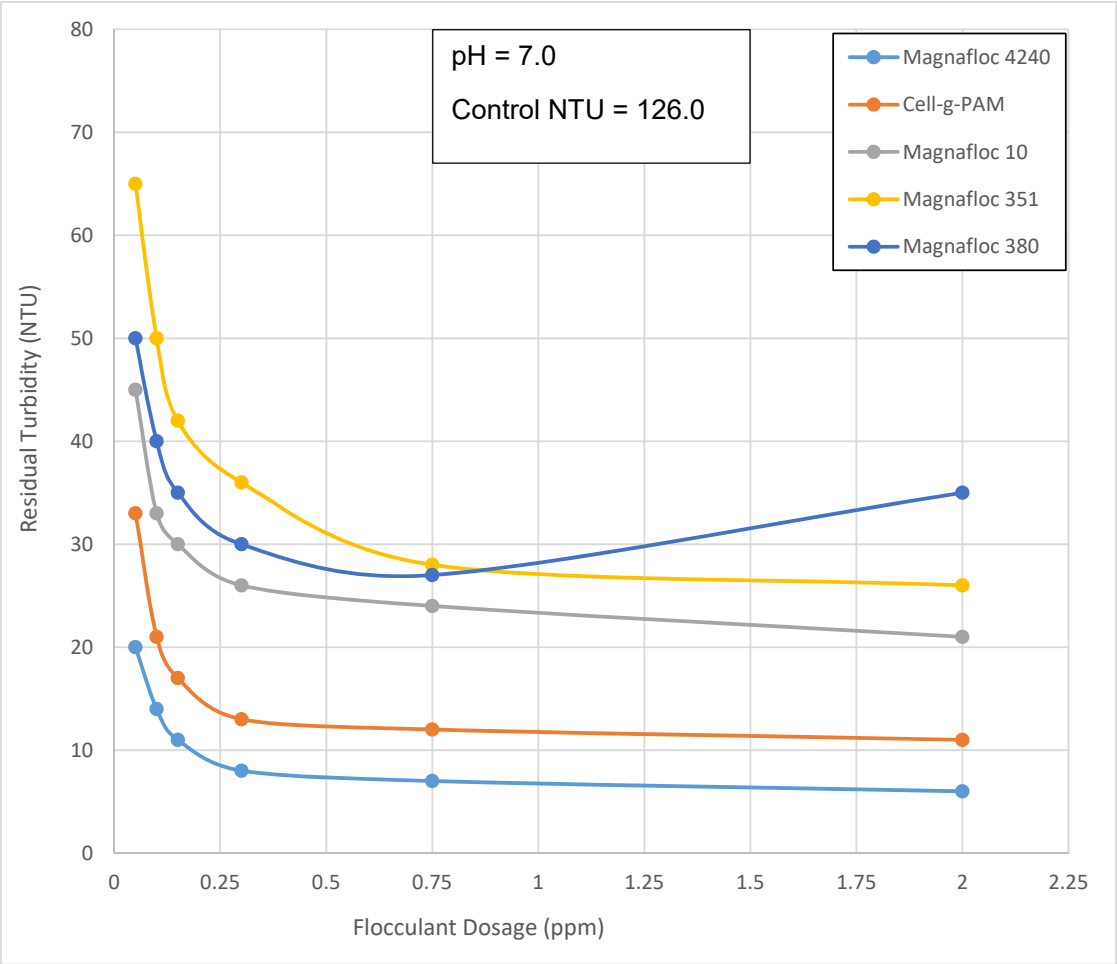

Figure 3.24: Jar test results in 0.25% (w/v) kaolinite suspension

Figure 3.24 shows the relationship between the residual turbidity of the kaolinite suspension and the concentration (dosage) of the flocculants. The flocculating abilities of the polymers were tested on a 0.25% (w/v) kaolinite suspension (in jar test apparatus) for dosages varying from 0 ppm (control) to 2.0 ppm. All results were obtained under the following conditions: a pH of 7.0, rapid mixing speed of 125 rpm for 2 minutes followed by a slow mixing speed of 20 rpm for 15 minutes, and a settling time of 30 minutes.

All polymers gave better flocculation performance than the natural, ungrafted cellulose at the low dosages applied – the turbidity of the suspension hardly changed from its original value of 126 NTU. All flocculants showed similar trends with respect to their flocculating abilities: Initially, even a very small dosage of the flocculants (as little as 0.25 ppm) caused a drastic drop in turbidity. Further increases in the flocculant dosage caused further, but slower reduction in the residual turbidity. The results also indicate that the dosage of cationic polymer flocculant (Magnafloc 380) exhibits an optimum flocculation beyond which the suspension

appears to restabilize. The nonionic and anionic flocculants (Magnafloc 351 and Magnafloc 10) show no such effect.

Interaction and flocculation of the kaolinite particles by organic polymer flocculants can occur by polymer bridging, charge compensation or neutralisation, polymer–kaolinite particle surface complex formation by a combination of these mechanisms [115].

For the non-ionic Magnafloc 351 – kaolinite system, polymer bridging between the flocculant and the kaolinite suspension particles is the dominant mechanism of flocculation. For bridging to occur, segments of the nonionic polymers need to firstly simultaneously adsorb onto different kaolinite particles. The nonionic Magnafloc 351 can adsorb onto the kaolinite particles through hydrogen bonding, hydrophobic interaction, and through ion-dipole interaction. These interactions are illustrated in Figure 3.25.

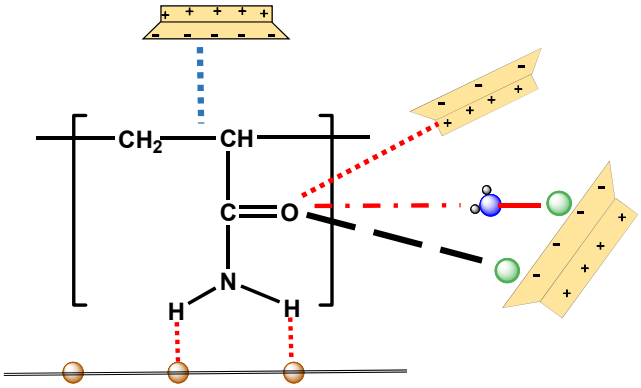

Figure 3.25: Possible interactions between kaolinite and nonionic polyacrylamide

In organic polymer flocculants, when hydrogen atoms are bonded to strongly electronegative atoms such as O, S, or N, the hydrogen atoms are able to accept electrons from atoms on the solid surface to form hydrogen bonds. In the case of the nonionic Magnafloc 351, the hydrogens of the amide group are able to attach themselves on the edge face of the kaolinite particles by forming hydrogen bonds with –OH groups of the aluminol and silanol groups. With the Magnafloc 351 – kaolinite system, the H of the aluminol group (Al-OH) on the edge face also bonds to the carbonyl (C=O) oxygen of polyacrylamide through hydrogen bonding. In the Magnafloc 351- kaolinite system, hydrophobic bonding between the hydrophobic backbone (CH_2–CH) of Magnafloc and the hydrophobic basal face (uncharged sites on the siloxane face) also takes place. The attraction of non-polar groups for each other is minimal and therefore plays only a minor role in the adsorption process. The surface of each kaolinite particle is negatively charged and therefore attracts and adsorbs positively charged cations. When water

is added to kaolinite, these cations move into solution but are still attracted to the kaolinite particle. These exchangeable cations on the kaolinite surface form bridges with the carbonyl oxygen (C=O) of Magnafloc 531 through ion-dipole interactions. In addition to these interactions, water molecules present in the solution also aid in attaching the kaolinite particle to the flocculant – the water molecules form bridges with the exchangeable cations and carbonyl oxygens through hydrogen bonding while at the same time forming bridges with exchangeable cations through ion-dipole interactions. Each of the above adsorption forces are weak forces and allows the Magnafloc polymer to expand and form loops and tails which then adsorb onto other kaolinite particles in the solution.

The flocculation of negatively charged fine particles by cationic polyacrylamide occurs by the adsorption of the PAM polymer chains on to the particle surface [116]. In cationic flocculation, charge neutralisation is the major mechanism, where the cationic PAM firstly neutralizes and then, if excess PAM is added, may reverse the particle surface charge. Collision with negative patches on neighbouring particles enable bridging and then flocculation to occur [117]. In this mechanism, Coulombic attraction forces are the dominant bonding mechanism between the kaolinite surface and cationic PAM molecules [118]. In the flocculation test carried out above, the positively charged trimethyl ammonium groups of cationic Magnafloc 380 PAM were attracted to the negatively charged sites along kaolinite particle surface, as shown in Figure 3.26.

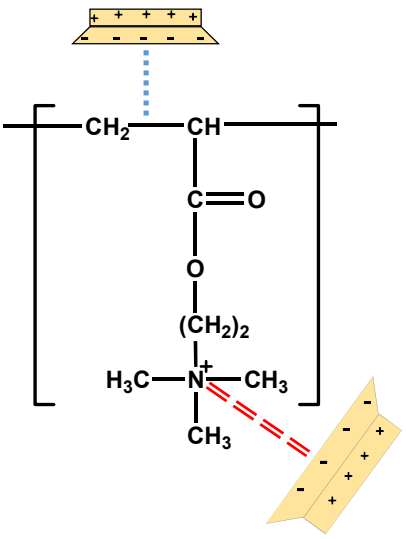

Figure 3.26: Possible interactions between kaolinite and cationic polyacrylamide

The critical coagulation concentration (CCC) is defined as the minimum concentration of counterions required to induce coagulation of the colloidal particles. At the critical coagulation concentration of the Magnafloc 380 treated kaolinite systems, all charges on the kaolinite

surface were neutralised. Once the CCC was reached, aggregation occurred through van der Waals force attractions and short-range ion–dipole interactions. In the Magnafloc 380-kaolinite system, hydrophobic bonding between the hydrophobic backbone of Magnafloc 380 and the hydrophobic basal face of kaolinite also took place as in the case for nonionic flocculants. The charged cationic groups of the Magnafloc flocculant also adsorbed onto more than one kaolinite particle, and thus contributed to flocculant bridging. Therefore, charge reversal may have occurred at a Magnafloc concentration at very low dosages, and repulsive forces between Magnafloc-adsorbed kaolinite increased with increasing dosage of Magnafloc 380 above 0.75 mg/L.

The electrostatic repulsion between the negatively charged kaolinite particles and anionic polyacrylamide flocculants would suggest that adsorption and subsequent flocculation by anionic polyacrylamides would be poor. However, in practice and in the current research, anionic polyacrylamides have proven to be very effective flocculants [119]. It would appear that the mutual repulsion between the kaolinite particles and the anionic polyacrylamide molecules allow some polymer adsorption whilst at the same time encouraging the formation of more open flocs. Thus the bridging mechanism is the dominant mechanism and the expanded loops and tails make this flocculant very effective. Since the anionic polyacrylamide is negatively charged (20-30 mol%), the main driving force for adsorption onto kaolinite particles is hydrogen bonding between the silanol/aluminol OH groups and the amide ($–NH_2$) groups of the polymer - as discussed in the case of nonionic polyacrylamide (Figure 3.27). The polymer COO^- pendant species acts to reduce adsorption onto the negatively charged kaolinite particles [120].

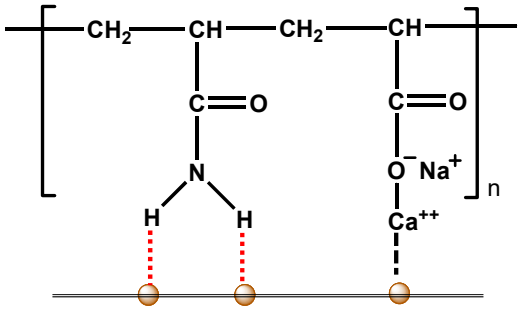

Figure 3.27: Possible interactions between kaolinite and anionic polyacrylamide

The tap water used to synthesize the kaolinite suspension had a Ca^{2+} and Mg^{2+} ion concentration of 11.8 mg/l and 1.32 mg/l respectively. These divalent cations also assist in reducing the electrostatic repulsion between the anionic Magnafloc 10 flocculant and the negatively-charged kaolinite particles, and hence aid in polyacrylamide adsorption and

flocculation. They provide anchoring and form bridges between the anionic Magnafloc flocculant molecules and the negatively charged kaolinite particles. The divalent cationic bridges between a Magnafloc molecule and two kaolinite particles can be represented as:

$Kao^- — {}^+M^+ — {}^-OOC\sim PAM\sim COO^- — {}^+M^+ — {}^-Kao.$

The grafted bio-flocculant, Cell-*g*-PAM, showed better flocculation efficacy than the natural ungrafted cellulose as well as the linear acrylamide based flocculants. All the mechanisms which caused the adsorption of kaolinite onto the nonionic polyacrylamide flocculant, as discussed above, also apply to the grafted flocculant. In the Cell-g-PAM – kaolinite system, polymer bridging was responsible for better flocculation of the grafted copolymer flocculant compared to the linear polymers. The better flocculation efficacy of the grafted polymer compared to the linear polymers is because of their structural differences. In both these systems, the segments of a polymer chain were adsorbed onto different kaolinite particles, thus linking the particles together. The graft copolymer however, has a comb-like structure, which is branched in nature. The flexible chains of polyacrylamide are grafted onto the rigid cellulose backbone and hence the approachability of the polyacrylamide chains to the kaolinite colloidal particles are significantly increased [121]. Due to the better approachability of the kaolinite particles to the dangling grafted chains, the kaolinite colloidal particles are easily adsorbed through bridging to form flocs. This type of intense bridging is not possible in the case of linear polymers (Figure 3.28). Hence, for graft copolymers, bridging will be better and easier than for linear polymers.

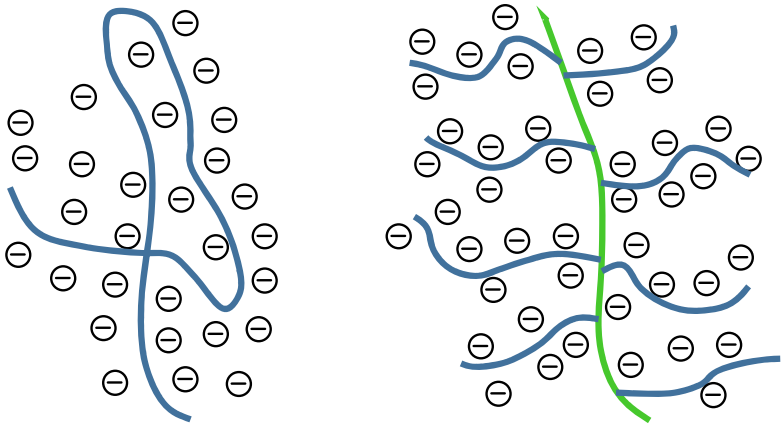

Figure 3.28: Singh's easy approachability model for grafted copolymers [121]

A study by Singh *et al*. [121] stated that due to the flexible polyacrylamide graft chains, the colloidal particles flocculate through the bridging mechanism and form larger net-like flocs. Then, in conjunction with the enhanced approachability of polyacrylamide chains and the

larger flocs with net-like structure, the flocculant begins to settle and in doing so further seize residual particles from water through sweep flocculation. These combined actions (bridging flocculation and sweep flocculation) gives the graft copolymer flocculant a superior flocculating ability compared to the linear acrylamide based flocculants.

The Magnafloc 4240 flocculant showed a slightly better flocculating efficiency compared to the Cell-*g*-PAM flocculant. As the molecular structure of Magnafloc 4240 is not available, the actual flocculating mechanism could not be described with certainty. However, literature has indicated that the manufacturer (BASF) had designed these polymeric molecular flocculants with unique molecular architecture (UMA) to enhance the flocculation process. It is claimed that this technology covers highly branched and interactive polymer chains containing a proportion of semi-particulate entities that extend in three dimensions and produce flocs that are denser and stronger with less intrafloccular water [122]. Another facet of the UMA technology (according to Pearce) is the manipulation of the production process to produce varying fractions of molar mass distribution that have a greater activity in efficient flocculation. Pearse [122] also claims and illustrates the mechanism difference of two dimensional and three dimensional polymeric flocculants as shown in Figure 3.29.

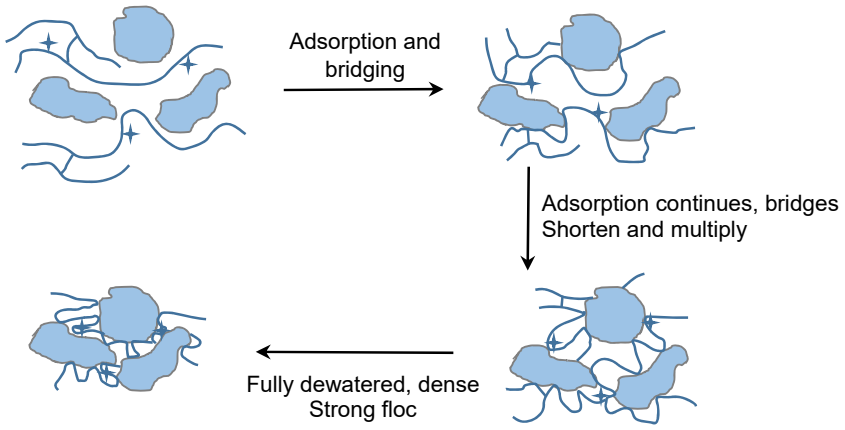

Figure 3.29: Flocculation with UMA Magnafloc macro-polymer [122]

The model proposed by Pearce *et al.* is similar to Singh's easy approachability model except that the flocculant chains are loosely cross-linked and contain semi-particulate entities.

3.9) Settling Tests

The settling tests were carried out using the same 0.25% (w/v) kaolinite suspension that was prepared for the jar tests. Figure 3.30 shows the settling characteristics of the kaolinite suspension under the activity of various commercially available flocculants (Magnafloc 351, Magnafloc 10, Magnafloc 380, Magnafloc 4240) as well as the in-house synthesized copolymer flocculant (Cell-g-PAM). The settling time was plotted against the height of interface. For all tests, the flocculant dosage was maintained at 0.75 ppm, *i.e.* at the optimized dosage as determined by the jar tests above.

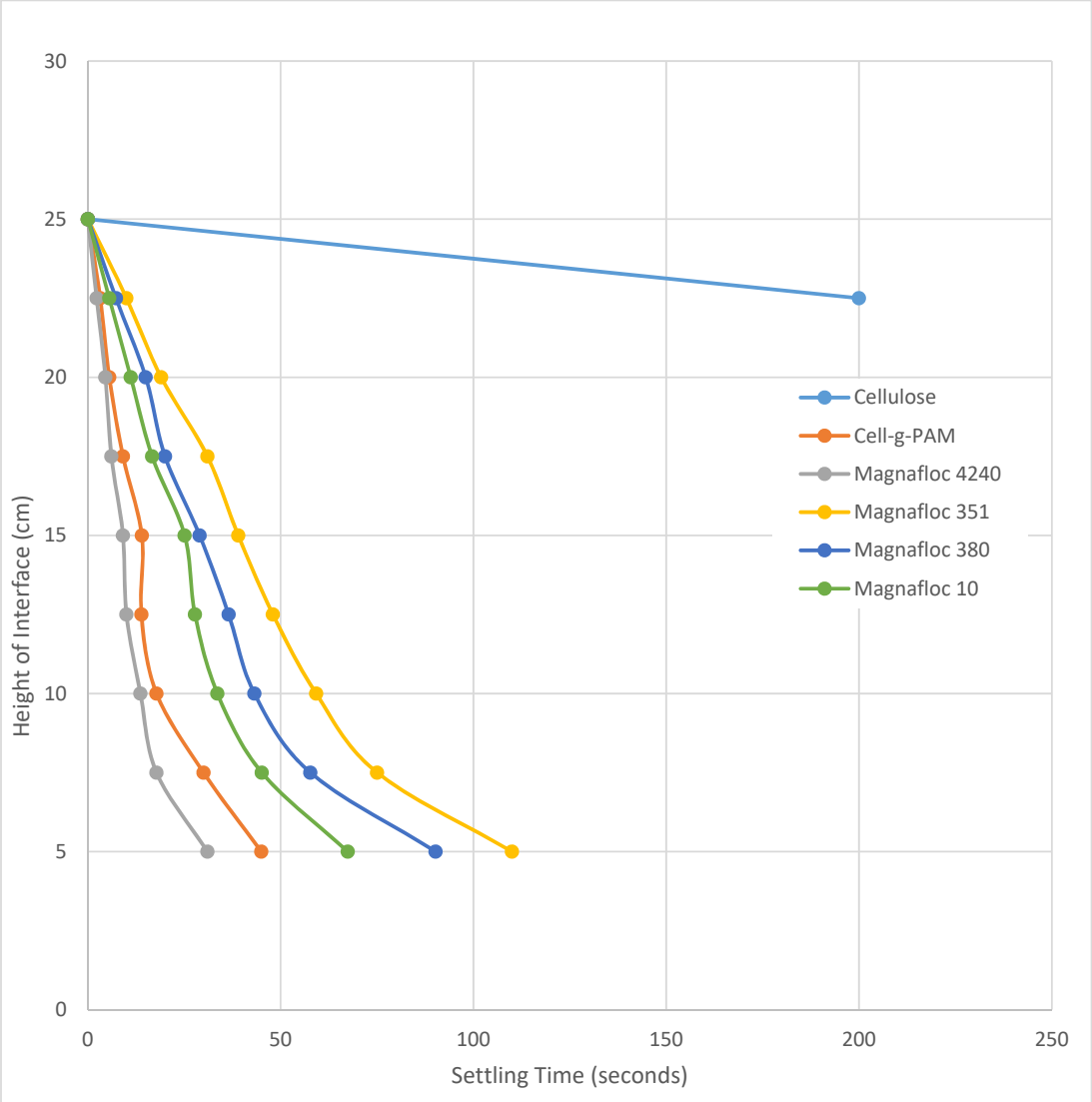

Figure 3.30: Settling characteristics of flocculants in 0.25% (w/v) kaolinite suspension

It was observed that settling rates obtained at the same polymer dosage for each flocculant type were different. These differences resulted from different mechanisms of polymer adsorption on the kaolinite particle surfaces and conformational differences in the flocculant polymer chains in suspension. It was observed that in the case where no flocculant was added to the suspension, no reduction in turbidity took place over the period of observation, indicating that the kaolinite remained suspended in solution. The kaolinite particles acted as a colloid and did not settle to the bottom of the column, as would heavier particles. As shown in Figure 3.30, for the case where pure α-cellulose was added as the flocculant, the suspension has a very slow settling rate of 0.45 m/h. This indicates that although cellulose can be used as a flocculant, its performance is very poor. The settling characteristics of kaolinite suspension using the nonionic, cationic and anionic linear polyacrylamide flocculants were in agreement with the jar tests experiments – the order of settling follow the same order as in jar test (anionic > cationic > nonionic). The better flocculation ability of the grafted copolymers (Magnafloc 4240 and Cell-*g*-PAM) over the linear flocculants was again confirmed using the settling test (Figure 3.30).

3.10 Conclusions

Cell-*g*-PAM graft polymers were successfully synthesized using the conventional chemical free-radical method. The CAN/HNO_3 initiator system was been found to be an efficient initiator in reducing the formation of ungrafted polyacrylamide by forming active sites mainly on the cellulose backbone. The percentage grafting was optimized using experimental design and response surface methodology. The percentage grafting of acrylamide onto cellulose was shown to be dependent on the molar ratio of monomer to cellulose, molar ratio of CAN to cellulose, molar ratio of HNO_3 to cellulose, temperature of reaction, and time duration of reaction. From the results obtained in this study, it can be concluded that the given predictive model described the studied grafting process very well. Results obtained from response surface methodology pointed out that the grafting percentage yield was affected by all the parameters studied. Using response surface methodology, the effects of the individual factors on the percentage grafting was elucidated and it was found that a maximum percentage grafting of 121% could be obtained.

The flocculants synthesized compared well with highly recommended UMA flocculants from commercial sources.

3.11 References

[1] Hebeish A, Guthrie JT. 1981. The chemistry and Technology of Cellulosic Copolymers. Springer, New York, NY.

[2] Misra M, Mohanty A K, Singh B C., J. Appl. Polym. Sci. 1987, 33, 2809–2819.

[3] Misra B N, Dogra R, Mehta I K., J Polym. Sci. Polym. Chem. 1980, 18, 749–52.

[4] Abdel-Razik E A., Polymer. 1990, 31, 1739–1744.

[5] Yang F, Li G, He Y G, Ren F X, Wang J X., Carbohydr. Polym. 2009, 78, 95–99.

[6] Bardhan K, Mukhopadhyay S, Chatterjee S R., J. Polym. Sci.: Polym. Chem. Ed. 1977, 15, 141–148.

[7] El-Hady B A, Ibrahim M M., J. Appl. Polym. Sci. 2004, 93, 271–278.

[8] Okieimen E F, Ebhoaye J E., J. Macromol. Chem. 1986, 23, 349–353.

[9] Bianchi E, Marsano E, Ricco L, Russo S., Carbohydr Polym. 1998, 36, 313–318.

[10] Misra B N, Jassal J K, Pande C S. Ind J Chem. 1978, 16, 1033–5.

[11] Sahoo P K, Samantaray H S, Samal R K., J Appl Polym Sci. 1986, 32, 5693–5703.

[12] Mukhopadhyay S, Prasad J, Chatterjee S R., Makromol Chem. 1975, 176, 1–7.

[13] Roy, D., Semsarilar, M., Guthrie, J.T., and Perrier, S., Chemical Society Reviews 2009, 38, 7, 2046–2064.

[14] Mino G, Kaizerman S, Rasmussen E., J Polym Sci. 1958, 31, 242–7.

[15] Schwab, E., Stannett, V, Rakowitz, D H. and Magrane, J K., Tappi. 1962, 45, 390-400.

[16] Gupta K C, Khandekar K., Polym Int. 2006, 55, 39–150.

[17] Hebeish A, Guthrie J T. 1981. Grafting by Chemical Activation of Cellulose, and Nature of Substrate. Springer, New York, NY.

[18] Hamma M A., Adama S A., Osemeahon P., and Barminas J T., IOSR Journal of Applied Chemistry. 2014, 7, 5, 11-17.

[19] Khullar R., V. K. Varshney, S. Naithani, Soni P. L., eXPRESS Polymer Letters. 2008, 2, 1, 12–18.

[20] Wassila D, D. Ghemati, A Oudia, D Liouche, Biochemical Engineering Journal. 2010, 8, 187-194.

[21] Okieimen EF, Ebhoaye J E., J Macromol Chem A. 1986, 23, 349–353.

[22] Singha, A.S. and Rana V.K., Polymer Composites. 2010, 31, 459–470.

[23] Ouajai S, Hodzic A, Shanks R A., J Appl Polym Sci. 2004, 94, 2456–2465.

[24] Imai, Y., Masuhara, E., and Iwakura, Y., J of Polymer Science, Part B. 1970, 75–79.

[25] Bergman, P C A., Boersma, A R., Zwart, R H., Kiel, J A., ECN report, ECN-C. 2005, 05-013.

[26] Imai, Y., Masuhara, E., and Iwakura, Y., Journal of Polymer Science, Part B.1970, 75–79.

[27] T. Terasaki and Matsuki M., Seni-i Gakkaishi. 1962, 18, 147.

[28] Arthur J C, Hinojosa O, Banis M S., J Appl Polym Sci. 1968, 12, 1411–1421.

[29] Hebeish, A. and Guthrie, J T. 1981. The Chemistry and Technology of Cellulosic Copolymers. Springer-Verlag.

[30] Hintz, H L., & Johnson, D C., Journal of Organic Chemistry. 1967, 32, 556–564.

[31] Mansour O Y, Nagaty A., Prog Polym Sci. 1985, 11, 91–165.

[32] Ogiwara Y, Ogiwara Y, Kubota H., J Appl Polym Sci. 1968, 12, 2575–2584.

[33] Varma D S, Narashinan V., J Appl Polym Sci. 1972, 16, 3325–3339.

[34] Chen, N., Zhang, Z., Feng, C., Li, M., Zhu, D., Sugiura, N., Mater. Chem. Phys. 2011,125, 293–298.

[35] Box G E., Wilson K B., J. R., Stat. Soc. 1951, 13, 1.

[36] Otto, M. 1999. Chemometrics: Statistics and Computer Application in Analytical Chemistry, Wiley–VCH, Weinheim.

[37] Doehlert D H., Appl. Stat. 1970, 19, 231.

[38] Myers, R H., & Montgomery, D C. 1995. Response Surface Methodology: Process and product optimization using designed experiments, John Wiley & Sons, New York.

[39] Ingersoll C D., Davis R E., Ind. Eng. Chem. Anal. Ed., 1930, 2, 3, 248–249.

[40] Goyal P, Kumar V, Sharma P., J Appl Polym Sci. 2008, 108, 3696–3701.

[41] Zhang G., Yi L. Deng H., Sun P., J. Environ Sci. 2014, 26, 1203–1211.

[42] Gonzalez-Olmos R, Kopinke K, Mackenzie A., Georgi Env Sci Tech. 2013, 47, 5, 2353-2360.

[43] Khalil, M I., Farag, S., Hattah, S E., J. Appl. Polym. Sci. 1995, 57, 335–340.

[44] Girod G., J. M. Lamarche and A. Foissy, J. Colloid Interface Sci. 1988,12, 265.

[45] Lepoutre, P. & Hui, S.H. J., Appl. Polym. Sci. 1975, 19, 1257-1268.

[46] Akhnazarova S, Kafarov V. 1982. Experiment Optimization in Chemistry and Chemical Engineering. Moscow, Mir.

[47] Gupta K C, Khandekar K., J Appl Polym Sci. 2002, 86, 2631–2642.

Chapter 4

Synthesis of cellulose-*g*-polyacrylamide through microwave-assisted and microwave-initiated copolymerization and its application as a flocculant

4.1) Introduction

Grafting is an effective technique to modify the properties of synthetic and natural polymers [1]. Chemical free-radical initiator induced graft copolymerization of polyacrylamide onto cellulose has been discussed in Chapter 3. In addition to the redox initiator-induced graft copolymerization, microwave-assisted graft copolymerization has also been employed. In the context of green chemistry, microwave irradiation provides an alternative method (to conventional heating) for introducing energy into chemical reactions and for reaction activation by using the ability of some liquids and solids to transform electromagnetic energy into heat [2]. Although the use of microwave energy for chemical modifications can be traced back to the 1950s, it began to gain wide acceptance only after the published papers in 1986 by the research groups of Gedye *et al.* [3] and Giguere *et al*. [4]. Gedye conducted a microwave-assisted hydrolysis of amides in a substantially shorter time than the corresponding reaction under conventional conditions. A few years later, in 1992, Mingos [5] demonstrated the possibility of heating liquids beyond their boiling points under microwave conditions. Since these publications microwave radiation has emerged as a promising technology in medicinal chemistry, polymer synthesis, material sciences, nanotechnology and biochemical processes.

The main advantages of microwave assisted chemistry are shorter reaction times, higher yields, and a reduction of side reactions compared with syntheses performed under conventional heating [6]. Although most of these enhancements can be described as thermal effects, the mechanism by which microwave irradiation improves reaction results is still a subject of great debate, with research groups divided over whether thermal effects alone, or “special microwave effects” are the cause of the enhancements [7].

Initially, microwave synthesis experiments were carried out in domestic microwave ovens that had little ability to control process conditions, such as temperature and pressure [8]. Domestic MW ovens also operated with pulsed irradiation and produced inhomogeneous microwave

fields. As a result, reactions were difficult to perform, results were hard to reproduce, and laboratory accidents were common due to the excessive pressure build up in the reactors [9]. Over the past decade, however, large strides have been made in developing safer microwave reactors capable of producing more reliable results with high reproducibility [10]. Several different reactor configurations have become commercially available. These commercially available microwave reactors are equipped with built-in magnetic stirrers and have the ability to monitor and control pressure and temperature. It has been proposed that with the above improvements microwave reactors may lead to the synthesis of novel products by permitting access to alternative kinetic pathways and stabilizing different energy minima in a reaction vessel [11].

In Chapter 3, details about the synthesis of polyacrylamide grafted cellulose (Cell-*g*-PAM) via the chemical free-radical initiated technique and its application as a polymeric flocculant has been discussed. It has been observed that partially hydrolyzed polyacrylamide shows better flocculation characteristics than polyacrylamide itself [12, 13]. This chapter therefore provides information on the synthesis of the bioflocculant, Cell-*g*-PAM, as well as the hydrolyzed Cell-*g*-PAM, by both the microwave-initiated and microwave-assisted graft copolymerization methods and its application in the flocculation of a synthetic wastewater system. First an explanation of microwave irradiation and its application in heating up a reaction mixture is provided, followed by a discussion of the different microwave reactor configurations. A literature survey on the application of microwave chemistry in the synthesis of polysaccharide copolymers is also carried out. The chapter concludes with testing the synthesized flocculants against commercially available flocculants for the flocculation of kaolinite suspensions.

4.2) Microwaves

Microwaves are a form of non-ionizing radiation and constitute a part of electromagnetic spectrum falling between the infrared and radio-wave region *i.e*. between the wavelengths 0.1 cm and 1 m, which correspond to frequencies between 30 MHz and 300 GHz respectively (Figure 4.1).

Of this bandwidth, radiations with wavelength 1 cm to 25 cm are used exclusively for radar transmissions while a major portion of the remaining range of wavelength is used for telecommunications. In order to avoid interferences with radar and communication systems, a

small bandwidth ranging from 0.82 cm to 16.95 cm (corresponding to frequencies of 896 to 3390 MHz) have been internationally agreed upon and allocated for the use of industrial, scientific and medical (ISM) equipment and applications. All domestic microwave ovens and dedicated microwave reactors for chemical synthesis use a frequency of 2.45 GHz in order to avoid interference with telecommunications and radar frequencies [14].

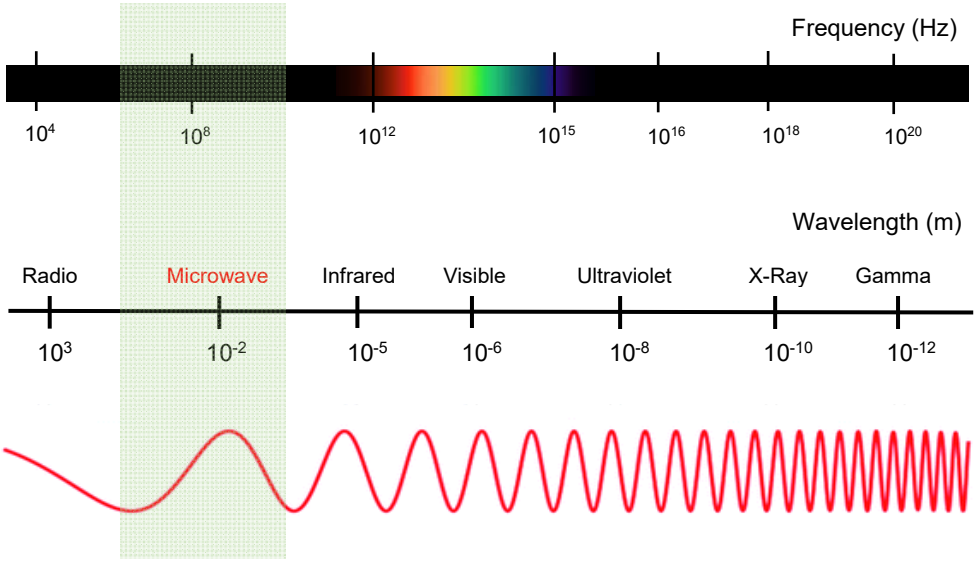

Figure 4.1: Electromagnetic Spectrum

Just like other electromagnetic radiations, microwaves consist of an electric wave and a magnetic wave component, with the magnetic wave oscillating in phase and at a 90° angle to the electric wave (Figure 4.2):

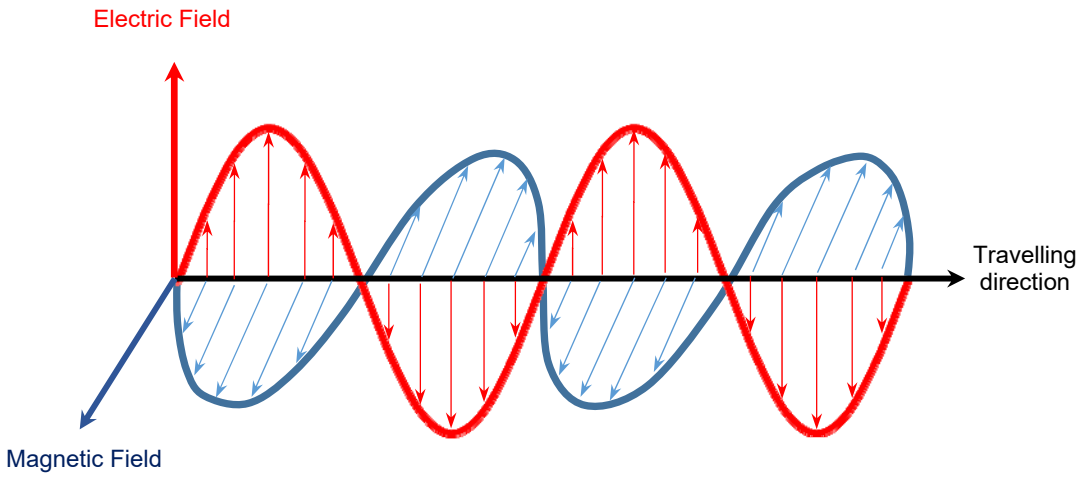

Figure 4.2: Electromagnetic wave with perpendicular, in-phase electric and magnetic fields [15]

The electric field component is generally considered to be responsible for microwave dielectic heating although in some instances the magnetic field component has also been shown to play a significant role (magnetic field interactions with transition metal oxides) [15].

The energy associated with microwaves, calculated using Planck's law $E = h\nu$ and corresponding to the microwave frequencies of 300 MHz - 300 GHz, falls between 1.24×10^{-6} and 1.24×10^{-3} eV. These energies are much lower than ionization energies of biological compounds (13.6 eV), of covalent bond energies such as -OH (5 eV), hydrogen bonds (2 eV), van der Waals intermolecular interactions (lower than 2 eV) and even lower than the energy associated with Brownian motion at 37°C ($2.7\ 10^{-3}$ eV) [16]. Because of the low energies associated with microwaves, microwave radiation alone cannot achieve any meaningful reactions in materials. However, if the material exposed to microwaves contains polar molecules and ions, then the radiation can accelerate chemical, biological and physical processes [17].

4.2.1) Microwave Effect on Heating

The observed increase in the rate of reactions and sometimes altered product distributions which occur when a reaction is carried out under microwave irradiation conditions can be attributed to both a "specific" (thermal) microwave effects and "non-thermal" (athermal) microwave effects.

4.2.1.1) Specific Microwave Effects

Specific microwave effects are reaction rate enhancements that are thermal in nature (i.e. a change in temperature), but cannot be achieved or duplicated by conventional heating. Specific microwave effects include the observed heating differences based on microwave absorptivity, the elimination of wall effects caused by inverted temperature gradients in reaction solutions being irradiated by microwaves, and the superheating effect of solvents at atmospheric pressure.

4.2.1.1.1) Thermal Effects of Microwave Radiation

Microwave heating is a non-contact energy transfer process that transforms electromagnetic energy into thermal energy at certain wavelengths. The electric component of an electromagnetic field causes heating in liquids by two main mechanisms: dipolar polarization and ionic conduction.

4.2.1.1.2) Dipolar Polarization

When certain atoms bond to form molecules, there will be a positive and negative atom, and it is the attraction between these atoms that causes a bond to form. The electrons within the bond will always be attracted to the electronegative side of the molecule causing the atoms to behave like a permanent dipole. Dipolar or orientation polarization occurs in these dielectric molecules due to the asymmetric charge distribution within the molecule. This means that under a time-alternating electric field they are highly sensitive to the field and re-orientate themselves in an attempt to align themselves and remain in phase with the oscillating field (Figure 4.3).

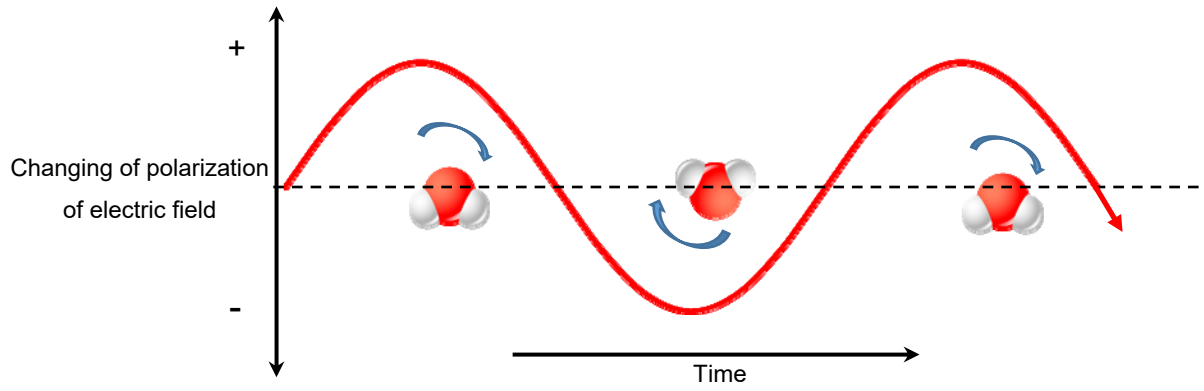

Figure 4.3: Effect of electromagnetic field on dipolar molecules [15]

The ability of the molecules in a liquid solution to align themselves with the alternating electric field depends on the frequency of the oscillations, the viscosity of the liquid, inertia of the molecules, and any inter-particle interactions. If a solution is composed of polar species which can freely move, then the oscillating electric field will induce movement in the entire liquid matrix. If the polar species/segments are, however, bonded to non-polar substrates, then their

movements are not completely free - the polar segments will try to move with the electromagnetic field until they become constrained by their bonds to the non-polar substrate.

Under low frequency, the molecule rotates in phase with the oscillating electric field. The molecule gains some energy by this behavior, but the overall heating effect is small. Under very high oscillating fields the dipoles do not have sufficient time to respond to the oscillations, do not rotate, and hence no energy transfer takes place. In the microwave frequency range however, the frequency of the electric field is low enough for the dipole to respond but it is also sufficiently high that the dipole cannot precisely follow the oscillating electric field. At microwave frequencies the inertia of molecules and their interactions with neighbours make changing orientation more difficult and the dipoles lag behind the field. Therefore, as the dipole re-orientates itself to align with the electric field, the field is already changing and this generates a phase difference between the orientation of the field and that of the dipole. This phase difference causes the polar molecules to vibrate at a rapid rate as they constantly try to realign themselves to the field and these rapid vibrations cause friction between polar molecules with each other and the surrounding medium resulting in a rapid heating of the system.

All the materials are not equally susceptible to microwave heating and the response of various materials to microwave radiation is diverse [18]. Microwave-induced heating efficiency for different materials is dependent on the dielectric properties of each material. A dielectric material contains either permanent or induced dipoles, such that the material acts as a capacitor when placed in an electric field i.e., the material allows an electrical charge to be stored with no conductivity observed. The extent to which a material heats up when subjected to an electromagnetic radiation such as microwave is mainly determined by its dielectric properties, which can be expressed by its permittivity (ε^*) which is made up of two components: a real part, the dielectric constant (ε') and an imaginary part, the dielectric loss factor (ε''). The permittivity is described by Equation 4.1.

$$\varepsilon^* = \varepsilon' - j\,\varepsilon'' \qquad (4.1)$$

The dielectric constant (ε') denotes the ability of a material to be polarized by an electric field, or to store electromagnetic energy from an electric field. The dielectric loss factor (ε'') quantifies the efficiency with which a molecule converts the incident electromagnetic irradiation into molecular rotation, and hence its efficiency in converting the stored electromagnetic energy into

heat [19]. The ratio of loss factor to dielectric constant is termed the dielectric loss tangent of a material and is defined by Equation 4.2.

$$\tan\delta = \frac{\varepsilon''}{\varepsilon'} \tag{4.2}$$

The dielectric loss tangent of a material determines its ability to absorb and convert the electromagnetic energy into thermal energy at a given temperature and frequency [19] when the electromagnetic field is applied to a sample. A material that has tan δ = 0 is completely transparent to microwave irradiation, and incident irradiation passes through with its path unchanged. For a perfectly absorbing material, tan δ = ∞. Here, the material under irradiation shows complete resistance to the incident irradiation. A general classification based on tan δ values can identify materials as high (tan δ **>** 0.5), medium (tan δ 0.1–0.5) and low (tan δ < 0.1) microwave absorbers [20]. The loss tangents for several organic solvents at room temperature are shown in Table 4.1

Table 4.1: Loss factors (tanδ) for commonly used solvents [20]

High efficiency		Medium efficiency		Low efficiency	
solvent	**tan δ**	**solvent**	**tan δ**	**solvent**	**tan δ**
Ethylene glycol	1.350	2-butanol	0.447	Chloroform	0.091
Ethanol	0.941	1,2-dichlorobenzene	0.280	Acetonitrile	0.062
DMSO	0.825	1-Me -2-pyrrolidone	0.275	Ethyl acetate	0.059
2-propanol	0.799	Acetic acid	0.174	Acetone	0.054
Formic acid	0.722	N,N – DMF	0.161	THF	0.047
Methanol	0.659	1,2-dichloroethane	0.127	Dichloromethane	0.042
Nitrobenzene	0.589	Water	0.123	Toluene	0.040
1-butanol	0.571	Chlorobenzene	0.101	Hexane	0.020

Based on their response to microwaves, materials can be broadly classified into three categories as follows:

(i) Materials that reflect microwaves, which are bulk metals and alloys, e.g. copper,

(ii) Materials that are transparent to microwaves, e.g. sulphur, ceramics, certain glass,

(iii) Materials that absorb microwaves, e.g. water, which constitute the most important class of materials for microwave synthesis.

4.2.1.1.3) Ionic Conduction

The ionic conduction mechanism applies to materials containing charged particles such as ionic solutions. Ions in solution do not have a dipole moment but in a solution containing ions or even an isolated ion, ions will move in a solution under the influence of an electric field as indicated in Figure 4.4.

During ionic conduction the dissolved ions oscillate back and forth under the influence of the microwave field, they collide with neighboring molecules and this increased collision rate converts kinetic energy to heat. When two samples containing equal amounts of distilled water and tap water, respectively, were heated by microwave irradiation at fixed radiation power, more rapid heating was found to occur in the tap water sample due to its ionic content [21].

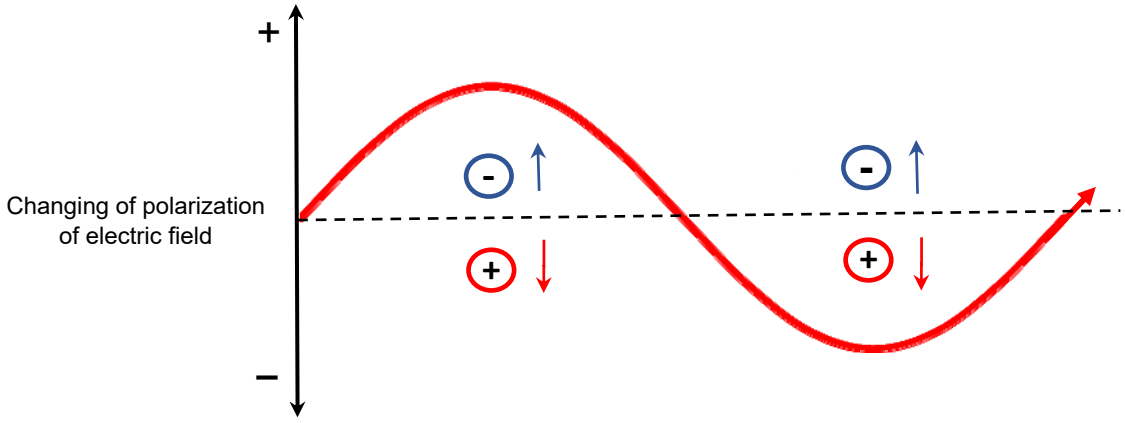

Figure 4.4: Effect of electromagnetic field on ions in solution [15]

The conductivity mechanism is a much stronger interaction than the dipolar mechanism with regard to the heat generating capacity [22].

4.2.1.1.4) Microwave Heating versus Conventional Heating

Conventional heating is carried out by conduction-convection heating, using external heat sources such as oil-baths or heating mantles. Conduction-convection heating is the transfer of heat as a result of differences in temperature between different parts of the system. The rate of heat flow between the two regions is proportional to the temperature difference between them

and the thermal conductivity of the substance. In solids, as in the case of the reaction vessel, the molecules making up the solid vessel are bound in a solid matrix and conduction of heat occurs by higher energy molecules vibrating against neighbouring molecules and transferring their heat. The conventional heating method is comparatively slow and inefficient since it depends on the thermal conductivity of the vessel material, on convection currents, and the specific heat and density of the various materials making up the system. In the conventional heating setup, heat must travel from the outside in, and the walls of the reaction vessel are generally the hottest part of the reaction. This is also called “wall heating”.

In contrast, microwave heating is an irradiation process that directly couples the microwave energy with the reacting solution molecules, thus generating heat across the entire reaction volume. A larger cross-section of the reaction solution reaches the ideal reaction temperature sooner than it would have with conventional heating. The reaction vessel itself is not affected thermally by microwave irradiation since it is made of microwave transparent materials. Thus an inverted thermal gradient exists from the reaction bulk into the vessel wall, resulting in greatly reduced hot wall effects.

The effect of the different mechanisms for microwave and conventional on the heating patterns in a reaction vessel are shown in Figure 4.5.

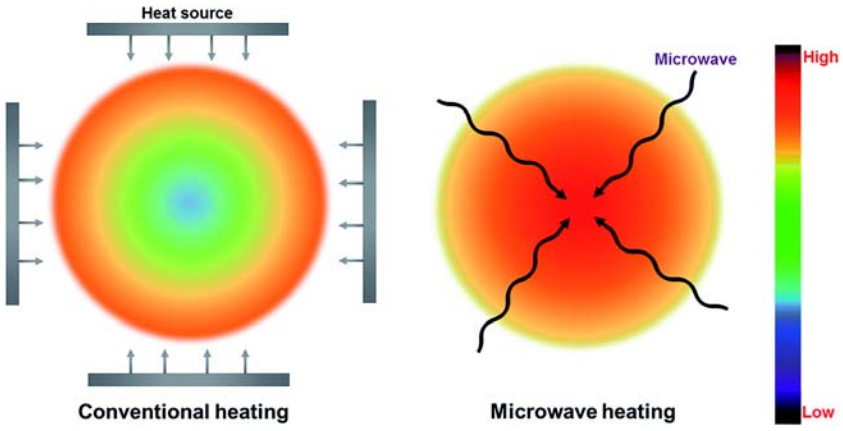

Figure 4.5: Microwave-induced and conventional heating patterns [23]

Unlike conventional heating, microwave heating shows a much higher and uniform temperature throughout the heated material. It must be noted though, that efficient stirring and controlled heating can generally mitigate temperature gradients in both microwave and conventionally heated reactions.

4.2.1.1.5) Macroscopic Superheating

According to experimental evidence, a solvent will boil only when it is in contact with its own vapour and, if this is not the case, then it can be heated to above its normal boiling point without the onset of boiling [24]. Imperfections in glassware or on boiling stones have areas that cannot be wetted by the solvents, and thus create small pockets of the solvent vapour, termed nucleation sites. In conventional heating, the inner surface of the reacting vessel normally provides nucleation sites for the formation of gas bubbles. Thus with conventional heating, the reacting solution cannot be heated to beyond its normal boiling point under atmospheric conditions.

When using microwave radiation, the surface of the reaction vessel does not heat up and is lower than the temperature of the heated liquid. Consequently, the tendency for the initiation of boiling is reduced, and superheating above the boiling point of the solvent is possible even at atmospheric pressure [25]. In these systems boiling occurs only when the energy delivered exceeds the intermolecular interactions in the liquid. In microwave heated systems, if the solution is not stirred, the observed boiling temperature is higher than a few to a few tens of degrees above the comparative conventionally boiled system [26]. Superheating may also occur when irradiating a strong microwave absorbing liquid and this results in a very large heating rate. Under these conditions the energy provided by the radiation surpasses the rate of energy dissipation by evaporation (at the boiling point) and heat begins to rapidly accumulate in the liquid phase. In this case the accumulation of heat will lead to an increase of the temperature above the boiling point. These effects, however, will not occur in the presence of boiling stones or agitation of the solution.

4.2.1.2) Non-thermal Effects of Microwave Radiation

Non-thermal or athermal effects of microwave radiation are increases in the rates of microwave assisted reactions that cannot be rationalized by either purely thermal/kinetic or specific

microwave effects [27]. These non-thermal effects result from the direct interaction of the electric field with specific molecules in the reaction medium. Researchers have used the Arrhenius equations (Equation 4.3) as the basis to explain these effects:

$$k = A \exp [-E_a/RT] \quad (4.3)$$

where k = reaction rate coefficient
A = pre-exponential factor
E_a = activation energy
T = temperature

From Equation 4.3, it can be noted that there are two possible ways to increase the rate of reaction. The first is by increasing the pre-exponential factor "A" and the other is to decrease the activation energy.

The pre-exponential factor represents the probability of molecular collisions in a system and is therefore related to the rate of a chemical reaction. The pre-exponential factor is defined by Equation 4.4.

$$A = \gamma \lambda^2 \Gamma \quad (4.4)$$

where γ = number of nearest-neighbour jump sites
λ = jump distance
Γ = jump frequency

It has been argued that the presence of an oscillating electric field leads to orientation effects of dipolar molecules and hence changes the pre-exponential factor, A [28]. As discussed under thermal effects of microwave radiation above, the application of a microwave field to a dielectric material induces rapid rotational movement of the molecular dipoles, which in turn, increases the probability of contact and collision between molecules. These increased collision rates, along with those generated by the movement of ionic species through the system, contribute to increasing the pre-exponential factor and consequently enhance the rate of reaction.

Another non-thermal effect is the decrease in the activation energy caused by electrostatic energy stabilization as shown in Figure 4.6 [29]. The example of Lewis *et al*. [30] of the unimolecular imidization of polyamic acid and the decomposition of sodium hydrogen carbonate in aqueous solution reported by Shibata [31] are two examples of a number of publications claiming a reduction in the activation energy of the transition state compared with the ground state (reactants). This type of effect is associated with reaction systems that involve an increase in polarity of the system from the ground state to the transition state.

The basis for this effect is that any system containing polar molecules should be stabilized to some extent as all the polar molecules align themselves simultaneously in the general direction of the electric field [32]. If the transition state of a reaction system is more polar than the ground state, then microwave radiation will stabilize it to a greater extent than the ground state. Since the difference in the energy of these states is the activation energy required for the reaction, the net result of unequal stabilization is a drop in activation energy.

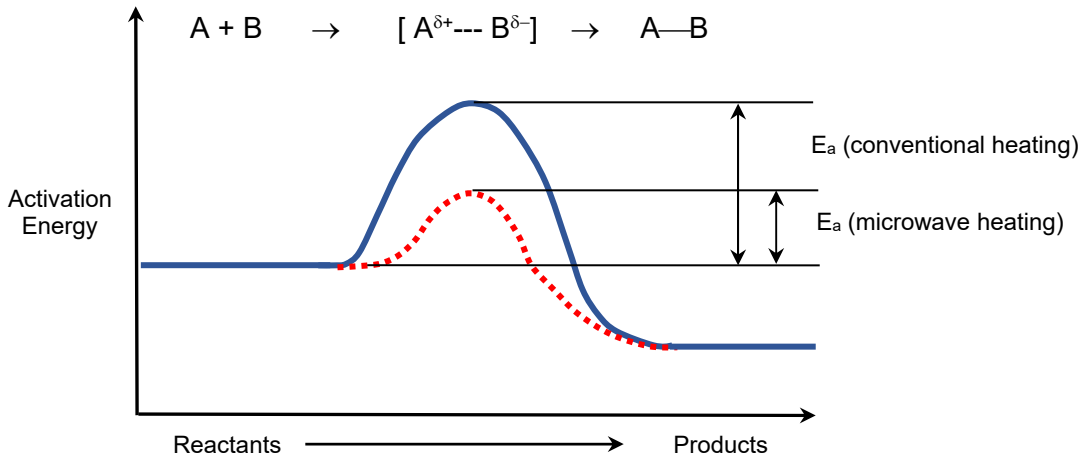

Figure 4.6: Gibb's free energy differences in conventional and microwave heating methods [32]

4.2.2) Benefits and Limitations of Microwave Heating

4.2.2.1) Benefits

Microwave assisted synthesis has several significant advantages over conventional technology:

Faster reaction: Based on experimental data it has been found that microwave enhanced chemical reactions can proceed at much larger rates (by as much as 1000-fold) compared to conventional heating methods. Heating rates of 2 – 4 °C s^{-1} can be achieved for common organic solvents - such heating rates would require furnaces heated to over 1000 °C using conventional heating methods [33]. Microwave irradiated reactions can also be conducted at higher temperatures than conventional heating systems, and hence can be completed in a few minutes instead of hours.

Better yield and higher purity: Microwave assisted synthesis reactions lead to the formation of fewer side reactions and products [34]. In general, microwave heating leads to yields that are 30 – 40% higher than those obtained using conventional heating. The product recovered has a higher yield and consequently results in faster and easier purification steps.

Energy saving: Microwave heating is a highly efficient process and results in significant energy saving. This is because microwaves heat up just the sample and not the reaction vessel as well, and this consumes far less energy. Further, microwave heating is more energy efficient than conventional heating because of direct molecular heating and inverted temperature gradients.

Uniform and selective heating: An important advantage of microwave heating is the “incore” heating of materials in a homogeneous and selective manner which results in a faster and more even heating of the reaction mixture. Selective heating is based on the principle that different materials respond differently to microwaves. The reaction vessel, for example can be selected such that it is transparent to the microwaves. Also, if the reactants of a process have low loss heating values, it would be possible to add inert metal powders to the reaction vessel to increase the heating rate.

Green synthesis: Reactions conducted using microwaves are cleaner and more eco-friendly than conventional heating methods [35]. Microwaves heat the compounds directly and therefore the usage of solvents can be drastically reduced or eliminated. The higher yields obtained with the use of microwaves also reduces the amount of purification required for the end products of chemical reactions, thus reducing the generation of waste.

Reproducibility: Reactions with microwave heating are more reproducible compared to the conventional heating because of uniform heating and better control of process parameters [36]. Easy on-line control of temperature, time, and pressure profiles is possible, which leads to more reproducible reaction conditions.

4.2.2.2) Limitations

Although microwave chemistry has many advantages it has certain limitations which should be kept in mind while carrying out reactions under microwaves irradiation. These limitations are linked to its scalability, limited application, and the hazards involved in its use.

Lack of scalability: The mass of products achievable by using currently available microwave equipment is restricted to only a few grams. Although some progress has been made in the recent past relating to the scalability of microwave equipment [37], there is still a large gap that needs to be spanned to upscale current rates of production to industrially required levels.

Limited applicability: The use of microwaves as a heating source is restricted only to materials that absorb them. Materials which are non-polar cannot be heated by microwaves as such materials are transparent to their radiation. In addition, although microwave heating increases the rate of reaction and yields in certain reactions, it can also results in yield reduction compared to conventional heating methods in other reactions [38].

Safety Hazards: Even though manufacturers have directed much attention to making microwaves a secure source of heating, some unexpected and uncontrolled reactions involving volatile reactants under superheated conditions may result in explosions [39]. Metals are reflective to microwaves and the radiation tends to bounce off them. Due to this, certain metal particles or metals have to be avoided because of the possibility of electric arcing in the oven.

Health hazards: While microwaves operating at a low frequency range are only able to penetrate the human skin, higher frequency-range microwaves (2.45 GHz) can reach body organs [40]. Research has also shown that on prolonged exposure microwaves, complete degeneration of body tissues and cells may also occur [40]. Experimental evidence has established that constant exposure of DNA to high frequency microwaves during a biochemical reaction result in complete degeneration of the DNA strand.

Other limitations:

- Sudden increases in reaction temperatures may lead to the distortion of molecular structures, which may lead to their degeneration and consequently to undesired products [41].
- Temperature sensitive reactions and reactions which involve effervescence are ordinarily difficult to perform in microwave reactors [42].
- Since heating takes place too fast, some reactions become vigorous and to some extent hazardous [43].

4.2.3) Microwave Reactors

Two types of microwave reactors have been used for the application of microwave radiation in chemistry field: multimode microwave reactors and monomode microwave reactors. Microwave reactors or ovens are available on the market in a variety of brands. However, for each mode, the underlying principles of operation of the various brands are very similar.

4.2.3.1) Multimodal Microwave Reactors

A schematic representation of multimode microwave oven and its working principle is illustrated in Figure 4.7.

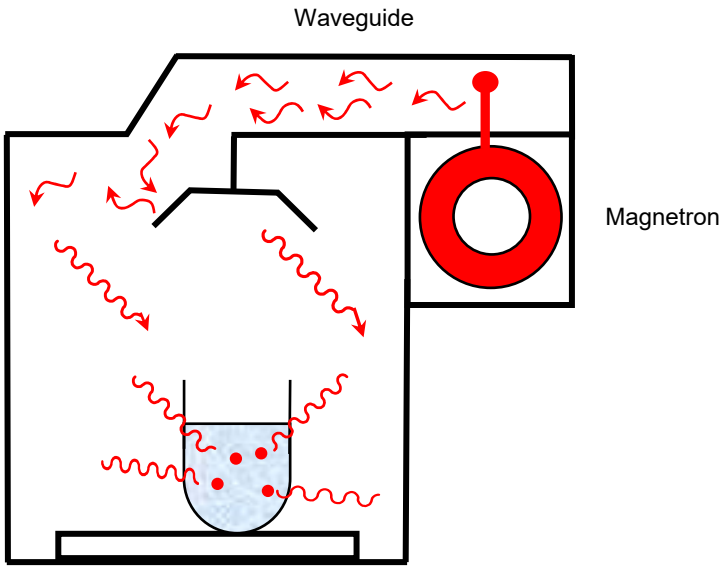

Figure 4.7: Microwave field distribution in a multimode reactor [44]

Multimode microwave reactors have been introduced on the market as domestic microwave ovens for cooking, heating and thawing of food. Although they were not designed for laboratory applications, multimode microwave applicators were the first to be used in laboratories. All cited publications thus far on graft polymerization on polysaccharides have been based on experiments carried out in domestic microwave ovens. These ovens have a maximum power rating of 1000 W and are characterized by a non-homogeneous distribution of electric fields due to the microwaves reflecting randomly off the walls of the oven and the multiple modes interacting with each other inside the microwave cavity. In order to optimize use of these ovens for synthesis purposes, researchers have resorted to mapping the hot spots of high energy using filter paper sheets impregnated with solutions of cobalt chloride [45]. Modifications made to multimode ovens include the addition of a mechanical mode stirrer that operates as a periodically moving metal vane that continuously changes the field pattern inside the cavity. This creates an electromagnetic field that is homogeneous in all directions and all locations throughout the cavity.

The advantage of this addition is that the reacting sample can be placed anywhere in the cavity. Also, the reacting sample placed inside the cavity will not permanently affect the distribution of the microwave field intensity. This implies that there are no limitations on the size and shape of the reaction vessel placed inside the cavity as well as the number of samples that can be simultaneously processed. Multimode reactors also have several limitations which include: (i) the reactors do not provide any reliable control over the emitted power and are not equipped with temperature or pressure sensors for reproducibility of experimental conditions; (ii) glass reactors (vessels) connected to cumbersome auxiliary components cannot be accommodated in the oven; (iii) openings in the walls of the microwave oven are severely limited, being permitted only by adopting very specific safety measures; (iv) the power is not tunable [46].

4.2.3.2) Monomode Microwave Reactors

Monomode microwave reactors have been designed to improve the energy intensity and distribution in the microwave cavity and to improve reproducibility in experiments. A schematic representation and working principle of a single-mode microwave applicators is shown in Figure 4.8.

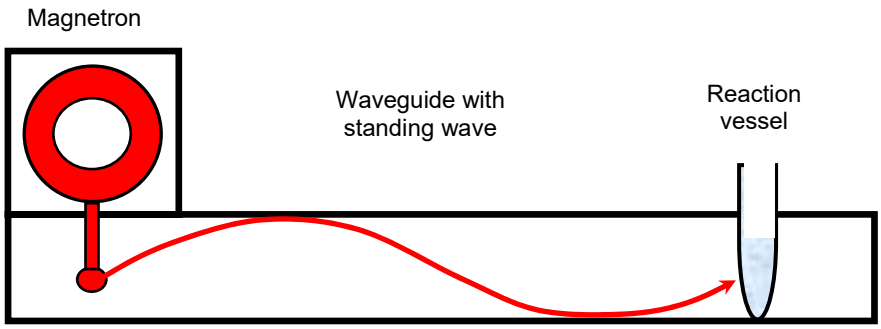

Figure 4.8: Monomode single-batch reactor [44]

The monomode microwave reactor operates with a continuously variable power but at a fixed frequency of 2.45 GHz. The distinguishing feature of the monomode microwave reactor is its ability to create a standing wave pattern, which is generated by the superposition of the incident and reflected waves in the resonant chamber. To obtain this, the dimensions of the waveguide are carefully calculated to correspond to the characteristic wavelength of the microwaves. The superposition of the incident and reflected waves generate an array of nodes where microwave energy intensity is zero, and an array of antinodes where the magnitude of microwave energy is at its maximum (Figure 4.9).

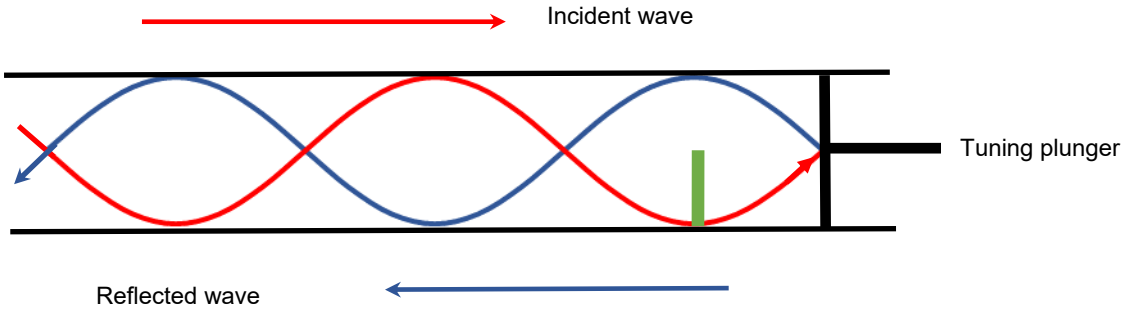

Figure 4.9: Formation of a standing wave

In the monomode microwave reactor the dimensions of the waveguide are calculated so to allow only one mode of propagation. The tuning plunger is adjusted so as to create a standing wave pattern in the resonating cavity and such that the dielectric material to be heated is precisely positioned in the antinode.

The advantage of the single mode microwave reactor is their high rate of heating, as the standing wave can always be adjusted so that the sample is always placed at the antinodes of the field, where the intensity of microwave radiation is the highest. Monomode microwave reactors, however, suffer from several disadvantages: (i) until now, there is no practical way of scaling up the process as the dimensions of a standing wave cavity cannot be extended indefinitely; (ii) these reactors do not lend themselves to simultaneous processing of multiple samples (reacting vessels)

4.2.3.3) Commercial Reactors

Specialized microwave reactors (both monomode and multimode) are available commercially from companies such as CEM, Milestone, Biotage, Anton Paar, and Plazmatronika. These reactors are equipped with built-in magnetic stirrers. Temperature measurement is achieved by means of IR pyrometers, shielded thermocouples or fiber-optical temperature sensors and feedback control enables the reaction mixture to be held at desired temperatures (without thermal runaways). Some of these reactors allow synthesis under reduced or elevated pressures within the cavity.

4.3) Copolymerization of Cellulose under Microwave Irradiation

The literature is rich in studies done on microwave-assisted and microwave-initiated grafting on polysaccharides. However, only a limited number of published studies could be found dealing specifically with copolymerization from cellulose.

Conventional chemical free-radical redox, microwave-initiated and microwave-assisted grafting methods have been successfully utilized to synthesize plant-based grafted bio-flocculants such as cellulose [47, 48]. Microwave-initiated grafting employs microwave radiation alone to create free radical sites on the cellulose substrate, from where the graft chains are attached [49]. Microwave-assisted grafting uses a combination of microwave radiation and a chemical free-radical initiator to create the free radical sites on the cellulose backbone, from where the graft chains grow [50].

4.3.1) Microwave-initiated Grafting

When a macromolecule such as cellulose is present, rotation or oscillation of the entire molecule under the influence of microwave irradiation is not possible [51]. The microwaves are absorbed by the polar groups present in the macromolecules, which then behave as if they were anchored to an immobile raft, and these polar groups then experience localized rotations in the microwave region. Researchers [52] have also postulated an acceleration of the reaction rate as a result of a reduction in the activation energy in polymerizations under microwave irradiation. The effect of localized oscillations and reduced activation energy results the severing of bonds and the formation of free radical sites [53]. It has also been reported [54] that the grafting in reaction mixtures without initiators does not occur under purely thermal heating. This may support the possibility of in situ formation of radicals in microwave-initiated grafting reactions, which could possibly be due to athermal or microwave effects.

Mishra *et al.* used the microwave-initiated technique to graft poly(acrylic acid) chains (PAA) onto carboxymethylcellulose (CMC) backbone. FTIR spectroscopy was used to provide the first ever experimental proof of the proposed mechanism of the microwave effect involved in microwave initiated grafting [55]. Mishra *et al.* studied the flocculation efficacy of the graft copolymer through standard Jar Test procedure in river water and the results were compared to that of the starting material (CMC) and with alum (coagulant). It was found that CMC-*g*-PAA showed the maximum flocculation efficacy, as predicted by “Singh’s easy approachability model” [56].

Arsad *et al.* [57] grafted chitosan onto cellulose obtained from empty fruit bunch (EFB) polymer by a microwave initiated method. In their investigation the effects of ratio chitosan to cellulose (0.2:1, 0.4:1, 0.6:1, 0.8:1 and 1:1) and irradiation time (1min, 2min, 3min, and 4min) on grafting were studied. Grafting was confirmed through gravimetry and element analysis. The synthesis method was found to be both efficient and selective for grafting.

Bao-Xiu *et al*. [58] prepared an adsorbent resin by graft copolymerization of acrylic acid and acrylamide onto cellulose under microwave irradiation. This material was examined for its adsorption capacity for Cu(II) from wastewater. At optimal adsorption conditions, a maximum adsorption capacity for Cu(II) of 49.6 mg/g was achieved.

4.3.2) Microwave-assisted Grafting

Microwave-assisted grafting involves the use of both microwave radiation and redox initiators. In the grafting reactions, the redox initiators produce free radicals, and their presence enhances the ability of the aqueous reaction mixture to convert the microwave energy to heat energy [59]. In microwave-assisted grafting reactions, where radical initiators are added from outside, ions produced from these salts create ionic drift which results in Joule heating to expedite the heating [60]. It has been postulated that localized heating of the initiator takes place at hot spots regions to generate free radicals faster than under the influence of thermal heating [61].

Zhao *et al.* [62] grafted acrylic acid (AA) and acrylamide (AM) under microwave-assisted conditions to cellulose to produce a heavy metal super-adsorbent polymer resin. In this system potassium persulfate/sodium thiosulfate were used as initiator and *N,N*-methylene bisacrylamide as cross-linker. The role of the initiator was to generate free radicals which were generated more easily and readily under the influence of microwaves as compared to the conventional thermal heating conditions. The reaction time (8 min) under microwaves (360 W power) was much shorter than the time required for grafting via thermal heating on a water-bath (10 h).

Matahwa *et al.* [63] copolymerized *N*-isopropyl acrylamide and methyl acrylate on α-cellulose in a heterogeneous medium. In their system, α-cellulose was dispersed in nitric acid and the reaction medium was exposed to microwaves. The reactions were initiated using the Ce^{4+} and/or the Ce^{4+}- KPS initiator system. The role of KPS was to oxidize Ce^{3+} back to Ce^{4+} (Ce^{4+} was the active species in the radical formation). The reaction time in microwave-assisted grafting was significantly less when compared to the conventional chemical free-radical process, but at higher temperatures (> 60 ^{o}C), the cross linked homopolymer was the only product.

Thakur *et al*. [64] investigated the effect of microwave radiation on the graft copolymerization of butyl acrylate (BA) onto cellulose derived from pine needles. The copolymerization was started off by immersing the cellulose in a specific amount of distilled water for 24 hours. This was then followed by the addition of a known amount of initiator, ferrous ammonium sulfate-potassium persulfate (FAS–KPS), in order to create sufficient free radical sites on the surface of the cellulose fibers. Then to start the copolymerization, the monomer (BA) was added to the reaction flask containing the cellulose fibers in the microwave oven. The reaction mixture was

stirred at selected doses for different time intervals to optimize different conditions of solvent, time, initiator and monomer concentration for maximum percentage grafting.

Kaith *et al.* [65] grafted methyl-methacrylate (MMA) on flax fiber using FAS–H_2O_2 under microwaves. They found that although the use of microwave irradiation reduced the reaction times compared the conventional free-radical technique, there was a negative effect on grafting percent – there was actually a drop in percentage grafting under microwave irradiation from 42% to 25%. They explained the drop in percentage grafting on the basis of rapid collisions between the different free radical active species generated under the influence of microwave irradiation. This resulted in the formation of a higher percentage of homopolymers rather than copolymers.

4.4) Mechanism

4.4.1) Microwave-assisted Copolymerization

The mechanism of acrylamide grafting on starch in the presence of CAN-HNO_3 initiator and under microwave-assisted irradiation was proposed by several authors [66, 67]. According to the authors, the electrophilic cerium ions have the possibility of attacking either the lone pair of oxygen in the hydroxyl groups at the secondary C_2–C_3 or at the C_6 hydroxyl. Under conventional chemical free-radical conditions, C_2–C_3 attack is preferred because of higher electron density. Sen *et al.* [68] proposed that when the starch is irradiated with microwaves, binding at C_6 hydroxyl occurs. The authors noted that copolymerization occurs without the disruption to the glucopyranose skeleton.

In the crystal structure of CAN, cerium (IV) is surrounded by oxygen atoms from six-bidentate nitrate ions resulting in a 12- coordinate icosahedral geometry [69]. Ce^{4+} takes electrons from C_6 alcoholic oxygen of starch to form a new Ce-O bond that is predominately ionic in character. This new bond being more polar than OH, cleaves readily in the presence of microwave irradiation. The process results in generation of free radical sites on the backbone of polysaccharide, from where the graft chains grow. Under their experimental conditions, the authors [70, 71] noted the formation of free radicals from the polysaccharide backbone and acrylamide monomers. These free radicals would recombine with each other through initiation, propagation and termination steps to produce graft copolymers.

Based on the above discussion, the following mechanism for the copolymerization of acrylamide onto cellulose in the presence of CAN-HNO_3 initiator is proposed (Scheme 4.1):

Initiation:

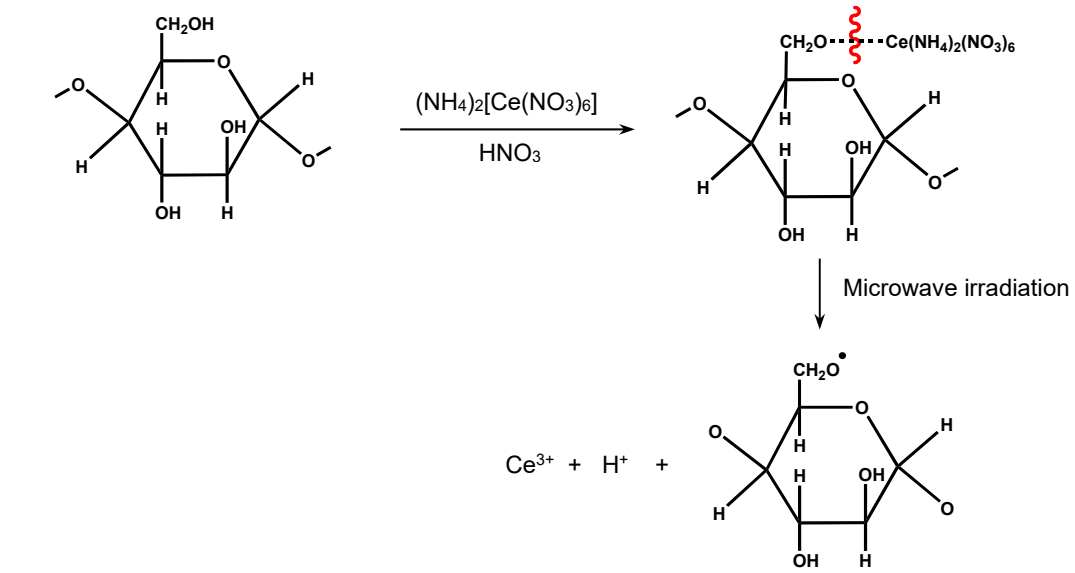

Propagation:

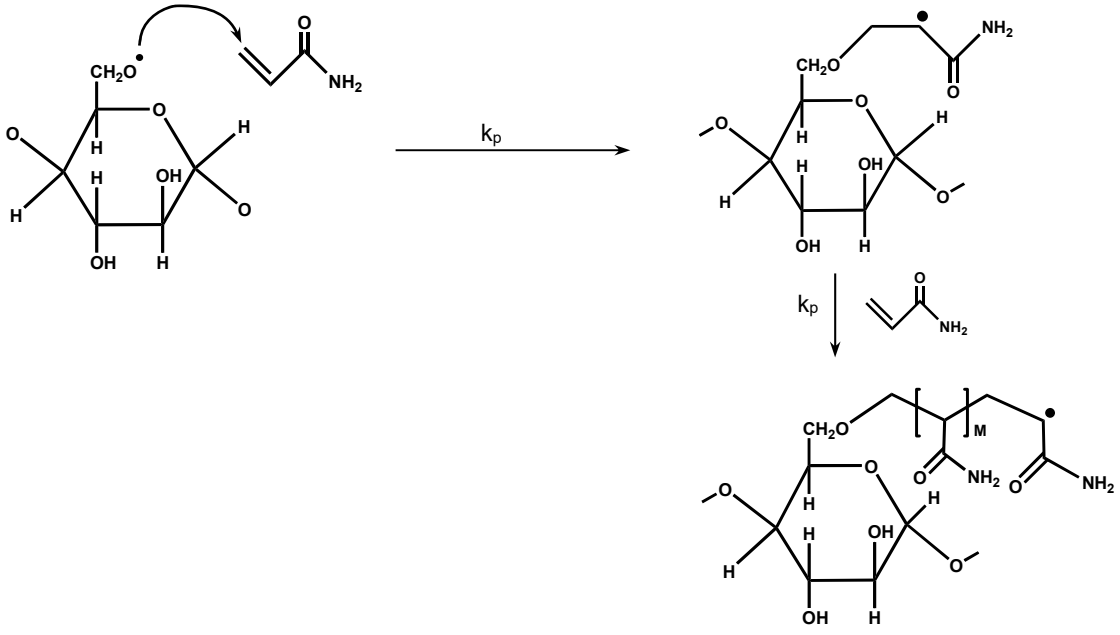

Scheme 4.1: Possible mechanism of graft copolymerization of acrylamide onto cellulose via microwave-assisted grafting

4.4.2) Microwave-initiated Grafting

Notwithstanding the discussion in Section 4.2, microwave-initiated copolymerization of polysaccharides have been observed to occur in the absence of chemical free-radical initiators by several researchers [72].

These researchers have proposed that since no grafting was observed to occur when a radical scavenger such as hydroquinone was added to the reaction mixture, a free radical mechanism for the grafting was most probable. As no radical initiator was added, the grafting observed could be initiated by the generation of the free radicals under the influence of the microwaves that can be explained as follows.

When small polar molecules like water are irradiated with microwave, it results in rotation of the molecules, leading to generation of heat. However, no free radicals are produced [73]. However, if bigger molecules or macromolecules such as polysaccharides are present, rotation of the entire molecule is not possible. In these cases, the microwave is absorbed by the pendant polar groups such as –OH groups which then behave as if they were anchored to an immobile substrate. Under these conditions localized rotations of the pendant groups occur in the microwave region. This results in severing of the bond leading to formation of free radical sites [74] – the authors suggest that with cellulose, free radical sites are expected to be generated at the primary hydroxyl group. Also, microwave energy absorbed by the water molecules is quickly transferred to the acrylamide molecules, causing dielectric heating of acrylamide molecules. Further, microwaves are also reported to have special effects of lowering of Gibbs energy of activation of the reactions [75]. These effects generate free radicals on the polar –OH groups of the polysaccharide backbone and on the monomer. In view of the above two effects, a plausible free radical mechanism for the grafting of acrylamide onto cellulose under microwave-initiated polymerization is shown in Scheme 4.2.

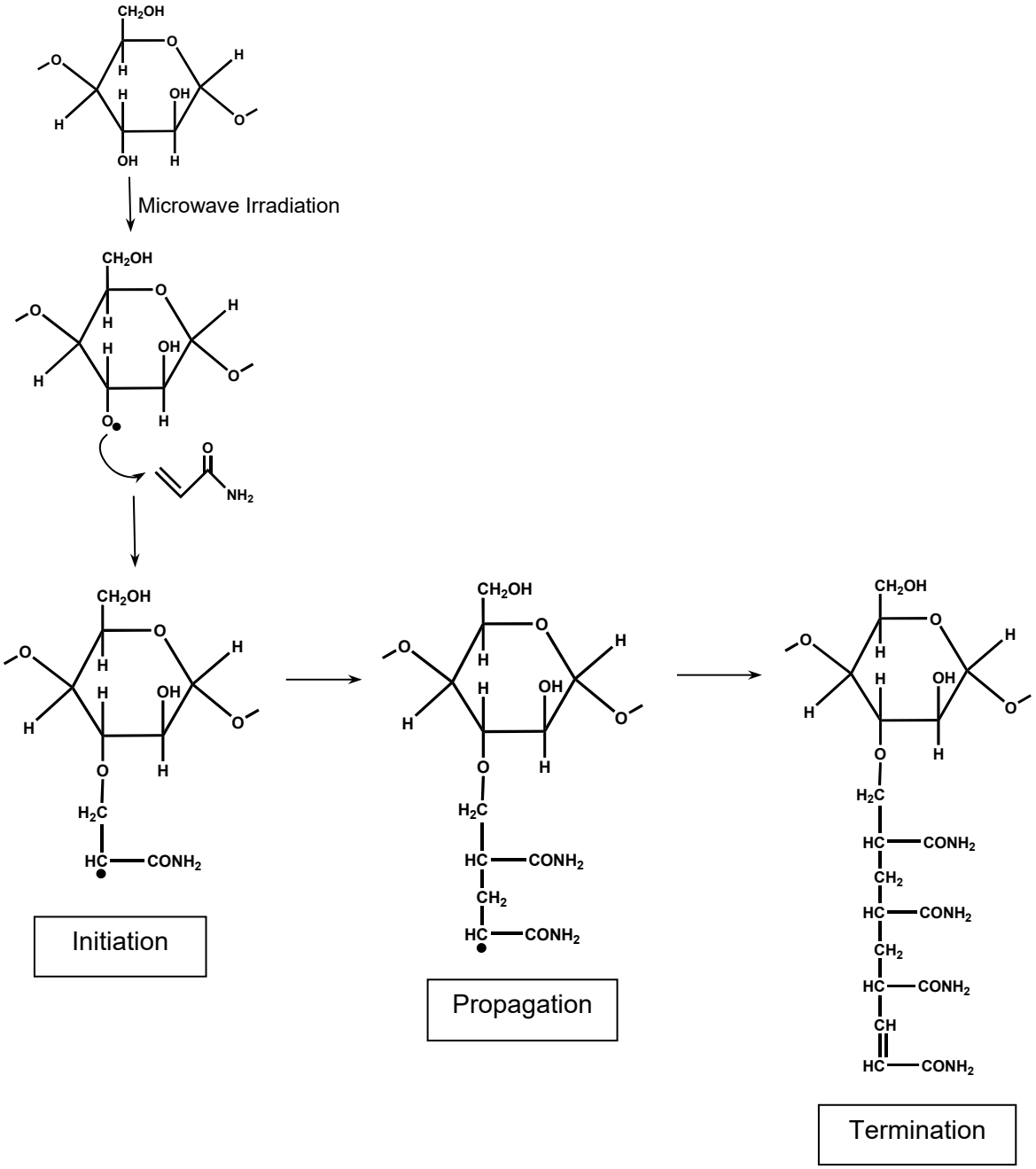

Scheme 4.2: Possible mechanism of graft copolymerization of acrylamide onto cellulose via microwave initiated grafting

4.5) Experimental

4.5.1) Reagents and Glassware

The following chemicals were required for the synthesis of Cell-*g*-PAM. The natural polymer, α-cellulose, was purchased from Sigma Aldrich (Germany) and was washed with water and then ethanol and vacuum dried at 60 °C to a constant weight before use. The monomer acrylamide, also from Sigma Aldrich, was recrystallized from acetone before use. Ceric ammonium nitrate (CAN) and hydroquinone were obtained from E. Merck, Germany and used as received. *N,N*-Dimethylformamide, acetone, and acetic acid, purchased from KIMIX (SA), used for extraction were reagent grade and used as received. Oxygen-free nitrogen (Afrox, SA) was used for purging the polymerization solution. All solutions were prepared by deionized water from a Millipore Direct-Q 5 ultrapure water system.

The following chemicals were purchased for the flocculation tests. Kaolinite powder, having a particle size range of 0.1 – 4 μm, was purchased from Sigma Chemicals and was used as received. Industrial flocculants: Magnafloc 351, Magnafloc 10, Magnafloc 380, and Magnafloc 4240 were purchased from BASF (SA). Hydrazine sulfate and hexamethylene tetramine, required to calibrate the turbidity meter was purchased from Sigma Aldrich (Germany).

All glassware was cleaned thoroughly before use. The vessels were first soaked in an alkali wash, rinsed with deionized water and left to stand in a dust-free cabinet. They were then dried in an oven prior to use.

4.5.2) Microwave Reactor

To overcome the limitations of the commercially available microwave reactors (as discussed in Section 4.2.3 above), Longo *et al.* [76] have designed and built a new, unique process involving a microwave applicator for in situ activation of the reaction. This new design also includes several advantages over previous microwave reactor setups: (i) the setup allows easy scale-up and continuous process of reactions; (ii) the setup can be easily modified to operate both as batch reactor and as a continuously stirred tank reactor (CSTR); (iii) Any auxiliary components can be added without affecting the operation of the microwave synthesis; the reactor can be

fabricated from any material, including metal, and hence can operate at extremely low or high pressures and temperatures.

The experimental appartus used in the current project is shown in Figure 4.10 and is based on the design of Longo *et al*. [76].

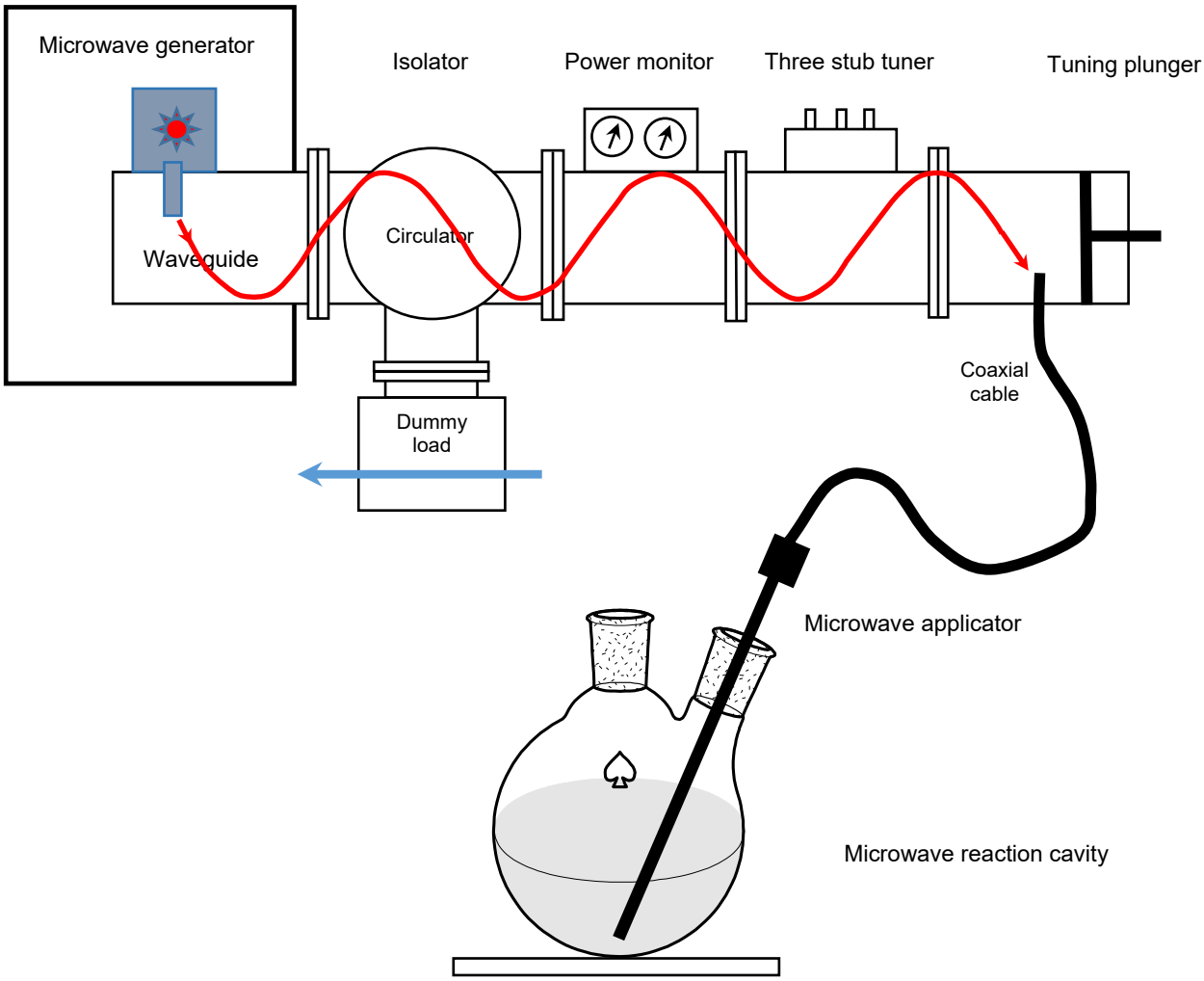

Figure 4.10: Schematic diagram of experimental setup

The microwave generation system consists of a power source to operate a magnetron, an isolator or circulator, a directional coupler with a meter to measure the forward and reverse power, a three stub manual tuner and a waveguide-to-coaxial cable transition.

4.5.2.1) Magnetron

The microwaves were generated by a water-cooled, low power National magnetron (Richardson Electronics, LaFox IL, USA) emitting at a frequency of 2.45 GHz. The magnetron was housed in a magnetron head which comprised the magnetron, a waveguide launcher, and the electronic circuitory to interface with a power supply. The microwave generator system was designed to provide a stable and controllable microwave power up to 800 W.

The magnetron used to generate the microwaves consists of an anode (shown in red) surrounding a cylindrical cathode (shown in green) (Figure 4.11). The anode has holes or cavities, called resonance chambers, cut into it. The anode is made up of an even number of small cavities, each of which acts as a tuned circuit. The anode is, therefore, a series of circuits, which are tuned to oscillate at a specific frequency. An antenna is connected to one cavity to transmit the generated microwaves.

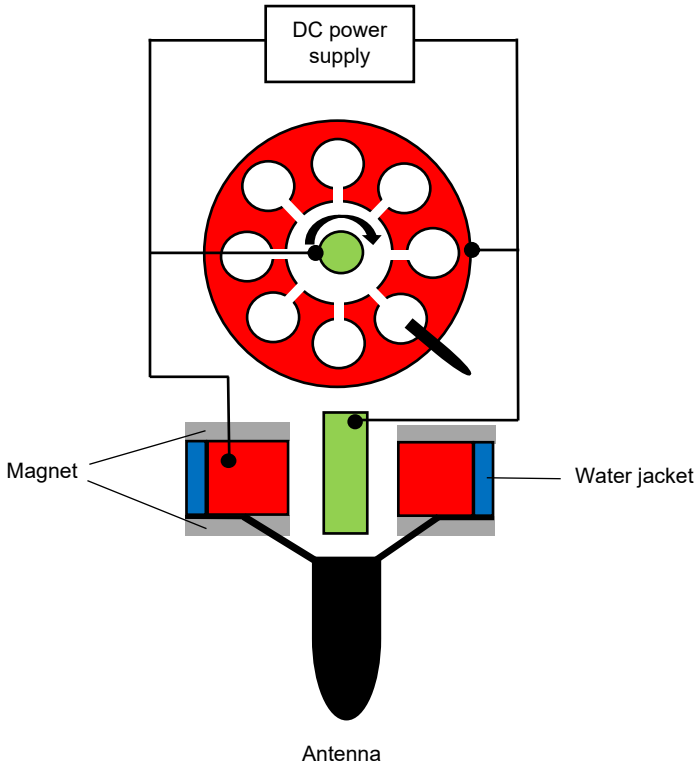

Figure 4.11: Microwave magneron

When the magnetron is switched on, the heated cathode emits electrons which would ordinarily migrate to the surrounding anode as a result of the eletric field set up between the cathode and the anode. However, due to a very powerful axial magnetic field generated by the permanent magnets, the elecrons are forced to move in a curved path in the vacuum space between the cathode and the anode. As the deflected electrons pass through the cavity gaps, they induce a small charge into the tuned circuit, resulting in the oscillation of the cavity. Alternate cavities are linked by two small wire straps, which ensure the correct phase relationship. The frequency at which this resonation occurs is in the microwave range. This process of oscillation continues until the oscillation has achieved a sufficiently high amplitude. It is then taken off by the anode via an antenna. The microwave radiation produced in the cavities is collected up and channeled by a kind of funnel called the waveguide. Only about 50% of the total electric power generated by the magnetron (1200 – 1500 W) is available as electromagnetic energy. The remainder is converted into heat and must be dissipated by an air or water cooling system.

4.5.2.2) Isolator

The microwaves that are generated by the magnetron travel down the waveguide, enter the coaxial cable and eventually end up in the reaction medium. That fraction of the incident microwave not entering the coaxial cable is reflected back in the direction of the generator. This power could potentially reach the magnetron and cause excess heating and damage to the delicate equipment and circuitory. To prevent damage to the generator, an isolator comprising a circulator and a dummy load is placed immediately after the generator unit. The circulator is a passive unit consisting of three ports with a water load attached to one of the ports and is used to absorb the reflected energy. Its physical geometry allows for the incident wave to be transmitted, whilst directing any reflected power into the flowing water load. The reflected microwave is thus rejected to water passing through the dummy load.

4.5.2.3) Directional Coupler

The directional coupler is a passive waveguide component that is used to measure forward and reflected microwave energy. It provides a simple, convenient, and accurate means for sampling microwave energy without moving parts and without the need for adjustments. In the current setup, a 60 dB bi-directional coupler was used to send a small fraction of the microwaves to a power meter to obtain a measure of the forward and reflected power.

4.5.2.4) Tuner

According to electronic theory the power dissipation from the energy source (magnetron) is maximized when the impedance of the generator is matched to that of the system [77]. The system is defined as everything attached to the generator and includes the waveguides, isolator, tuning devices, transmission line and the load (reaction medium). If impedance is not matched energy will be reflected back to the generator, reducing efficiency and the operational lifetime of the magnetron.

In the experimental setup, the stub tuner consisted of three capacitive stubs inserted into the waveguide between the magnetron generator and the reaction medium. The stubs could be adjusted by inserting the metallic stubs at different lengths into the waveguide and fine tuning the depth using vertical micrometer screws. Although the stub tuners came standard with the equipment, they were not used because of the low range power (0 – 800 W) used.

4.5.2.5) Coaxial Line

The coaxial cable is a transmission line used to carry the microwaves from the waveguide to the microwave applicator. It was constructed using a short section (500 mm) of semi-rigid commercial 50 Ω metal core surrounded by a low-density polytetrafluoroethylene (PTFE) for working at temperatures in the range from –65 °C to +250 °C. This was then surrounded by another metallic shield and finally insulated with a plastic sheath (Figure 4.12). The coaxial cable had an external diameter of 6.3 mm, a characteristic impedance of 50, and a maximum continuous power handling capacity of 800 W at 2.45 GHz.

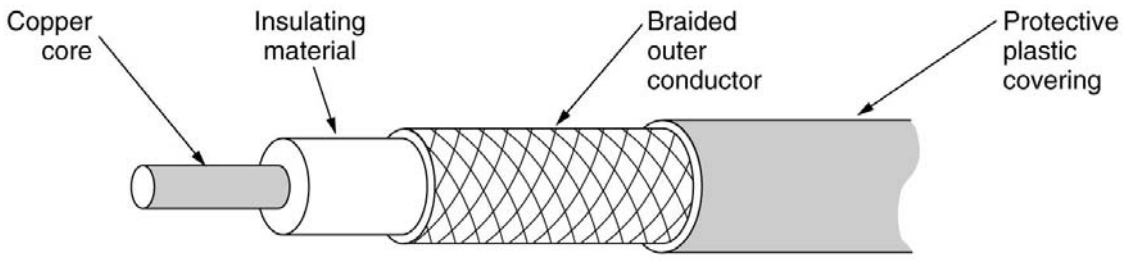

Figure 4.12: Microwave co-axial cable

4.5.2.6) Microwave Applicator

The microwave applicator that was fabricated and used in the experiments is depicted in Figure 4.13.

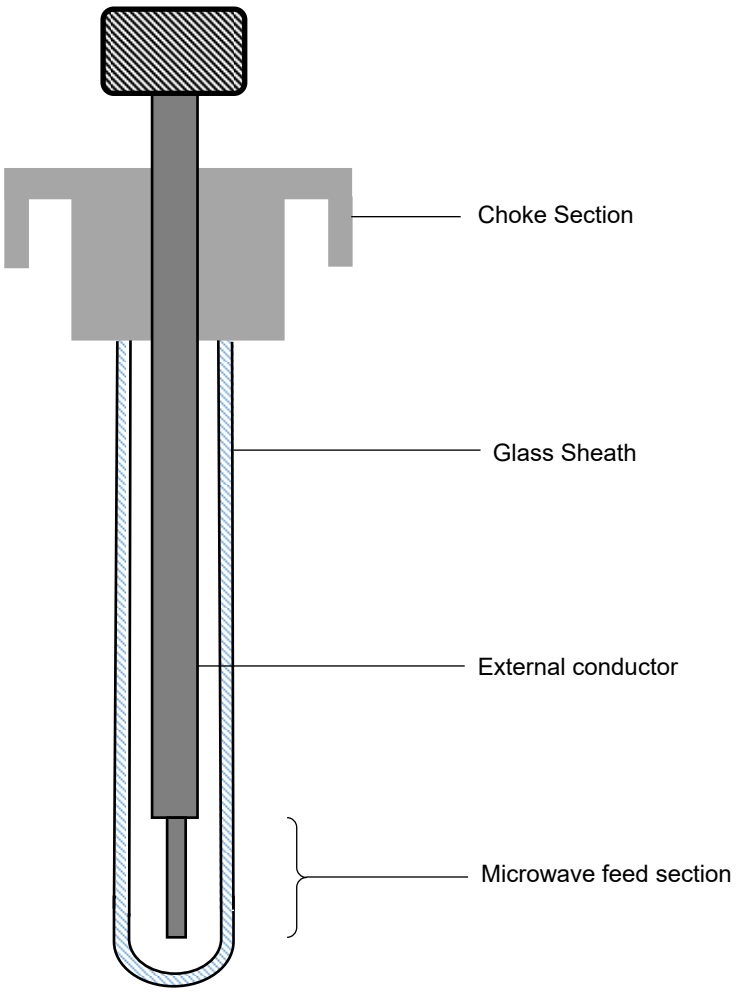

Figure 4.13: Longitudinal section of microwave applicator

The inner core of the applicator was a continuation of the coaxial cable used to transmit the microwaves from the waveguide. The radiating section of the applicator was obtained by stripping off 25 mm from the end of the external conductor cable. A brass choke section was designed to block the backward flow of microwaves flowing along the surface of the coaxial cable. This section was also specifically designed to accommodate the neck of a standard 250 mL round bottom glass flask. To protect the coaxial cable from damage when operating in reactive chemicals, it was surrounded by a protective glass sheath that isolated the coaxial cable from the reactive medium. The glass sheath was made using a 7 mm (inner diameter) 9

mm (outer diameter) borosilicate glass tubing, which was fitted to the choke using a high-temperature two-component epoxy glue.

4.5.2.7) Microwave Reactor Cavity

The microwave chemical reactor consisted of a 2-necked, 250-mL round bottom glass flask, filled with the reaction medium to be heated and activated by the immersed insulated microwave applicator, as shown in Figure 4.10. The second neck of the round bottom flask was used to add reagents and permit any possible vaporization of the reactants during the microwave assisted chemical process.

4.5.3) Synthesis of Graft Copolymer (Cell-*g*-PAM)

The grafting reaction was carried out by two different methods. The most commonly used method employs microwave in presence of a free radical initiator (microwave-assisted grafting) [78]. The lesser known method involves the use of microwave radiation in absence of any free radical initiator (microwave-initiated grafting) [79]. Since the microwave-initiated method does not require any catalyst (free radical initiator), it is considered to be more ecofriendly.

4.5.3.1) Microwave-Assisted Copolymerization

Microwave irradiation and the chemical free-radical initiator, CAN-HNO_3, were used to generate the free radical sites on the cellulose backbone. The synthesis procedure is shown in Figure 4.14 and is based on the method described by Singh *et al.* [80].

The reaction procedure commenced with the addition of 4 g (0.025 mol, based on 1 anhydroglucose pyranose unit) of cellulose which was soaked overnight in 70 mL distilled water to a 250 mL round-bottomed reactor vessel. The reactor vessel was placed on a magnetic stirrer and the desired amount of acrylamide monomer (0.05 – 0.246 mol), which was dissolved in 20 mL distilled water, was added to the reaction mixture. The reaction vessel was then fitted with a reflux condenser and an oxygen-free nitrogen inlet line which was used to purge the system until the end of the reaction period. A freshly prepared, 10 mL solution of CAN (4.9×10^{-4} – 4.9×10^{-3} mol) in nitric acid was added to the solution and the entire setup was enclosed in a Faraday cage.

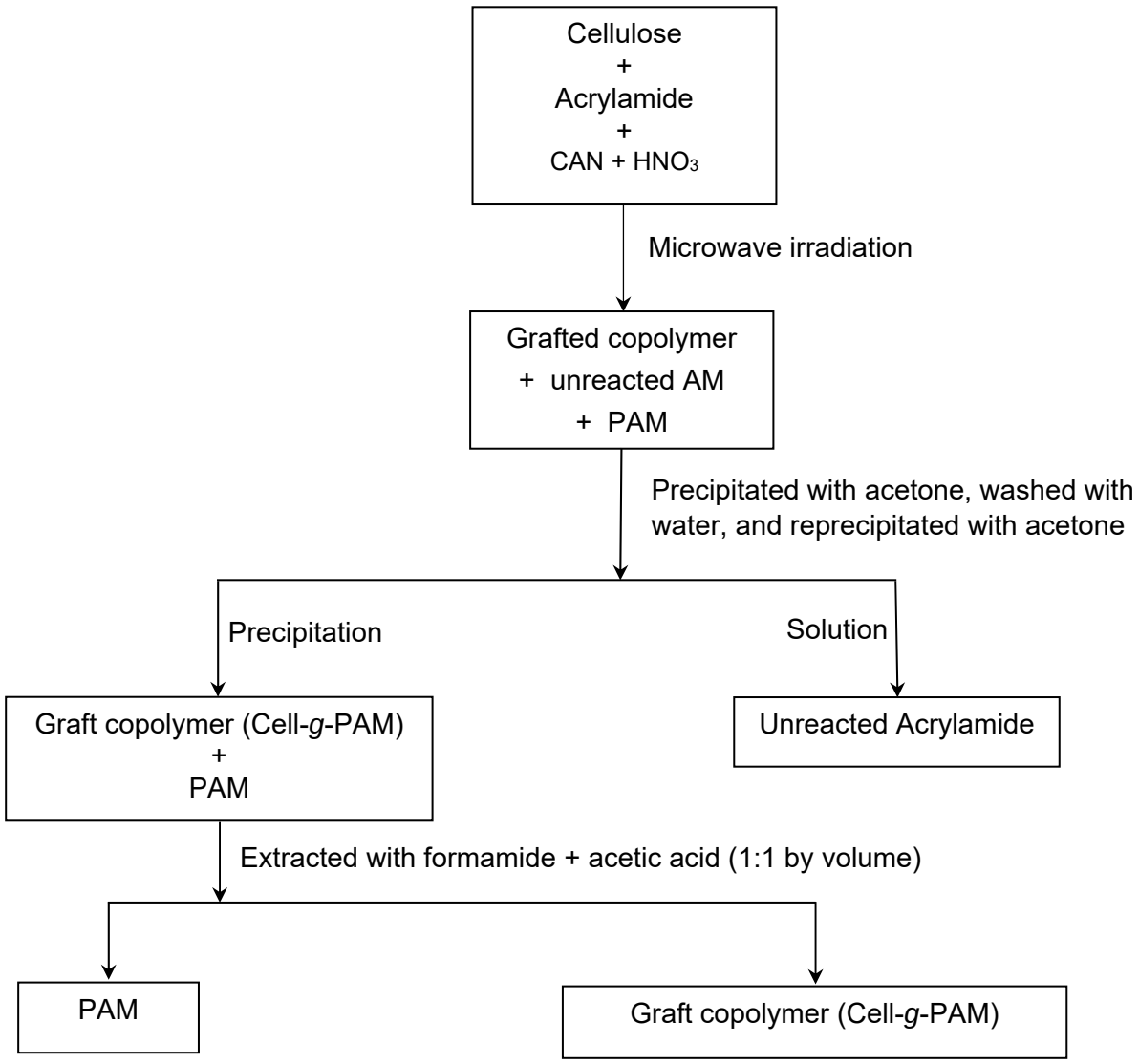

Figure 4.14: Procedure to synthesize and purify Cell-*g*-PAM via microwave-assisted technique

The reaction mixture was then irradiated with microwaves of different power settings (100 – 500 W) and the reaction allowed to proceed for the desired time period (1 – 5 minutes). The reaction was stopped by the addition of 1 mL of 2% hydroquinone solution to the reaction mixture.

At the end of the reaction, the reaction mixture may contain a small amount of unreacted acrylamide monomer. The reaction mixture was therefore poured into a 1-L beaker, in which it was made into a homogeneous slurry with the addition of distilled water. The viscous slurry was then precipitated by the addition of an excess quantity of acetone. The precipitated product was

centrifuged and dried overnight in a vacuum oven at 40 °C. The dried product from the above step was then extracted with a dimethylformamide : acetic acid mixture (1:1) for 24 h and washed with methanol to remove the homopolymer (polyacrylamide). The grafted cellulose (cell-*g*-AM) was finally dried to a constant weight under vacuum for 24 h at 40 °C.

It should be noted that although researchers have conducted microwave-assisted copolymerizations in the presence of air, preliminary experiments indicated a much lower percentage grafting when compared to experiments conducted in an inert atmosphere. Based on this, it was decided to conduct all experiments in an atmosphere of nitrogen.

4.5.3.2) Microwave-initiated Copolymerization

In this method, microwave irradiation was used to generate the free radical sites on the cellulose backbone no free radical initiator was used in the process. The details of the method of synthesis employed were as follows: 4 g (0.025 mol, based on an anhydroglucose pyranose unit) of cellulose was dissolved in 70mL distilled water in the 250 mL round-bottomed reactor vessel. The desired amount of acrylamide monomer (0.05 – 0.246 mol) was then dissolved in 20 mL distilled water and added to the reaction mixture. The reaction vessel was then fitted with a reflux condenser and an oxygen-free nitrogen inlet line. The reaction vessel was placed on a magnetic stirrer and the solution mixed well for 5 minutes. The entire setup was then enclosed in a Faraday cage and the reaction initiated by irradiating the mixture with microwaves of different power settings (100 – 500 W). The reaction was allowed to proceed for the desired time period (1 – 5 minutes) and then stopped by the addition of 1 mL of 2% hydroquinone solution to the reaction mixture. The reactor vessel was continuously purged with the supply of nitrogen throughout the reaction period. Any occluded polyacrylamide (PAM) formed by competing homopolymer formation reaction was removed from the graft copolymers by solvent extraction using a mixture of formamide and acetic acid (1:1 by volume), as in the case of the microwave-assisted copolymerization.

The percentage grafting (%G) for both the microwave-assisted and microwave-initiated copolymerization was determined from the increase in the weight of cellulose after grafting according to Equation 4.5:

$$\% \text{ grafting} = \frac{\text{wt. of graft copolymer - wt. of cellulose}}{\text{wt. of cellulose}} \text{ x } 100 \qquad (4.5)$$

4.5.4) Synthesis of Hydrolyzed Polyacrylamide grafted Cellulose

Partial alkaline hydrolysis of the highest percentage grafted Cell-*g*-PAM was performed as follows: 1 g of the graft copolymer was dissolved in 100 mL of distilled water in a 200 mL round bottomed flask and 2 mL of a 1 N NaOH solution was added to the solution. The mixture was placed in a thermo-stated water bath at a temperature of 50 °C and stirred for 3 hours. At the end of the reaction time, the reaction mixture was added to a beaker containing 300 mL of acetone with stirring to precipitate the hydrolyzed product. The product was then washed with ethanol–water (70:30) mixture. The resulting precipitate was collected, and dried in a vacuum oven at 50 °C for 6 h.

The reaction is schematically depicted in Scheme 4.3.

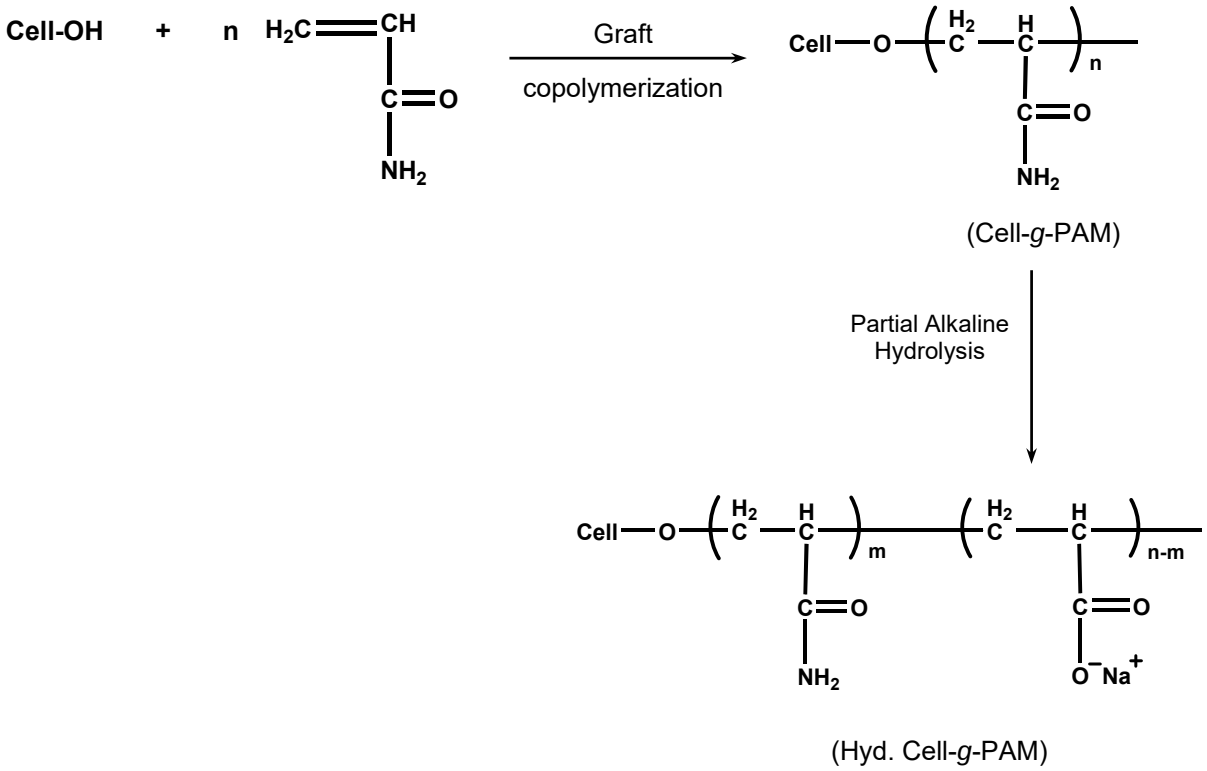

Scheme 4.3: Schematic representation of synthesis of Hyd. Cell-*g*-PAM

4.5.5) Experimental Design and Statistical Analysis

The basic principle behind response surface methodology (RSM) analysis is to relate the observed value (dependent variables) to process parameters (independent variables) using statistical methods, yielding a multivariate regression equation, often of second-order. RSM takes into consideration any possible interactions between the variables and optimizes the process variables, whilst requiring the least number of experimental runs [81]. Therefore, it was considered an effective method for optimizing the conditions for copolymerizing acrylamide onto cellulose. A central composite design (CCD) was used in this study.

4.5.5.1) Microwave-assisted Copolymerization

Four factors (monomer to cellulose molar ratio, time period of reaction, power of microwave irradiation, and initiator to cellulose molar ratio) were identified as factors affecting the grafting percentage and were varied simultaneously using a factorial design template. Although temperature is an important parameter affecting the percentage grafting, it was not possible to independently vary the value of temperature – in a batch reaction system such as the one used in this study, temperature changes integrally with change in power and time. A five-level-four-factor fractional central composite design (CCD) was employed, requiring 30 experimental runs (calculated based on Equation 4.6) which consist of 16 factorial runs, 8 axial runs and 6 replicate runs at the centre.

$$N = 2^n + 2n + N_c = 2^4 + 2(4) + 6 = 30 \tag{4.6}$$

where N is the total experimental runs, n the number of variables, and N_c is the number of central runs. The effect of the independent variables on the %G were determined at 5 levels ($-\alpha$, -1, 0, +1, $+\alpha$). The alpha value depends on the number of independent factors (variables) in the factorial design and is determined by Equation 4.7.

$$\alpha = \left(2^n\right)^{1/4} \tag{4.7}$$

where n is the number of independent factors. For four factors, as in the case of microwave-assisted grafting, α = 2. The coded and actual levels of the independent variables are given in Table 4.2 and can be related using Equation 4.8.

$$X = \frac{x_i - x_o}{\Delta x} \tag{4.8}$$

where X is the coded value of the independent variable, x_i is the actual value of the independent variable, x_o is the midpoint value of the actual variable, and Δx is the interval of the original range.

Table 4.2: Experimental range and levels of the independent variables for microwave-assisted copolymerization

Independent variables	Code	Units	Factor level				
			-2	-1	0	1	2
Time	X_1	min	1	2	3	4	5
[AM] : [cellulose]	X_2	-	2	4	6	8	10
[CAN] : [cellulose]	X_3	-	0.02	0.065	0.1	0.16	0.2
Power	X_4	W	100	200	300	400	500

In all experimental runs, the mass of cellulose was held constant at 4 g (0.025 mol – based on an anhydroglucose pyranose unit). The factor ranges were selected based on the prior knowledge about the system from preliminary experimental trials.

The behavior of the system can be described by the second-order polynomial Equation 4.9:

$$Y = \beta_o + \sum_{i=1}^{4} \beta_i x_i + \sum_{i=1}^{4} \beta_{ii} x_i^2 + \sum_{i=1}^{3} \sum_{j=i+1}^{4} \beta_{ij} x_i x_j + \varepsilon \qquad (4.9)$$

where Y is the response (percentage grafting), β_o the value of the fitted response at the center point, and β_i, β_{ii}, and β_{ij} are the linear, quadratic, and cross-product (interaction) regression terms, respectively.

In order to obtain the general form of the probability distribution of the error term, four assumptions have been made [82]:

i) The mean of the probability distribution of ε is zero.
ii) The variance of the probability distribution of ε is constant for all settings of the independent variables.
iii) The probability distribution of ε is normal.
iv) The errors associated with two different observations are independent.

Residual plots and test statistics allow one to check the validity of these assumptions.

4.5.5.2) Microwave-initiated Copolymerization

For the graft copolymerization of acrylamide onto cellulose using microwave-initiated technique, the independent variables that were considered significant were the microwave power, the time period for microwave irradiation, and the acrylamide to cellulose molar ratio. In this research, the central composite design (CCD) was used to study the effect of these variables, and any possible interactions between them, on the percentage grafting. The variables were examined at five levels, namely the factorial points levels (+1 and -1), the replication point level (0) that was situated in the cubic design center, and the axial points that were placed at the outer edge of the cubic design relating to the α values (±1.68) for each factors. The ranges and levels of the variables studied are shown in Table 4.3.

Table 4.3: Experimental range and levels of the independent variables for microwave-initiated copolymerization

Independent variables	Code	Units	Factor level				
			-2	-1	0	1	2
Time	X_1	min	1	2	3	4	5
[AM] : [cellulose]	X_2	-	2	4	6	8	10
Power	X_3	W	100	200	300	400	500

As the number of independent variables were low (three), a full factorial experimental design consisting of 20 points, including six replications at the central point, were carried out in a random order. The full quadratic model for microwave-initiated copolymerization was established by using the mathematical equation (Equation 4.10)

$$Y = \beta_o + \sum_{i=1}^{3} \beta_i x_i + \sum_{i=1}^{3} \beta_{ii} x_i^2 + \sum_{i=1}^{2} \sum_{j=i+1}^{3} \beta_{ij} x_i x_j$$

$$= \beta_o + \beta_1 X_1 + \beta_2 X_2 + \beta_3 X_3 + \beta_{11} X_1^2 + \beta_{22} X_2^2 + \beta_{33} X_3^2 + \beta_{12} X_1 X_2 + \beta_{13} X_1 X_3 + \beta_{23} X_2 X_3 \quad (4.10)$$

where Y is the response variable (percentage grafting), β_i are regression coefficients for linear effects; β_{ik} are regression coefficients for effects from interaction; β_{ii} are regression coefficients for quadratic effects; and X_i are the coded experimental levels of the variables.

4.5.6) Data Processing

Numerical and graphical optimization was carried out for the process parameters for both the microwave-assisted and microwave-initiated copolymerization of acrylamide onto cellulose. This optimization was performed using the Design Expert software program (V7.0.0) (Stat-Ease, Inc., Minneapolis, MN, USA). The software package was utilized to analyze the statistical characteristics of the data and to develop a regression equation between the input process variables and the percentage grafting (%G). The statistical testing of the model, which includes linear, quadratic and interaction coefficient, was performed by ANOVA analysis with F-test to obtain the empirical correlation between input and output parameters. According to the experimental data, the fitting model represented by Equation 4.9 was constructed and the statistical significance of the model terms was examined by regression analysis and analysis of variance (ANOVA). The reliabilities of the models were determined by model analysis, lack of fit tests, and R^2 (coefficient of determination) analysis. The determination coefficient (R^2) indicates the goodness of fit for the model. The values of the determination coefficient (R^2) indicate that the model does not explain only less than 5% of the total variations [83]. The values of adjusted determination coefficient (adjusted R^2) should be high, which indicates a high significance of the model. Predicted R^2 denotes the agreement with the adjusted R^2. The coefficient of variation (CV) indicates the relative dispersion of the experimental points from the model prediction. The experimental and predicted percentage grafting were compared in order to determine the validity of the model.

4.5.7) Flocculation Studies

The flocculation characteristics of the highest percentage grafted Cell-*g*-PAM copolymer, the hydrolyzed Cell-g-PAM as well as the best performing commercially available flocculant (Magnafloc 4240) from the previous study (Chapter 3) were investigated using a Jar Test and Settling Test method. A 0.25% (w/v) kaolinite suspension was used as the synthetic wastewater.

4.5.7.1) Jar Tests

The Jar-test studies were carried out using a Phipps and Bird Six-Paddle Stirrer, model PB-7790910 jar test apparatus. The following procedure was adopted uniformly for all the

flocculants. Synthetic effluent suspensions (1000 mL) were placed in six, 1.5 L Gator Jars. The jars were placed on the flocculator bench, with the stirrer blades dipped in the suspension. Varying dosages of the flocculants were added to each jar under slow stirring conditions. Immediately after the addition of the flocculant to all the jars, the suspensions were stirred at a constant high speed of 125 rpm for 2 minutes. This was followed by slow stirring at 20 rpm for 15 minutes. When the flocculants were added to the effluent suspensions, flocs developed in the solutions. The flocs were allowed to settle for a period of 30 minutes. A sample of the supernatant liquid was then drawn, and its turbidity measured with a digital Nephelo turbidity meter (HANNA model HI88703). The turbidity was expressed in Nephelo turbidity units (NTUs).

4.5.7.2) Settling Test

The column-settling studies were carried out using the same 0.25% (w/v) synthetic suspensions used for the Jar Tests. This test employed a 1000 mL, stoppered, graduated cylinder and stopwatch. The tests started with adding 1000 mL of the kaolinite suspension to a Gator Jar, adding a dosage of flocculant and rapidly stirring the mixture at 125 rpm for 2 minutes. The dosage of flocculants to be added was determined from the Jar Test – it was the optimally determined dosage of the hydrolyzed Cell-*g*-PAM flocculant. The mixed slurry sample from the Gator Jar was poured into the graduated cylinder and the cylinder was then inverted 10 times for thorough mixing. After the cylinder was set upright, the height of the interface between the water and settling solid bed was measured over time.

4.6) Results and Discussion

4.6.1) Percentage Grafting of Cell-*g*-PAM

The experimental design matrix, in terms of real and coded independent variables and the results, is presented in Table 4.4 for the microwave-assisted grafting of polyacrylamide onto cellulose and in Table 4.5 for the case of microwave-initiated grafting. The experiments in both cases were conducted according to the run order, which is a random order, to minimize errors from systematic trends in the variables.

Table 4.4: Experimental design matrix for the synthesis of Cell-*g*-PAM (microwave-assisted) with results

Std Order	Run Order	Time	[AM] / [Cell]	[CAN] / [Cell]	Power	%G (Actual)	%G (Predicted)
1	26	-1 (2)	-1 (4)	-1 (0.07)	-1 (200)	143.2	143.7
2	10	1 (4)	-1 (4)	-1 (0.07)	-1 (200)	139.1	138.8
3	29	-1 (2)	1 (8)	-1 (0.07)	-1 (200)	153.4	152.0
4	19	1 (4)	1 (8)	-1 (0.07)	-1 (200)	161.1	163.8
5	6	-1 (2)	-1 (4)	1 (0.16)	-1 (200)	152.9	151.0
6	12	1 (4)	-1 (4)	1 (0.16)	-1 (200)	150.1	152.3
7	22	-1 (2)	1 (8)	1 (0.16)	-1 (200)	160.9	156.5
8	4	1 (4)	1 (8)	1 (0.16)	-1 (200)	172.8	174.6
9	27	-1 (2)	-1 (4)	-1 (0.07)	1 (400)	173.1	168.1
10	8	1 (4)	-1 (4)	-1 (0.07)	1 (400)	168.3	175.5
11	5	-1 (2)	1 (8)	-1 (0.07)	1 (400)	164.8	165.7
12	18	1 (4)	1 (8)	-1 (0.07)	1 (400)	190.9	189.8
13	23	-1 (2)	-1 (4)	1 (0.16)	1 (400)	175.2	175.2
14	7	1 (4)	-1 (4)	1 (0.16)	1 (400)	190.7	188.8
15	16	-1 (2)	1 (8)	1 (0.16)	1 (400)	173.1	170.0
16	28	1 (4)	1 (8)	1 (0.16)	1 (400)	197.9	200.3
17	25	-2 (1)	0 (6)	0 (0.1)	0 (300)	143.4	149.9
18	17	2 (4)	0 (6)	0 (0.1)	0 (300)	181.7	175.4
19	20	0 (3)	-2 (2)	0 (0.1)	0 (300)	158.9	158.2
20	11	0 (3)	2 (10)	0 (0.1)	0 (300)	177.3	178.0
21	1	0 (3)	0 (6)	-2 (0.02)	0 (300)	154.8	152.7
22	21	0 (3)	0 (6)	2 (0.2)	0 (300)	168.5	170.5
23	14	0 (3)	0 (6)	0 (0.1)	-2 (100)	148.9	149.0
24	9	0 (3)	0 (6)	0 (0.1)	2 (500)	199.0	199.2
25	30	0 (3)	0 (6)	0 (0.1)	0 (300)	181.1	180.8
26	2	0 (3)	0 (6)	0 (0.1)	0 (300)	179.2	180.8
27	13	0 (3)	0 (6)	0 (0.1)	0 (300)	181.9	180.8
28	24	0 (3)	0 (6)	0 (0.1)	0 (300)	182.0	180.8
29	3	0 (3)	0 (6)	0 (0.1)	0 (300)	181.1	180.8
30	15	0 (3)	0 (6)	0 (0.1)	0 (300)	179.8	180.8

Using different combinations of reaction conditions, the percentage grafting varied from 139.1 % to 199.0 %. The highest %G of 199.0 % was synthesized under the following conditions: time = 3 minutes, acrylamide to cellulose molar ratio = 6, CAN to cellulose molar ratio = 0.1, and power = 500 W.

Table 4.5: Experimental design matrix for the synthesis of Cell-*g*-PAM (microwave-initiated) with results

Std Order	Run Order	Time	[AM] / [Cell]	Power	%G (Actual)	%G (Predicted)
1	17	-1 (2)	-1 (4)	-1 (200)	46.9	46.3
2	3	1 (4)	-1 (4)	-1 (200)	50.6	50.6
3	10	-1 (2)	1 (8)	-1 (200)	53.3	51.9
4	2	1 (4)	1 (8)	-1 (200)	62.4	61.1
5	4	-1 (2)	-1 (4)	1 (400)	53.1	52.5
6	16	1 (4)	-1 (4)	1 (400)	63.2	62.7
7	12	-1 (2)	1 (8)	1 (400)	51.8	49.9
8	9	1 (4)	1 (8)	1 (400)	66.2	64.9
9	8	-1.68 (1)	0 (6)	0 (300)	44.6	46.3
10	15	1.68 (5)	0 (6)	0 (300)	61.6	62.6
11	7	0 (3)	-1.68 (2)	0 (300)	48	48.1
12	11	0 (3)	1.68 (10)	0 (300)	52.2	54.8
13	13	0 (3)	0 (6)	-1.68 (100)	54.1	55.2
14	20	0 (3)	0 (6)	1.68 (500)	62	63.6
15	18	0 (3)	0 (6)	0 (300)	56.9	57.4
16	19	0 (3)	0 (6)	0 (300)	57.8	57.4
17	5	0 (3)	0 (6)	0 (300)	56.2	57.4
18	1	0 (3)	0 (6)	0 (300)	57.4	57.4
19	14	0 (3)	0 (6)	0 (300)	58.7	57.4
20	6	0 (3)	0 (6)	0 (300)	58.1	57.4

Using different combinations of reaction conditions, the percentage grafting varied from 44.6 % to 66.2 %. The highest %G of 66.2 % was synthesized under the following conditions: time = 4 minutes, acrylamide to cellulose molar ratio = 8, CAN to cellulose molar ratio = 0.1, and power = 400 W.

4.6.2) Model Selection

Design-Expert collects the important statistics used to select the correct starting point for the final model. The software then provides a suggested model. The software fits linear, two-factor interaction (2FI), quadratic, and cubic polynomials to the experimental data to obtain the regression equations. To decide on the adequacy of models among these various models to represent the percentage grafting, two different tests, namely lack of fit and model summary statistics were carried out in the present study. Table 4.6 presents a summary of relevant statistics for the model for this step.

Table 4.6: Lack of Fit and Model Summary Statistics

Microwave-assisted Grafting					
Lack of Fit Test					
Source	Sum of Squares	Mean Square	F-Value	P-Value	Comment
Linear	2009.13	100.46	73.50	<0.0001	
2FI	1416.26	101.16	74.02	<0.0001	
Quadratic	248.25	24.82	18.16	0.0260	Suggested
Cubic	39.25	19.63	14.36	0.0085	Aliased
Model Summary Statistics					
Source	Std. Deviation	R^2	Adjusted R^2	Predicted R^2	Comment
Linear	8.98	0.7426	0.7015	0.6470	
2FI	8.65	0.8183	0.7227	0.6298	
Quadratic	4.12	0.9674	0.9370	0.8162	Suggested
Cubic	2.57	0.9941	0.9756	0.2772	Aliased
Microwave-initiated Grafting					
Lack of Fit Test					
Source	Sum of Squares	Mean Square	F-Value	P-Value	Comment
Linear	175.40	16.04	20.31	0.0019	
2FI	113.50	14.19	17.97	0.0028	
Quadratic	24.66	4.93	6.25	0.0329	Suggested
Cubic	18.64	18.64	23.61	0.0046	Aliased
Model Summary Statistics					
Source	Std. Deviation	R^2	Adjusted R^2	Predicted R^2	Comment
Linear	3.36	0.7173	0.6644	0.5063	
2FI	3.01	0.8159	0.7310	0.6641	
Quadratic	1.69	0.9552	0.9148	0.6985	Suggested
Cubic	1.94	0.9646	0.8879	-5.4491	Aliased

The “lack of fit” test compares the residual error to the pure error from the replicated design points. The results in Table 4.6 indicate that the quadratic model for both the microwave-assisted and microwave-initiated grafting does not show significant lack of fit, hence the adequacy of quadratic model is confirmed. The cubic model is aliased, so it is not chosen. In the second test, the “model summary statistics,” the predicted R^2 and adjusted R^2 values are

important parameters to consider in determining how well the model can predict the %G responses. The predicted R^2 value predicts how well the model can predict the response while the adjusted R^2 value gives a measure of the amount of variation around the mean explained by the model. For the model to be statistically significant, the adjusted R^2 value and predicted R^2 value should be as high as possible and within approximately 0.20 of each other. As shown in Table 4.6, the quadratic model has higher R^2, adjusted R^2 value and predicted R^2 values than the other models for both microwave-assisted and microwave-initiated grafting. Further, in the quadratic model, the difference between the adjusted R^2 and predicted R^2 is 0.0304 for microwave-assisted grafting and 0.0404 for microwave-initiated grafting – well lower than the 0.2 limit. The quadratic model was therefore chosen as the predictive model.

4.6.3) ANOVA and Fitting of Quadratic Model

When a model has been selected, an analysis of variance (ANOVA) is performed to assess how well the model represented the data. The analysis of variance is a statistical technique that subdivides the total variation in a set of data into component parts associated with specific sources of variation for the purpose of testing hypotheses on the parameters of the model [83].

4.6.3.1) Microwave-assisted Grafting

The analysis of variance for microwave-assisted grafting of polyacrylamide onto cellulose is shown in Table 4.7. The model F-value is 31.83, implying that the model is significant. According to the statistic Prob>F (P-value), there is less than a 0.01% chance that a model F-value this large could occur due to noise. Values of Prob>F less than 0.05 indicate that model terms are significant, while values greater than 0.1 indicate that the model terms are not significant. The lack of fit F-value of 18.16 implies the lack of fit is not significant relative to the pure error. There is also a 0.26% chance that a lack of fit F-value this large could occur due to noise. Nonsignificant lack of fit is desired, and the statistics therefore indicate that the model closely fits the experimental data. The Predicted R^2 is a measure of how good the model is able to predict a response value. Further, the Adjusted R^2 and Predicted R^2 should be within approximately 0.20 of each other to be in reasonable agreement. If they are not, there may be a problem with either the data or the model. In this case, the Predicted R^2 of 0.8162 is in reasonable agreement with the Adjusted R^2 of 0.9320. Adequate precision is a measure of the range in predicted response relative to its associated error, in other words a signal-to-noise ratio

[84]. Its desired value is 4 or more. Therefore, the ratio of 21.105 indicates a good signal to noise signal. The coefficient of variation (C.V.) for this model is the error expressed as a percentage of the mean. The regression coefficient values for the equation relating the %G to the various independent variables are also given in Table 4.7. The P-values were used as a tool to check the significance of each coefficient, which in turn might indicate the pattern of the interactions between the variables. The smaller the value of P is, the more significant the corresponding coefficient is values of "Prob > F" less than 0.05 indicate model terms are significant. In this case A, B, C, D, A^2, B^2, C^2, AB, AD, BD are significant model terms. The other term coefficients were not significant (P > 0.05).

Table 4.7: ANOVA of Response Surface Quadratic Model for percentage grafting for microwave-assisted grafting

Source	Coeff	Sum of Squares	DF	Mean Square	F Value	Prob > F	Significant (Y/N)
A	6.38	975.38	1	975.38	57.36	< 0.0001	Y
B	4.96	590.04	1	590.04	34.70	< 0.0001	Y
C	4.46	477.04	1	477.04	28.05	< 0.0001	Y
D	12.54	3775.04	1	3775.04	221.99	< 0.0001	Y
A^2	-4.55	568.36	1	568.36	33.42	< 0.0001	Y
B^2	-3.18	276.86	1	276.86	16.28	0.0011	Y
C^2	-4.80	632.50	1	632.50	37.19	< 0.0001	Y
D^2	-1.68	77.15	1	77.15	4.54	0.0501	N
AB	4.19	280.56	1	280.56	16.50	0.0010	Y
AC	1.56	39.06	1	39.06	2.30	0.1504	N
AD	3.06	150.06	1	150.06	8.82	0.0095	Y
BC	-0.69	7.56	1	7.56	0.44	0.5150	N
BD	-2.69	115.56	1	115.56	6.80	0.0598	N
CD	-0.06	0.06	1	0.06	0.00	0.9525	N
Model		7578.38	14	541.31	31.83	< 0.0001	Y
Residual		255.08	15	17.01			
Lack of Fit		248.25	10	24.83	18.16	0.0026	Y
Pure Error		6.83	5	1.37			
Cor Total		7833.47	29				

Standard Deviation	4.12	R-Squared	0.9674
Mean	169.47	Adjusted R-Squared	0.9370
C.V.	2.43	Predicted R-Squared	0.8162
PRESS	143.76	Adequate Precision	21.105

Multiple regression analysis of the experimental data yielded the following second-order polynomial equation (Equation 4.11) for the grafting of acrylamide onto cellulose using microwave-assisted grafting:

$$\%G = 180.83 + 6.37\,A + 4.96\,B + 4.46\,C + 12.54\,D - 4.55\,A^2 - 3.18\,B^2 - 4.80\,C^2 + 4.19\,AB + 3.06\,AD \quad (4.11)$$

The results predicted by the model equation (Eq. 4.11) from RSM indicated that a combination of adjusting the reaction time to 3.8 minutes, the acrylamide to cellulose molar ratio to 7.4, CAN to cellulose molar ratio to 0.17, and the irradiation power to 400 W would favour a maximum percentage grafting of 199.6%. In order to confirm these optimized parameters, the reaction was conducted under the suggested conditions and the percentage grafting obtained was 197 %, which was almost equal to the actual predicted value of 199.6%.

4.6.3.2) Microwave-initiated Grafting

The ANOVA for the fitted quadratic polynomial model of microwave-initiated grafting of polyacrylamide onto cellulose is shown in Table 4.8. The quadratic regression model showed the value of determination coefficient (R^2) to be 0.9552, which means that the calculated model was able to explain 95.52% of the results. The results indicate that the model used to fit response variable is significant ($P < 0.0001$) and adequate to represent the relationship between the response (%G) and the independent variables (time duration of reaction, acrylamide to cellulose molar ratio, and power of microwave radiation). The significance of the model was also judged by F-test, which suggested that the model had a high model F-value of 23.67. Adjusted R^2 (adjusted determination coefficient) is the correlation measure for testing the goodness-of-fit of the regression equation [84]. It is observed that the coefficient of variation (C.V.) value is 3.03, which implies that there is a high degree of precision and a good reliability of the experimental values in the reaction model [85]. Also, a small value of the standard deviation of 1.69 indicates good precision, reproducibility, and reliability of the experimental model. The precision of the model reflects the signal-to-noise ratio, and a value larger than 4 is normally desirable [86]. The obtained precision value for the model of 15.579 is well above the

desirable value and further suggests that the proposed model can be used to navigate the design space [87].

The effect of the linear factors i.e. duration of reaction, acrylamide to cellulose molar ratio, and microwave irradiation power are highly significant ($P < 0.0001$, $P = 0.0015$, and $P = 0.0003$) on the percentage grafting of polyacrylamide onto cellulose. Two of the square terms are also significant with the power of irradiation not being significant ($P = 0.1481$). For the significant squared terms, it means that there is a curved line relationship between percentage grafting and the square factors. The interaction term i.e. AC and BC are found to be significant. A positive sign of the coefficients represented a synergistic effect, while a negative sign indicated an antagonistic effect. The significant square terms have a negative relationship indicating that with an increase of these factors there will be a decrease in the percentage grafting. The linear terms and interaction term (duration x power) have a positive effect on the percentage grafting which indicates that with an increase of these factors there will be an increase in the response.

Table 4.8: ANOVA of Response Surface Quadratic Model for percentage grafting for microwave-initiated grafting

Source	Coeff	Sum of Squares	DF	Mean Square	F Value	Prob > F	Significant (Y/N)
A	4.82	317.90	1	317.90	111.11	< 0.0001	Y
B	1.97	53.24	1	53.24	18.61	0.0015	Y
C	2.52	86.58	1	86.58	30.26	0.0003	Y
A^2	-1.05	15.94	1	15.94	5.57	0.0399	Y
B^2	-2.11	64.30	1	64.30	22.47	0.0008	Y
C^2	0.70	7.03	1	7.03	2.46	0.1481	N
AB	1.21	11.76	1	11.76	4.11	0.0701	N
AC	1.46	17.11	1	17.11	5.98	0.0345	Y
BC	-2.06	34.03	1	34.03	11.89	0.0062	Y
Model		609.46	9	67.72	23.67	< 0.0001	Y
Residual		28.61	10	2.86			
Lack of Fit		24.66	5	4.93	6.25	0.0329	Y
Pure Error		3.95	5	0.79			
Cor Total		638.07	19				

Standard Deviation	1.69	R-Squared	0.9552
Mean	55.75	Adjusted R-Squared	0.9148
C.V.	3.03	Predicted R-Squared	0.6985
PRESS	192.35	Adequate Precision	15.579

Multiple regression analysis of the experimental data yielded the following second-order polynomial equation (Equation 4. 12) for the grafting of acrylamide onto cellulose using microwave-initiated grafting:

$$\%G = +57.44 + 4.82\,A + 1.97\,B + 2.52\,C - 1.05\,A^2 - 2.11\,B^2 + 1.46\,AC - 2.06\,BC \qquad (4.12)$$

The results predicted by the model equation (Eq. 4.12) from RSM suggested that a combination of adjusting the reaction time to 4 minutes, the acrylamide to cellulose molar ratio to 6.5, and the irradiation power to 400 W would favour a maximum percentage grafting of 66%. In order to confirm these optimized parameters, the reaction was conducted under the suggested conditions and the percentage grafting obtained was 64%, which was almost equal to the actual predicted value of 66%.

In general, proceeding with further exploration and optimization using a theoretically derived fitted response surface may produce misleading results unless the theoretical model generated exhibits an adequate fit to the experimentally generated data [88]. This implies that checking of the model adequacy is essential and vitally important. Three further tests were therefore done to verify the adequacy and accuracy of the generated model equations to predict the observed responses. These were plots of predicted verus actual responses, normal plots of residuals, and the plot of residual versus predicted responses.

The plots of the actual responses versus the predicted responses for both the microwave-assisted and microwave-initiated grafting is shown in Figure 4.15. As can be seen from Figure 4.15 the developed model successfully captures the correlation of the grafting variables with the grafting percentage response because the predicted values obtained are close to the experimental values. From the graph, the R^2 value is 0.9674 for the microwave-assisted grafting, which indicates that 96.74% of the total variation in the grafting percentage can be attributed to the experimental variables. The corresponding R^2 value for microwave-initiated grafting is 0.9552.

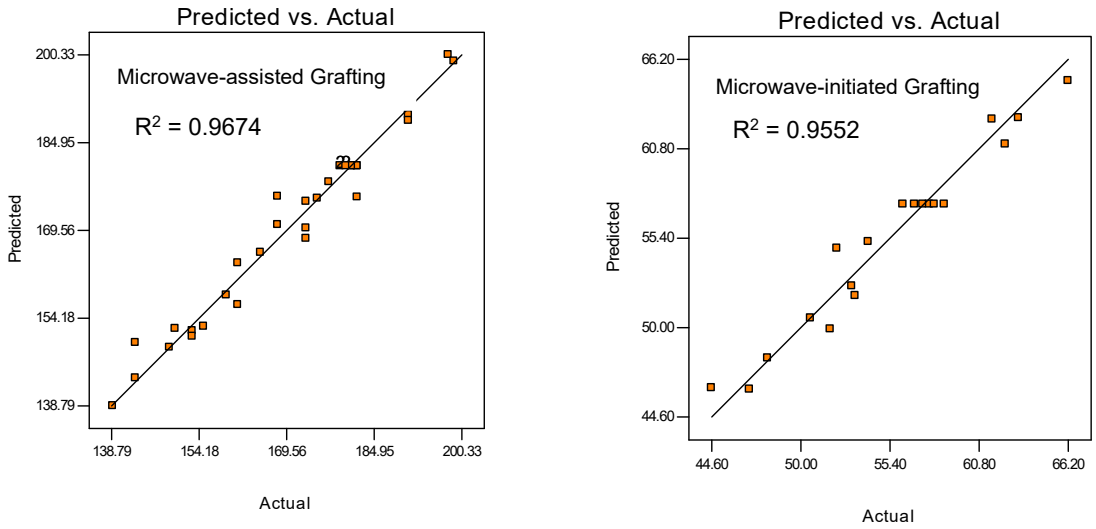

Figure 4. 15: Plot of predicted vs. actual percentage grafting for microwave-assisted and initiated grafting

There are two further plots that must be investigated to verify the assumptions made in Section 4.5.5.1. The first is the residual plots of normal probability, and the second is the plot of residual versus predicted response.

Normality assumption needs to be validated and satisfied based on the residual plots of normal probability. The normal probability plot of the residuals for both the microwave-assisted and microwave-initiated grafting are shown in Figure 4.16.

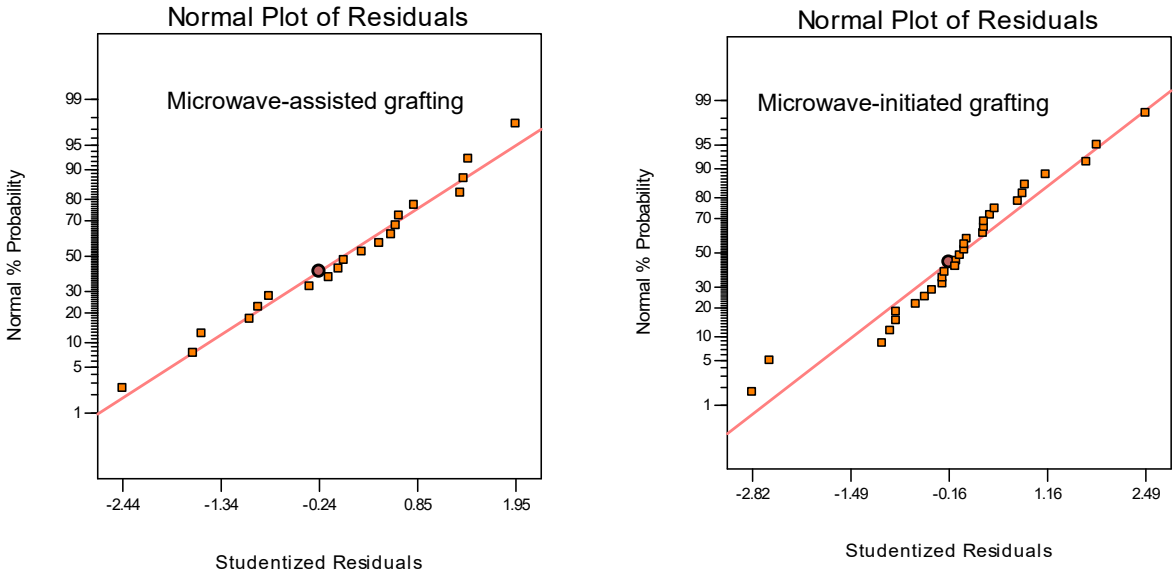

Figure 4.16: Normal plot of residuals for percentage grafting for microwave-assisted and initiated grafting

The normality assumption is satisfied when the residual plot approximately falls along a straight line [89]. Figure 4.16 shows that the residuals approximately fall on a straight line for both cases, which implies that the normality assumption is satisfied.

Residuals versus Predicted Values plots of the regression models are shown in Figure 4.17.

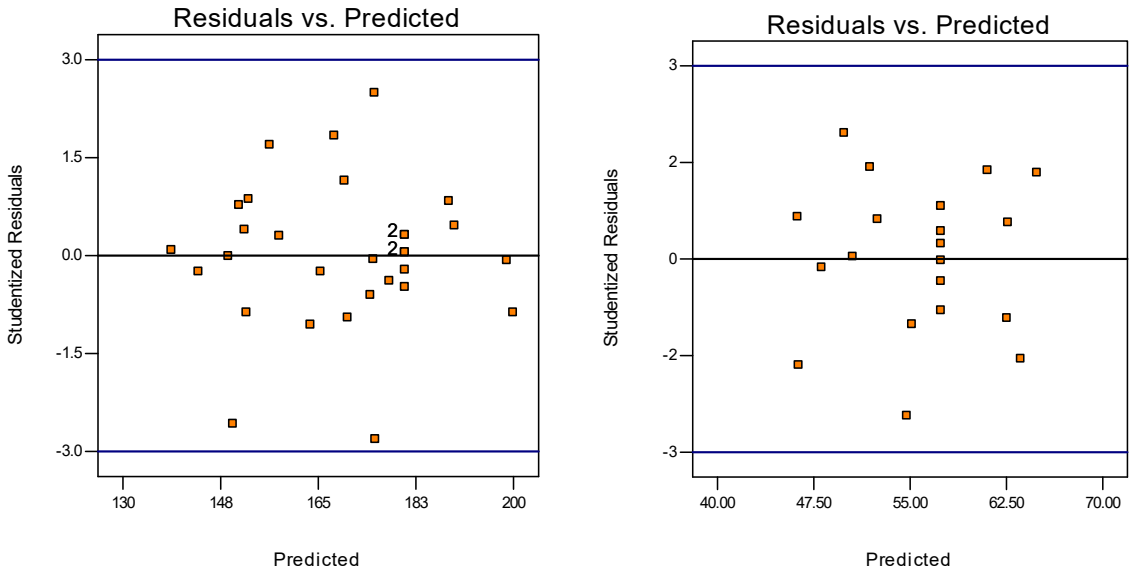

Figure 4.17: Plot of residual vs predicted response for percentage grafting

Figure 4.17 shows that the residuals are randomly scattered around the mean of the response variable for the plot of the residuals versus predicted response - the random and even distribution of the residuals above and below the centerline suggests that the models of microwave-assisted and microwave-initiated grafting are statistically significant. These findings indicate no violations of the basic regression assumptions and reconfirms that the model is adequate and that no violation of independence or constant variance assumption exists.

4.6.4) Determination of optimal grafting conditions under microwave irradiation

For microwave-assisted graft polymerization, the irradiation time, acrylamide to cellulose molar ratio, CAN to cellulose molar ratio and power of irradiation were considered significant and varied simultaneously. For microwave-initiated graft polymerization, three factors: irradiation time, power of irradiation, and acrylamide to cellulose molar ratio were varied simultaneously.

From the model equations generated it is possible to extract the effect of each variable (main effects) alone on the percentage grafting. When extracting the effect of each variable alone, the effect of the other variables need to be kept constant – these constant values could be any value within the experimental range. For the purposes of discussion, when discussing the effect of each variable, the other variables were maintained constant at their centre points.

4.6.4.1) Effect of Time

The effect of duration of reaction on the percentage grafting for both the microwave-assisted and microwave-initiated grafting is shown in Figure 4.18.

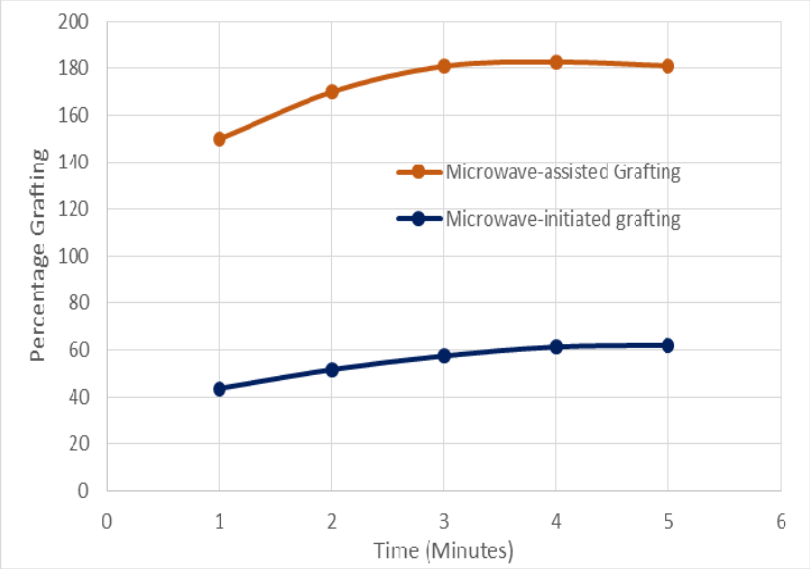

Figure 4.18: Effect of time on percentage grafting of acrylamide on cellulose

Preliminary experiments conducted with and without the chemical free-radical initiator indicated that no grafting took place before 30 seconds even when the microwave power was increased to 500 W. When the reaction was run for longer than 5 minutes at the higher power of 500 W, the reaction solution began to boil and evaporate at around 6 minutes. Based on these observations, it was decided to set the lower and upper time limits at 1 minute and 5 minutes respectively.

From Figure 4.18 it can be seen that the percentage grafting profile is similar for both microwave-assisted and microwave-initiated grafting. The profile is also similar to that observed

under conventional chemical free-radical copolymerization. For both cases, the percentage grafting initially increases with time, reaches a maximum and then levels off. With microwave-assisted grafting, a maximum grafting of 182.7 % was reached at 3.5 minutes while a maximum grafting percentage of 61.9% was attained at 4.5 minutes. The initial increase in percentage grafting with time can be ascribed to the availability of more microwave energy, resulting in an incease in the number of grafting sites being generated on the cellulose backbone with time and the adding of acrylamide groups onto the growing grafted polyacrylamide chains. The levelling off of the percentage grafting after the maximum grafting percentage had been attained can be attributed to firstly, a decline in the concentration of CAN-HNO_3 initiator and acrylamide monomer (microwave-assisted grafting) and monomer (microwave-initiated grafting). Secondly, with time there is a decrease in the number of available sites on the cellulose substrate for copolymerization. From research performed on other polysaccharides systems, it has been postulated that after the time corresponding to the maximum percentage graft, homopolymerization reaction becomes competitive with the copolymerization reaction [90].

The percentage grafting is much higher (150 – 182%) for microwave-assisted grafting compared to microwave-initiated grafting (44 – 62%). This vast difference in percentage grafting can be ascribed to the synergistic effects of the CAN-HNO_3 initiator and microwave irradiation acting simultaneously on the cellulose substrate and increasing the rate at which active sites are generated.

4.6.4.2) Effect of Initiator Concentration

The molar ratio of CAN-HNO_3 to cellulose was varied from 0.02 to 0.2. The effect of this change in molar ratio on the percentage grafting is shown in Figure 4.19.

Information gathered from microwave-initiated grafting indicates that acrylamide can be grafted onto cellulose even in the absence of the CAN-HNO_3 initiator. The maximum percentage grafting in the absence of the chemical free-radical initiator was 66.2%. When the initiator to cellulose molar ratio was increased to 0.02, there was a sharp increase in the percentage grafting to 152.7% implying that even a small amount of initiator causes a drastic increase in the percentage grafting. A possible reason for this jump in percentage grafting could be the synergistic effect of the chemical free-radical and the microwave electromagnetic energy that results in a specific initiation on cellulose as opposed to a more random grafting process.

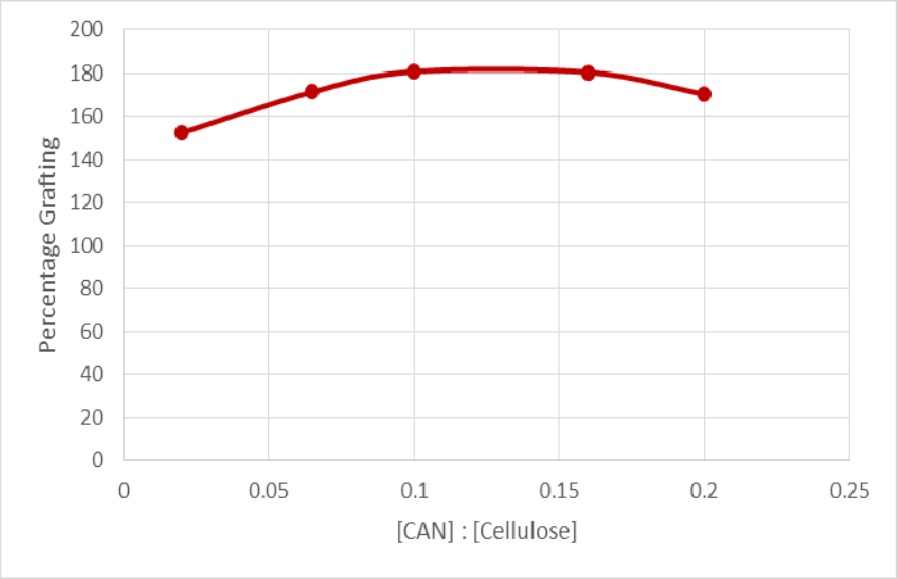

Figure 4.19: Effect of CAN to cellulose molar ratio on percentage grafting of acrylamide on cellulose

As shown in Figure 4.19, the percentage grafting increased from 152.7% to a maximum of 180.8% at an initiator to cellulose molar ratio of 0.125, and later decreased with an additional increase in CAN-HNO_3 concentration. The microwave-assisted method is based on free-radical polymerization mechanism using microwave radiation which leads to synergism with chemical free-radical initiator to create free-radical sites on the cellulose polymer chain [91]. Ce^{4+} radicals are formed as a result of thermal decomposition of ceric ammonium nitrate in the presence of microwave irradiation and these radicals abstract hydrogen from the hydroxyl groups of cellulose. The formed macro-radicals initiate grafting of acrylamide onto cellulose. When the CAN-HNO_3 concentration is increased in the polymerization medium, the number of Ce^{4+} radicals increases as well. These radicals lead to the formation of more active sites on the cellulose polymer chain.

Increasing the concentration of CAN-HNO_3 initiator beyond what was required for maximum percentage grafting, causes an increase in the number of acrylamide radicals to form. This causes the percentage grafting to drop as the generation of competing polyacrylamide homopolymers increases. Also an increase in the concentration of CAN makes it easier for Ce^{4+} to be involved in termination reaction, thereby causing a drop in the percentage grafting.

4.6.4.3) Effect of Monomer Concentration

In order to investigate the effect of monomer concentration on graft copolymerization, the molar ratio of acrylamide to cellulose was varied between 2:1 to 10:1 while simultaneously varying the other parameters as per the experimental design matrix. The results obtained for both microwave-assisted and microwave-initiated grafting is given in Figure 4.20.

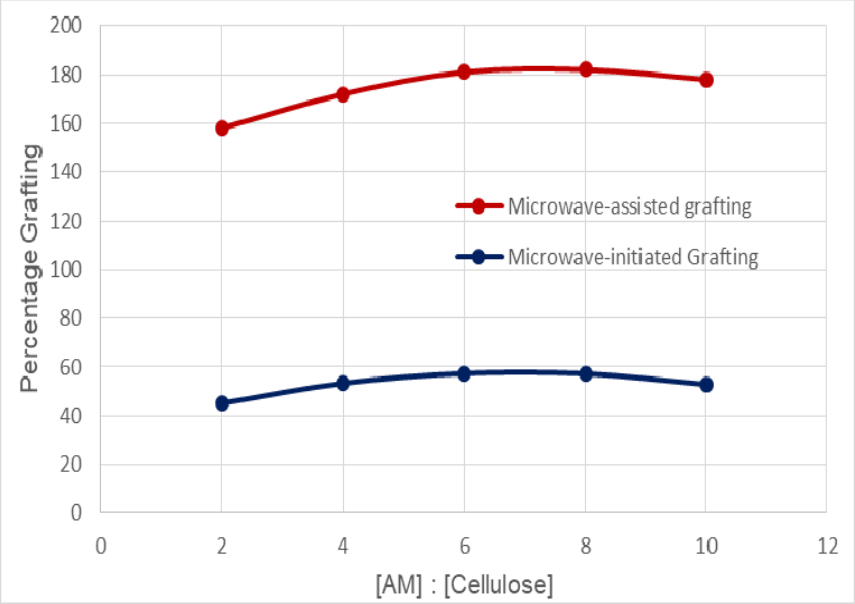

Figure 4.20: Effect of acrylamide to cellulose molar ration on percentage grafting of acrylamide on cellulose

The percentage grafting profile for both cases are similar with the percentage grafting initially increasing, reaching a maximum and then decreasing with increasing monomer to cellulose molar ratio. The maximum percentage grafting for microwave-assisted grafting and microwave-initiated grafting was 182% and 57.3% respectively and these maximum percentage grafting occurred at a monomer to cellulose molar ratio of 7. The initial increase in percentage with monomer concentration can be explained by the fact that with an increase in the acrylamide concentration more monomer molecules become available in close proximity to the reactive sites on the cellulose backbone. After the maximum grafting percentage had been attained, it was noticed that the mixture formed a gel-like mass. It may thus be likely that as the monomer concentration increased and copolymerization progressed, the viscosity of the resulting solution increased to the extent of reducing the rate of diffusion of the acrylamide monomer to the active sites.

4.6.4.4) Effect of Microwave Irradiation Power

The impact of microwave power on the percentage grafting was studied by varying the microwave power between 100 and 500 W, whilst simultaneously varying the other parameters. The results for both microwave-assisted and microwave-initiated grafting are displayed in Figure 4.21.

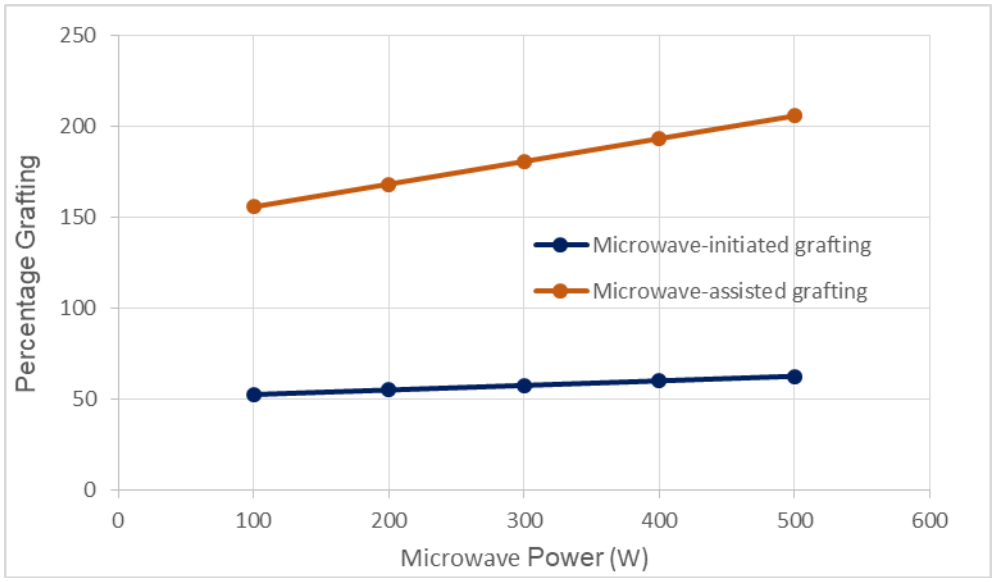

Figure 4.21: Effect of microwave power on percentage grafting of acrylamide on cellulose

The limits of the microwave irradiation power were decided upon after conducting preliminary experiments – at below 100 W, no discernable grafting of acrylamide onto cellulose occurred when using microwave-initiated grafting. At above 500 W there was very rapid heating and evaporation of the solution mixture, and also very likely degradation of the cellulose substrate. It was therefore decided to limit the microwave power to between 100 W and 500 W.

It can be seen from Figure 4.21 that the percentage grafting increased linearly with increasing power for both microwave-assisted and microwave-initiated grafting. The increase in the percentage grating with increasing microwave power may be due to the increased formation of monomer and cellulose macro-radicals because of fast energy transfer among the molecules. With an increase in the microwave radiation power, the rotation of the acrylamide molecules is increased, which leads to more and more elongation of its bond [92]. As the C-C double bond elongates, the pi bond electron cloud splits up into two localized clouds (i.e. free radical sites on

the constituent carbon atoms). The free radical sites created on the cellulose backbone and on the acrylamide molecules by microwave radiation interact rapidly through free radical reaction mechanism, to yield higher percentage grafting [93].

Researchers have reported a decrease in the percentage grafting after the maximum percentage grafting had been achieved and attributed this decrease to the formation of homopolymers and to the decomposition of the grafting copolymers at high microwave power [94, 95].

4.6.5) Interactive Effects

The regression model equations (Eq. 4.11 and Eq. 4.12) allowed the prediction of the effects of the independent parameters on the percentage grafting of acrylamide onto cellulose. The relationship between the independent and dependent variables can also be illustrated in three-dimensional representations (response surfaces) as well as two-dimensional contour plots. In these representations, two variables are depicted at a time while the other variables are kept constant at any value within the experimental range. For purposes of discussion, these values have been maintained constant at their central values.

4.6.5.1) Microwave-assisted Grafting

The significant two-factor interactions for microwave-assisted grafting are time/acrylamide to cellulose molar ratio (AB) and reaction time/irradiation power (AD).

The combined effect of time duration of grafting (A) and the molar ratio of acrylamide to cellulose (B) on the percentage grafting is shown in Figure 4.22.

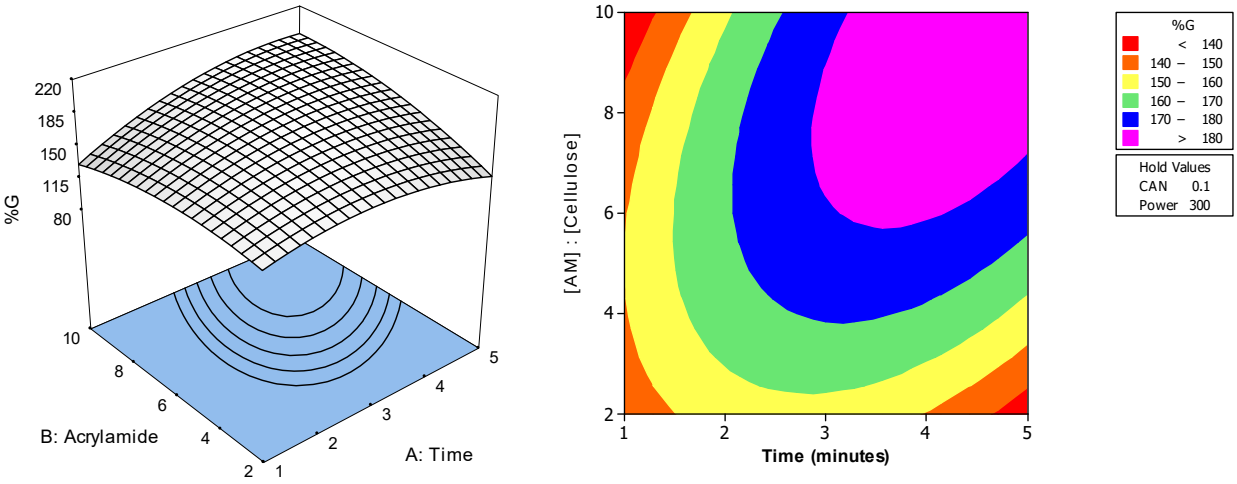

Figure 4.22: Response surface plot and contour plot showing the combined effects of reaction time and acrylamide to cellulose molar ratio on percentage grafting

At the conditions shown in Figure 4.22, the power of microwave irradiation and the molar ratio of CAN to cellulose were held constant at their central values of 300 W and 0.1 respectively. As shown in Table 4.7, the effects of the interactions between reaction time (A) and acrylamide to cellulose molar ratio (B) on the percentage grafting (%G) are positive effects - having a positive interaction coefficient of 4.19. This synergetic effect is observed in Figure 4.22 - increasing both factors (A and B) simultaneously results in an increase in the percentage grafting. As shown in Figure 4.22, maintaining the acrylamide to cellulose ratio above 5 and increasing the reaction time from 1 minute to 5 minutes results in an initial increase and then levelling off in the percentage grafting. This is in line with the main effect of time as discussed in Section 4.6.4.1. When the acrylamide to cellulose ratio was kept constant at levels below 5 and the reaction time increased from 1 to 5 minutes, it is noticed that the percentage grafting increases, reaches a maximum and then begins to decrease – this decrease, however, is not significant. The slight decrease in the percentage grafting may be due to the activated acrylamide molecules not having sufficient time to reach the activated sites on the cellulose substrate and instead forming homopolymers. The symmetric contour lines on the contour map indicate the almost equal contribution of factors A and B to the interaction. The maximum percentage grafting of 188% was obtained at a reaction time of 4.4 minutes and at an acrylamide to cellulose molar ratio of 9.

Figure 4.23 shows the 3-D plot of the interaction between reaction time (A) and microwave irradiation power (D) and their combined effect on the percentage grafting. The acrylamide to cellulose molar ratio and the CAN to cellulose molar ratio were fixed at their central values of 6 and 0.1 respectively.

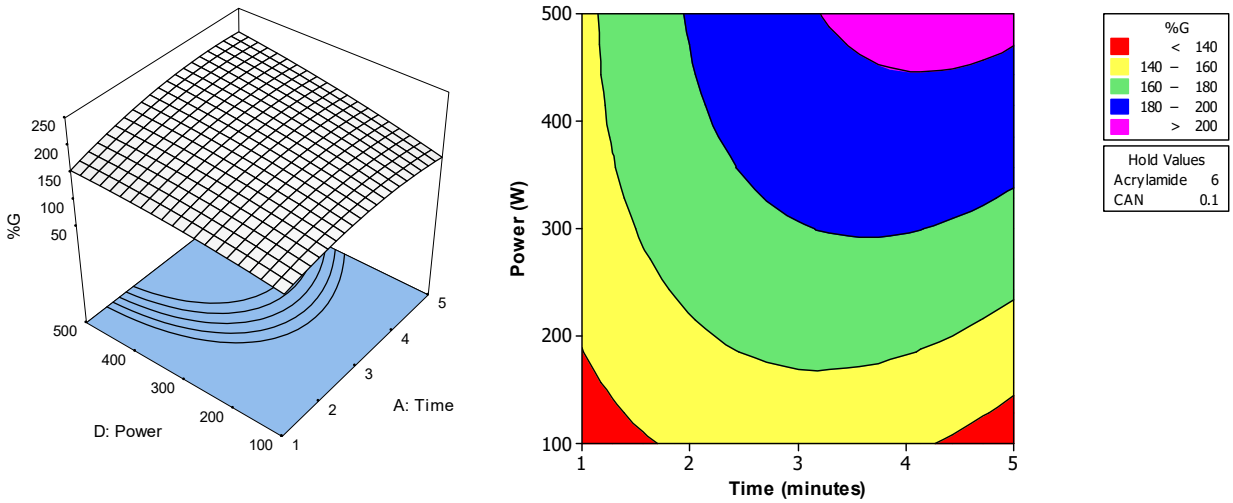

Figure 4.23: Response surface plot and contour plot showing the combined effects of reaction time and microwave power on percentage grafting

The effect of the interactions between reaction time (A) and irradiation power (D) on the percentage grafting are synergetic with the coefficient of interaction being positive (+ 3.06). From Figure 4.23 it can be seen that increasing both factors (A and D) simultaneously results in an increase in the percentage grafting. A higher percentage grafting is obtained at high values of reaction time and high values of irradiation power while lower percentage grafting occurs at reversed operating conditions. At higher values of power and time the increase in the grafting percentage may be due to the formation of greater amounts of free radicals and better transfer of energy. It was seen from the main effects (Figure 4.21) that the percentage grafting increased linearly with irradiation power. From Figure 4. 23 it is seen that interaction with time introduces some curvature in the percentage grafting with power of microwave irradiation. Under the experimental conditions, a maximum grafting percentage of 205.7 % was achieved at 4.3 minutes and at a power setting of 500 W.

4.6.5.2) Microwave-initiated Grafting

From Table 4.8 the significant two-factor interactions for microwave-initiated grafting are time/irradiation power (AC) and acrylamide to cellulose molar ratio/irradiation power (BC).

The combined effect of reaction time (A) and power of microwave irradiation (C) on the percentage grafting at a constant acrylamide to cellulose molar ratio of 6 is shown in Figure 4.24.

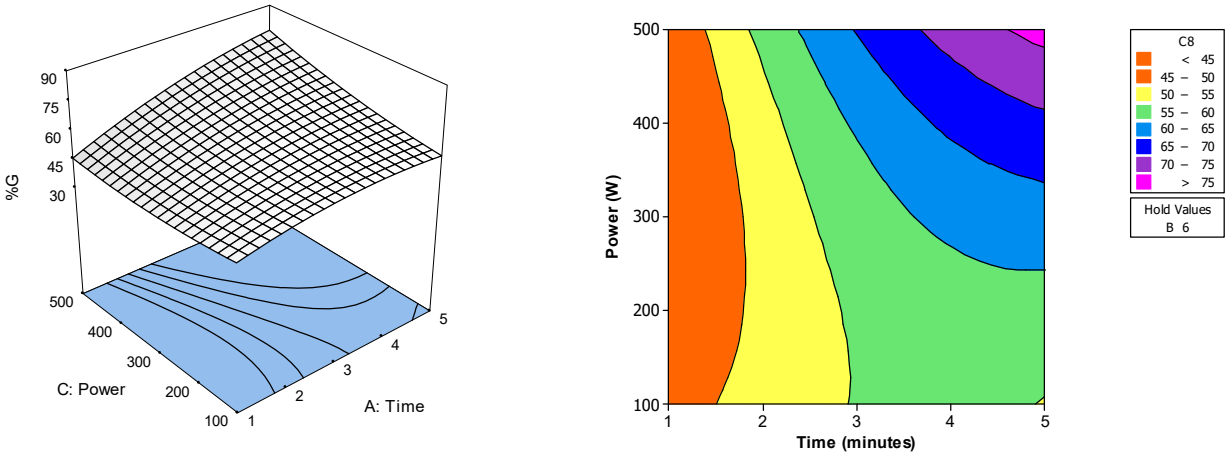

Figure 4.24: Response surface plot and contour plot showing the combined effects of reaction time and microwave power on percentage grafting

The effect of the interactions between reaction time (A) and irradiation power (C) on the percentage grafting are synergetic with the coefficient of interaction being positive (+ 1.46). From Figure 4.24 it can be seen that increasing both factors (A and C) simultaneously results in an increase in the percentage grafting. At low values of time (< 2 minutes) the percentage grafting remains almost constant with increasing irradiation power. At high values of time, however, there is a significant increase in percentage with increasing irradiation power. At higher reaction times, there may be an incease in the number of grafting sites being generated on the cellulose backbone and an increase in the addition of acrylamide groups onto the growing grafted polyacrylamide chains. The maximum grafting perentage (76.3%) occurred at a power setting of 500W and at a reaction time of 5 minutes.

The combined effect of acrylamide to cellulose molar ratio (B) and power of microwave irradiation (C) on the percentage grafting at a constant reaction time of 3 minutes is shown in Figure 4.25.

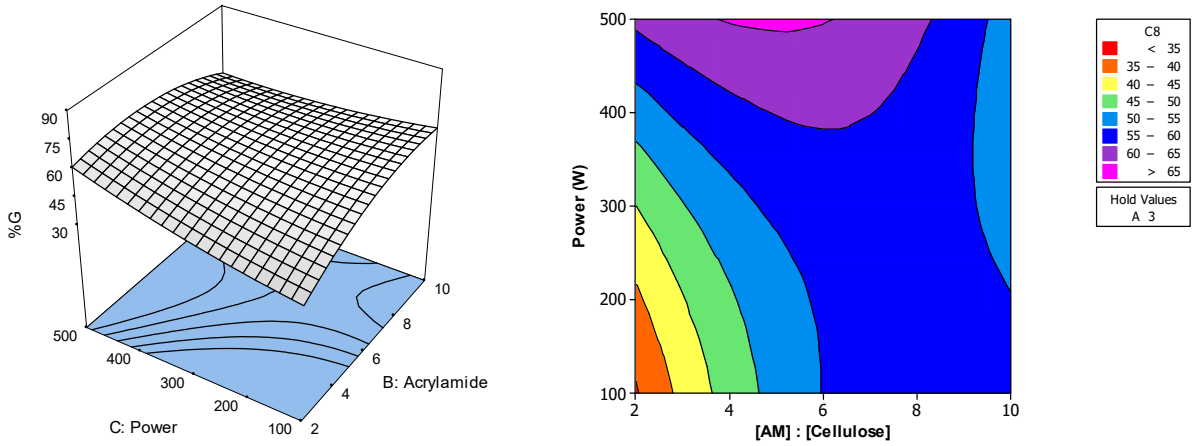

Figure 4.25: Response surface plot and contour plot showing the combined effects of acrylamide to cellulose molar ratio and microwave power on percentage grafting

As shown in Table 4.8, the effects of the interactions between acrylamide to cellulose molar ratio (B) and the irradiation power (C) on the percentage grafting (%G) are negative effects - having a negative interaction coefficient of -2.06. Figure 4.25 displays the antagonist interaction between the acrylamide concentration and microwave power, with one factor modifying the effect of the other. At high values of microwave power (> 400 W), increasing the concentration of acrylamide resulted in decrease in grafting percentage. The highest percentage grafting of 63.5% was obtained at a microwave power setting of 500 W and an acrylamide to cellulose molar ratio of 5.7.

4.6.6) Results of Flocculation Tests

A standard Jar Test and Settling Test procedure was followed to compare the flocculation performance of the prepared flocculants as well as Magnafloc 4240. A 0.25% (w/v) kaolinite suspension was used as the synthetic wastewater.

4.6.6.1) Jar Tests

The performance of the prepared flocculants as well as that of Magnafloc 4240 using the Jar Tests is shown in Figure 4.26.

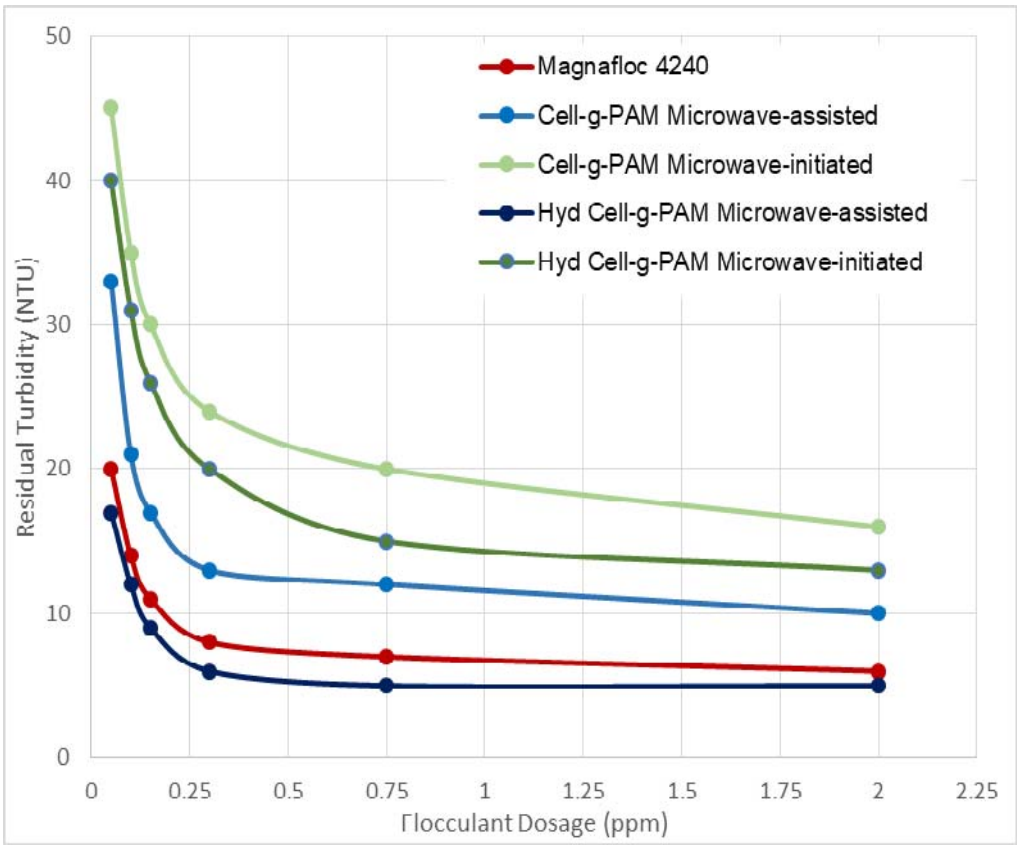

Figure 4.26: Jar test results in 0.25% (w/v) kaolinite suspension

Figure 4.26 shows the relationship between the residual turbidity of the kaolinite suspension and the concentration (dosage) of flocculants for both the microwave-assisted and microwave-initiated Cell-*g*-PAM bioflocculants as well as their partially hydrolyzed derivatives. The results shown were obtained under the following conditions: a pH of 7.0, original turbidity of kaolinite suspension of 132.0 NTU, rapid mixing speed of 125 rpm for 2 minutes followed by a slow mixing speed of 20 rpm for 15 minutes, and a settling time of 30 minutes.

All flocculants showed similar trends with respect to their flocculating abilities: Initially, even a very small dosage of the flocculants (as little as 0.25 ppm) caused a drastic drop in turbidity.

Further increases in the flocculant dosage caused further, but slower reduction in the residual turbidity. Among the hydrolyzed and unhydrolyzed graft copolymers, the hydrolyzed copolymers showed better performance than the unhydrolyzed graft copolymer. The hydrolyzed microwave-assisted graft copolymer, Hyd Cell-*g*-PAM, showed the best flocculating ability, surpassing that of the best performing commercial flocculant (Magnafloc 2042).

Hyd Cell-*g*-PAM can interact and adsorb onto the kaolinite particles through several mechanisms as shown in Figure 4.27.

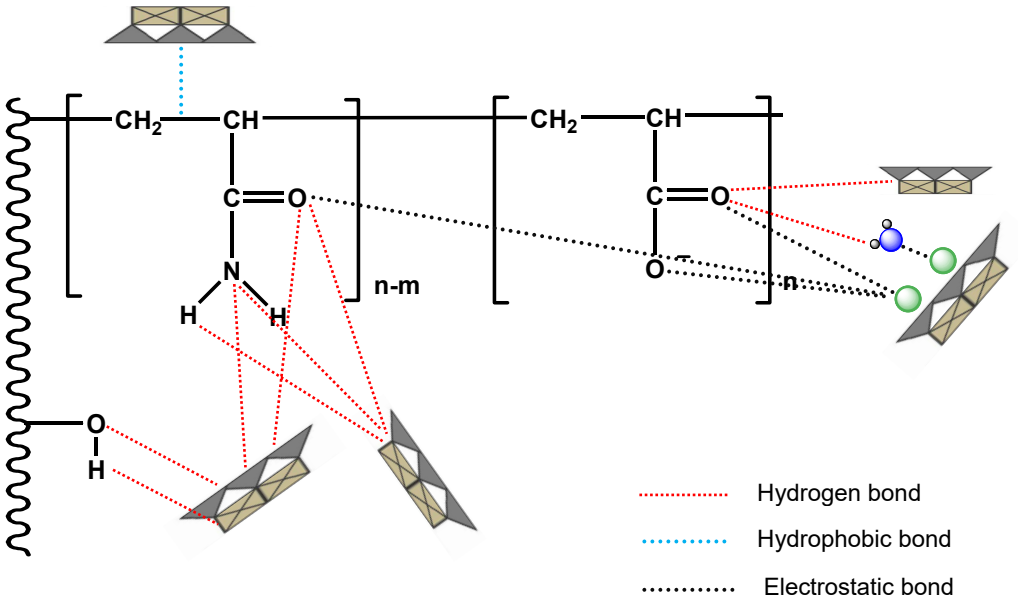

Figure 4.27: Possible interactions between kaolinite and Hyd. Cell-*g*-PAM

The microwave-assisted and microwave-initiated grafted Cell-*g*-PAM flocculants performed better than those generated via the conventional chemical free-radical method. This is because ring opening of the cellulose molecule does not take place under microwave grafting and the rigidity of the cellulose chain is maintained. The higher rigidity has the effect of extending the flocculant chain further into the aqueous phase, enabling the pendant PAM chains to capture more contaminant (kaolinite) particles and hence resulting in higher efficiency. Further, alkaline hydrolysis of the -$CONH_2$ groups of the grafted PAM chains converts these groups into carboxylate groups (-COO^-). The presence of the two negative pendant groups on adjacent carbon atoms repel each other and as a result, the chain becomes straightened to some extent. As a result, there is further increase in the hydrodynamic volume of the partially hydrated

flocculant molecule [96]. The higher hydrodynamic volume of Hyd. Cell-*g*-PAM than its parent material (Cell-*g*-PAM) is expected to make it a more efficient flocculant [97].

The major mechanism of flocculation by Hyd. Cell-*g*-PAM polymers is bridging. Bridging flocculation occurs when segments of the same flocculant polymer molecule become attached to more than one kaolinite particle, thereby linking the particles together. In polymer bridging, the high molecular weight hydrated anionic polymer chains become adsorbed onto the kaolinite particle surface and form bridges between adjacent particles. When the long-chain Hyd. Cell-*g*-PAM polymer molecules adsorb on the surface of the kaolinite particles, they tend to form loops and tails that extend some distance from the surface of the adsorbed kaolinite particle into the aqueous phase. Adsorption of Hyd. Cell-*g*-PAM onto the kaolinite particles occurs by electrostatic forces, van der Waal forces, and hydrogen bonding as shown in Figure 4.27.

Hydrogen bonding is possible when a hydrogen atom is bonded to a strongly electronegative atom such as O or N and assumes a δ positive charge. In the case of Hyd. Cell-*g*-PAM flocculant and kaolinite particles, the free basal silanol groups as well as the formation of Si−OH and Al−OH groups on the kaolinite edge surfaces provide suitable adsorption sites. There are two possible sites as H-bonding acceptor on the flocculant molecule: the carbonyl group and the nitrogen atom. In addition to this, hydrogen bonds can form between the amide hydrogens of the Hyd. Cell-*g*-PAM flocculant and the -OH groups of the aluminol and silanol groups present on the edge faces of the kaolinite particle. A third source of hydrogen bonding occurs as the exchangeable cations surrounding the kaolinite particle are hydrated and allows the flocculant to interact with the exchangeable cations through water bridging. In this case the amide groups of the flocculant form H-bonds with water molecules in the hydration shells of the exchangeable cations. Whilst the individual hydrogen bond may be weak (in the order of 2×10^4 J/mol) the overall adsorption is strong due to the relatively large numbers of bonds that can be formed.

Hydrophobic bonds arise due to the desire of hydrophobic moieties, which form part of a polymer, to “escape” the aqueous environment and attach to less polar surroundings [98]. In the Hyd. Cell-*g*-PAM–kaolinite system, hydrophobic bonding occurs between the hydrophobic backbone of the flocculant and the hydrophobic basal siloxane surfaces of kaolinite, which consists of Si-O-Si bonds. The magnitude of this interaction is still debatable with some groups [99] suggesting that the hydrophobic chains interact more strongly with the kaolinite surfaces than do the amide groups. Other researchers [100] conclude that a substantial contribution of

hydrophobic bonding is unlikely as the hydrophobic backbone of the polymer becomes shielded by the polar amide groups in a water solution.

Electrostatic interaction is a coulombic type of interaction between oppositely charged (or similarly charged) polymer molecules and mineral particle surfaces [101]. In the Hyd. Cell-*g*-PAM-kaolinite system, electrostatic repulsion forces may be said to exist between the anionic polymeric $–COO^-$ group of the flocculant and the negatively charged kaolinite surfaces. This electrostatic repulsion force would suggest that adsorption and flocculation between the flocculant and kaolinite would be poor. In practice, however, the opposite is experienced. The electrostatic repulsion between the charged segments of the flocculant causes it to adopt a more extended conformation than a neutral polymer [102]. An extended conformation is beneficial for flocculation as it increases the hydrodynamic radius of the polymer. This allows the flocculant polymer to better extend past the electrostatic barriers of the kaolinite particles, leading to more effective bridging.

The kaolinite colloidal particle is negatively charged and immediately surrounded by water molecules and exchangeable cations such as Na^+, Mg^{2+} or Ca^{2+} (as discussed in Chapter 2). The amide group ($CONH_2$) of the non-ionic segment of Hyd. Cell-*g*-PAM is dipolar. Ion dipole interactions therefore occur between the carbonyl oxygen (C=O) and the exchangeable cations through $CO–M^{n+}$ bonding. The alkaline earth cations Ca^{2+} and Mg^{2+} have higher charge densities than the alkali Na^+ cations and therefore have stronger ion-dipole interactions with the amide group. The divalent cations (Ca^{2+} and Mg^{2+}) present in the system are also highly effective at reducing the electrostatic repulsion between anionic segment of Hyd. Cell-*g*-PAM and the negatively charged kaolinite particles. These divalent cations not only reduce the electrostatic repulsion between negatively charged kaolinite particles themselves, but also provide anchoring and bridging sites for the anionic flocculant segments. They consequently enhance adsorption and flocculation by building divalent cationic bridges between the flocculant molecules and the kaolinite colloidal particles. In addition to these interactions, water molecules present in the system also aid in attaching the kaolinite particle to the flocculant – the water molecules form bridges with the exchangeable cations and carbonyl oxygens through hydrogen bonding while at the same time forming bridges with exchangeable cations through ion-dipole interactions.

4.6.6.2) Settling Tests

The flocculation efficiency of the flocculants used in the Jar Tests were again tested using Settling Tests and the results depicted in Figure 4.28. For all tests, the flocculant dosage was maintained at 0.5 ppm, *i.e.* at the optimized dosage as determined by the jar tests above.

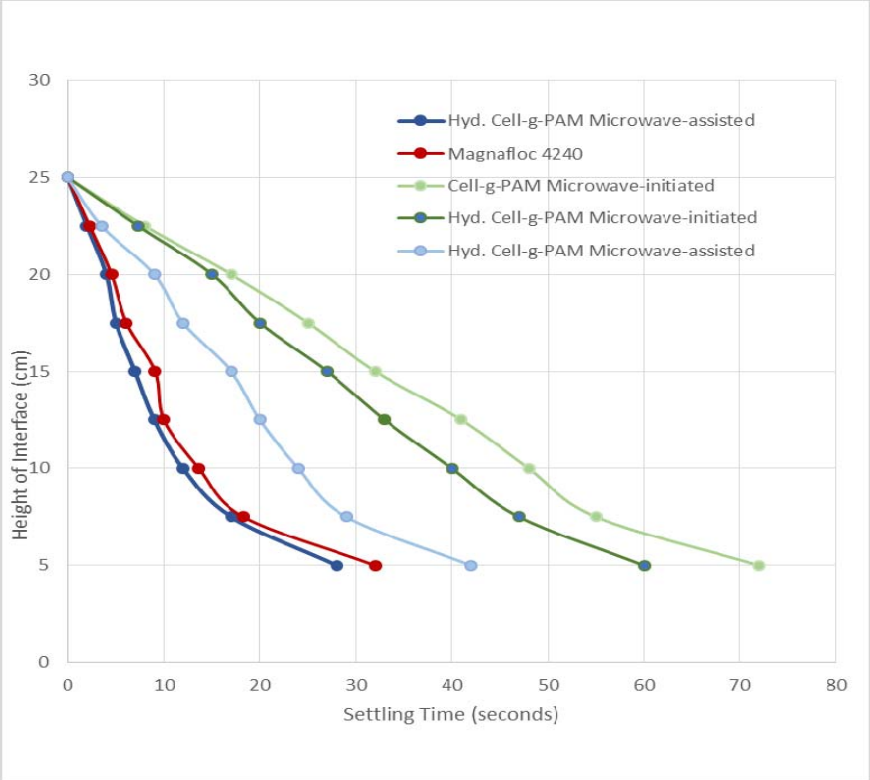

Figure 4.28: Settling characteristics of flocculants in 0.25% (w/v) kaolinite suspension

In Figure 4.28, the height of the interface between the solid and liquid (mud line) is plotted against time. The flocculation performance of a particular copolymer can be correlated with settling velocity. The greater the settling velocity of the floc containing contaminants, the greater will be its flocculation performance. From Figure 4.28 it is again evident that increasing the anionic content of the copolymer through hydrolysis increases its flocculation performance. The best performing flocculant for the Settling Tests was again the Hyd. Cell-*g*-PAM copolymer. In this flocculant, on hydrolysis, the grafted chains get straightened and expanded but still maintain some flexibility. This enhances the approachability of the colloidal particles towards the flocculant macromolecules. The settling characteristics of kaolinite suspension were in

agreement with the jar tests experiments – the order of settling follow the same order as in jar test.

4.7) Conclusions

Polyacrylamide grafted cellulose flocculants were successfully synthesized by using both the microwave-assisted and microwave-initiated methods. The synthesis procedure was optimized to target maximum percentage grafting. For microwave-assisted grafting, the grafting was optimized in terms of reaction time, acrylamide to cellulose molar ratio, CAN to cellulose molar ratio, and microwave irradiation power. For microwave-initiated grafting, the grafting was optimized in terms of reaction time, acrylamide to cellulose molar ratio, and microwave irradiation power. The optimization was performed using a central composite design and response surface methodology (RSM). Using this method, the optimized conditions for synthesis of Cell-*g*-PAM under microwave-assisted grafting were a reaction time to 3.8 minutes, an acrylamide to cellulose molar ratio to 7.4, a CAN to cellulose molar ratio to 0.17, and an irradiation power to 400 W. When these conditions were experimentally verified a grafting percentage of 197% was obtained – this was close to the predicted value of 199.6%. For the microwave-initiated grafting method, the suggested conditions were a reaction time to 4 minutes, an acrylamide to cellulose molar ratio to 6.5, and an irradiation power to 400 W. Again, when verified, a maximum percentage grafting of 64% was obtained, which was very close to the predicted value of 66%. It may thus be concluded that using design of experiment with RSM, with a minimum number of experiments, can effectively optimize the conditions for grafting of acrylamide onto cellulose. The mathematical models generated reveals the complexity of the reaction process with different sets of conditions.

From information gleaned when conducting flocculation tests with chemical free-radical initiated copolymer flocculants, it was decided to try and improve the flocculating performance of the Cell-*g*-PAM flocculant by partial alkaline hydrolysis. Flocculants synthesized by the microwave-assisted and microwave-initiated methods as well as their hydrolyzed products were tested against commercially available flocculants. The flocculation efficacy of the various flocculants was studied through standard Jar Test and Settling Test procedures using a 0.25 (w/v) kaolinite suspension. The Hyd. Cell-*g*-PAM flocculant performed the best due to its expanded structure and polyelectrolyte nature – the expanded nature of the flocculant enhanced its approachability to the colloidal particles.

4.8 References

[1] Stannett V T., Fanta, G. F., Daone W M., Chatterjee P K., 2002. In P. K. Chatterjee, & B. S. Gupta (Eds.), Absorbent Technology, Elsevier Science.

[2] Kappe C. O., Angew. Chem. Int. Ed. 2004, 43, 6250.

[3] Gedye R., Smith F., Westway K., Ali H., Baldisera L., Laberge L., Rusell J., Tetrahedron Lett. 1986, 27, 279.

[4] Giguere R J., Bray T L., Duncan S M., Majetich G., Tetrahedron Lett. 1986, 27, 4945.

[5] Gabriel C., Gabriel S., Grant E H., Halstead B S., Mingos D M P., Chem. Soc. Rev. 1998, 27, 213.

[6] Dickmeis M., Ritter H., Macromol Chem Phys. 2009, 210:776–82.

[7] Loupy A., Microwaves in Organic Synthesis. 2002. 1st edition, Wiley-VCH, Weinheim.

[8] Jachuck R J J., Selvaraj D. K., Varma R S., Green Chem. 2006, 8, 29.

[9] Hayes B L., Microwave Synthesis: Chemistry at the Speed of Light. 2002. CEM Publishing, Matthews, NC.

[10] Nüchter M., Ondruschka B., Bonrath W., Gun A., Green Chem. 2004, 6, 128.

[11] Loupy A., C R Chim. 2004, 7,103–12.

[12] Kudryavtsev Y V., Litmanovich A D., Plate N. A., Macromolecules.1998, 31, 4642-4644.

[13] Ye M., Han D., Shi L., J. App. Polym. Sci. 1996, 60, 317-322.

[14] Kappe C O., Dallinger D., Nat. Rev. Drug Discovery. 2006, 5, 51-63.

[15] Herrero M A., Kremsner J. M., Kappe C O., J. Org. Chem. 2008, 73, 36.

[16] Lidstrom P., Tierney J., Wathey B., Westman J., Tetrahedron. 2001, 57, 9225.

[17] Lared M., Moberg C., Hallberg A., Acc. Chem. Res. 2002, 35, 717.

[18] Zhang X., Hayward D. O., Mingos D M P., Chem. Commun. 1999, 975.

[19] Kappe O. C., Angew. Chem., Int. Ed. 2004, 43, 6250.

[20] Nuchter M., Ondruschka B., Bonrath W., Gum, A., Green Chemistry. 2004, 6,128.

[21] Baghurst D R., Mingos D M P., J. Chem. Soc. Chem. Commun. 1992, 674.

[22] Gabriel C., Grant E H., Halstead B S J., Mingos D M P., Chem. Soc. Rev. 1998, 27, 213.

[23] Bhattacharya M., Basak T., Energy, 2016, 97, 306–338.

[24] Loupy A., Microwaves in Organic Synthesis. 2002. 1st edition, Wiley-VCH, Weinheim.

[25] Stadler A., Yousefi B H., Dallinger D., Walla P., van der Eycken E., Kaval N., Kappe C O., Org. Process Res. Dev., 2003, 7, 707.

[26] Arvela R K., Leadbeater N. E., Collins M. J., Tetrahedron. 2005, 61, 9349.

[27] Miklavc A., Chem. Phys. Chem. 2001, 2, 552.

[28] de la Hoz A., Diaz-Ortiz A., Moreno A., Chem. Soc. Rev. 2005, 34, 164.

[29] Loupy A., Pigeon P., Ramdani M., Jacqualt P., Synth. Commun. 1994, 24, 159.

[30] Lewis D A., Summers J. D., Ward T. C., McGrath J. E., Polymer Preprints. 1988, 29, 1, 174.

[31] Shibata, C., Hashima, T., Ohuchi, K. Japanese J. of Applied Physics, Part 1. 1995, 35, 316-319.

[32] Yildiz G., Pronk M., Djokic M., van Geem K M., Ronsse F., van Duren R., Prins W., J. Anal. Appl. Pyrolysis. 2013, 103, 343–351.

[33] Herzog A., Klingner R., Vogt U., Graule T., J. Am. Ceram. Soc., 2004, 87, 784.

[34] Meng X K., Tang S C., Vongehr S., J. Mater. Sci. Technol. 2010, 26, 487.

[35] Hicks R., Majetich G., J Microwave Power Electromagn Eng. 1995, 30, 27

[36] Challa, S., Little, W. E., Cha, C. Y. J. Microw. Power Electromagn. Energy. 1994, 29, 131.

[37] Limousin C., Cleophax J., Petit A., Loupy A., Lukacs G., J. Carbohydr. Chem. 1997, 16, 327.

[38] Mladenovic M., Marincic A., Milovanovic B., J. Microwave Power EE.1989, 24, 166.

[39] Binner J G P., Hassine N A., Cross, T. E., J. Mater. Sci. 1995, 30, 5389.

[40] Westaway, K. C., Gedye, R., J. Microwave Power. 1995, 30, 219.

[41] Berlan J., Giboreau P., Lefeuvre S., Marchand C., Tetrahedron Lett. 1991, 32, 2363.

[42] Lewis D A., Summers J D., Ward T C., McGrath J E., J. Polymer Sci: Polymer Chem. 1992, 30, 1647.

[43] Loupy, A., Maurel, F., Sabatie-Gogova, A., Tetrahedron. 2004, 60, 1683.

[44] Hayes B L., Aldrichimica ACTA, 2004, 37, 66-76.

[45] Carlson T R., Tompsett G. A., Conner W. C., Huber G. W., Top. Catal. 2009, 52, 241–252.

[46] Malik P K., Sanyal S. K., Separation and Purification Technology. 2004, 36, 3, 167–175.

[47] Singh V, Tiwari A, Tripathi D N, Malviya T., Tetrahedron Lett. 2003, 44, 7295–7.

[48] Sen G., Pal S., Macromol Symp. 2009, 277,100–11.

[49] Stuerga D, Gaillard P. Tetrahedron. 1996, 52, 5505–10.

[50] Zhang X., Hayward D O., Mingos D M P., Catal Commun.1999, 11, 975–96.

[51] Mishra S., A. Mukul, G. Sen, U. Jha, Int. J. Biol. Macromol. 2011, 48, 106–111.

[52] Princi, E., Vicini, S., Pedemonte, E., Mulas, A., Franceschi, E., Luciano, G., Thermochimica Acta. 2005, 425, 173–179.

[53] Singh, V., Tiwari, A., Tripathi, D. N., & Sanghi, R., J. Applied Polymer Sci. 2004, 95, 820–825.

[54] Peng, Y. and Song, G. Green Chem. 2001, 3, 302.

[55] S. Pal, G. Sen, S. Mishra, R.K. Dey, U. Jha, J. Appl. Polym. Sci. 2008, 110, 392–400.

[56] Rani, P., Mishra, S., & Sen, G., Carbohydrate Polymers. 2013, 91, 686–692.

[57] Arsad N. J., Applied Mechanics and Materials. 2016, 818, 281-284.

[58] Jing, W., Peng, Z. Tong, Z. Bao-Xiu, J. Appl. Polym. Sci. 2006, 100, 2244.

[59] Sen G., R. Kumar, S. Ghosh, S. Pal, Carbohydr. Polym. 2009, 77, 822–831.

[60] Miyazaki S., A. Nakayama, M. Takada, D. Attwood, Biol. Pharm. Bull. 1994, 7, 745–747.

[61] Yao D.K., T. Peng, H.B. Feng, Y.Y. He, J. Polym. Sci. Part A: Polym. Chem. 1994, 32, 1213–1223.

[62] Wei Yin, Yuan Ma, Jiaxi Xu, Yufen Zhao, Journal of Organic Chemistry. 2006, 71, 11, 4312-4315.

[63] Matahwa, H., Ramiah, V., Jarrett, W. L., McLeary, J. B. and Sanderson, R. D., Macromol. Symp. 2007, 255, 50–56.

[64] Thakur, V.K., Thakur, M.K., Gupta, R.K., Carbohydr. Polym. 2013, 97, 18–25.

[65] Kaith, B. S., Susheel, K. Polymer Composites. 2008, 29, 791–797.

[66] Pal S., G. Sen, S. Mishra, R.K. Dey, U. Jha, J. Appl. Polym. Sci. 2008, 110, 392–400.

[67] Ge, H., Wan, P., & Luo, D., Carbohydrate Polymers. 2006, 6, 3, 372–378.

[68] Sen, G., Ghosh, S., Jha, U., Pal, S., Chemical Engineering Journal. 2011, 171, 495–501.

[69] Bhattacharya, A., Misra, B. N.,Progress in Polymer Sciences. 2004, 29, 767–814.

[70] Misra, S., Mukul, A., Sen, G., Jha, U. International Journal of Biological Macromolecules. 2010, 48, 1, 106–111.

[71] Sen, G., Singh, R. P., Pal, S., Journal of Applied Polymer Sciences. 2010, 115, 63–71.

[72] Singha, A. S., Thakur, B. P., and Pathania, D., Int. J. Polym. Anal. Char. 2014, 19, 115–119.

[73] Wiesbrock, F., Hoogenboom, R., & Schubert, U. S., Rapid Comm. 2004, 25, 1739–1764.

[74] Sen, G., Singh, R. P., & Pal, S. Journal of Applied Polymer Sciences. 2010, 115, 63–71.

[75] Du, G. D., Wang, J. Q., Guo, Z. P., Chen, Z. X., Liu, H. K. Mater. Lett. 2011, 65, 1319.

[76] Longo I and Ricci A. S., J. Microwave Power and Electromagnetic Energy. 2007, 41, 1, 4–19.

[77] Ferrari C, I. Longo, E. Tombari, and L. Gasperini, International Journal of Chemical Reactor Engineering. 2010, 8, 72.

[78] Cırkva V and S. Relich, Current Organic Chemistry. 2011, 15, 2, 248–264.

[79] Ondruschka B. and M. Nüchter. 2003. Recent Applications of Microwave Power for Applied Organic Chemistry, in Advances in Microwave and Radio Frequency Processing, ed. M. Willert-Porada, Springer Verlag, Berlin.

[80] Singh V., P.L. Kumari, A. Tiwari, S. Pandey, J. Appl. Polym.Sci. 2010, 117, 3630–3638.

[81] Montgomery D.C. 1997. Design and Analysis of Experiments, fourth ed. Wiley, New York.

[82] Myers, R. H., Montgomery, D. C. 1995. Response Surface Methodology: Process and product optimization using designed experiments. John Wiley & Sons, Inc., New York.

[83] Penny, D. J., Lindfield, G. 1999. Numerical methods using MATLAB. Prentice-Hall Inc., New Jersey.

[84] Cornell J.A. 1990. Experiments with Mixtures: Designs, Models and the Analysis of Mixture Data, Wiley, New York.

[85] Otto M. 1999. Chemometrics: Statistics and Computer Application in Analytical Chemistry, Wiley–VCH, Weinheim.

[86] Cartwright H.M. 1993. Application of Artificial Intelligence in Chemistry, Oxford Science Publications, Oxford.

[87] Amaro J.A.D., S.L.C. Ferreira, J. Anal. At. Spectrom. 2004, 19, 246.

[88] Box G.E.P., J.S. Hunter, W.G. Hunter. 2005. Statistics for Experimenters, second ed., Wiley-Interscience, New York.

[89] Box G.E.P., N.R. Draper.1987. Empirical Model-Building and Response Surfaces, Wiley, New York.

[90] O'Connell, D.W., Birkinshaw, C., O'Dwyer, T.F., Journal of Applied Polymer Science. 2006, 99, 6, 2888–2897.

[91] Raman, G., and Gaikar, V. G., Ind. Eng. Chem. Res. 2002, 41, 10 , 2521-2528.

[92] Zhu, S., Wu, Y., Yu, Z., Zhang, X., Li, H., Gao, M., Bioresour. Technol. 2006, 97, 15, 1964-1968.

[93] Reddy, N., and Yang, Y., Trends Biotechnol. 2005, 23, 1, 22-27.

[94] Okieimen F.E., Ogbeifun D.E., and Jideonwo J. Macromol. Sci. Macromolecular Reports. 1996, 33, 391.

[95] Rout A., Singh B., and Santapa M. Euro. Polym. J. 1977, 13, 497.

[96] Bratskaya S., S. Schwarz, T. Liebert, T. Heinze, Colloids Surf. A. 2005, 254, 75–80.

[97] Singh V, Tiwari A, Singh SP, Kumari P, Tiwari S., J Appl Polym Sci. 2008, 110, 1477–1484.

[98] Addai-Mensah J., Powder Technol. 2007, 179, 73–78.

[99] Theng B.K.G., Clays Clay Miner. 1982, 30, 1, 1–10.

[100] Mahdavinia G.R., Pourjavadi A., Hosseinzadeh H., Zohuriaan M J., Eur Polym J. 2004, 40, 1399-1407.

[101] Tripathy T., R.P. Singh, Eur. Polym. J. 2000, 36, 1471–1476.

[102] Setty C M., Deshmukh A S., Badiger A M., Int. J. Biological Macromolecules. 2014, 70, 1–9.

Chapter 5

Linear block polymers as flocculants for wastewater treatment

5.1 Introduction

A polymer which consists of only one type of structural repeating unit (monomer) is called homopolymer and when two or more different monomers are interconnected, the polymeric molecule is called a copolymer. A block copolymer contains at least two chemically different polymer chains that are covalently bound to each other (Figure 5.1). Linear block copolymers are an attractive class of polymeric materials which consist of different polymeric segments covalently bonded together to form a material with hybrid properties [1]. Linear block copolymers may be used in oil exploitation, papermaking, wastewater treatment, mining, printing and dyeing of textiles, daily chemical industry, slurry dehydration, etc. [2].

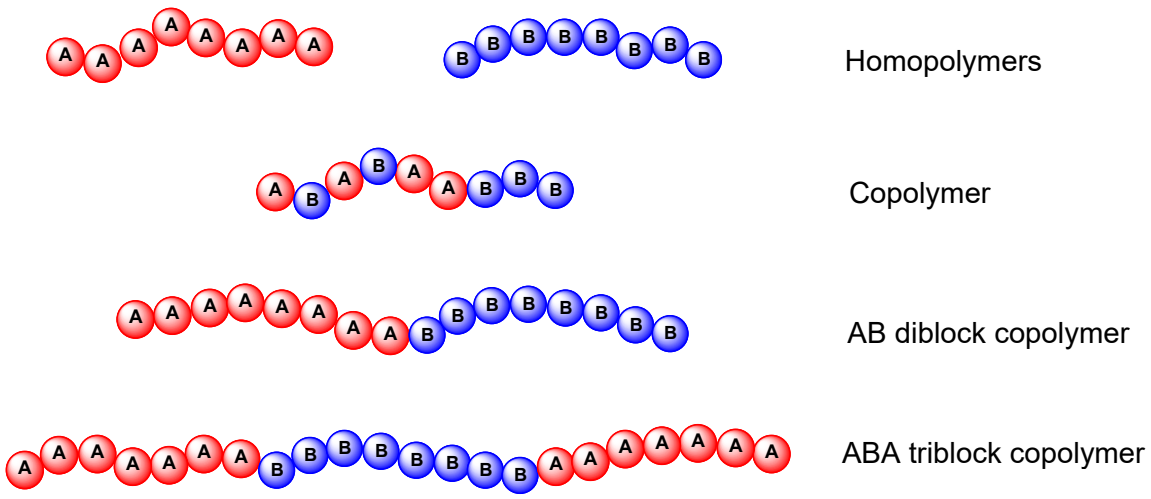

Figure 5.1: Types of polymers

Flocculation is an important step in the purification process of waste water treatment and has been widely applied due to its advantages of high efficiency, low cost and simple operation [3]. Synthetic flocculants have received much attention in waste water treatment because of their excellent solid-water separation performance. During the solid-water separation process, the main mechanisms involved are charge neutralization, bridging and electrostatic patching.

However, if the flocculant consists of a disordered and random distribution of the adsorption segments within the polymer chain then the flocculating ability of the flocculant will be greatly compromised - the adsorption units located on the loops and tails of the chain will be wasted while insufficient adsorption sites will be available for adsorption onto the colloidal particles, as shown in Figure 5.2 (a).

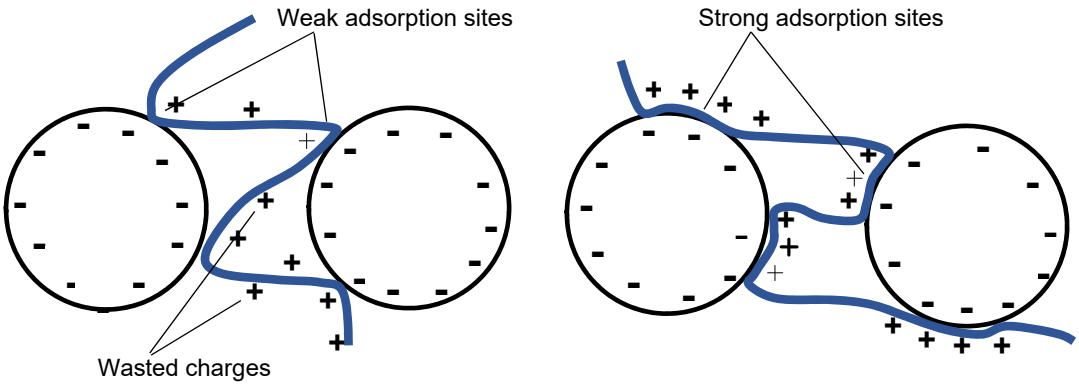

(a) Random Polymer (b) Blocked copolymer

Figure 5.2: Adsorption of random and blocked copolymer flocculants

By contrast, if the adsorption segments are orderly distributed in a block structure, as shown in Figure 5.2(b), then this will strengthen the adsorption between the linear block copolymer and the colloidal particles, making the flocculant more effective.

The most widely used techniques for synthesis of linear block copolymers are anionic polymerization, cationic polymerization and living/controlled radical polymerization methods, nowadays formally referred to as reversible-deactivation radical polymerization (RDRP) [4]. Although the older techniques of anionic and cationic polymerization are still widely used in industry for the manufacture of block copolymers, the most important advances in block copolymer synthesis in the last two decades, has been the development of techniques of living radical polymerization [5]. A number of RDRP techniques have been reported. Rizzardo *et al*. [6] reported on the nitroxide stable radical in 1985. Georges *et al.* [7] reported the first low dispersity (*Đ*) polymers synthesized through Nitroxide Mediated Polymerization (NMP). After NMP, a number of new RDRP methods such as Atom Transfer Radical Polymerization (ATRP), Reversible Addition Fragmentation chain Transfer (RAFT), and Single-Electron-Transfer Living Radical Polymerization (SET-LRP) have been reported.

This study employs different molecular weights of triblock copolymer as flocculants for the treatment of wastewater. The triblock copolymers consist of a poly(ethylene glycol) central block with two outer blocks – these being either polyacrylamide (PAM) or poly(2-dimethylaminoethyl methacrylate) *(*PDMAEMA). The objective of this work is to investigate the synergistic effects of using different lengths of central and outer blocks on the performance of the flocculant. The turbidity of the wastewater will be used as an evaluating parameter in determining the effectiveness of the various flocculants synthesized. The flocculants will be tested in pH neutral simulated wastewater so that their flocculating performance can be compared with the Cell-*g*-PAM graft copolymers synthesized and tested previously. PDMAEMA-*b*-PEO-*b*-PDMAEMA block copolymers are however pH sensitive macromolecules and changes in pH will affect the extent of their intermolecular interactions and flocculating performance [8]. Lowering the pH of the flocculant solution will result in protonation of the DMAEMA segments of the macromolecule. These charged polymers assume a more extended configuration than their neutral counterparts due to the mutual repulsion caused by the charged groups. This, in principle, will enable these polymers, to extend and “reach out” to more colloidal particles through the bridging flocculation mechanism. In this research, the effect of pH on the flocculating performance of PDMAEMA-*b*-PEO-*b*-PDMAEMA will therefore also be tested.

5.2 Nitroxide-mediated Polymerization (NMP)

The use of NMP as a reversible-deactivation radical polymerization (RDRP) technique was first reported by Solomon *et al*. in 1985 [6]. In their work, Solomon *et al.* utilized 2,2,6,6-tetramethylpiperidinyl-1-oxy (TEMPO) as the stable, persistent nitroxide free radical. However it was only in the 1990s, when Georges *et al.* [9] demonstrated the ability of nitroxides to react reversibly with growing polymer chains and produce polymers with low dispersity, that the method gained prominence. NMP involves a dynamic equilibrium between a dormant alkoxyamine and transient propagating radicals, while persistent nitroxide radicals ensure control over the system, as shown in Scheme 5.1.

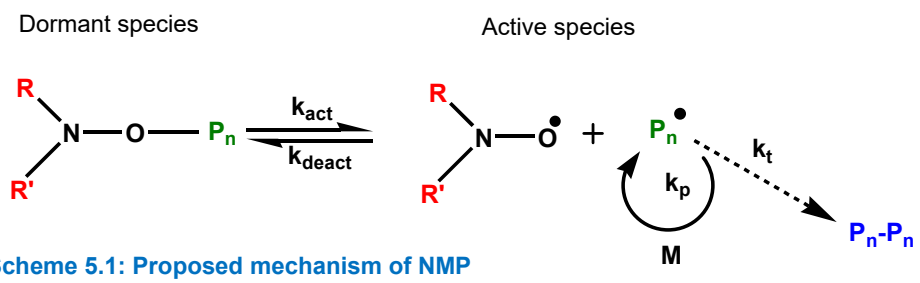

Scheme 5.1: Proposed mechanism of NMP

Control of the reaction is provided by reversible capping and de-capping of the growing (radical) polymer chain by the nitroxide radical. The equilibrium lies greatly towards the alkoxyamine. As a result, the concentration of the growing radical species is decreased and the rate of the polymerization is significantly reduced. The propagating radical concentration is much lower than the dormant species which results in a RDRP with good control of the molecular weight and dispersity. The polymer chains also grow at a (quasi) uniform rate, with side reactions and bimolecular termination kept to a minimum.

The major drawbacks of NMP with TEMPO are the high temperatures required (125 – 140 ^{o}C) along with the long reaction times (1 - 3 days). Further, relatively narrow molecular weight distributions can be achieved only for a narrow pool of monomers [10]. To overcome the problem of high required temperatures, second generation alkoxyamines capable of operating below 100 ^{o}C, were introduced [11]. With the introduction of these second generation alkoxyamine radicals (other than the TEMPO radical), nitroxide-mediated polymerizations have regained interest because of the growing number of monomers that can now be polymerized in a controlled manner via this method.

5.3 Reversible Addition-Fragmentation Chain Transfer (RAFT) Polymerization

Reversible addition-fragmentation chain transfer (RAFT) polymerization was first reported in 1998 by Chiefari *et al.* [12]. The RAFT process involves a conventional radical initiator (e.g. AIBN), a monomer, and a chain transfer agent (CTA - also referred to as RAFT agent). The chain transfer agent, in the form of thiocarbonylthio compounds such as dithioesters, is used to maintain control over chain growth via a rapid equilibrium between the active propagating radicals and the dormant species. The proposed mechanism for the RAFT polymerization is described in Scheme 5.2.

Initiation occurs by the decomposition of the conventional free radical initiator to form a propagating species ($P_n^{\bullet}$). $P_n^{\bullet}$ adds to the RAFT agent to give an intermediate radical (2) which then undergoes fragmentation to give a dormant macro-CTA species (3) and radical $R^{\bullet}$. This new radical reacts with another monomer to form a new propagating radical ($P_m^{\bullet}$). Further addition-fragmentation results in an equilibrium between the propagating radicals $P_n^{\bullet}$ and $P_m^{\bullet}$ and the dormant species (3) and (4) via intermediate (5). The rapid equilibrium between the propagating species and the dormant polymeric thiocarbonylthio compounds allows for equal chain growth and generates well-defined polymers.

Initiation:

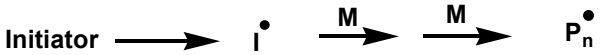

Reversible chain transfer/propagation:

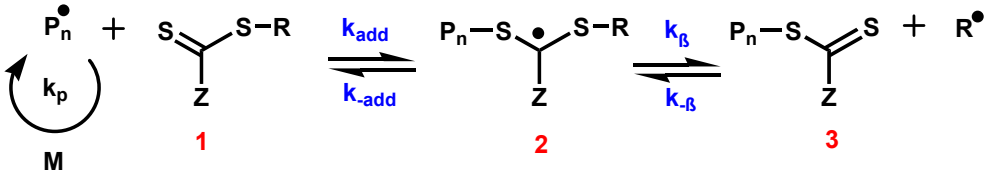

Reinitiation:

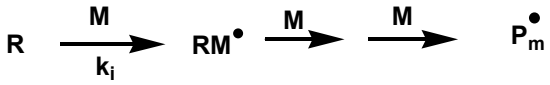

Chain equilibration/propagation:

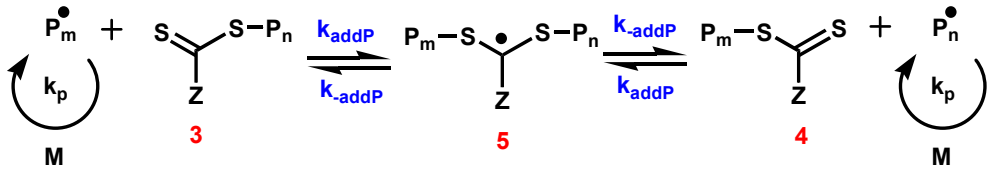

Termination:

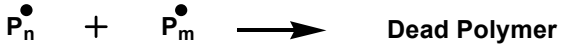

Scheme 5.2: Mechanism of RAFT Polymerization

The versatility and robustness of RAFT with respect to the number of polymerizable monomers makes it a powerful method for achieving LRP. The advantage of RAFT polymerization is that it has proven to be an efficient, versatile and robust tool for the synthesis of polymeric materials with a wide range of design compositions, structures and topologies such as multiblock copolymers and stars [13]. The main drawbacks of RAFT polymerization are that the RAFT transfer agents are not commercially available and are not stable for extended periods of time [14]. Therefore, extra synthetic reaction steps are required for the synthesis of the chain transfer agent. In addition, the polymers are produced with some associated sulphur (odours) and colours which might be undesirable for some applications. Further, with regard to polymerization of acrylamides, although RAFT gives good control over the MWDs, the reaction generally requires a long period of 24 h to reach 94% conversion at ambient temperature conditions [15].

5.4 Atom Transfer Radical Polymerization (ATRP)

Atom Transfer Radical Polymerization (ATRP) was first reported in 1995 almost simultaneously by Sawamoto *et al.* [16] and Matyjaszewski *et al.* [17]. Both systems were based on catalytic systems used for the atom transfer radical addition reaction (ATRA), or the well-known Kharasch reaction. Sawamoto reported ruthenium-mediated polymerization while Matyjaszewski used the more popular copper-catalyzed version of ATRA.

ATRP involves an alkyl halide (P_n-X) as an initiator to generate radicals and control over the growing chain is gained by a reversible activation/deactivation process using a deactivating species (Scheme 5.3).

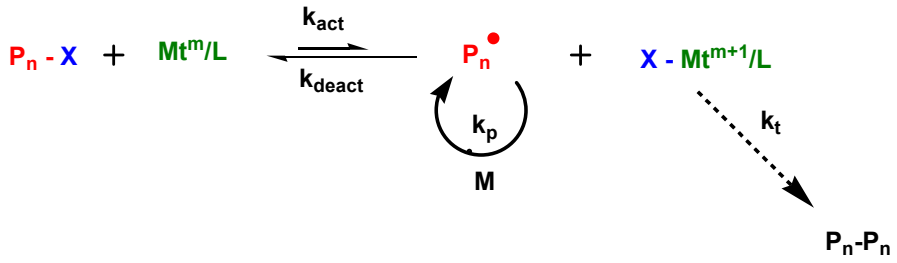

Scheme 5.3: ATRP Equilibrium

Initially, a transition metal compound such as cuprous halide, (Mt^n-X, where X is a halogen atom) is mixed with a nitrogen based ligand (L), to form the transition-metal complex catalyst ([Mt^m(L)X]). The catalyst abstracts the halogen atom X from the organic halide (P_n-X) yielding the oxidized catalyst (deactivating complex), Mt^{m+1}-X, and the radical ($P_n^{\bullet}$). This radical subsequently reacts with the monomer (M) to initiate the intermediate radical species, also known as propagating radical species ($P_n^{\bullet}$) (active species). Then, the deactivating species Mt^{m+1}-X caps the polymer propagating radical ($P_n^{\bullet}$) resulting in the target product (P_n-X) (dormant species) and the reduced transition metal species Mt^m-X which further activates P_n-X and so on. As in all RDRP methods, termination will always occur.

ATRP provides control in the polymerization of many different monomers under various reaction conditions and makes it possible to prepare polymers having a wide range of architectures including blocks, grafts, gradient copolymers, stars, combs, branched, and hyper-branched [18]. Major drawbacks associated with ATRP are the relative sensitivity of the metal complex towards air and the fact that the final product contains substantial amounts of metal that need to be

removed - ATRP requires a relatively high copper concentration in order to compensate for a constant decrease in the Cu(I) caused by bimolecular termination which could eventually terminate the reaction. Efforts to reduce the catalyst loading and air-sensitivity of the metal complex led to the development of Activator Regenerated by Electron Transfer (ARGET-ATRP) and Initiators for Continuous Activator Regeneration (ICAR-ATRP) (Scheme 5.4) [19].

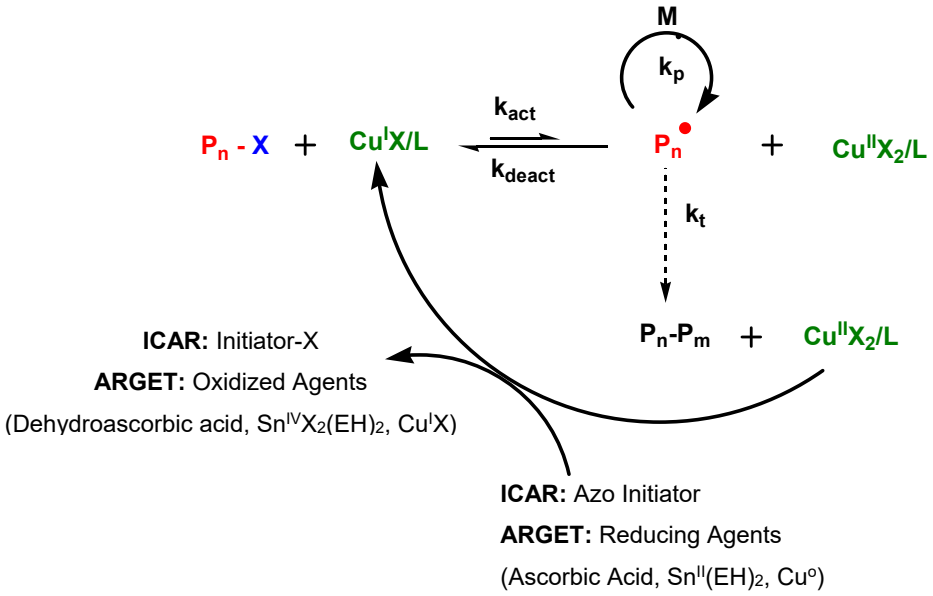

Scheme 5.4: Mechanism of ARGET-ATRP and ICAR-ATRP

In ARGET-ATRP a reducing agent is utilized to (re)generate the active catalyst from the deactivating species that accumulate *via* unavoidable termination reactions. A wide range of reducing agents including tin(II) 2-ethylhexanoate ($Sn(EH)_2$), glucose, ascorbic acid, phenol, hydrazine, phenylhydrazine and nitrogen containing ligands have been successfully used. These reducing agents enable the reaction to proceed even in the presence of oxygen. In ICAR-ATRP the copper complex in its higher oxidation state Cu (II) and a source of organic free radicals (*e.g.* AIBN) is used as the starting components of the process. Free radicals are slowly and continuously generated by conventional radical initiators throughout the polymerization process to reduce Cu (II) as a persistent radical and consequently generate the Cu (I) activator.

Both ARGET-ATRP and ICAR-ATRP generate well-defined polymers, with narrow molecular weight distributions while the low concentration of metal reduces the need for extensive purification. Both ARGET-ATRP and ICAR-ATRP, however, have relatively long reaction times

(typically 24–48 h), have moderate conversions (typically 10 - 80%) and the macroinitiators need to be purified prior to block copolymerization.

5.5 Single Electron Transfer Living Radical Polymerization (SET-LRP)

The concept of SET-LRP (or Cu(0) mediated RDRP) was initially introduced by Percec and co-workers in 2002 [20]. The process has drawn increasing attention since 2006 when the Percec group reported that this process was capable of providing an “ultrafast” synthesis of “ultrahigh” molecular weight polymers. They further demonstrated that this was possible at ambient temperatures and below, in polar media (such as DMSO, alcohols and water) and in the presence of nitrogen-based ligands and alkyl halide initiators as previously used in ATRP [21]. As with other RDRP techniques, in SET-LRP an effective reversible-deactivation between the propagating radicals and dormant species is necessary to ensure a low radical concentration, and reducing bimolecular termination and other side reactions (Scheme 5.5):

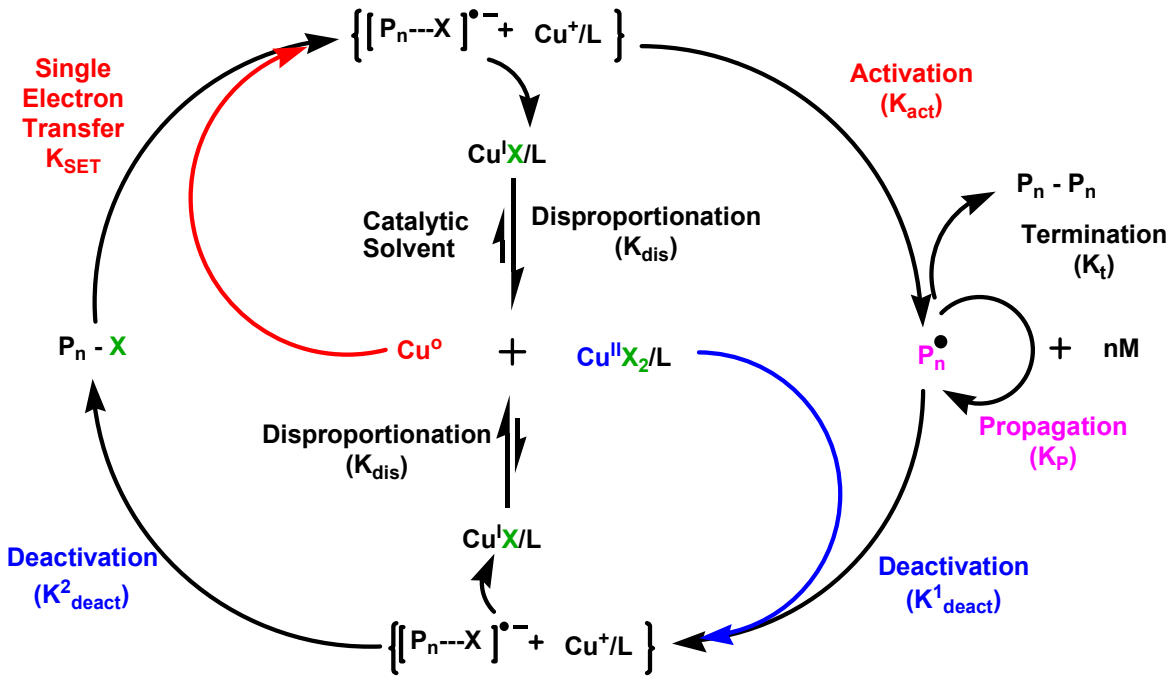

Scheme 5.5: Proposed mechanism for SET-LRP

In SET-LRP, the Cu(0) species acts as an electron donor, while the initiator/dormant propagating species (P_n-X) acts as an electron acceptor. In the process, Cu(0) donates an electron to P_n–X to simultaneously generate a radical-anion intermediate (P_n-$X^{\bullet -}$) and Cu^+/L. The active radical ($P_n^{\bullet}$)

is then generated by the heterolytic cleavage of the radical anion intermediate (P_n-$X^{\bullet -}$). The Cu(I) species generated during the formation of the radicals spontaneously disproportionates into extremely reactive Cu(0) atoms and a Cu(II)X_2/L species, which mediate the initiation and the reversible termination, respectively. The equilibrium between the dormant chains and the propagating radicals relies on the rapid disproportionation of in situ produced Cu(I)X by activating Cu(0) and deactivating Cu(II)X_2 in presence of polar solvents (*e.g.* H_2O and DMSO) and suitable nitrogen containing ligands (*e.g*. Me_6-Tren).

SET-LRP is a robust and versatile polymerization tool that allows rapid polymerization of a range of monomers [22]. The polymerization reactions can be completed in less than 15 minutes and can be conducted at or below ambient temperature conditions. The polymerization procedure does not require strict deoxygenating procedures (just bubbling with nitrogen or argon) or complex apparatus - a vial can be used in place of a Schlenk tube [23]. Further, the very low levels of catalyst employed (parts per million) result in colorless polymerization mixtures and may be used without the need for further separation in many applications. It is important to mention that in comparison with the other LRP methods that provide polymers with narrow molecular weight distribution, only SET-LRP generates polymers with both narrow molecular weight distribution and quantitative or near quantitative chain-end functionality [24].

Like all polymerization techniques, SET-LRP has some limitations. Currently it cannot mediate the polymerization of less activated monomers such as N-vinylpyrrolidone (VP) and vinyl acetate (VA) [25]. Also, acidic monomers cannot be directly homopolymerized due to complexation of the catalyst. In addition, cessation of the polymerization can occur due to gradual accumulation of Cu(II)Br_2 species. Solvent choice is also limited, with DMSO, methanol and water being the most studied solvents [26].

Based on the needs of the current research project (linear block copolymerization of monomers) and weighing the advantages and disadvantages of each of the LRP systems, it was decided to use SET-LRP to synthesize the linear block copolymers for use as flocculants.

5.6 Components of SET-LRP

When using a zero-valent metal as a catalyst in SET-LRP, the monomer, solvent, catalyst system, and initiator are all important factors that influence the reaction and quality of the product.

5.6.1 Monomer Compatibility

Various monomers have been successfully polymerized by SET-LRP using zero-valent metals as catalysts. These monomers include acrylates [27], methacrylates [28], acrylamides [29], methacrylamides [30], acrylonitrile [31], vinyl chloride [32], styrene [33], and other monomers [34]. With regard to acrylates, copper-based systems have been the most extensively studied and are effective at controlling the polydispersity. Functional and pH-responsive acrylates such as 2-dimethylaminoethyl acrylate (DMAEA) have been demonstrated to be efficiently polymerized by SET-LRP [35]. Although SET-LRP has not been as extensively applied for methacrylates, several studies, including poly(2-(dimethylamino)ethyl methacrylate) (PDMAEMA), have been carried out which have resulted in well-defined polymers [36]. In 2013, the introduction of aqueous SET-LRP by Haddleton and co-workers gave access to the rapid and quantitative (100% conversion in 15 min) polymerization of acrylamide monomers with controlled chain lengths and narrow molecular weight distributions [37].

5.6.2 Solvent Compatibility

Polar solvents, such as DMSO and H_2O, favour the disproportionation of Cu(I)Br and present a first order rate of polymerization. These solvents maintain a very high end-group functionality [38]. Alcohols, including methanol, ethanol, phenol, isopropanol, and tert-butanol have also shown excellent compatibility with SET-LRP, resulting in the preparation of well-defined polymers with narrow molecular weight distributions [39].

DMSO is by far the most commonly used solvent to date for SET-LRP [40]. DMSO enhances the polarity of the medium, thereby aiding electron transfer. DMSO has also been reported to be a coordinating solvent that stabilizes CuX_2, shifting the K_{dis} further to the right and hence facilitating disproportionation. More recently, the Haddleton group [41] had shown that H_2O also showed excellent compatibility with SET-LRP. Haddleton proposed that the key step to using water as the solvent was to allow full disproportionation of CuBr/Me_6-Tren to Cu(0) powder and Cu(II)Br prior to addition of both monomer and initiator. Following this protocol enables the synthesis of functional water-soluble polymers with controlled molecular weight, narrow molecular weight distributions and high chain end fidelity – this is important for chain extensions or multi-block copolymerization via sequential monomer addition.

5.6.3 Ligand Compatibility

Ligands are an important component of the catalyst system used in SET LRP. They help to solubilize the transition metal salts and alter the redox potential of the metal center for the exchange between the dormant and active species [42]. The appropriate choice of ligand is critical for successful SET-LRP. A minimal ligand concentration is required to achieve both acceptable reaction rate and good control over the MWDs and small changes in ligand concentration can dramatically affect the end-group fidelity of the polymer chains [43].

A number of nitrogen containing ligands that promote the disproportionation of Cu(I)Br have been used in SET-LRP. Of these Me_6-Tren has been the most widely used. Commercially available ligands including *N,N,N′,N″,N″*-pentamethyldiethylenetriamine (PMDETA) and tris(2-aminoethyl) amine (Tren) have also been used - disproportionation in the presence of these ligands is near quantitative and polymerization proceeds with equally high end-group fidelity, although at a slower rate compared to Me_6-Tren. 2,2′-Bipyridine (Bipy) and 4,4′-dinonyl-2,2′-bipyridine (diNbpy) have also been employed, although the disproportionation in the presence of these two ligands is negligible and, thus, a mixture of Cu(0) and Cu(I) activation occurs [44].

5.6.4 Catalyst Compatibility

SET-LRP processes have been initially reported to be activated, almost exclusively, by zero-valent copper or copper derivatives [45]. Polymers prepared by SET-LRP utilizing Cu(0) powder as the catalyst generate perfect or near-perfect end-group functionality in a large diversity of solvents [46]. Cu(0) wire catalysts presents several advantages over Cu(0) powder, including greater control over MWDs, predictability, easy catalyst preparation and removal. In addition to adding copper wire or powder directly to the reaction mixture, Cu(0) particles can be also generated *in situ* via the disproportionation of Cu(I)Br in the presence of Me_6-Tren in various solvents, including water. In situ chain extension up to a triblock was also successfully conducted (final $Đ \sim 1.15$), demonstrating that high end-group fidelity could be maintained [47].

Over the last three years, several groups have investigated alternative metallic catalytic sources, including silver (Ag), iron (Fe), nickel (Ni), ytterbium (Yb), lanthanum (La), gadolinium (Gd), magnesium (Mg), tin (Sn), and samarium (Sm) [48]. Of these, Fe proved to be highly attractive as it is inexpensive, nontoxic, abundant, environmentally benign, biocompatible, and easy to remove [49].

5.6.5 Initiator Compatibility

A variety of monofunctional, bifunctional, multifunctional, and macro initiators have successfully been used in SET-LRP. The initiators (which can be represented by R-X) consist of a leaving group (X) (which is almost exclusively a halogen atom) and the component R – which should contain some radical-stabilizing groups in order to facilitate radical generation. An organic halide, the structure of which is similar to that of the dormant chain end of the polymer, is preferentially used so that the activity of the carbon-halogen bond in the initiator is similar to that of the dormant polymer terminus [50].

The two most commonly employed monofunctional initiators are methyl bromopropionate (MBP), which is mainly utilized for the polymerization of acrylates, and ethyl-α-bromoisobutyrate (EBiB), which has been employed for the polymerization of a diversity of monomers, including acrylates, methacrylates, and acrylonitrile [51]. Poly(ethylene oxide) macroinitiator (PEO-Br) has also been used for the polymerization of acrylates [52].

SET-LRP has shown excellent compatibility with a range of bifunctional initiators including ethylene bis(2-bromoisobutyrate) (BrIBE), bis(2-bromopropionyl)ethane (BPE), dimethyl 2,5-dibromohexanedionate (MBHD), and dimethyl-2,6-dibromoheptanedioate (DMDBH) for the polymerization of acrylates and acrylonitrile [53]. Poly(ethylene glycol) bis(2-bromoisobutyrate) (PEG-BEBiB) and bis(2-(2′-bromoisobutyryloxy)ethyl)disulfide $(BiBOE)_2S_2$ have also been utilized for the polymerization of acrylates, methacrylates, and acrylamides [54].

5.7 Experimental

5.7.1 Materials

Poly(ethylene glycol) (10 000, 20,000, and 30 000 g/mol), purchased from Sigma-Aldrich, was dried in vacuum for 24 h before use. *N,N*-dimethylamino-2-ethyl methacrylate (DMAEMA, 97%) was obtained from Sigma–Aldrich and purified by passing through a basic alumina column. It was then distilled from CaH_2 under reduced pressure prior to use. Triethylamine (Aldrich, 99.5%) was dried over KOH for several days and then distilled from CaH_2 under reduced pressure before use. Tetrahydrofuran (THF, Aldrich, 99%) was fractionally refluxed over sodium in the presence of benzophenone and then stored over dried molecular sieves. Methylene chloride (DCM), purchased from Kimix South Africa, was refluxed with CaH_2 and then stored over dried molecular sieves. Copper(I) bromide (CuBr, Aldrich, 98%) was purified by stirring overnight over CH_3COOH at room temperature, followed by washing the solid with ethanol, diethyl ether, and acetone prior to drying under vacuum at 40^{o}C for one day. The following chemicals, from Sigma-Aldrich, were analytical grade and used as received: Acrylamide (≥99% for electrophoresis), magnesium sulfate, anhydrous (MgSO4), α-bromoisobutyryl bromide (BiBB) (98%), 4-dimethylaminopyridine (DMAP, 99 %), tris[2-(dimethylamino)ethyl]amine (Me_6TREN).

5.7.2 Synthesis Procedures

Triblock copolymers flocculants, PAM-*b*-PEG-*b*-PAM and PDMAEMA-*b*-PEG-*b*-PDMAEMA, were synthesized using the SET-LRP technique for copolymerization. For both polymer flocculants, three molecular weights of the central PEG (10 000, 20 000, and 30 000 g/mol) were used. The lengths of outer blocks were varied to obtain flocculants of various lengths.

The triblock copolymers PAM-*b*-PEG-*b*-PAM and PDMAEMA-*b*-PEG-*b*-PDMAEMA were synthesized using a two-step process. The first step involved the synthesis of a difunctional macroinitiator.

5.7.2.1 Synthesis of Poly(ethylene oxide) Macroinitiators

The difunctional macroinitiator, Br-PEG-Br, was synthesized by the method proposed by Kop *et al*. [55]. Reaction of poly(ethylene glycol) with excess of 2-bromoisobutyryl bromide was carried

out in the presence of *N,N*-dimethylamino pyridine (DMAP) and triethyl amine (TEA) as hydrogen bromide acceptors (Scheme 5.6).

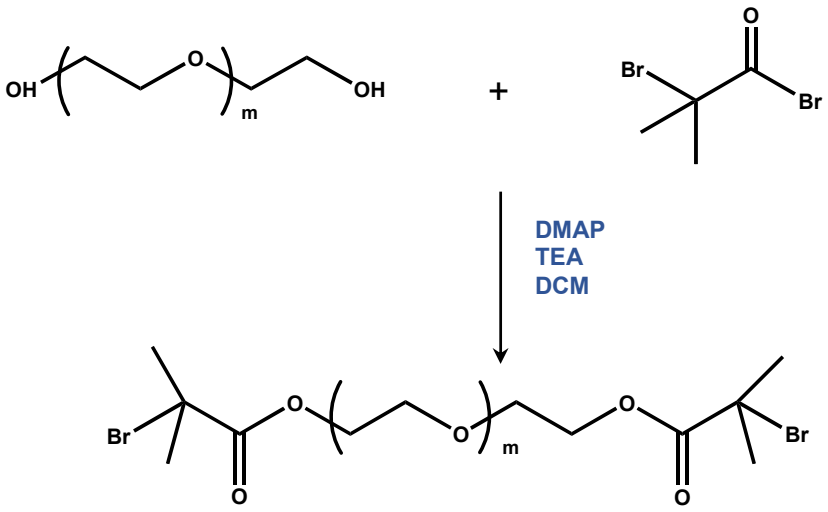

Scheme 5.6: Synthesis of Br-PEG-Br macroinitiator

The procedure described below was for the synthesis of a PEG_{20k}. An equivalent procedure was used to synthesize macroinitiators using PEG_{10k} and PEG_{30k} as the central block. Throughout the synthesis procedure, the system was continuously purged with a stream of dry argon gas.

A dried 500 mL three-necked round bottom flask, fitted with a condenser and a dropping funnel was placed in an ice bath and the entire setup was placed atop a stirrer unit. The round bottom flask was then charged with 10 mL dry methylene chloride, *N,N*-dimethylamino pyridine (0.22 g, 1.8 x 10^{-3} mol) and triethyl amine (0.22 g 2.5 x 10^{-3} mol) and the mixture stirred for 15 minutes. 2-Bromoisobutyryl bromide (0.51 g, 2.5 x 10^{-3} mol) in dry dichloromethane (10 mL) was added over a period of 10 minutes to the reaction mixture, followed by dropwise addition of poly(ethylene glycol) (15 g, 7.5 x 10^{-4} mol) in dichloromethane (100 mL) over a period of 1.5 h under inert atmosphere. The reaction mixture was then allowed to attain room temperature and stirred overnight at room temperature. The next morning, the mixture was filtered and washed with saturated sodium bicarbonate solution (3 x 100 mL) and water (3 x 100 mL). The solution was dried over anhydrous sodium sulphate, filtered and the dichloromethane removed under vacuum to obtain the Br-PEO-Br macroinitiator. The macroinitiator was purified by dissolution in dichloromethane (10 mL) and precipitation into excess hexane. The purification procedure was repeated three times and macroinitiator was dried under vacuum at room temperature for 24 h.

5.7.2.2 Synthesis of PAM-*b*-PEG-*b*-PAM Triblock Copolymers by SET-LRP

The preparation of the Cu(0) catalyst by the disproportionation of the CuBr "in situ" and the block copolymerization follows the previously reported procedure by Percec and Haddleton [56] and is illustrated in Scheme 5.7 and Figure 5.3.

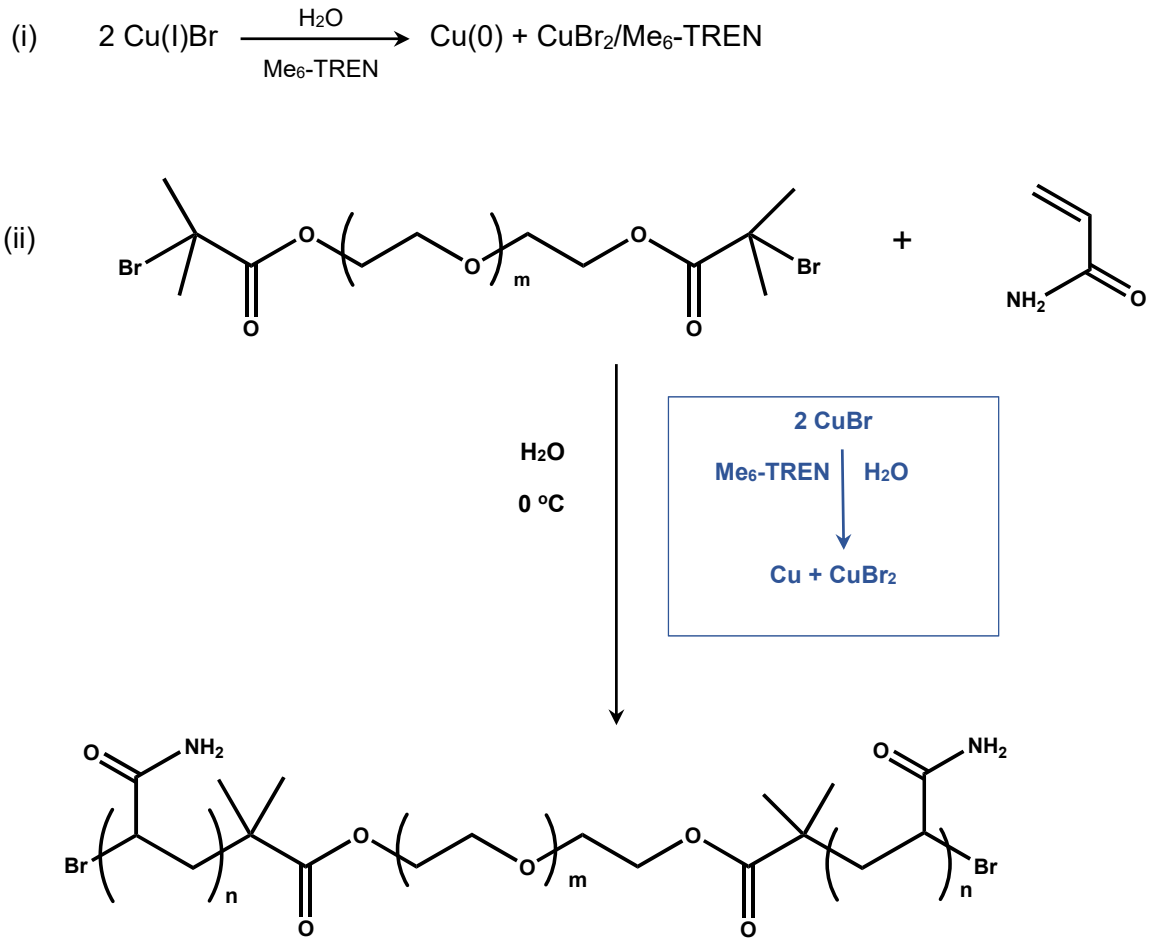

Scheme 5.7: Synthesis of PAM-*b*-PEG-*b*-PAM

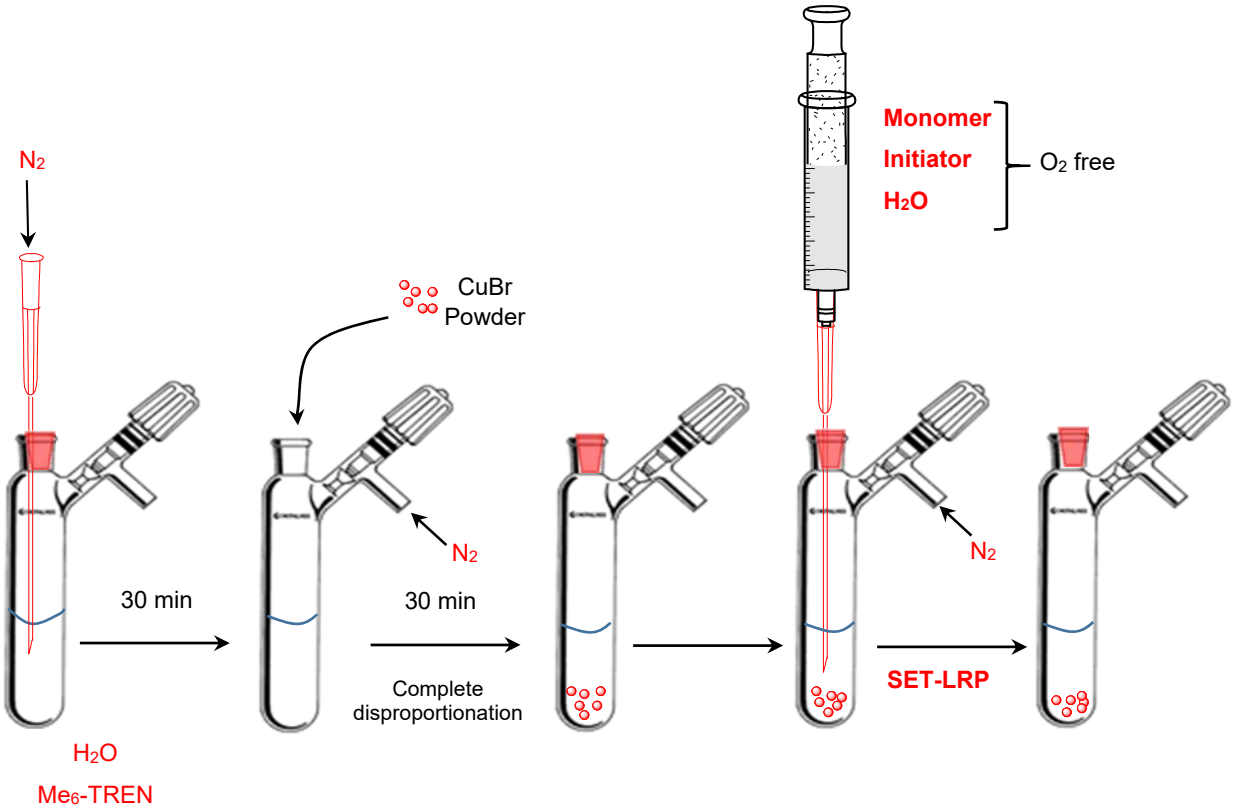

Figure 5.3: Schematic representation of the aqueous SET-LRP catalyzed with Cu(0) generated "in situ"

The procedure described below is based on 1 g (0.05 mmol) of macroinitiator (Br-PEG-Br). To an oven dried Schlenk tube fitted with a magnetic stirrer bar and a rubber septum, H_2O (10 mL) and Me_6TREN (7.9 μL, 29.6 μmol, 0.6 equiv) were charged and the mixture was bubbled with nitrogen for 30 minutes. Cu(I)Br (8.5 mg, 59.1 μmol, 1.2 equiv) was then carefully added under slight positive pressure of nitrogen. The disproportionated solution was placed in an ice bath and deoxygenated for a further 30 minutes. In a separate tube fitted with a magnetic stirrer bar and a rubber septum, acrylamide monomer (3.50 g, 49.2 mmol, 500 equiv) was dissolved in H_2O (10 mL) prior to addition of the Br-PEG-Br initiator (1 g, 0.05 mmol) and the resulting mixture was bubbled with nitrogen for 30 minutes. The degassed monomer-initiator aqueous solution was then transferred via a degassed syringe to the Schlenk tube containing the Cu(0)/$CuBr_2$/Me_6TREN catalyst. The Schlenk tube was sealed and the mixed solution was allowed to polymerize at 0°C for 30 minutes.

The resultant solution was first evaporated to dryness under vacuum. The residue was then diluted with THF and passed through an alumina column to remove the copper catalyst. The

product was precipitated from diethyether three times and then dried under vacuum overnight at room temperature to produce the block copolymer.

The above procedure was repeated for two other lengths of acrylamide – twice the length of PEG (DP_n =1000) and half the length of PEG (DP_n = 250). The entire procedure was then repeated for PEG_{10k} and PEG_{30k}. The values of the reagents used is given in Table 5.1.

Table 5.1: SET-LRP of acrylamide with varied degree of polymerization

PEG	[M]:[I]:[Cu(I)Br]:[Me_6TREN]		Initiator (mol)	Acrylamide mass (g)	Cu(I)Br mass (mg)	Me_6-TREN Vol (μL)
10 k	PA1	250 : 1 : 1.2 : 0.6	9.7E-05	1.73	5.68	5.3
	PA2	500 : 1 : 1.2 : 0.6	9.7E-05	3.45	5.68	5.3
	PA3	1000 : 1 : 1.2 : 0.6	9.7E-05	6.90	5.68	5.3
20 k	PA4	500 : 1 : 1.2 : 0.6	4.9E-05	1.75	8.48	7.9
	PA5	1000 : 1 : 1.2 : 0.6	4.9E-05	3.50	8.48	7.9
	PA6	2000 : 1 : 1.2 : 0.6	4.9E-05	7.00	8.48	7.9
30 k	PA7	750 : 1 : 1.2 : 0.6	3.3E-05	1.75	16.72	15.5
	PA8	1500 : 1 : 1.2 : 0.6	3.3E-05	3.52	16.72	15.5
	PA9	3000 : 1 : 1.2 : 0.6	3.3E-05	7.40	16.72	15.5

5.7.2.3 Synthesis of PDMAEMA-*b*-PEG-*b*-PDMAEMA Triblock Copolymers by SET-LRP

The triblock copolymers, PDMAEMA-*b*-PEG-*b*-PDMAEMA, were synthesized by the SET-LRP method in accordance with the procedure proposed by Percec and Haddleton [56] and is shown in Scheme 5.8.

In accordance with the reported procedure, CuBr was allowed to fully disproportionate in an aqueous solution of the tetradentate tertiary amine ligand Me_6-TREN. An aqueous mixture consisting of the macroinitiator (Br-PEG-Br), monomer (DMAEMA), and water-methanol was

subsequently added and polymerization was allowed to proceed under a nitrogen atmosphere. Three different molecular weights of the central PEG polymers were used: 10 000, 20 000, and 30 000 g/mol. For each of these central blocks three lengths of outer blocks were polymerized. In the first case an outer chain having the same number of monomer units as the PEG central block was synthesized. In the second copolymer, the outer chain with twice the number of monomer units as the central PEG block was synthesized. The third copolymer had outer chains equivalent to half the number of monomer units of the central PEG block. The masses/moles of the reagents used are given in Table 5.2.

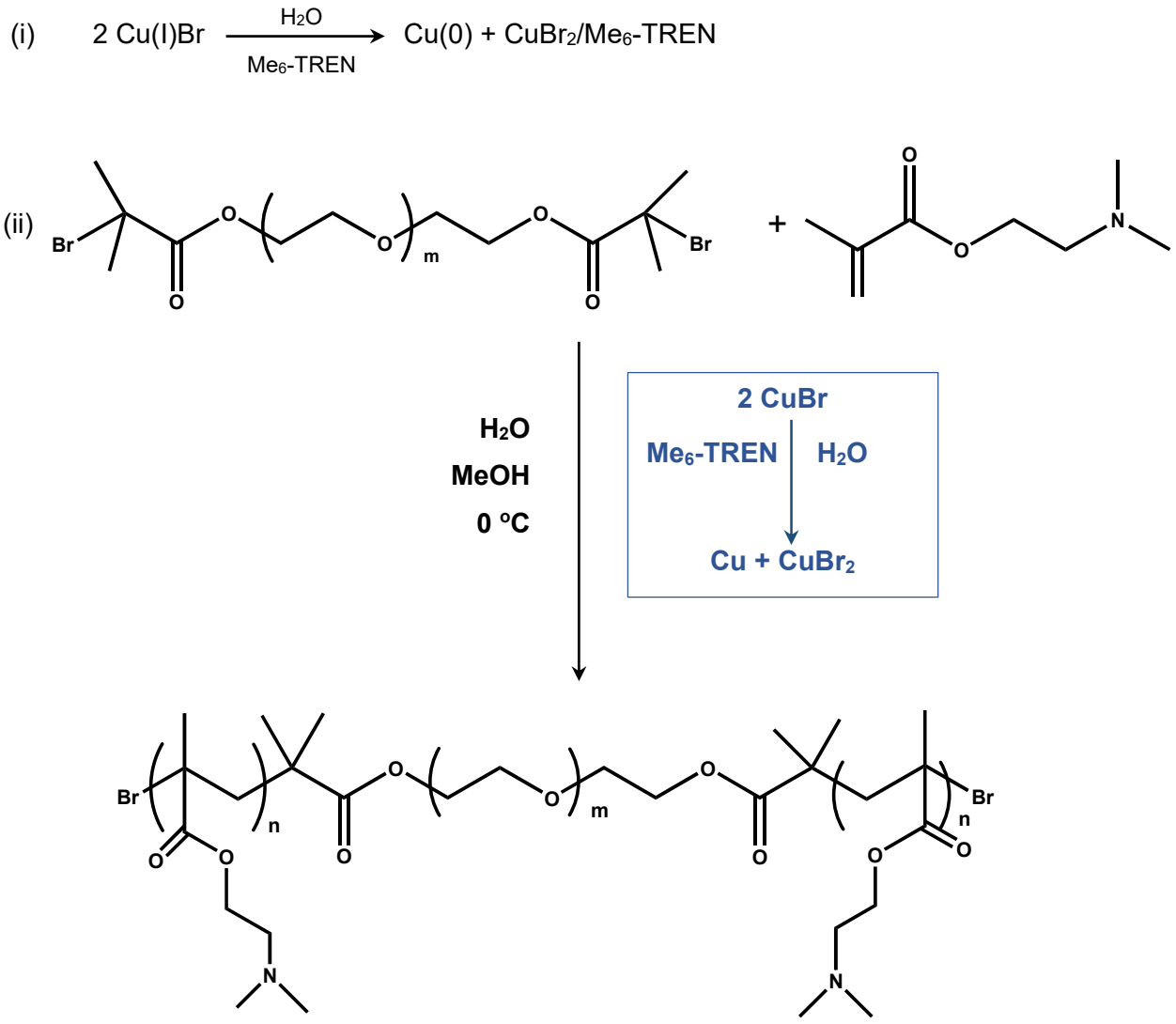

Scheme 5.8: Synthesis of PDMAEMA-*b*-PEG-*b*-PDMAEMA

Table 5.2: SET-LRP of 2-(dimethylamino)ethyl methacrylate (DMAEMA) with varied degree of polymerization

PEG		[M]:[I]:[Cu(I)Br]:[Me_6TREN]	Initiator (mol)	DMAEMA Vol (mL)	Cu(I)Br mass (mg)	Me_6-TREN Vol (μL)
10 000	PB1	250 : 1 : 1.2 : 0.6	9.7E-05	3.8	5.68	5.3
	PB2	500 : 1 : 1.2 : 0.6	9.7E-05	7.6	5.68	5.3
	PB3	1000 : 1 : 1.2 : 0.6	9.7E-05	15.2	5.68	5.3
20 000	PB4	500 : 1 : 1.2 : 0.6	4.9E-05	3.9	8.48	7.9
	PB5	1000 : 1 : 1.2 : 0.6	4.9E-05	7.7	8.48	7.9
	PB6	2000 : 1 : 1.2 : 0.6	4.9E-05	15.5	8.48	7.9
30 000	PB7	750 : 1 : 1.2 : 0.6	3.3E-05	3.9	16.72	15.5
	PB8	1500 : 1 : 1.2 : 0.6	3.3E-05	7.8	16.72	15.5
	PB9	3000 : 1 : 1.2 : 0.6	3.3E-05	15.6	16.72	15.5

5.7.2.4 Characterization

Different analytical techniques were used to confirm that all intermediates and final products were indeed obtained. The macroinitiators and the triblock copolymers were characterized using both Fourier transform infrared spectroscopy (FTIR) and proton nuclear magnetic resonance (^{1}H NMR) spectroscopy.

FTIR spectroscopy was carried out on a Perkin Elmer FT-IR transmission spectrophotometer ranging from 400–4500 cm^{-1} with a resolution of 4 cm^{-1}. KBr was used to prepare the sample discs for analysis. The software that was used on the system to do the data analysis was Spectrum 10 Software.

The ^{1}H-NMR measurements were carried out at 50°C on a Varian Mercury 400 MHz or Varian Unity Inova 600 MHz spectrometer in either deuterated dimethyl sulfoxide (DMSO-d_6) or deuterated chloroform ($CDCl_3$). Mestranova software version 6.02 was used to view and analyze the NMR data obtained from the spectrometer.

5.7.2.5 Flocculation Studies

The flocculation characteristics of the synthesized triblock copolymer flocculants were investigated using the Standard Jar Test and Settling Test methods. A 0.25% (w/v) kaolinite suspension was used as the synthetic wastewater.

5.7.2.5.1 Jar Tests

Conventional turbidity tests of the various triblock copolymer based flocculants were carried out using a Phipps and Bird Six-Paddle Stirrer, model PB-7790910 jar test apparatus. A 0.25 wt% suspension of kaolinite was used for flocculation study. The suspensions were poured into 1.5-L Gator Jars under slow stirring conditions and different flocculant doses were added to the suspensions. Immediately after the addition of flocculant, the suspension was stirred at a constant speed of 125 rpm for 2 minutes, followed by slow stirring at 20 rpm for 15 minutes. The flocs were then allowed to settle for 30 minutes. At the end of the settling period, a sample of supernatant liquid was drawn, and its turbidity measured using a turbidity meter (HANNA model HI88703). Distilled water was used as a reference.

5.7.2.5.2 Settling Test

The column-settling studies were carried out using the same 0.25% (w/v) synthetic suspensions used for the Jar Tests. This test employed a 1000 mL, stoppered, graduated cylinder and stopwatch. The tests started with adding 1000 mL of the kaolinite suspension to a Gator Jar, adding a dosage of flocculant and rapidly stirring the mixture at 125 rpm for 2 minutes. The dosage of flocculants to be added was determined from the Jar Test – it was the optimally determined dosage from the best performing flocculant from the Jar Test. The mixed slurry sample from the Gator Jar was poured into the graduated cylinder and the cylinder was then inverted 10 times for thorough mixing. After the cylinder was set upright, the height of the interface between the water and settling solid bed was measured over time.

5.8 Results and Discussion

5.8.1 Synthesis and characterization of difunctional Br-PEG-Br macroinitiator

Kops *et al*. [55] functionalized poly(ethylene glycol) by transforming the hydroxyl groups into 2-bromo propionate groups to obtain mono or difunctional PEG macroinitiators. They found PEO macroinitiators to be efficient initiators for ATRP of styrene and obtained PEO-*b*-PS and PS-*b*-PEO-*b*-PS copolymers with predetermined molecular weight and narrow MWD. In order to avoid cleavage of the polymer chains, as found in other derivatizations of PEG, Kops *et al.* carried out the reaction at 0 °C in CH_2Cl_2 and in the presence of TEA and DMAP. In the current research, difunctional Br-PEG-Br macroinitiators were synthesized according the procedure reported by Kops *et al*. The reaction of poly(ethylene glycol) with an excess of 2- bromoisobutyryl bromide was carried out in the presence of *N,N*-dimethylamino pyridine and triethylamine as hydrogen bromide acceptors (Scheme 5.6). A high mean yield of 88.5% was obtained using this process.

The macroinitiator was successfully synthesized and the structural integrity of the macroinitiator was confirmed by FTIR spectroscopy (Figure 5.4 and Figure 5.5) and ^{1}H NMR analysis (Figure 5.6 and Figure 5.7). The characteristic peaks of poly(ethylene glycol) observed at 3445 cm^{-1}, 3051 cm^{-1}, 1481 cm^{-1} and 1161 cm^{-1} are those attributed to -OH stretching vibrations, C-H stretching vibrations, C-H bending vibrations and C-O stretching vibrations, respectively [57]. It is observed that after incorporation of the bromo-ester group onto PEG, the -OH stretching vibration band (3445 cm^{-1}) almost disappeared, while the -CH_3 bending vibration (1343 cm^{-1}) as well as carbonyl stretching vibration (1736 cm^{-1}) of ester carbonyl group of difunctional macroinitiator were observed, suggesting the successful acylation of the PEG molecule.

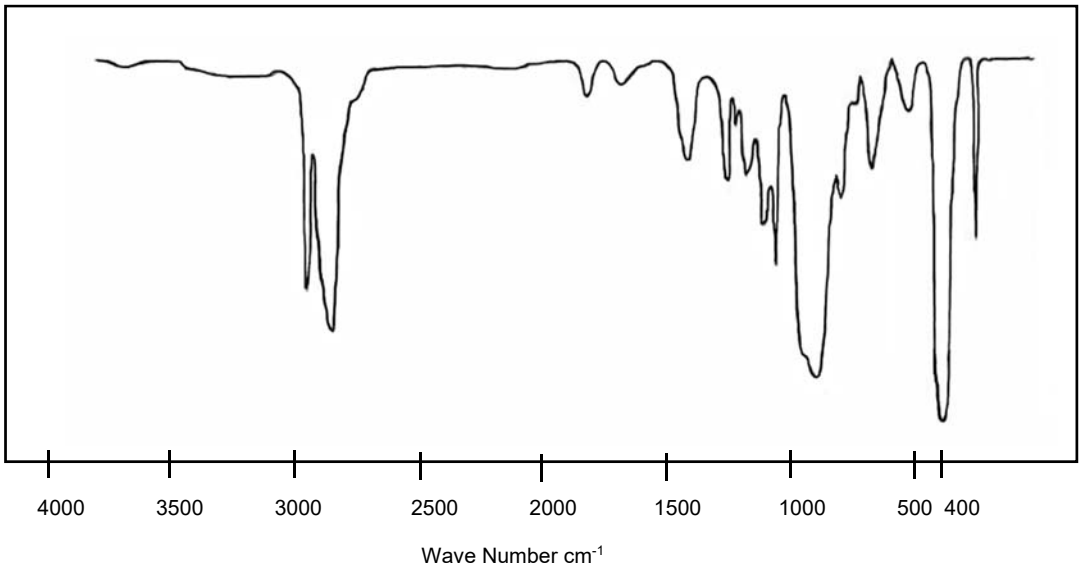

Figure 5.4: FTIR spectrum for poly(ethylene glycol)

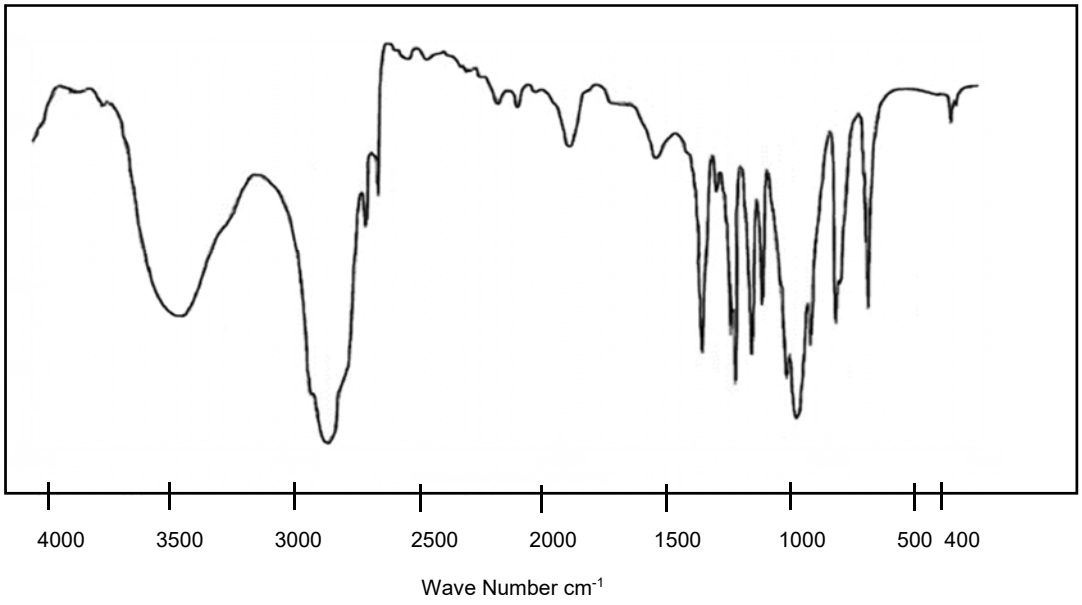

Figure 5.5: FTIR spectrum for Br-PEG-Br macroinitiator

The ^{1}H NMR spectra of poly(ethylene glycol) (Figure 5.6) and the macroinitiator (Br-PEG-Br) (Figure 5.7) confirm the successful synthesis of the macroinitiator.

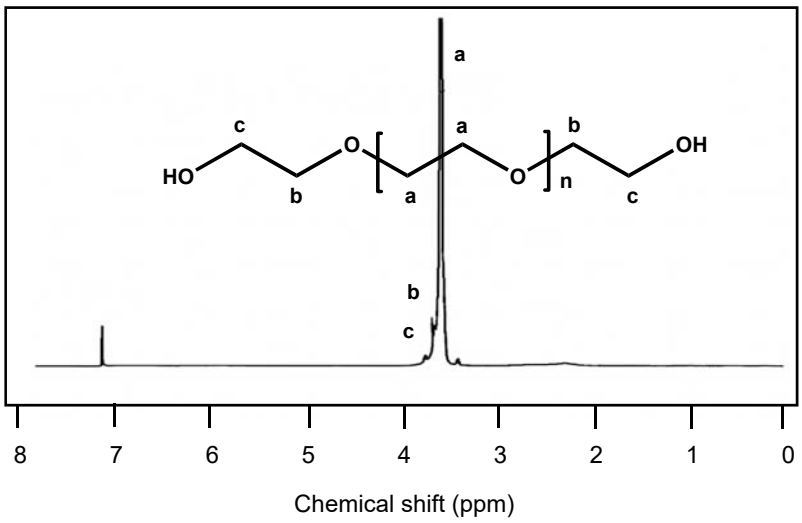

Figure 5.6: ^{1}H NMR spectrum for PEG

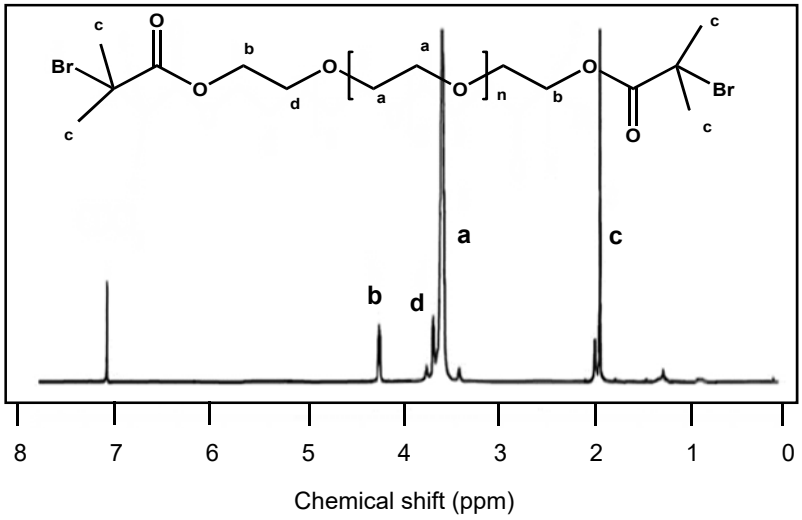

Figure 5.7: ^{1}H NMR spectrum for Br-PEG-Br macroinitiator

From Figure 5.7 it is observed that the peak of the hydroxyl group of PEG in $CDCl_3$ at around 2.45 ppm disappears completely and two new peaks appear at 4.33 and 1.94 ppm. The peak at 1.94 ppm is attributed to the protons from four methyl groups (-OCO-C(CH_3)$_2$) and the multiplet at 4.33 ppm is assigned to methylene protons attached to the ester group. The peak at 3.65 ppm corresponds to the oxy-ethylene protons of Br-PEO-Br macroinitiator [58].

5.8.2 Synthesis and Characterization of PAM-*b*-PEG-*b*-PAM Triblock Copolymers

Reversible addition−fragmentation chain transfer (RAFT) methodology has traditionally been used to polymerize and generate well-defined polyacrylamide and polyacrylamide derivatives [59]. Although RAFT gives good control over the MWDs, the reaction generally requires 24 h to reach 94% conversion at ambient temperature conditions. Atom transfer radical polymerization (ATRP) of acrylamide and its derivatives has also been attempted in various organic solvents and mixed aqueous media with varying degrees of success [60]. The most recent example of copolymer block synthesis involving polyacrylamide was by Matyjaszewski and coworkers in 2015 [61]. They used electrochemistry (eATRP) to polymerize acrylamide from a poly(ethylene glycol) macroinitiator. Their results showed good agreement between theoretical and experimentally determined molecular weights and they obtained a low dispersity of 1.09 for lower targeted molecular weight species. They, however, used a water/DMF mixture instead of pure water and the integrity of the diblock copolymer obtained was compromised when the macroinitiator reached a conversion of only 84% prior to the subsequent monomer addition.

In 2013, Haddleton and co-workers [37] introduced a successful new procedure for the polymerization of acrylamide monomers in an aqueous solution using SET-LRP. The key to the success of their procedure was to firstly completely disproportionate Cu(I)Br to Cu(0) and Cu(II) species in an aqueous solution of Me_6TREN prior to the addition of the monomer and initiator. This protocol has proved to be an extremely powerful tool for the synthesis of both polyacrylamides and other water-soluble monomers such as PEG-based acrylates. Haddleton and coworkers [62] reported that they were able to synthesize polyacrylamides with narrow molecular weight distributions, in a quantitative manner (>99% conversion) and within a short time period of 15 minutes using the above protocol. Haddleton and coworkers also targeted various degrees of polymerization using different ratios of [AM]:[I]:[Cu(I)Br]:[Me_6TREN]. When targeting low degrees of polymerization (< 40), they obtained good polymerizations with a ratio of [20]:[1]:[0.4]:[0.4]. Similar results were obtained for a targeted degree of polymerization of 80 when the ratio of [Cu(I)Br]:[Me_6TREN] was increased to [0.8:0.6]. In order to probe the potential of the technique to obtain higher molecular weight polyacrylamide, a reaction targeting DP_n = 640 was conducted. Using optimized ratios of [1]:[1.2]:[0.6] ([I]:[Cu(I)Br]:[Me_6TREN]), they were able to successfully polymerize acrylamide to high conversion (>99%) and low dispersity.

In the current research, the symmetric linear PAM-*b*-PEG-*b*-PAM triblock copolymer was successfully synthesized via SET-LRP using the above protocol. The structural integrity of the linear triblock copolymer was confirmed by FTIR spectroscopy and ^{1}H NMR.

Sample FTIR spectra of acrylamide, polyethylene glycol, and the linear block copolymer PAM-*b*-PEG-*b*-PAM are shown in Figures 5.8, 5.9, and 5.10 respectively.

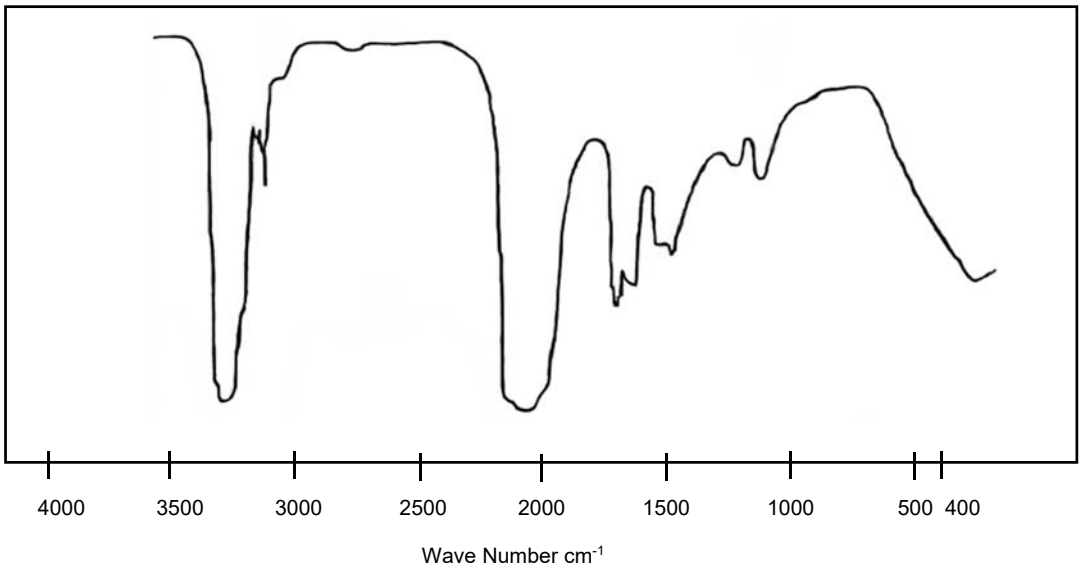

Figure 5.8: FTIR spectrum of polyacrylamide

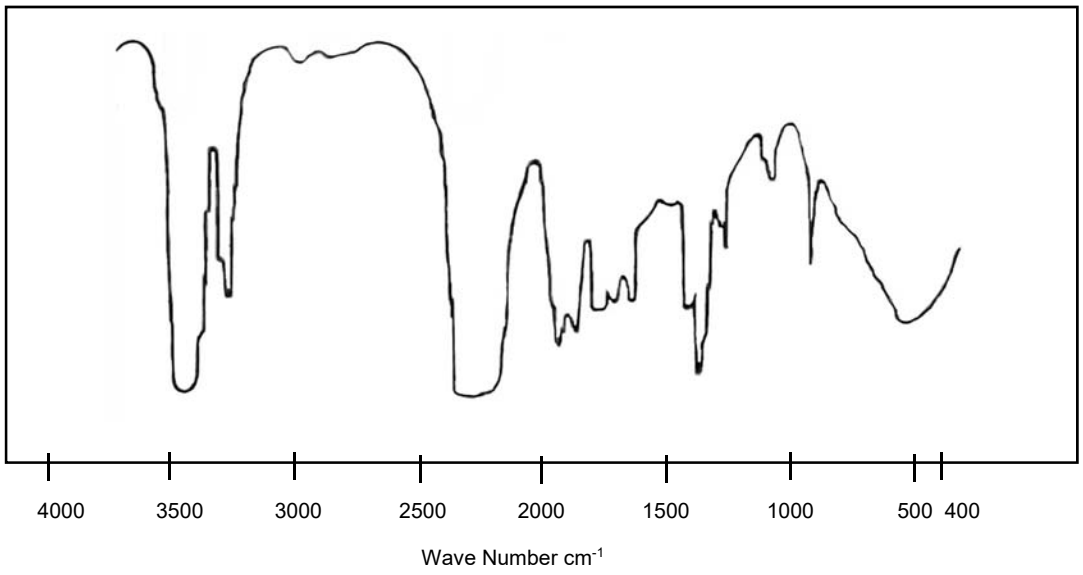

Figure 5.9: FTIR spectrum for poly(ethylene glycol)

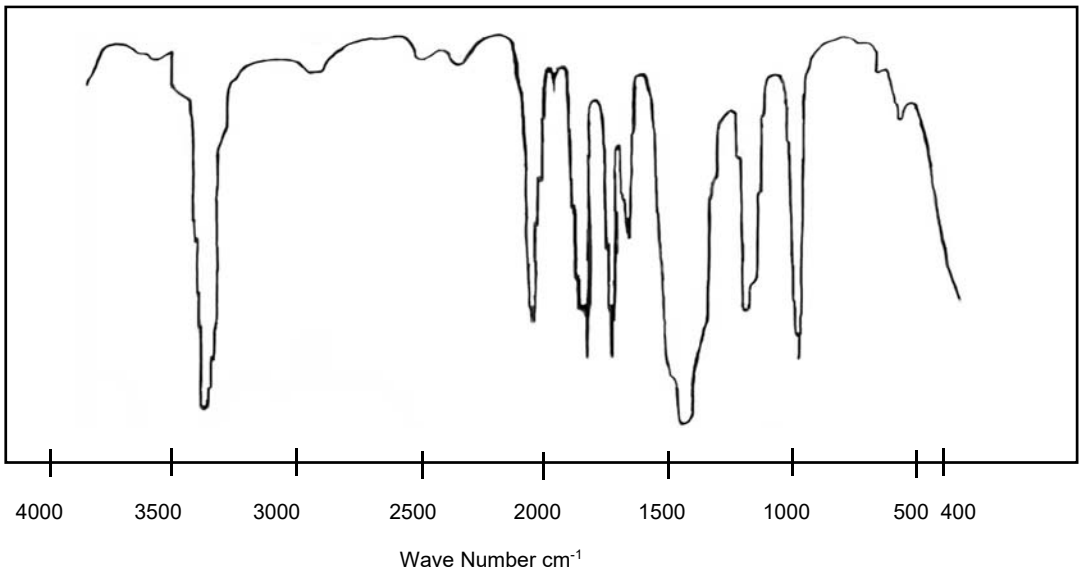

Figure 5.10: FTIR spectrum for PAM-*b*-PEG-*b*-PAM

In the FTIR spectrum of polyacrylamide (Figure 5.8), the characteristics bands at 3350 cm^{-1}, 2950 cm^{-1}, 1680 cm^{-1} and 1460 cm^{-1} were assigned for the stretching vibrations of the NH_2 group C-H bond, C=O group and CH_2 scissoring, respectively. In the FTIR spectrum of PEG (Figure 5.9), characteristic OH bonds were observed. The absorption band at 2920 cm^{-1} was attributed to C-C bond. The bands at 1465 cm^{-1}, 960 cm^{-1} to 1060 cm^{-1} were ascribed to the CH_2 bending vibrations, C-OH stretching vibrations respectively. The FTIR spectrum of the triblock copolymer (Figure 5.10) showed a characteristic peak of NH_2 group at 3433 cm^{-1} which was also present in the spectrum of pure acrylamide. A weakened peak for the stretching band of OH group was observed. The characteristic C-H bond stretching vibrations were also observed at a slightly shifted position. The presence of additional peaks for amide (1660 cm^{-1}), and C-N (1456 cm^{-1}) stretching vibrations, gave the confirmation for the grafting of polyacrylamide chains onto the PEG backbone.

A sample ^1H NMR spectra for poly(ethylene glycol) and the triblock copolymer (PAM-*b*-PEG-*b*-PAM) is shown in Figures 5.11 and 5.12 respectively.

The ^1H NMR spectrum in Figure 5.11 for poly(ethylene glycol) shows chemical shifts between, 1 and 2.5 for ^1H protons (a) and in $–CH_2$ and –CH (b) of the acrylamide units.

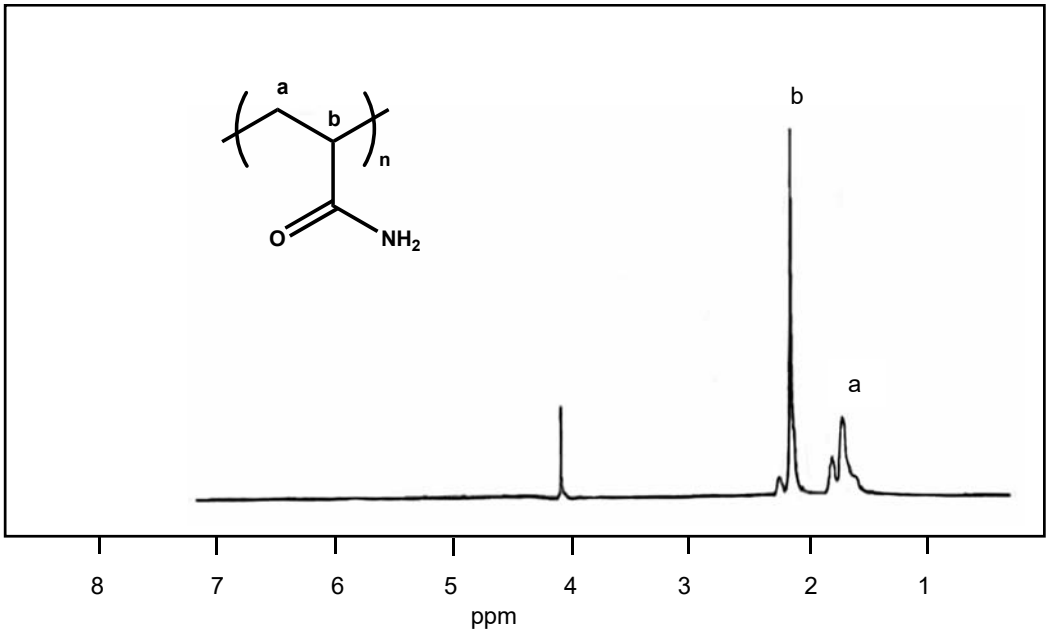

Figure 5.11: ^{1}H NMR spectrum for polyacrylamide

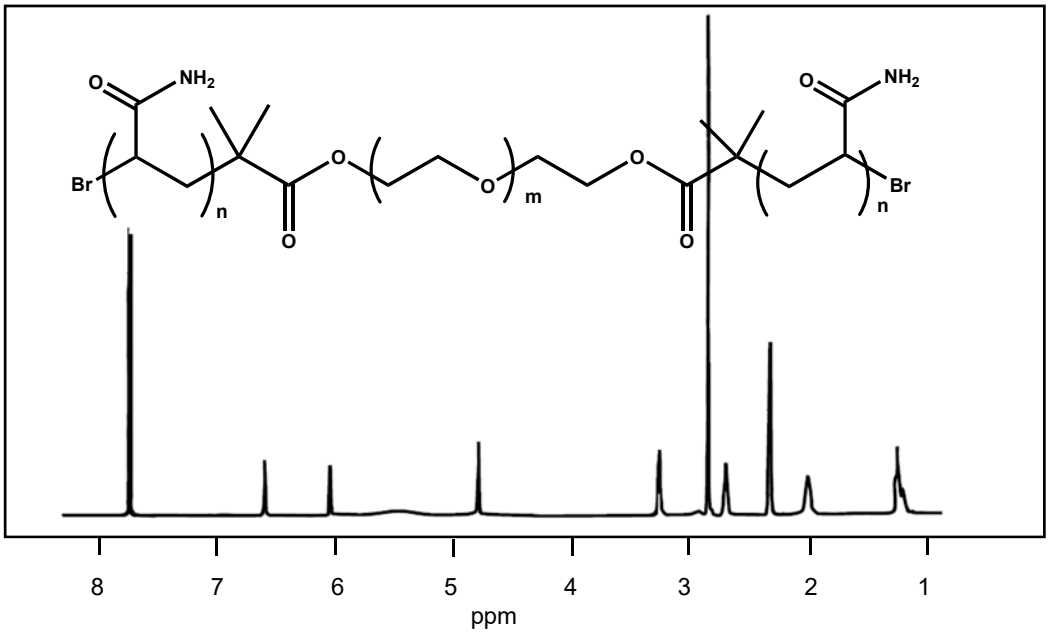

Figure 5.12: ^{1}H NMR spectrum for PAM-*b*-PEG-*b*-PAM

The ^{1}H NMR spectra of the triblock copolymer (PAM-b-PEG-PAM) in Figure 5.12 shows the methyl proton peak of bromo ester compound has been shifted to δ = 2.09 ppm. The other methylene protons that are connected with bromo-ester group and bromine atom were observed at δ = 2.99 ppm and δ =5.14 - 5.17 ppm, respectively. The -NH_2 protons of acrylamide were found at δ = 6.64 ppm. This result confirms the successful polymerization.

5.8.3 Synthesis and Characterization of PDMAEMA–*b*–PEG–*b*–PDMAEMA Triblock Copolymers

Various lengths of the triblock copolymers were synthesized by varying the lengths of both the central PEG block as well as the outer PDMAEMA blocks. The triblock copolymers, PDEAEMA–*b*–PEG–*b*–PDEAEMA, were synthesized by SET-LRP using Br–PEG–Br as a macroinitiator.

Tertiary amine monomers and their corresponding polymers have good solubility in a range of organic solvents, such as acetone, alcohols, *N*, -*N*-dimethylformamide (DMF), dimethyl sulfoxide (DMSO), dichlorobenzene, ethyl acetate and tetrahydrofuran (THF) [63]. Controlled polymerizations of DMAEMA have been conducted in such organic solvents or aqueous solution with a high ratio of organic solvent [64]. In the current research, an aqueous solution of methanol-water, which strongly favours the disproportionation of Cu(I), has been chosen as a solvent for the Cu(0)-LRP of DMAEMA onto the PEG macroinitiator.

After the copolymers were purified, the chemical structures were characterized by ^{1}H NMR spectroscopy (Figures 5.13 and 5.14). The structure and the ^{1}H NMR spectra of the PDMAEMA-*b*-PEG-*b*-PDMAEMA copolymer are shown in Figure 5.14. The signal at 2.14 ppm is attributed to the methyl protons next to the nitrogen atom (-N(C**H**$_3$)$_2$) of the DMAEMA units. The peak at δ = 2.45 ppm is attributed to the methylene protons (-C**H**$_2$-N(CH$_3$)$_2$) and the chemical shift at 3.45 ppm is attributed to the methylene protons on PEG units (-C**H**$_2$-C**H**$_2$-O-). Figure 5.14 shows that there were no signals at 5.6 and 6.1 ppm assigned to the two protons of CH$_2$=C of DMEAEMA monomer, proving that the copolymers were successfully synthesized and purified.

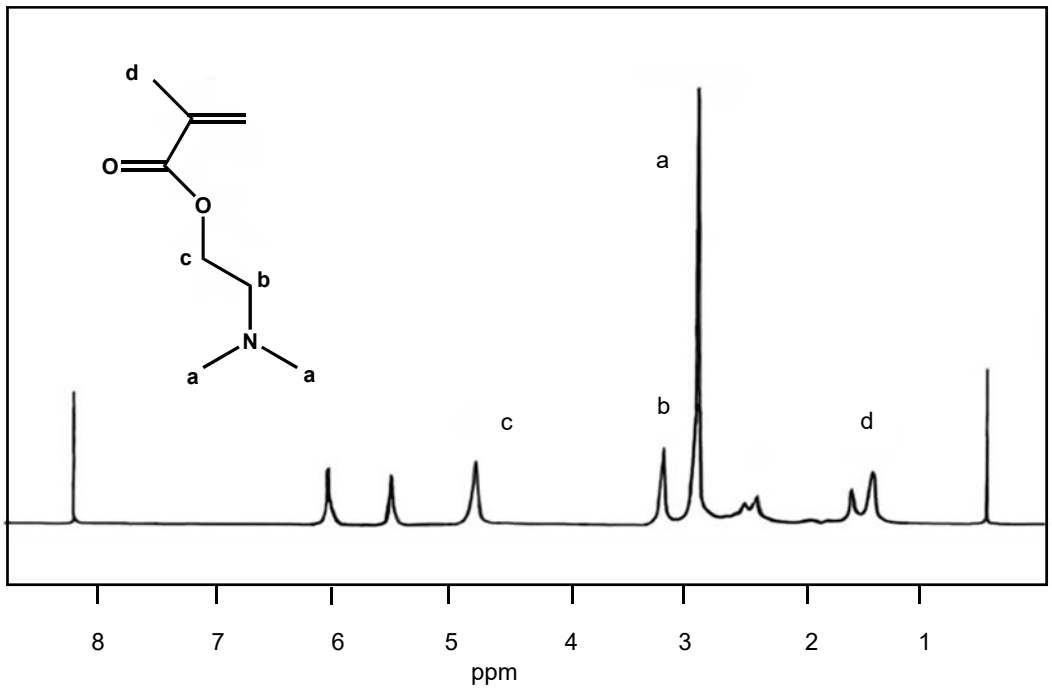

Figure 5.13: ^{1}H NMR spectrum for DMAEMA

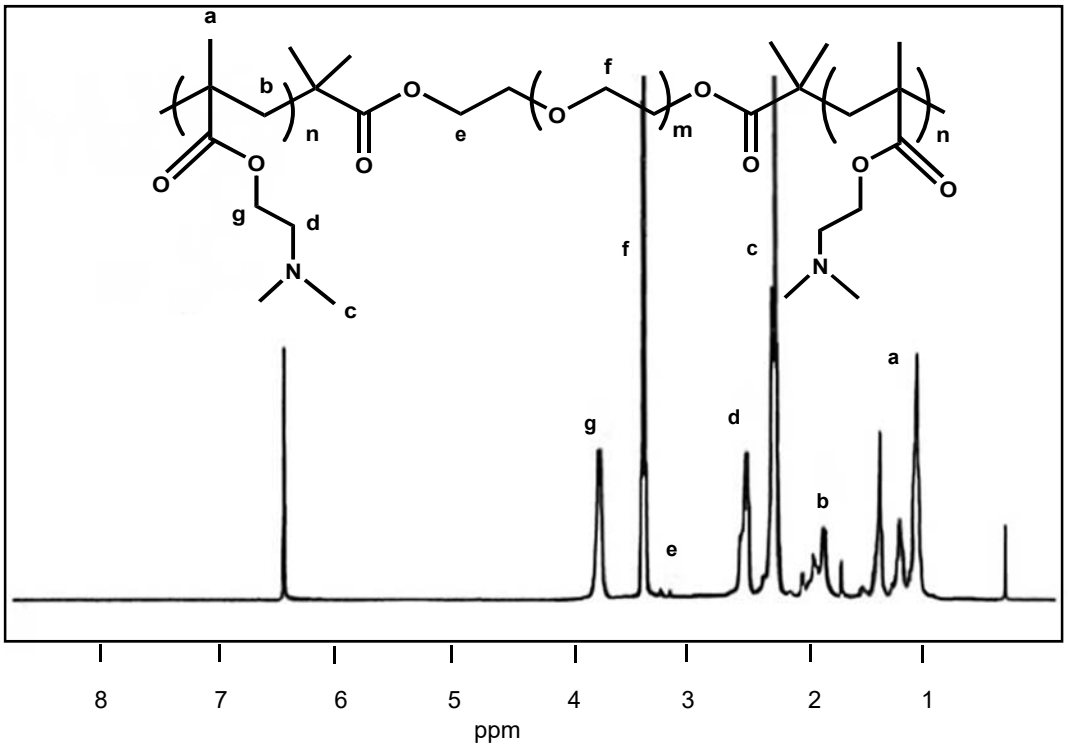

Figure 5.14: ^{1}H NMR spectrum for PDEAEMA–*b*–PEG–*b*–PDEAEMA

5.8.4 Flocculation Characteristics of PAM-*b*-PEG-*b*-PAM Flocculant

An effective flocculant for the aggregation/flocculation of colloidal particles must be of the correct molecular weight and charge density and contain functional groups that are predisposed to interact favourably with specific sites on the colloidal particle surface [65]. It must also have an extended and flexible configuration in the solution to achieve better particle bridging and to produce flocs capable of withstanding moderate shear forces without rupturing [66]. Both polyacrylamides (PAMs) and poly(ethylene oxides) (PEOs) meet these requirements and have been used widely as flocculants in the mineral industry [67]. A comparison of these two polymers on flocculation performance has shown PEO to have a greater settling efficiency and higher turbidity removal than PAM [68]. Furthermore, PEO treatment of the colloidal suspensions yielded more stable and stronger flocs. PEO is a water-soluble nonionic polymer, $HO\text{-}(CH_2\text{-}CH_2\text{-}O)_n\text{-}H$, which is available commercially in a wide range of molecular weights. The ether oxygen in the polymer chain interacts with water, causing the polymer to be water-soluble, while the $\text{-}CH_2\text{-}CH_2\text{-}$ groups are hydrophobic in nature. Previous studies on PEO and PEG (separately) indicate that a block copolymer such as PAM-*b*-PEG-*b*-PAM will adsorb onto kaolinite particles by a combination of hydrogen bonding, hydrophobic interaction, electrostatic interaction, and cation-bridge mechanisms [69]. These mechanisms have been discussed previously with respect to PAM. With respect to PEO, it has been postulated that the main mechanism of adsorption is hydrogen bonding. It has been suggested [68] that the two lone pairs of electrons in the outer orbital of the ether oxygen act as electron donors while the hydroxyl groups on the kaolinite particle are electron acceptors to form the hydrogen bond. The hydrogen bonding between PEO and kaolinite is shown in Figure 5.15.

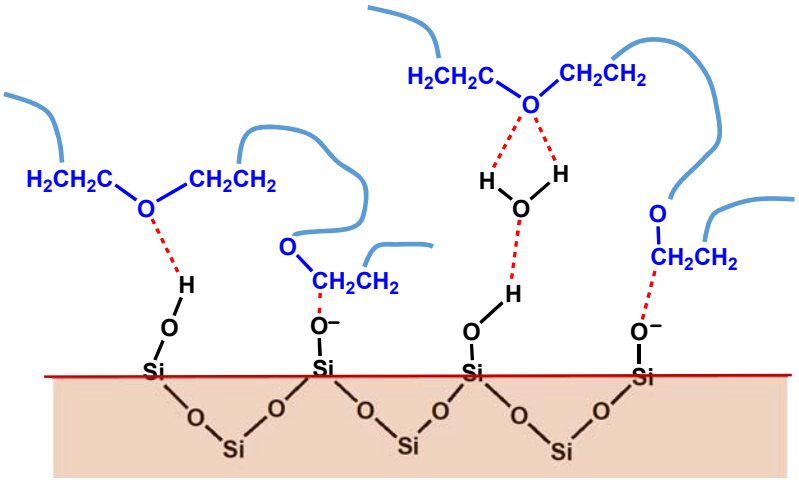

Figure 5.15: Schematic diagram of the conformation of PEO chains adsorbed on kaolinite surface

In addition to hydrogen bonding, hydrophobic interactions between the siloxane (Si-O-Si) surface and PEO has also been suggested [69]. PEO contains hydrophilic segments and a very long hydrophobic hydrocarbon chain. The hydrophobic backbone ($–CH_2 – CH_2–$) of the polymer is attracted to the hydrophobic siloxane surfaces of kaolinite because they both have a tendency to avoid water molecules. When compared to hydrogen bonding, it is found that hydrogen bonding mechanism is more influential than hydrophobic interactions. Hydrophobic interactions are therefore considered as an assistive mechanism of hydrogen bonding [70].

The flocculation characteristics of the various block copolymers were evaluated using a 0.25% (w/v) kaolinite suspension and the effect of the flocculant dosage on residual turbidity of the suspension is shown in Figure 5.16.

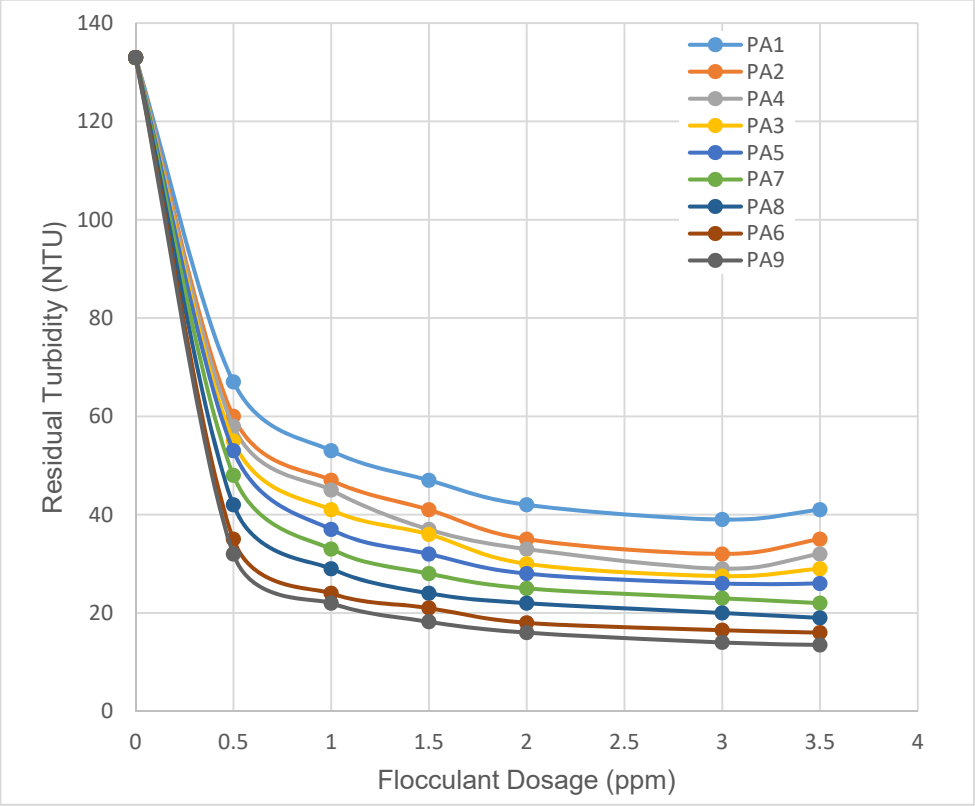

Figure 5.16: Jar test results of PAM-*b*-PEG-*b*-PAM flocculant on a 0.25% (w/v) kaolinite suspension

The results shown were obtained under the following conditions: a pH of 7.0, original turbidity of kaolinite suspension of 135.0 NTU, rapid mixing speed of 125 rpm for 2 minutes followed by a slow mixing speed of 20 rpm for 15 minutes, and a settling time of 30 minutes. As with previous studies (Cell-*g*-PAM flocculants), all PAM-*b*-PEG-*b*-PAM flocculants showed similar trends with

respect to their flocculating abilities: Initially, even a very small dosage of the flocculants (as little as 0.5 ppm) caused a drastic drop in turbidity. Further increases in the flocculant dosage caused further, but slower reduction in the residual turbidity.

In general, polymeric flocculants cause aggregation/flocculation of colloidal particles by either polymer bridging or charge neutralization (including 'electrostatic patch' effects) [71]. The major mechanism of flocculation by polymers is, however, bridging. Bridging takes place by adsorption of a polymer flocculant at more than one site on a colloidal particle or at sites on different particles. When long chain polymer molecules adsorb onto the surface of particles, they tend to form loops and tails that extend some distance from the particle surface into the aqueous phase. These loops and tails adsorb onto the surface of neighbouring particles, thus forming bridges between the particles. For effective bridging to occur, the length of polymer chains should be long so that they can extend from one particle surface to another. The effect of polymer length on flocculation performance is clearly visible in the data presented in Figure 5.16 – the poorest performing polymers (PA1, PA2, PA3, and PA4) are also the shortest length polymers. These polymers may not be long enough to effectively bridge neighbouring particles and the primary mechanism of flocculation for these flocculants may be electrostatic patch mechanism. Also, for these flocculants, the suspension turbidity decreases by increasing the added polymer from 0.5 ppm to 3 ppm after which it begins to increase. Most probably, increasing the flocculant beyond 3 ppm results in the surface of the colloidal particle becoming completely covered with the flocculant and restabilizing the colloidal particles - in the over dosage region, residual turbidity of the supernatant liquid increases probably because of steric stabilization and electrostatic repulsion.

The flocculation efficiency of the flocculants used in the Jar Tests were again tested using Settling Tests and the results are depicted in Figure 5.17. For all tests, the flocculant dosage was maintained at 3 ppm, *i.e.* at the optimum dosage as determined by the Jar Tests. The Settling Test results (Figure 5.17) confirm the results obtained from the Standard Jar Tests – the longer flocculants produced bigger flocs which settle at a faster rate. The flocculation performance of a particular copolymer can be correlated with the settling velocity. The settling profiles of the graft copolymers do not show any retarded settling behavior and from the settling curves, it is observed that the fall of interface is initially linear before it becomes non-linear. The settling velocity is measured from the slope of the linear portion of the settling curves. The greater the settling velocity of the floc containing kaolinite particles, the greater will be its flocculation performance. The faster the rate at which kaolinite particles are flocculated and settle, the steeper will be the curves for interphase height versus time.

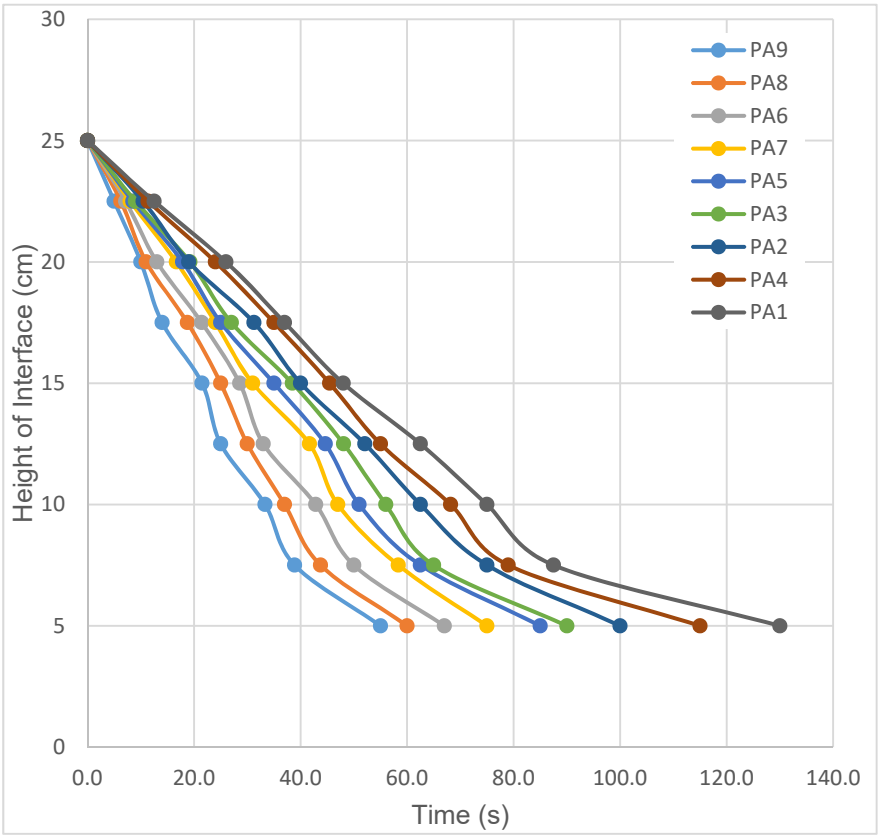

Figure 5.17: Settling characteristics of PAM-*b*-PEG-*b*-PAM flocculants in 0.25% (w/v) kaolinite suspension

When the flocculating performance of the PAM-*b*-PEG-*b*-PAM block copolymers (as evidenced by both the Standard Jar Test and Settling Test) is compared with that of Cell-*g*-PAM (Chapter 3), it seen that the graft copolymers perform better than the linear block copolymers. In case of linear polymers, the polymer segments attach to the surface of colloidal particles and project into the solution as tails and loops. In this way, they form bridges between colloidal particles to form flocs. In the case of graft copolymers such as Cell-*g*-PAM, the PAM polymer segments dangle from the rigid cellulose backbone in a comb-like structure. This enables better approach of the flocculant segments towards the colloidal particles as proposed by the Easy Approachability Model. With graft copolymers, due to the better approachability of the grafted chains, they can easily bind onto more colloidal particles through bridging. This type of intense bridging is not possible in the case of linear polymers and hence their approachability towards suspended particles and flocculation efficiency is lower.

5.8.5 Flocculation Characteristics of PDMAEMA-*b*-PEG-*b*-PDMAEMA Flocculant

The triblock copolymer, PDMAEMA-*b*-PEG-*b*-PDMAEMA, is a double-hydrophilic block copolymer (DHBC). DHBCs consist of two or more water-soluble blocks, each with a different chemical nature. However, only one of them can be converted to be hydrophobic by changing the temperature, pH, ionic strength, or complexation with appropriate molecules [72]. Poly(ethylene glycol) (PEG) does not exhibit any pH-dependent hydrolysis or charging behaviour in the 3-12 pH range. PEG has been included as one hydrophilic block of the DHBC because of its nontoxicity and well-known flocculating ability. Poly(*N,N*-dimethylaminoethyl methacrylate) (PDMAEMA) is the pH-responsive segment. The tertiary amine groups along its main chain can be charged or uncharged at low or high pH, respectively. At low pH, the tertiary amine groups are protonated and become positively charged. Under these conditions PDMAEMA is water-soluble and can be considered to be a typical cationic polyelectrolyte. The amino groups of PDMAEMA are deprotonated at high pH and PDMAEMA becomes hydrophobic.

The interaction and flocculation of kaolinite particles by PDMAEMA-*b*-PEG-*b*-PDMAEMA may be induced by one of two mechanisms, namely, interparticle bridging and charge neutralization. Interparticle bridging requires that the block copolymer be adsorbed to two or more particles at the same time. Interparticle bridging would occur through hydrogen bonding between the PDMAEMA-PEG segments of the triblock copolymer. Charge neutralization would occur when the positively charged PDMAEMA segments adsorb to kaolinite particles carrying negative charges. Changing the pH of the suspension would therefore result in varying modes of flocculation.

Kadla *et al*. [73] gained insight into the mechanism of lignin aggregation with PDMAEMA-PEO triblock copolymers at different pH values by following the changes in the system using NMR analyses. At a pH value of 10 they found the lignin and copolymer to be dissolved and existing as separate non-interacting polymers. When the pH was reduced to pH 8, the proton signals disappeared. The absence of NMR signals demonstrates that strong intermolecular association occur between the lignin and the copolymer, resulting in aggregation and precipitation from the solution. At this pH, they also found the appearance of PEO methylene protons and lack of PDMAEMA protons suggesting that the PDMAEMA is located in the core of the aggregates with lignin, while the PEO is located in the corona. This confirms that the lignin preferentially interacts with the PDMAEMA component of the triblock copolymer. At a pH value of 2, the

protonated PDMAEMA proton signals reappear but those associated with the PEO-block become negligible. Under these acidic conditions, protonation of the tertiary amine stops its interaction (hydrogen bonding) with lignin, and also dramatically enhances its hydrophilicity. Under these conditions the lignin/PEO interactions become dominant, resulting in lignin/PEO aggregation forming the core of the assemblies, with the PDMAEMA blocks extending to form the corona.

The flocculation characteristics of the various synthesized PDMAEMA-*b*-PEG-*b*-PDMAEMA block copolymers were evaluated at neutral pH using a 0.25% (w/v) kaolinite suspension. The effects of the triblock copolymers on the flocculation of kaolinite particles are shown in Figure 5.18 (Standard Jar Test) and in Figure 5.19 (Settling Test).

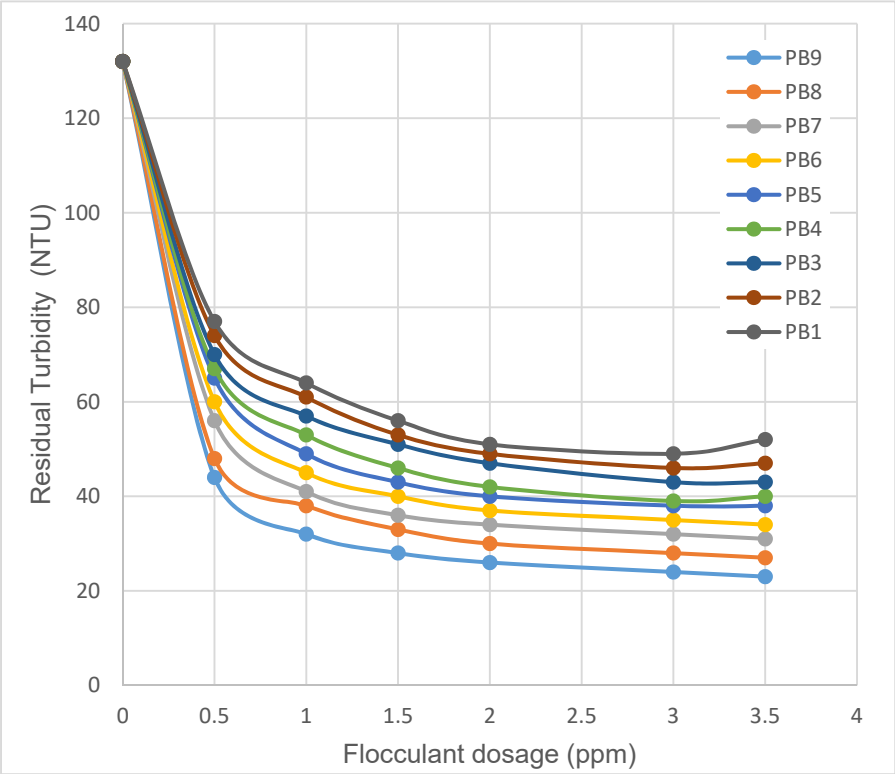

Figure 5.18: Jar test results of PDMAEMA-*b*-PEG-*b*-PDMAEMA flocculant on a 0.25% (w/v) kaolinite suspension

The results shown in the Jar Test experiments (Figure 5.18) were obtained under the following conditions: a pH of 7.0, original turbidity of kaolinite suspension of 135.0 NTU, rapid mixing speed of 125 rpm for 2 minutes followed by a slow mixing speed of 20 rpm for 15 minutes, and a settling time of 30 minutes. The Settling Tests were conducted at a flocculant dosage of 3 ppm.

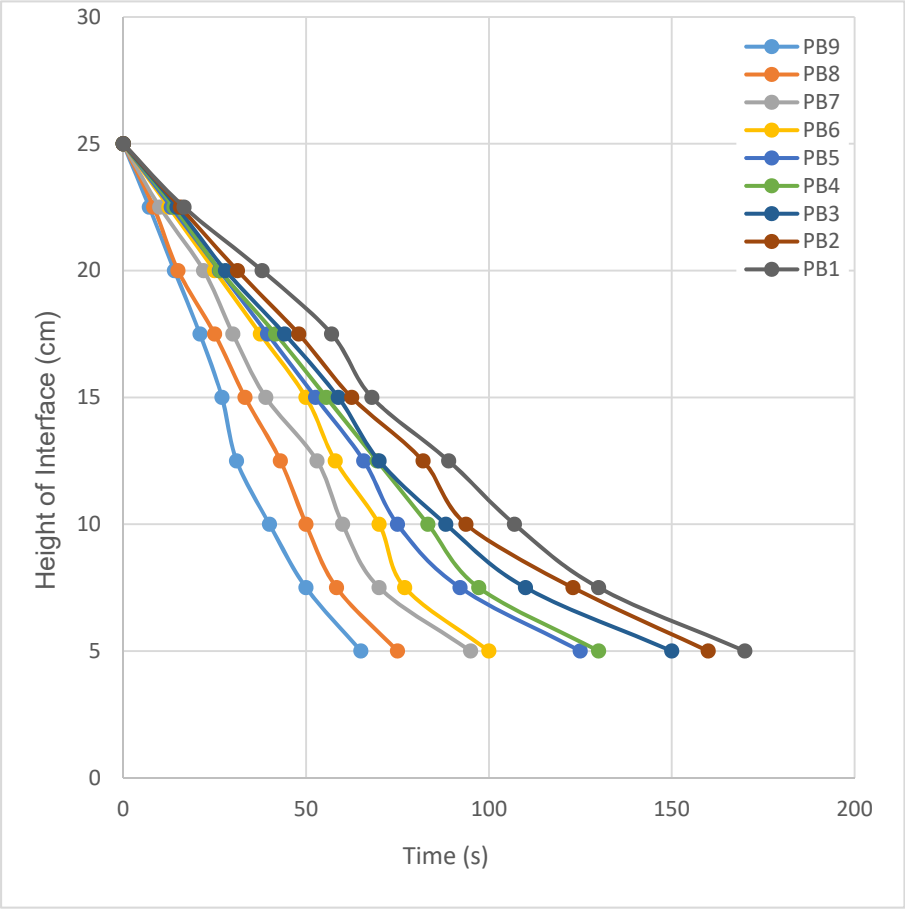

Figure 5.19: Settling characteristics of PDMAEMA-*b*-PEG-*b*-PDMAEMA flocculants in 0.25% (w/v) kaolinite suspension

From Figure 5.18 it can be seen that the turbidity drops rapidly with initial increase in flocculant dosage. Further increases in the flocculant dosage then cause further, but slower reduction in the residual turbidity. It is observed that the overall length of the block copolymer determines the efficiency of the flocculant (as opposed to the composition of the copolymer). For the shorter length polymers (PB1, PB2, PB3, and PB4) there is a slight increase in turbidity after the optimum dosage of flocculant at 3 ppm. The primary mechanism of flocculation for the shorter length flocculants is by charge patch formation. It has been suggested by many researchers [74] that optimum flocculation occurs when half the surface of the colloidal particle is covered with flocculants. At higher dosages of the flocculant polymer, there is insufficient particle surface for attachment of the polymer segments leading to destabilization of the flocs. From Figure 5.18, it is seen that in all the cases, this optimal dosage is 3 ppm (in the 0.25% kaolinite suspension). The flocculation by the longer length flocculants (PB5 – PB9) may be explained by polymer bridging

mechanism - if the flocculants are sufficiently long and for neutral flocculants/slightly ionic flocculants in a pH neutral suspension, the major mechanism is polymer bridging [70]. The flocculant polymer (PB9) with the longest grafted chains would be the most efficient flocculant. For the longer chain flocculants there was no over-dozing in the range 0 – 3.5 ppm.

Settling tests were carried out in 0.25t% (w/v) kaolinite suspension and the settling characteristics of the PDMAEMA-*b*-PEG-*b*-PDMAEMA flocculant and its various grades are illustrated in Figure 5.19. From the settling curves above, it is observed that the fall of the interface is linear for a considerable height before it becomes non-linear. This means that initially the rate of fall of the interface is constant, after which it gradually declines. In conformity with the Jar Test results discussed above, the longest flocculant (PB9) has the highest settling velocity. This relationship between the length of flocculant and settling velocity is followed by the remaining grades of flocculant as well.

The pH of the flocculation system can affect or activate both the kaolinite surface and/or the flocculant polymer functional groups. In the present study, the turbidity of the kaolinite suspensions was measured at different values of pH ranging from 3 to 10. The results of these measurements are shown in Figure 5.20.

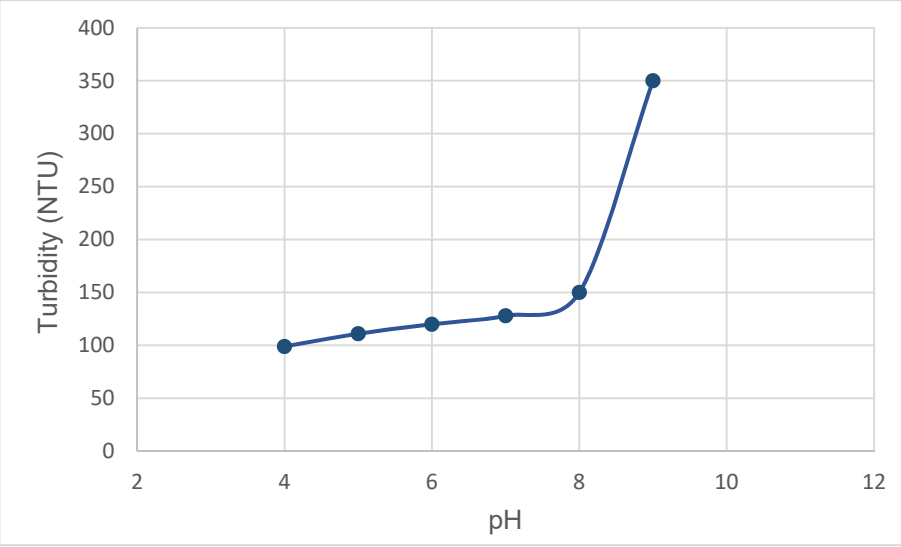

Figure 5.20: Effect of pH on the turbidity of kaolinite suspension (0.25% (w/v))

These measurements indicate that the turbidity of the kaolinite suspension increases with increasing pH. The observed changes in turbidity with pH are closely related to the molecular

structure of the kaolinite particles. Kaolinite has a platelet structure with a tetrahedral silica sheet attached to an octahedral alumina sheet [75]. At the edges of the kaolinite particles, the silica and alumina sheets are disrupted, exposing broken bonds comprising of silanol (Si-OH) and aluminol (Al-OH) groups. The basal faces, comprising of tetrahedral silica sheets, carry permanent negative charges as a result of the isomorphous substitution of Si^{4+} by Al^{3+} and these charges do not change with solution pH. The octahedral alumina sheets and Al-OH and Si- OH edge sites, on the other hand, are pH-dependent - these surface hydroxyl groups protonate and deprotonate according to the pH of the slurry. The change in charge on the kaolinite particle with pH is shown in Figure 5.21.

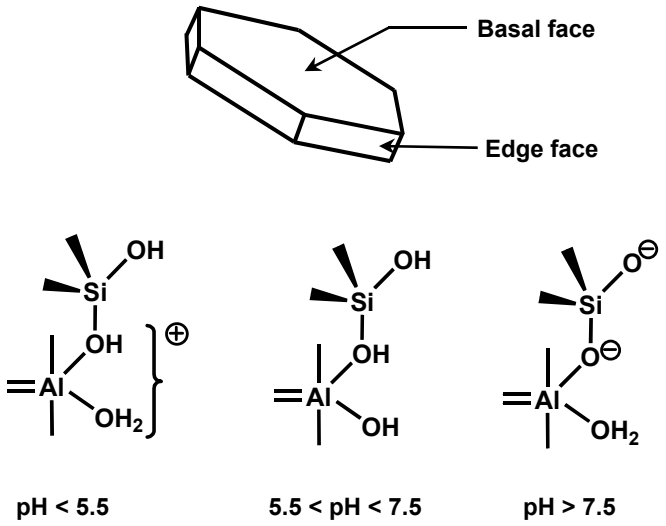

Figure 5.21: pH-dependence of surface chemistry of the edge face of kaolinite particle [75]

At a low pH value, the positively-charged octahedral alumina sheets become attracted to the negatively charged tetrahedral silica sheets, thus forming tightly bonded face-face platelets. In addition to this, the positively charged edges are attracted to the negatively charged tetrahedral silica sheets, forming slightly porous edge-face connections. At high pH values (pH>7.5) all faces and edges are negatively charged and repel each other. This increases the turbidity of the solution, as observed in Figure 5.20.

Further flocculation investigations were carried out to see if the polymer structure dependent behavior, observed at pH 7, is displayed at other pH values. The best performing PDMAEMA-*b*-PEG-*b*-PDMAEMA block copolymer (PB9) was used as the flocculant. The effect of changing the pH of the flocculation system on the residual turbidity is shown in Figure 5.22.

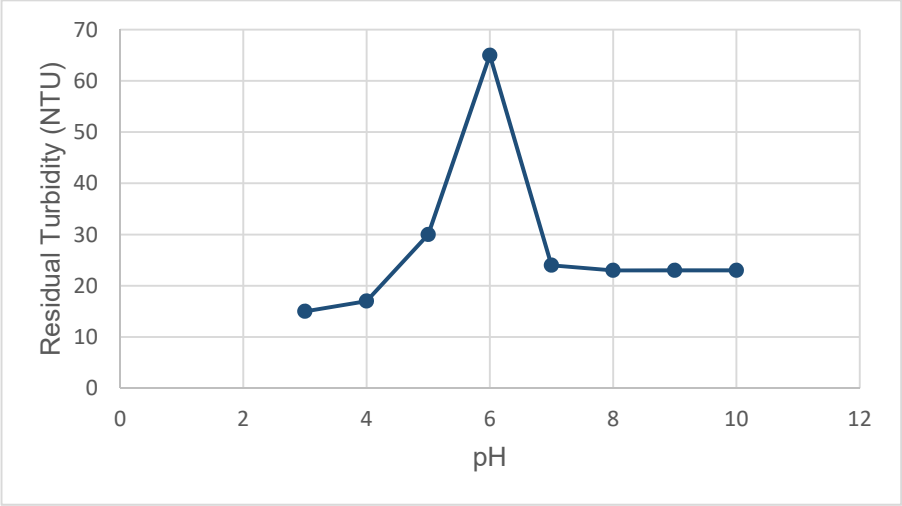

Figure 5.22: Effect of pH on residual turbidity of kaolinite (0.25% (w/v)) with PDMAEMA-*b*-PEG-*b*-PDMAEMA as flocculant

The results shown in Figure 5.22 were obtained under the following conditions: original turbidity of kaolinite suspension of 135.0 NTU, flocculant: PB9, flocculant dosage: 3 ppm (optimum dosage from Standard Jar Test), rapid mixing speed of 125 rpm for 2 minutes followed by a slow mixing speed of 20 rpm for 15 minutes, and a settling time of 30 minutes.

As shown in Figure 5.22, the turbidity of the solution was low (15 NTU) at the lower values of pH. The turbidity of the colloidal solution increased sharply when the pH of the solution increases beyond 4 and then reaches the maximum value. When the pH is further increased, the turbidity begins to reduce significantly and when the pH reaches above 7, the solution becomes clearer again. The DMAEMA monomer is soluble in water with a pH of 8.4, whereas the pK_a of PDMAEMA-*b*-PEG-*b*-PDMAEMA ranges from 7.4 to 7.8 depending on its molecular weight [76]. At a pH lower than its pK_a, the amine group of DMAEMA gets protonated whereas at high pH (above the pK_a of the polymer), the amine group loses its protonation as shown in Scheme 5.9.

At low pH values, the DMAEMA segments of the copolymer assume a positive charge as result of the protonation of the amine groups. These positively charged groups become attracted to the negatively charged tetrahedral silica sheets, which now become more approachable because of the effect of low pH on the kaolinite structure. These strong electrostatic attractions result in flocculation of the kaolinite particles through charge neutralization. The high turbidity values

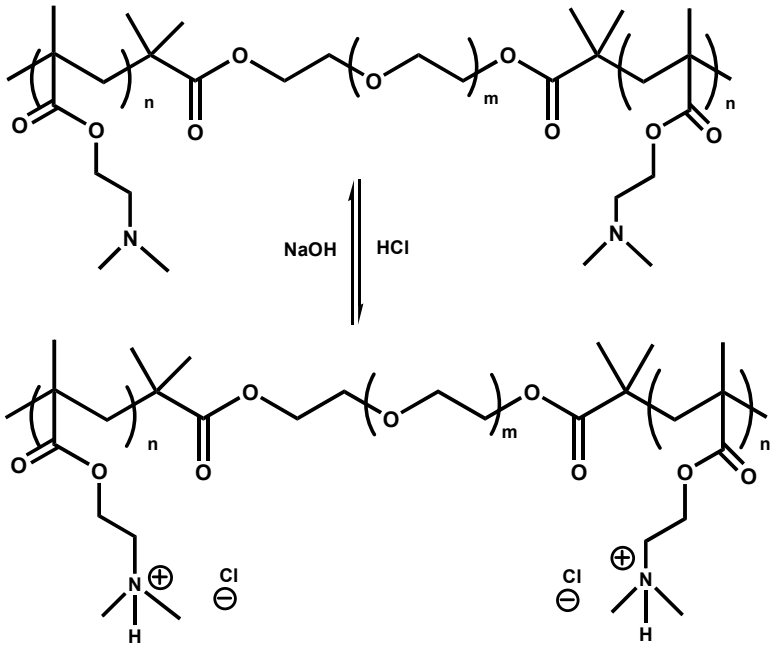

Scheme 5.9: Effect of pH on PDMAEMA-*b*-PEG-*b*-PDMAEMA

around the pH value of 6 may be attributed to the fact that around this pH value the block copolymer is nonionic and has a more coiled conformation that is less effective for bridging. In the case of nonionic polymers, the most likely mechanism of adsorption is through hydrogen bonding between the oxygen atoms associated with hydrated metal ions at the particle surface and amide groups on the polymer [77]. At higher values of pH (> 6.5) the DMAEMA segments are deprotonated while the kaolinite particles are negatively charged. The polymer interactions with the highly negatively charged kaolinite particles at higher pH (6 – 8) result in the formation of more open and weak flocs.

For non-ionic PEO, which does not exhibit pH-dependent hydrolysis or charging behaviour in the pH range 3-12, no significant conformational changes are expected. A change in pH does however affect the colloidal particles. Kaolinite, which exist as hexagonal platelets, have different chemistries occurring at the basal face and at the edge face. The basal face has a net negative charge due to isomorphous replacements by impurities, and is unaffected by changes in pH. The edge face, however, can be positive, neutral, or negative, depending on the pH of the solution. A decrease in the Brønsted acid sites at the kaolinite particle surface with increasing dispersion pH occurs and negatively impacts the flocculation performance of PEO. Hence, as the pH is increased, the flocculation rate decreases. These results are consistent with the fact that as pH

is increased, a poor interaction of kaolinite particles with the PEO results from weakened hydrogen bonding.

5.9 Conclusions

Two triblock copolymer flocculants, PAM-*b*-PEG-*b*-PAM and PDMAEMA-*b*-PEG-*b*-PDMAEMA have been successfully synthesized using the SET-LRP method. For both types of copolymers the lengths of both the central PEG segments and outer block were varied. The synthesized block copolymers were characterized using FTIR and ^{1}H NMR analysis. The flocculation efficacy of the block copolymers was studied through standard jar test and settling test procedures in kaolinite suspensions (0.25% w/v), at dosage ranging from 0.5 ppm to 3.5 ppm. For both the PAM-*b*-PEG-*b*-PAM and PDMAEMA-*b*-PEG-*b*-PDMAEMA flocculants, the polymers with the longest lengths gave the best flocculation results – minimum residual turbidity and fastest settling velocity. It was postulated that the longer polymers induced flocculation through the bridging mechanism while the shorter polymers flocculated through the charge patch mechanism. For the PDMAEMA-*b*-PEG-*b*-PDMAEMA flocculant, the effect of pH on the flocculation performance was further investigated. It was found that because of the response of both the DMAEMA segments and the kaolinite particles to changing pH, the optimum flocculation occurs when the pH of the kaolinite suspension is below 5.5.

5.10 References

[1] Zaman A.A., Bjelopavlic M., Moudgil B.M., J. Colloid Interface Sci. 2000, 226, 290.

[2] Mpofu P., Addai-Mensah J., Ralston J., Int. J. Miner. Process. 2003, 7, 247.

[3] Deng Y J., Dixon J B., White G N., Colloid. Polymer Sci. 2006, 284, 347–356.

[4] Wang W., Zhao J., Zhou N., Zhu J., Zhang W., Pan X., Zhang Z., Zhu X., Polym. Chem. 2014, 5, 3533−3546.

[5] Alsubaie F., Anastasaki A., Nikolaou V., Simula S., Nurumbetov G., Wilson P., Kempe K., Haddleton D M., Macromolecules. 2015, 48, 5517−5525.

[6] Polymerization process and polymers produced thereby, US Patent 4581429, 1986.

[7] Georges M K., Veregin R P N., Kazmaier P M., Hamer G K., Macromolecules. 1993, 26, 2987-2988.

[8] Wang G., Chen M., Guo S., Hu A., J. Polym. Sci., Part A: Polym. Chem. 2014, 52, 2684–2691.

[9] Georges M K., Veregin R P N., Kazmaier P M., Hamer G. K., Macromolecules. 1993, 26, 2987-2988.

[10] Hibi Y., Tokuoka S., Terashima T., Ouchi M., Sawamoto M., Polym. Chem, 2011, 2, 341-347.

[11] McHale R., Patterson J. P., Zetterlund P. B., O'Reilly R. K., Nat Chem. 2012, 4, 491-497.

[12] Chiefari J., Chong Y. K., Ercole F., Krstina J., Jeffery J., Le P T., Mayadunne R T A., Meijs G. F., Moad C. L., Moad G., Macromolecules. 1998, 31, 5559-5562.

[13] Moad, G., Chiefari, J., Polym. Int., 2000, 49(9), 993-1001.

[14] Moad G., Rizzardo E., Thang S. H., Aust. J. Chem. 2009, 62, 1402-1472.

[15] Moad G., Rizzardo E., Thang S. H., Aust. J. Chem. 2005, 58, 379-410.

[16] Kato M., Kamigaito M., Sawamoto M., Higashimura T., Macromolecules. 1995, 28, 1721-1723.

[17] Wang J S., Matyjaszewski K., J. Am. Chem. Soc. 1995, 117, 5614-5615.

[18] Haddleton D M., Crossman M C., Dana B H., Duncalf D J., Heming A M., Kukulj D., Shooter A J., Macromolecules. 1999, 32, 2110-2119.

[19] Percec V., Guliashvili T., Ladislaw J S., Wistrand A., Stjerndahl A., Sienkowska M J., Monteiro M J., Sahoo S., J. Am. Chem. Soc. 2006, 128, 14156-14165.

[20] Rosen M., Percec V., J. Polym. Sci., Part A: Polym. Chem. 2007, 45, 21, 4950-4964.

[21] Nguyen N H., Rosen B M., Lligadas G., Percec V., Macromolecules. 2009, 42, 2379-2386.

[22] Rosen B M., Percec V., Chem. Rev. 2009, 109, 5069-5119.

[23] Percec V., Guliashvili T., Ladislaw J S., Wistrand A., Stjerndahl A., Sienkowska M J., Monteiro M J., Sahoo S., J. Am. Chem. Soc. 2006, 128, 14156-14165.

[24] Liu D., Chen H., Yin P., Hao Z., Fan L., J. Polym. Sci., Part A: Polym. Chem. 2012, 50, 4809-4813.

[25] Hao Z., Chen H., Liu D., Fan L., J. Polym. Sci., Part A: Polym. Chem. 2012, 50, 4995-4999.

[26] Rosen B M., Percec V., Chem. Rev. 2009, 109, 5069-5119.

[27] Nguyen N H., Rosen B M., Lligadas G., Percec V., Macromolecules. 2009, 42, 2379-2386.

[28] Nguyen N H., Rosen B M., Percec V., J. Polym. Sci., Part A: Polym. Chem. 2010, 48, 1752-1763.

[29] Nguyen N H., Rodriguez-Emmenegger C., Brynda E., Sedlakova Z., Percec V., Polym. Chem. 2013, 4, 2424-2427.

[30] Liu X H., Zhang G B., Li B X., Bai Y G., Li Y S., J. Polym. Sci., Part A: Polym. Chem. 2010, 48, 5439-5445.

[31] Whittaker M R., Urbani C N., Monteiro M J., J. Polym. Sci., Part A: Polym. Chem. 2008, 46, 6346-6357.

[32] Samanta S R., Cai R., Percec V., Polym. Chem. 2014, 5, 5479-5491

[33] Tom J., Hornby B., West A., Harrisson S., Perrier S., Polym. Chem. 2010, 1, 420−422.

[34] Gao J., Zhang Z., Zhou N., Cheng Z., Zhu J., Zhu X., Macromolecules. 2011, 44, 3227−3232.

[35] Li Y., Lu G., Dai B., Xu C., Huang X J., Polym. Sci., Part A: Polym. Chem. 2013, 51, 1942−1949.

[36] Truong N P., Gu W., Prasadam I., Jia Z., Crawford R., Xiao Y., Monteiro M. J., Nat. Commun. 2013, 4, 1902.

[37] Zhang Q., Wilson P., Li Z., McHale R., Godfrey J., Anastasaki A., Waldron C., Haddleton D M., J. Am. Chem. Soc. 2013, 135, 7355−7363.

[38] Nguyen N H., Percec V., J. Polym. Sci., Part A: Polym. Chem. 2011, 49, 4756−4765.

[39] Nguyen N H., Kulis J., Sun H J., Jia Z., van Beusekom B., Levere M E., Wilson, D A., Monteiro M J., Percec V., Polym. Chem. 2013, 4, 144−155.

[40] Samanta S R., Nikolaou V., Keller S., Monteiro M J., Wilson D A., Haddleton D M., Percec V., Polym. Chem. 2015, 6, 2084−2097.

[41] Zhang Q., Wilson P., Li Z., McHale R., Godfrey J., Anastasaki A., Waldron C., Haddleton D M., J. Am. Chem. Soc. 2013, 135, 7355−7363

[42] Nguyen N H., Jiang X., Fleischmann S., Rosen B M., Percec V J., Polym. Sci., Part A: Polym. Chem. 2009, 47, 5629−5638.

[43] Simula A., Nikolaou V., Anastasaki A., Alsubaie F., Nurumbetov G., Wilson P., Kempe K., Haddleton D M., Polym. Chem. 2015, 6, 2226−2233.

[44] Hornby B D., West A G., Tom J C., Waterson C., Harrisson S., Perrier S., Macromol. Rapid Commun. 2010, 31, 1276−1280.

[45] Lligadas G., Ladislaw J S., Guliashvili T., Percec V., J. Polym. Sci., Part A: Polym. Chem. 2008, 46, 278−288.

[46] Nguyen N H., Rosen B M., Lligadas G., Percec V., Macromolecules. 2009, 42, 2379−2386.

[47] Jiang X., Rosen B M., Percec V., J. Polym. Sci., Part A: Polym. Chem. 2010, 48, 403−409.

[48] Chen H., Zong G., Chen L., Zhang M., Wang C., Qu R., J. Polym. Sci., Part A: Polym. Chem. 2011, 49, 2924−2930.

[49] Wang G X., Lu M., Hou Z H., Li J., Zhong M., Wu H., J. Polym. Sci., Part A: Polym. Chem. 2013, 51, 2919−2924.

[50] Rosen B M., Percec V., J. Polym. Sci., Part A: Polym. Chem. 2008, 46, 5663−5697.

[51] Hornby B D., West A G., Tom J C., Waterson C., Harrisson S., Perrier S., Macromol. Rapid Commun. 2010, 31, 1276−1280.

[52] Nguyen N H., Kulis J., Sun H J., Jia Z., van Beusekom B., Levere M E., Wilson D A., Monteiro M J., Percec V., A. Polym. Chem. 2013, 4, 144−155.

[53] Ayres L., Vos M R J., Adams P J H M., Shklyarevskiy I O., van Hest J C M., Macromolecules. 2003, 36, 5967−5973.

[54] Li Z., Kesselman E., Talmon Y., Hillmyer M A., Lodge T P., Science. 2004, 306, 98−101.

[55] Jankova K., Chen X., Kops J., Batsberg W., Macromolecules. 1998, 31, 538.

[56] Samanta S R., Nikolaou V., Keller S., Monteiro M J., Wilson D A., Haddleton D M., Percec V., Polym. Chem. 2015, 6, 2084−2097.

[57] Piirma I. 1992. Polymeric Sufactants, Sufactant Science Series, M. Dekker, New York.

[58] Hamley I. W. 2004. Developments in Block Copolymer Science and Technology, John Wiley and Sons, England.

[59] Wang J S., Matyjaszewski K., Macromolecules. 1995, 28, 7901–7910.

[60] Zeng F Q., Shen Y Q., Zhu S P., Pelton, R., J. Polym. Sci., Part A: Polym. Chem. 2000, 38, 3821–3827.

[61] Siegwart D. J., Oh J K., Matyjaszewski K., Prog. Polym. Sci. 2012, 37, 18–37.

[62] Waldron C., Anastasaki A., McHale R., Wilson P., Li Z., Smith T., Haddleton D M., Polym. Chem. 2014, 5, 892-898.

[63] Zhao Y., Lord M S., Stenzel M H., J. Mater. Chem. B. 2013, 1, 1635−1643.

[64] Shenoi R A., Kalathottukaren M T., Travers R J., Lai B F L., Creagh A L., Lange D., Yu K., Weinhart M., Chew B H., Du C., Brooks D E., Carter C J., Morrissey J H., Haynes C A., Kizhakkedathu J N., Sci. Transl. Med. 2014, 6, 260.

[65] Mpofu, P., Addai-Mensah J., Ralston J., International Journal of Mineral Processing. 2005, 75, 155-171.

[66] Nabzar L., Carroy A., Pefferkorn E., Journal of Colloid Interface Sci. 1986, 14, 2,113-119.

[67] Hwang J Y., Dixon J B., Clay Science. 2000, 11, 137-146.

[68] Mpofu, P., Addai-Mensah J., Ralston J., Minerals Engineering. 2004, 17, 3, 411-423.

[69] Thompson J G., Uwins P., Whittaker, A K., Mackinnon I., Clays and Clay Minerals 1992, 40, 4, 369– 380.

[70] Kristof E., Zoltan A J., Vassanyj I., Clays and Clay Minerals. 1993, 415, 608–612.

[71] Frost L., Clays and Clay Minerals. 1998, 46, 3, 280– 289.

[72] Fox M E., Szoka F C., Fréchet J M J., Acc. Chem. Res. 2009, 42, 1141–1151.

[73] Gao G., Xu W Z., Kadla J F., Journal of Wood Chemistry and Technology. 2015, 35, 1.

[74] Dos Santos A B., Cervantes F J., van Lier J B., Bioresour. Technol. 2007, 98, 12.

[75] Johnson R A., Gallanger S M., J. Water Pollut. Control Fed. 1984, 56, 8.

[76] Hocking M B., Klimchuk K A., Lowen S., Journal of Macromolecular Science, Part C: Polymer Reviews. 1999, 39, 2, 177-203

[77] Kikuchi A., Okano T., Adv. Drug Delivery Rev. 2002, 54, 53–77.

Chapter 6

Conclusions and Recommendations

6.1 Conclusions

The research can effectively be divided into four sections: synthesis of graft copolymers flocculants using a chemical free-radical method, synthesis of graft copolymer flocculants using a microwave-assisted approach, synthesis of graft copolymer flocculants using a microwave-initiated approach, and synthesis of triblock copolymer flocculants. Conclusions for each of these methods will be discussed separately.

6.1.1 Chemical Free-radical Initiated Graft Copolymerization of Cell-*g*-PAM

In recent years, due to the increasing costs and environmental considerations associated with the use of commercially available flocculants, research work aimed at developing new, low cost flocculants derived from renewable resources has intensified. In this context, the advantages of using cellulose as the basis for new flocculants (due to its high abundance, low cost and the relative ease with which it can be modified chemically) has been identified. In this research the chemical free-radical grafting of acrylamide onto cellulose using ceric ammonium nitrate/nitric acid as the initiator has been successfully accomplished. The CAN/HNO_3 initiator system has been found to be an efficient initiator in reducing the formation of ungrafted polyacrylamide by forming active sites mainly on the cellulose backbone. The percentage grafting was optimized using experimental design and response surface methodology. Traditional methods to obtain the optimum conditions for the synthesis of Cell-*g*-PAM used the one-factor-at-a-time approach. This research used, for the first time, an experimental design approach with response surface methodology. The percentage grafting of acrylamide onto cellulose was shown to be dependent on the molar ratio of monomer to cellulose, molar ratio of CAN to cellulose, molar ratio of HNO_3 to cellulose, temperature of reaction, and time duration of reaction. From the results obtained in this study, it can be concluded that the given predictive model described the studied grafting process very well. The model can be used to predict the grafting percentage under any given conditions within the experimental range. Results obtained from response surface methodology pointed out that the grafting percentage yield is affected by all the parameters studied. Using

response surface methodology, the effects of the individual factors on the percentage grafting was elucidated and it was found that a maximum percentage grafting of 121% could be obtained.

Further, the flocculation efficacy of the highest percentage grafted copolymer was tested against highly recommended commercially available polyacrylamide based flocculants. These flocculants were studied using the Standard Jar Test as well as the Settling Test procedure in 0.25% kaolinite suspension. It was found that the synthesized Cell-*g*-PAM bioflocculant performed just as well as the best performing commercial flocculants. Based on the observed results, it can be concluded that synthesized bioflocculant may be used as a high performance flocculant for the treatment of wastewaters.

6.1.2 Microwave-assisted Grafting of Acrylamide onto Cellulose

In this research, polyacrylamide grafted cellulose (Cell-*g*-PAM) has been successfully synthesized by the microwave-assisted technique. This method involved the synergism of microwave radiation and ceric ammonium nitrate/nitric acid (chemical free-radical initiator) to initiate the free radical grafting reaction. All sited literature indicated the use of the domestic microwave oven to carry out the copolymerization reactions. In this research, a novel monomode reactor was designed, fabricated, and utilized to carry out the reactions. The designed reactor can easily be adapted to operate in a continuous flow reactor and hence is capable of producing copolymer flocculants on a commercial scale – a major limitation of previously designed microwave reactors. The synthesized grades of the graft copolymer were characterized through gravimetric techniques. In this study, the process of grafting of acrylamide onto was optimized by response surface methodology. The process was most suitably described with a quadratic model. The conditions for optimizing the grafting of acrylamide onto cellulose was predicted with the model. From the results obtained in this study, it can be concluded that the given predictive model described the studied grafting process very well. The results predicted by the model equation from RSM indicated that a combination of adjusting the reaction time to 3.8 minutes, the acrylamide to cellulose molar ratio to 7.4, CAN to cellulose molar ratio to 0.17, and the irradiation power to 400 W would favour a maximum percentage grafting of 199.6%.

The flocculation efficacy of the synthesized bioflocculant with the highest percentage grafting was compared with commercial flocculants using a 0.25% (w/v) kaolinite suspension as the synthetic wastewater. The synthesized bioflocculant outperformed the flocculating ability of the best performing commercial flocculants. It can be concluded that microwave dielectric heating is not

only an alternative for conventional thermal heating for cellulose modifications, but it also offers an alternative environment friendly, cleaner, greener approach resulting in greater control and higher reproducibility of percentage grafting in the final product, suitable for commercial mass production.

6.1.3 Microwave-initiated Grafting of Acrylamide onto Cellulose

Polyacrylamide grafted cellulose (Cell-*g*-PAM) has been successfully synthesized by microwave-initiated method, which involved microwave radiation alone to initiate synthesis of the graft copolymer. The percentage grafting was optimized using response surface methodology with input parameters being the molar ratio of monomer to cellulose, microwave exposure time, and molar ratio of CAN to cellulose. The percentage grafting of the synthesized graft copolymers was characterized through gravimetric analysis. The results predicted by the model equation from RSM suggested that a combination of adjusting the reaction time to 4 minutes, the acrylamide to cellulose molar ratio to 6.5, and the irradiation power to 400 W would favour a maximum percentage grafting of 66%. In order to confirm these optimized parameters, the reaction was conducted under the suggested conditions and the percentage grafting obtained was 64%, which was almost equal to the actual predicted value of 66%. It was found that the percentage grafting was lower than those obtained by both the conventional chemical free-radical technique and the microwave-assisted method.

As a result of the lower percentage grafting, the flocculating performance of the flocculants were also lower than those produced by the chemical free-radical technique and the microwave-assisted method. The performance of the flocculants improved by hydrolyzing the polyacrylamide side chains.

6.1.4 Block Copolymers

Two triblock copolymer flocculants, PAM-*b*-PEG-*b*-PAM and PDMAEMA-*b*-PEG-*b*-PDMAEMA were successfully synthesized. The integrity of these copolymers were verified using FTIR spectroscopy and ^{1}H NMR spectroscopy. The triblock copolymers were synthesized by SET-LRP using difunctional Br-PEG-Br macroinitiators in the presence of Cu(0)/Me_6-TREN as a catalyst. The difunctional Br-PEG-Br macroinitiators were derived from commercially available poly(ethylene glycol) with various molecular weights (M_n = 10 000, 20 000, and 30 000 g/mol).

Strictly adhering to the protocol for the synthesis of the block copolymer (as proposed by the Haddleton research group) ensured almost complete conversion, with very little monomers being formed. The SET-LRP synthesis was fast (< 20 minutes) and was conducted under relatively mild conditions.

The block copolymers were effective in flocculating a simulated wastewater system of kaolinite suspension. The mechanism of flocculation changed from patch mechanism to bridging mechanism as the overall length of the polymer increased. The flocculating performance of these linear block copolymers were lower than the graft copolymerized flocculants and the quality of the flocculated wastewater could not be considered to be potable. The performance of the PDMAEMA-*b*-PEG-*b*-PDMAEMA flocculant changed with varying pH levels of the kaolinite suspension. The pH of the suspension affected the orientation of the kaolinite particles. Changing the pH from acidic to basic also resulted in the PDMAEMA segments changing from being protonated to deprotonated.

6.2 Recommendations

In the research just completed, various types of flocculants were synthesized and their flocculating ability tested in a model kaolinite suspension at a pH of 7. For the Cell-*g*-PAM graft copolymer, when the PAM was hydrolyzed, an improvement in the flocculation was observed. Changing the pH of the suspension also improved the flocculation when PDMAEMA-*b*-PEG-*b*-PDMAEMA was used as the flocculant. There are several factors, in addition to the ones just mentioned, that affect the overall performance of a flocculant.

The most relevant factors that affect the flocculation of a wastewater system include flocculant type, pH of suspension, temperature of suspension, flocculant dosage, initial turbidity of wastewater, and molecular weight and charge of flocculant. These factors, individually and collectively, will influence the type of flocculant that will provide optimum performance. It is therefore recommended that when a flocculant is designed and synthesized, its performance be tested against currently available flocculants bearing the above factors in mind. It is further recommended that the optimum conditions for the flocculation process be established by using response surface methodology – response surface methodology enables one to assess the effects of these factors simultaneously on the turbidity while reducing the number of experiments. Response surface methodology also determines the effect of each factor on other factors.

In the synthesis of Cell-*g*-PAM, some of the acrylamide will not have polymerized, resulting in unreacted acrylamide being present in the treated water system. The International Agency for Research on Cancer (IARC) states that acrylamide could be classified as “probably carcinogenic to humans” and the World Health Organization (WHO) guideline value associated with a lifetime cancer risk of 10^{-5} is 0.5 μg L^{-1} in drinking water. In this research, attempts had been made to remove any unreacted acrylamide in the synthesized flocculant by washing repeatedly with acetone and water. No attempt, however, had been made to quantify the amount of acrylamide present in the final flocculant sample. Several acceptable methods, such as direct injection and reversed-phase HPLC–UV, solid-phase extraction (SPE), and extraction with activated carbon filter and GC–MS analysis are available to quantify the amount of acrylamide present. It is therefore recommended that one of these methods be used to ensure that the synthesized flocculant is well within the recommended toxicity limits.